UNIVERSIDAD DE CHILE
FACULTAD DE CIENCIAS FÍSICAS Y MATEMÁTICAS
DEPARTAMENTO DE ASTRONOMÍA

SPECTRAL ANALYSIS OF TYPE II SUPERNOVAE

TESIS PARA OPTAR AL GRADO DE
DOCTOR EN CIENCIAS
MENCIÓN ASTRONOMÍA

CLAUDIA PATRICIA GUTIÉRREZ AVENDAÑO

PROFESOR GUÍA:

MARIO HAMUY WACKENHUT

MIEMBROS DE LA COMISIÓN:

JOSEPH PAUL ANDERSON
PAULINA LIRA TEILLERY
RENÉ MENDEZ BUSSARD

SANTIAGO DE CHILE
2016

Resúmen

La idea principal de esta tesis es el análisis de los espectros ópticos de las supernovas de tipo II (SNs II) y sus correlaciones con los parámetros fotométricos. Este análisis se basa en la caracterización de la diversidad espectral y el uso de esta para entender de una mejor forma los mecanismos físicos que involucran a las SNs II. Un objetivo clave es vincular la evolución transitoria a las propiedades del progenitor antes de la explosión. Para este propósito utilizo 893 espectros ópticos (entre 3 y 363 días) de 123 SNs II que se obtuvieron entre 1986 y 2009.

Con el fin de comparar consistentemente las propiedades observadas de las SNs II, es necesario tener una época común. Para ello, estimo las fechas de explosión usando imágenes antes de la explosión y del descubrimiento y la técnica de ajuste espectral, los cuales muestran muy buenos resultados. Centrándome en el perfil P-Cygni de H_α, encuentro que SNs con menor componente de absorción con respecto a la emisión (valores pequeños en a/e), son más brillantes en el máximo, tienen una tasa de declinación más rápida en las curvas de luz, duraciones más cortas en la fase opticamente gruesa y velocidades de expansión más altas. Teniendo en cuenta estos resultados, sugiero que las diferencias entre las SNs de rápido declive (IIL) y las SNs con meseta (IIP) están relacionados con la masa de la envoltura de hidrógeno al momento de la explosión.

Expandiendo el análisis a la cobertura total de los espectros, analizo la aparición de las líneas de Fe II y su evolución con el tiempo con respecto a las diferencias en a/e y la velocidad de H_α en una época dada, la magnitud en el máximo, la la tasa de declive, y la metalicidad del medio. Especulo que la evolución de líneas podría indicar diferencias en las temperaturas y/o metalicidad. Además, encuentro un componente adicional de absorción en el lado azul de H_α. Concluyo de que este componente en los espectros tempranos está asociado a Si II $\lambda6355$, mientras que en la fase de la meseta está relacionado con una característica de alta velocidad en las líneas de hidrógeno, las cuales podrían indicar señales de interacción entre el material expulsado y el viento de la supergigante roja. Por otro lado, la presencia de Si II podría estar relacionada con el radio progenitor.

Analizando las propiedades espectrales y sus correlaciones con parámetros fotométricos, encuentro que SNs con velocidades más altas son más brillantes, tienen seudo-anchos equivalentes más pequeños, tasas de declive más rápidas, duraciones más cortas en la fase opticamente gruesa y en la meseta y masas de niquel más altas. Relacionando estos parámetros con las propiedades físicas de la explosión y del progenitor, especulo que la duración de la meseta está relacionado con la masa de la envoltura de hidrógeno, la tasa de declive en la curva de luz está relacionada con el radio del progenitor, y las velocidades de expansión del material expulsado con la energía de la explosión.

Abstract

The basis of this thesis is the analysis of optical wavelength spectroscopy of type II supernovae (SNe II) and their correlations with photometric parameters. This analysis involves characterising the diversity of the spectral evolution of SNe II, and using this characterisation to further understand the physical mechanisms behind SNe II. A key aim is to link the transient evolution to pre-explosion progenitor properties. To that purpose, I use 893 optical wavelength spectra of 123 SNe II obtained between 1986 and 2009, and ranging from between 3 and 363 days post explosion.

In order to consistently compare observed properties of SNe II, it is necessary to have a common epoch. For this, I estimate the explosion epochs using pre-explosion images and spectral matching technique, which have very good agreements. Concentrating on the dominant H_α P-Cygni profile, I find that SNe with less absorption component with respect to emission have faster declining light curves, shorter optically thick phase durations, higher ejecta velocities and are brighter at maximum. I suggest that the differences between fast declining (IIL) and plateau (IIP) SNe are related with the pre-explosion hydrogen envelope mass and that they do not come from different progenitor families.

Expanding the analysis to the full coverage of the spectra, I analyse the appearance of lines in SNe II and their time evolution with respect to differences in the ratio of absorption to emission (a/e) and H_α velocity at a particular epoch, the magnitude at maximum, the decline rate, and environment metallicity. I speculate that line evolution could indicate differences in temperatures and/or metallicity. I also find an extra absorption component on the blue side of H_α. I conclude that this component in early spectra (before 35 days) is associated with Si II λ6355, while in the plateau phase is related with high velocity (HV) features of hydrogen lines. These HV features could imply signs of interaction between the SNe ejecta and the red supergiant (RSG) wind, and could be used to constrain the nature of the circumstellar environment of SNe II. On the other hand, I speculate that the presence of Si II is related with larger progenitor radius.

Spectral properties are analysed and correlated with photometric parameters. I find that SNe with higher velocities are brighter, have smaller pseudo-equivalent widths, faster declining light curves, shorter optically thick duration phases and plateau durations, and higher Ni masses. I attempt to relate observable SNe parameters with physical properties of the explosion and progenitor. Thus, I speculate that the plateau duration is related with the hydrogen envelope mass at the moment of the explosion, the initial light-curve decline rate is related with the radius of the progenitor, and the expansion ejecta velocities with the explosion energy.

A los que están... A los que estuvieron

Agradecimientos

En primer lugar quiero agradecer a mis supervisores, Joe Anderson y Mario Hamuy. A Joe le doy infinitas gracias por su apoyo incondicional, paciencia, entusiasmo y toda la experiencia científica que me transmitió durante largas horas de discusiones; a Mario por haberme impulsado a seguir siempre adelante, por darme la oportunidad de trabajar en su grupo. A ambos agradezco la confianza que depositaron en mi. También agradezco a los profesores de Calán por haberme ayudado a crecer científicamente, especialmente a Paulina Lira por su paciencia y dedicación. A Luc Dessart por su buena disposición a la hora de responder mis múltiples inquietudes y a Christophe Martayan por su confianza. Agradezco al grupo de supernovas: Thomas de Jaeger, Lluis Galbany, Hanin Kuncarayakti, Francisco Forster, Giuliano Pignata, y con mucha más gratitud a Santiago González, por haberme apoyado cuando más lo necesitaba. También le doy las gracias a mis compañeros de generación (Fernando Becerra, Fernando Olguín, Elise Servajean, Paula López, Jesús Umanzor, Nicola Astudillo) por haberme incluido en su grupo y ayudado a adaptarme con más facilidad. A Lara y Lucerito, compañeras de oficina y de aventuras. A mis compañeros de oficina, de almuerzo, de la van, etc... Julián Mejia, Regis Cartier, Paula Sánchez, Ismael Botti, Angel Rincón, Celia Verdugo, Felipe Santana por estar dispuestos a invertir su tiempo en ocio. A los funcionarios (Lucho Lalo, Natalie, la Señora Nelly, Marta, Alejandro, José, Rogelio, Alejandro, doña Mary, don Jorge y don Richard) por su amabilidad y cariño. También quiero agradecer a los compañeros y amigos de la ESO y de la Universidad: Kora, Julio, Jesús, Daniel, Liz, Tomek, Paul, Elyar, Pascale, Amal, Gaby, Francisco.

Quiero agredecer profundamente a Alejo por haberme acompañado en los momentos mas difíciles, por haberme impulsado a seguir mi sueño. A mi familia y amigos por apoyarme desde la distancia y por creer en mi.

Agradezco a CONICYT-AGCI por apoyarme a través del Programa Nacional de Becas de Postgrado para extranjeros. Al Centro de Excelencia en Astrofísica y Tecnologías Afines (CATA), a la Iniciativa Científica Milenio por apoyarme a través del Núcleo Milenio de Supernovas (MCSS) y del Instituto Milenio de Astrofísica (MAS), y al Observatorio Europeo Austral (ESO).

Contents

List of Figures

List of Tables

Chapter 1

Introduction

1.1 Supernova explosions

The word supernovae was introduced by Baade & Zwicky in 1934, to refer to a bright "new" star in the sky. However, the first remarks on such "new stars" comes from the second century A.D. by Chinese astronomers. They reported the appearance of a new star in the sky, which after than certain length of time, faded away. One of the most famous such events is the Crab nebula. This object was observed in AD 1054, with a maximum apparent magnitude of -4, in the constellation Taurus. It was visible for more than six months, outshining even many bright stars. Later, in A.D. 1572 and 1604, two "new stars" were discovered. The first one by Tycho Brahe in the constellation Cassiopeia, and the second one by Johannes Kepler only a few years before the invention of the telescope. These days, the rate of discovery of "new stars", i.e. supernovae, has significantly increased due to modern telescopes and detectors, together with systematic searches.

It is now known that Supernovae (SNe hereafter) are the explosions of stars ending their lives and that they represent some of the most energetic events that occur in the Universe. During the explosion $\sim 10^{51}$ ergs (or 1 foe) of energy is released, and the interstellar medium is enriched by heavy elements synthesized by the star during its evolution and explosion. Their peak luminosities can be comparable to the total light of their host-galaxies ($\sim 10^{10}$ $L_\odot$). They play a very important role in stellar evolution and in the chemical evolution of galaxies, and they are also powerful cosmological tools, most famously as distance indicators.

1.2 Supernovae classification

The initial SN classification was achieved by Minkowski (1941) based on spectroscopic differences: SNe with broad emission features and no clear signs of hydrogen in the spectrum were classified as Type I, while SNe with strong broad Balmer lines, Type II. Later, new SN types were introduced and in the '80s a classification scheme was established. Thus, the Type I class was sub-classified into three classes according to the presence or absent of different lines:

- **SNe Ia:** the spectra show Si II lines.
- **SNe Ib:** spectra display He I lines but absent of Si II.
- **SNe Ic:** spectra do not show neither Si II nor He I.

Similarly, the Type II was also divided into subgroups based on spectral features (Filippenko et al., 1993, Schlegel, 1990, Filippenko, 1997), and in some cases on photometric behaviour (Barbon et al., 1979) as follows:

- **SNe IIb:** the spectra show strong hydrogen lines during the first weeks since explosion. Later, the Balmer lines disappear and He I lines emerge.
- **SNe IIn:** show narrow emission lines in their spectra, attributed to interaction with circumstellar medium (CSM).
- **SNe IIP:** the light curve shows a "plateau" or quasi-constant luminosity for a few months.
- **SNe IIL:** the light curve shows a linear decline of luminosity after maximum.

However, recent studies (e.g. Anderson et al., 2014b, Sanders et al., 2014, Valenti et al., 2016) have shown that the last two classes (IIL and IIP) display a continuum in their light curve properties and it is not possible to divide them into two different groups. Figure 1.1 shows the spectra of the SN types at maximum, three weeks and one year since maximum.

Although the initial classification was done according the spectral information, SNe can be classified according to their explosion mechanism into two groups: core-collapse SNe (CC-SNe) from massive stars, and thermonuclear SNe from white dwarf (WD) stars in binary systems (see Figure 1.2). The accepted picture is that young massive stars with $M_{ZAMS} > 8$ $M_\odot$ collapse when their iron core reaches the Chandrasekhar mass near 1.4 $M_\odot$ (Smartt, 2009). At this point the pressure provided by the electrons becomes insufficient to balance gravity and the core becomes condemned to gravitational collapse. This is followed by the explosion of the star, presumably due to heat deposited by the neutrinos created in the center. This process leads to the formation of a neutron star or a black hole, which depends on the initial mass of the star and the amount of material falling to the core in the collapse. Belonging to the CC-SNe class are SNe II, Ib/c, IIn, and

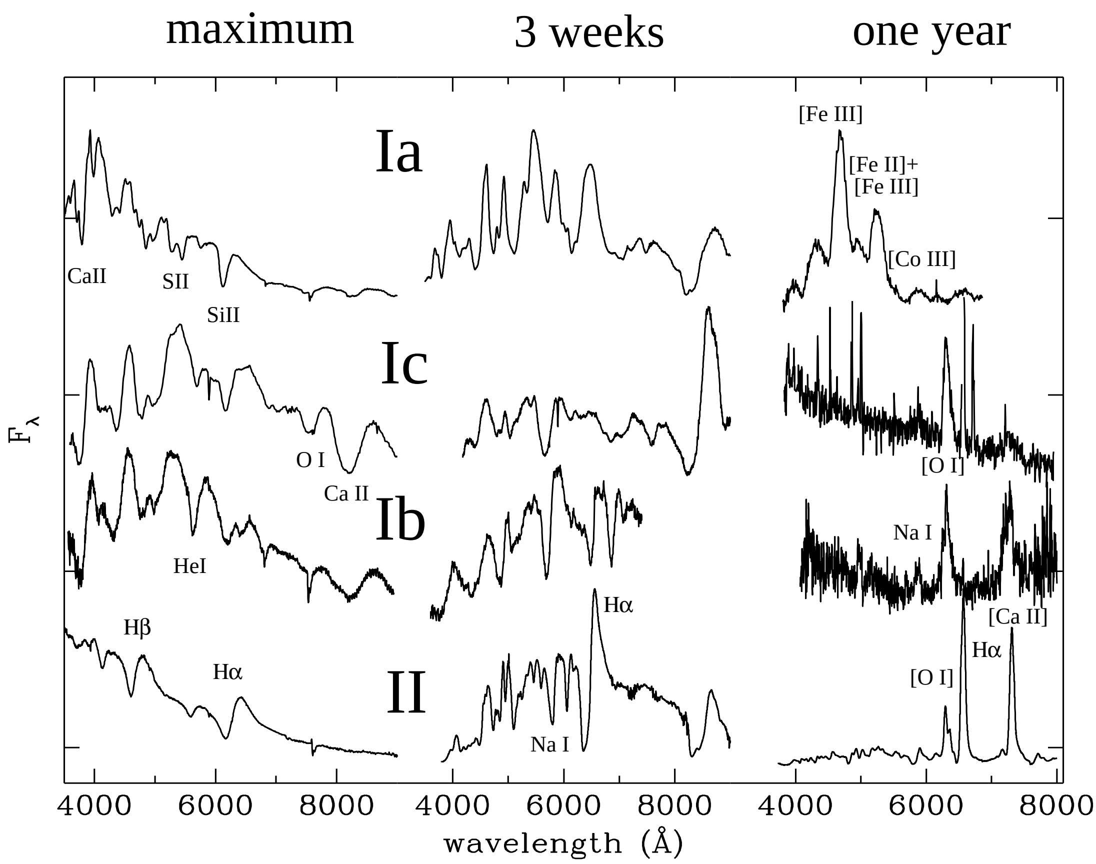

Figure 1.1 The spectra of the main SN types at maximum, three weeks and one year after maximum (from Turatto 2003).

IIb. Their spectral differences are possibly due to the amount of mass loss during the life of the star. In this scenario, SNe II keep a significant fraction of H at the moment of the explosion, while SNe Ib/c lose their H envelope due to strong stellar winds or transfer to a binary companion (Podsiadlowski et al., 1992, Nomoto et al., 1996, Yoon et al., 2010).

On the other hand, Type Ia SNe come from the thermonuclear burning of a carbon-oxygen white dwarf either triggered by the interaction with the companion in a close binary system (Hoyle and Fowler, 1960) or by direct collisions of white dwarfs (Raskin et al., 2009). In the leading scenario of a close binary system, the nature of the explosion and companion star is still debated. Two of the most popular models considered are the single degenerate (SD; Nomoto 1982, Iben and Tutukov 1984) and the double degenerate (DD) scenarios (Iben and Tutukov, 1984, Webbink, 1984). In the former, a white dwarf accretes matter from the companion, which can be a subgiant or main-sequence star, while in the latter the SN is produced by the merging of two white dwarfs. SNe Ia are thought to explode near the Chandrasekhar mass, although recent simulations of sub-Chandrasekhar mass explosions have been successful for both

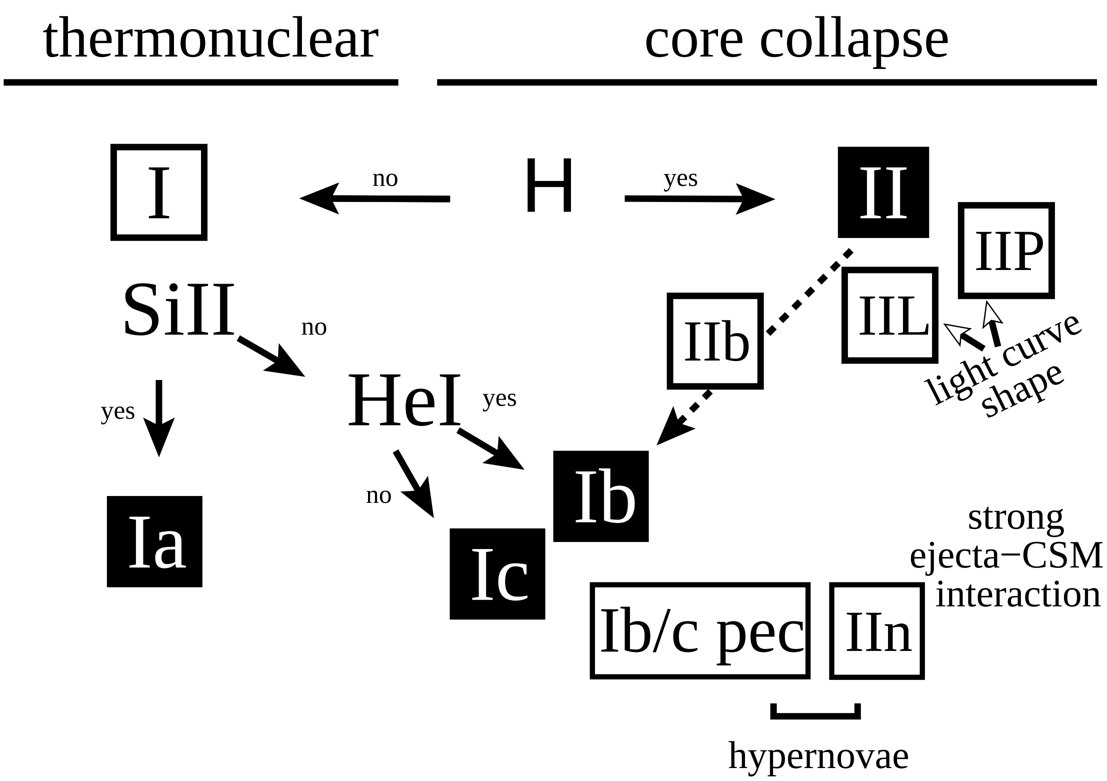

Figure 1.2 The classical classification scheme of supernovae (from Turatto 2003).

scenarios (Sim et al., 2012, Kromer et al., 2010, Pakmor et al., 2012). Unlike CC-SNe, in the thermonuclear explosion the entire star is disrupted and the iron and intermediate-mass elements produced in the explosion are expelled at great velocities to the interstellar medium leaving no compact object at its center.

1.3 General properties of type II supernovae

During the evolution and explosion of the stars, chemical elements heavier than boron are produced and are driven out through the interstellar medium thanks to the enormous kinetic energies liberated during stellar deaths (Smartt et al., 2009). At the beginning, the SN luminosity increases due to the diffusion of internal energy, and the light curve reaches the optical maximum. In this stage, the ejecta is dense and opaque, however with the expansion of the ejecta, the density and temperature decrease and the photosphere recedes. At this moment, the ionized hydrogen matter begins to recombine. The opacity goes down and the residual trapped internal energy can be released. When the recombination phase ends, the envelope is transparent and the light curve settles onto the exponential tail, during which the radioactive decay of ^{56}Co represents the main energy source (Arnett, 1979, Barbon et al., 1984).

Generally, SN II evolution is studied in two phases: photospheric and nebular. In the photospheric phase, the SNe II spectra exhibit the Balmer lines, Ca II, Na I D, and iron group lines. With time, the photosphere becomes transparent and the nebular phase starts. At this moment, the inner regions are exposed and the spectra are dominated by forbidden lines. For details of the spectral lines see Appendix A.

1.4 Goals of this dissertation

SNe II are the most frequent stellar explosions in nature (Li et al., 2011) and they have a significant role in the chemical evolution of galaxies. They are produced by the final explosion of massive (> 8 $M_\odot$) stars, which retain a significant part of their hydrogen envelope at the time of the explosion, and hence their spectra show prominent Balmer lines. The direct identification of Red Supergiant (RSG) stars on pre-explosion images (e.g. Van Dyk et al., 2003, Smartt et al., 2004, Maund and Smartt, 2005, Smartt et al., 2009, Smartt, 2015) suggests that SNe II arise from this stellar type. SNe II display a huge diversity both spectroscopic and photometric. However it is not clear how this diversity is associated to progenitor and explosion properties.

The goal of this thesis is to do an analysis of optical wavelength spectroscopy of SNe II and their correlations with photometric parameters. This analysis involves characterising the diversity of the spectral evolution of SNe II, and using this characterisation to further understand the physical mechanisms behind SNe II. A key aim is to link the transient evolution to pre-explosion progenitor properties.

The thesis is organized as follows. In Chapter 2, I present the study of the H_α P-Cygni profile diversity for 52 SNe II at a common epoch (t_{tran}). Chapter 2 has been published in the The Astrophysical Journal Letters as Gutiérrez et al. 2014, ApJL, 786, 15. In Chapter 3, I present the characterization of the spectral diversity of SNe II. Chapter 4 shows the correlations between spectral and photometric parameters of SNe II at 50 days since explosion. Chapter 3 and Chapter 4 will each be submitted separately in The Astrophysical Journal. Finally, in Chapter 5, I summarize the main conclusions of this work.

Chapter 2

H_α spectral diversity of type II supernovae: correlations with photometric properties

*This chapter is published in The Astrophysical Journal Letters as Gutiérrez, C. P.; Anderson, J. P.; Hamuy, M.; González-Gaitán, S.; Folatelli, G.; Morrell, N. I.; Stritzinger, M. D.; Phillips, M. M.; McCarthy, P.; Suntzeff, N. B. and Thomas-Osip, J. **2014**, ApJL, 786, 15*

2.1 Abstract

We present a spectroscopic analysis of the H_α profiles of hydrogen-rich type II supernovae. A total of 58 type II supernovae having well sampled optical light curves and spectral sequences were analyzed. Concentrating on the H_α P-Cygni profile we measure its velocity from the FWHM of emission and the ratio of absorption to emission (a/e) at the epoch of transition between initial and plateau decline phases, and search for correlations between these spectral parameters and photometric properties of the V-band light curves. Testing the strength of various correlations we find that a/e appears to be the dominant spectral parameter in terms of describing the diversity in our measured supernova properties. It is found that supernovae with smaller a/e have higher H_α velocities, more rapidly declining light curves from maximum, during the plateau and radioactive tail phase, are brighter at maximum light and have shorter optically thick phase durations. We discuss possible explanations of these results in terms of physical properties of type II supernovae, speculating that the most likely parameters which influence the morphologies of H_α profiles are the mass and density profile of the hydrogen envelope, together with

additional emission components due to circumstellar interaction.

2.2 Introduction

Type II Supernovae (SNe II) are produced by the final explosion of massive (> 8 $M_\odot$) stars. They retain a significant part of their hydrogen envelope at the time of the explosion, and hence their spectra show strong Balmer lines. Studies of the variety of SNe II have relied on photometric analysis, cataloging this group in two sub-classes according to the shape of the light curve: SNe with a plateau (quasi-constant luminosity for a period of a few months) are classified as SNe IIP, while SNe with steeper declining linear light curves as SNe IIL (Barbon et al., 1979). However, despite the role played by SNe II in stellar evolution, the impact on their environments and their importance as standardized candles, an overall picture describing the physics which underpins their diversity is lacking. It has been suggested that SNe IIL are produced by progenitors which explode with smaller mass H envelopes, which then lead to SNe with more linearly declining light curves and shorter or non-existent 'plateaus' (Popov, 1993). Indeed, this was argued to be the case for the prototype SN IIL 1979C (Branch et al., 1981). This would imply that SNe IIL progenitors suffer from a higher level of mass-loss than their IIP counterparts. In addition, a number of SNe IIL have shown evidence for circumstellar (CSM) interaction at late times (e.g. SN 1986E, Cappellaro et al. 1995b; SN 1979C, Milisavljevic et al. 2009), which has been interpreted as evidence of interaction of the ejecta with the pre-supernova CSM (see e.g. Sahu et al. 2006, Inserra et al. 2013). However, a number of authors have also claimed evidence for signs of CSM interaction in SNe IIP (e.g. SN 1999em, Pooley et al. 2002; SN 2004et, Kotak et al. 2009; SN 2007od, Inserra et al. 2011, Andrews et al. 2010; SN 2009bw, Inserra et al. 2012).

In recent years many individual studies have been published focusing on particular properties of individual SNe, but few statistical studies where the spectral and photometric properties have been directly related are available. Patat et al. (1994) found correlations and anti-correlations between the maximum B-band magnitude (M^B_{max}), the color at maximum ($(B-V)_{max}$) and the ratio of absorption to emission (e/a) in H_α, concluding that SNe IIL have shallower P-Cygni profiles (larger e/a values) than SNe IIP. Hamuy and Pinto (2002) analysed 17 SNe IIP and found that SNe with brighter plateaus have higher expansion velocities. Similar results were found by Pastorello et al. (2004) with four SNe II, who concluded that low luminosity SNe have narrow spectral lines indicating low expansion velocities. Hamuy (2003) used observations together with the analytical models of Litvinova and Nadezhin (1983, 1985) to derive physical SN IIP properties. He found that more massive progenitors produce more energetic explosions and in turn produce more nickel. These results were confirmed by Pastorello et al. (2003) with a heterogeneous group of SNe II that share a very wide range of physical properties.

Despite the above results, it is currently unclear whether underlying spectral and photometric relations exist for the whole ensemble of SN II events. Therefore, here we attempt to remedy this situation by presenting an initial statistical analysis of some spectroscopic and photometric properties of a large sample of SNe II.

In this chapter we present results showing the diversity of H_α P-Cygni profiles, and relations between spectral and photometric parameters for a sample of 58 SNe. The chapter is organized as follows. In § 2.3 we outline our SN sample and we define the measurements, then in § 2.4 we present the results. In § 2.5 possible physical explanations of those results are discussed, and finally in § 2.6 we list our conclusions. We note that a detailed analysis of the V-band light curve properties of the currently analyzed sample of SN II is being presented in (Anderson et al. 2014b, hereafter A14).

2.3 SN II data and measurements

The sample of SNe II employed in this study was obtained by the Carnegie Supernova Project (CSP, Hamuy et al. 2006) between 2004 and 2009 plus previous campaings: the Calan/Tololo Supernova Survey (CT), the Cerro Tololo SN program, the Supernova Optical and Infrared Survey (SOIRS) and the Carnegie Type II Supernova Survey (CATS). The full spectroscopic sample will be published in an upcoming paper. Data reductions were performed with IRAF[1] using the standard routines (bias subtracted, flat-field correction, 1-D extraction and wavelength correction). Detailed discussion of spectroscopic observations and reductions for CSP was first presented in Hamuy et al. (2006), then outlined further in Folatelli et al. (2013). These are also applicable to previous data. From this database we selected a sub-sample of events with sufficient data to measure our spectral and photometric parameters. SN IIn and SN IIb were not analysed in this work.

SNe II show a large diversity in their spectra. As the dominant spectral feature is the H_α P-cygni profile, for this initial study we concentrate on this line's properties. The H_α line presents a diversity that can be derived from the shape and strength in the emission and absorption, and in the line width. Figure 1 shows the variety in SNe II H_α P-Cygni profiles, where the SNe are ordered in terms of an increasing ratio of absorption to emission (a/e) components (as defined below) around the transition time between

[1]IRAF is distributed by the National Optical Astronomy Observatories (NOAO), which are operated by the Association of Universities for Research in Astronomy (AURA), Inc., under cooperative agreement with the National Science Foundation.

initial and plateau decline phases. We see that the absorption is the component which changes most from one SN to another rather than the emission. There are SNe with little absorption (e.g. SN 2006ai, SN 2006Y), while there are others with boxy absorption profiles (e.g. SN 2003cx, SN 2007X). One can observe in Figure 1 that the first SNe show little absorption compared to emission. Gradually the SNe change to show more classic P-Cygni profiles with significant absorption components. A number of SNe show an extra absorption component on the blue side of H_α (e.g. SN 2003hn, SN 2007od, SN 2008aw).

To analyze the SNe spectra within our sample we define two measurements: **(1)** the expansion velocity in H_α via the FWHM of the emission, and **(2)** the ratio of equivalent widths of absorption to emission (a/e) components of H_α. This ratio was initially proposed by Patat et al. (1994) as the flux ratio of the emission to absorption. However, we choose a/e because in a few SNe H_α shows an extremely weak absorption component. In order to relate spectral and light curve properties we use the V-band photometric properties as defined by A14: s_1: initial decline from the maximum (magnitudes $100d^{-1}$), s_2: 'plateau' decline rate (magnitudes $100d^{-1}$), s_3: radioactive tail decline (magnitudes $100d^{-1}$), M_{max}: magnitude at V-band maximum, and $OPTd$: optically thick phase duration (days): time from the explosion epoch through to the end of the plateau phase. We define a common epoch in order to measure spectral properties, which we identified in the light curves: the B-band transition time (t_{tran}). This common epoch is defined as the transition between s_1 and s_2 determined by chi-square minimization. We interpolate all the spectral measurements to this epoch. These parameters are all labeled in the light-curve parameter schematic presented in Figure 2 (left).

To estimate SN ejecta expansion velocities through H_α the minimum flux of the absorption component of P-Cygni line profile is commonly used. However, a few SNe in this sample present an extremely weak absorption component, complicating this method. Therefore, we employ the FWHM of emission line for velocity estimations. To verify the concordance between these methods we measure velocities from the minima of absorption and the FWHM of the emission in H_α in SNe with a well defined absorption, finding consistent results. The ratio of absorption to emission (a/e) in H_α was obtained by measuring the equivalent widths (EW) of each component. Examples of these measurements are shown in Figure 2 (right). The top panel shows a normal H_α P-Cygni profile, i.e., a profile with well defined absorption and emission components, while the bottom panel shows a peculiar profile with an extra absorption component on the blue side. Similar features were identified by Leonard et al. (2001), Leonard et al. (2002b) and Leonard et al. (2002a) in SN 1999em as high velocity (HV) features, while in the case of SN 2005cs the line was identified as Si II $\lambda6355$ absorption (Pastorello et al., 2006). This peculiar structure complicates measurements of the EW of absorption, because it is hard

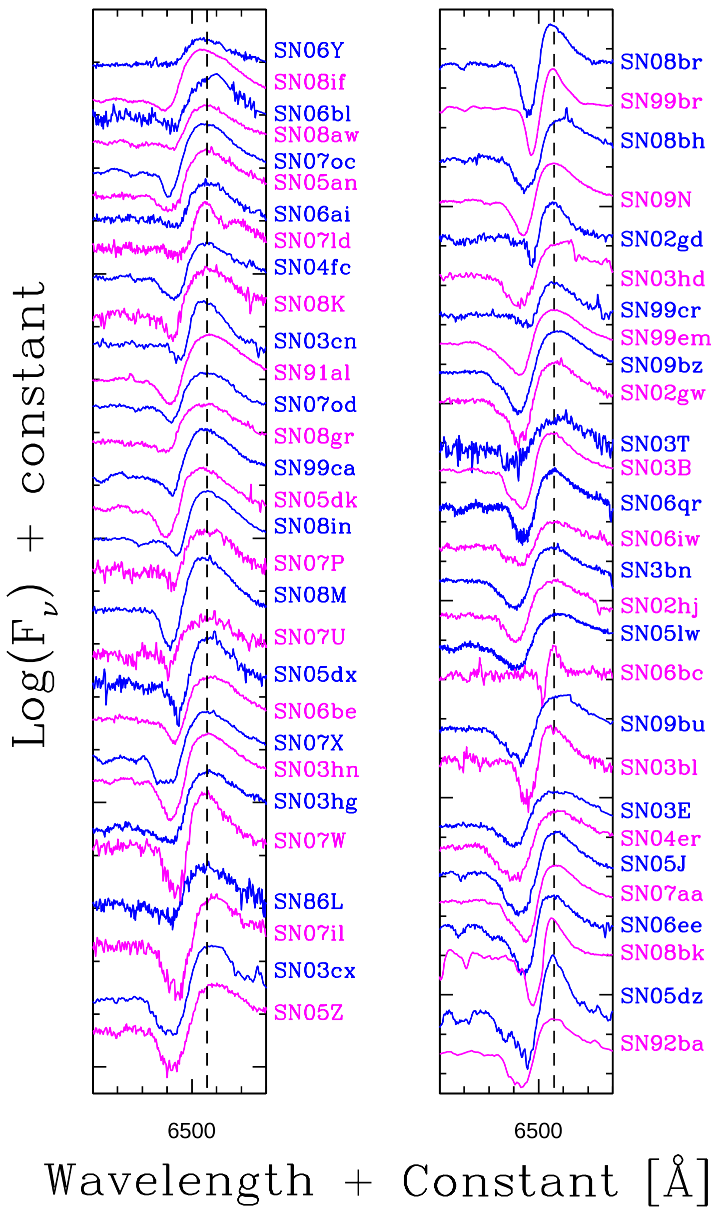

Figure 2.1 Variety in SN II H_α P-Cygni profiles ordered in terms of increasing a/e starting top left, finishing bottom right. The Host galaxy features were removed and the spectra are shifted to be centered on the peak of H_α emission. The epoch of the spectra shown are those in closest time proximity to t_{tran}. In general the difference between epochs of the spectra and t_{tran} is within ±10 days.

to objectively define the continuum. Therefore, we simply trace a straight line along the absorption feature to mimic the continuum flux, which can be seen in Figure 2 (right). All spectral measurements were performed with IRAF using the *splot* package. The errors for the H_α velocity and a/e are mainly dominated by how the continuum is defined. Errors

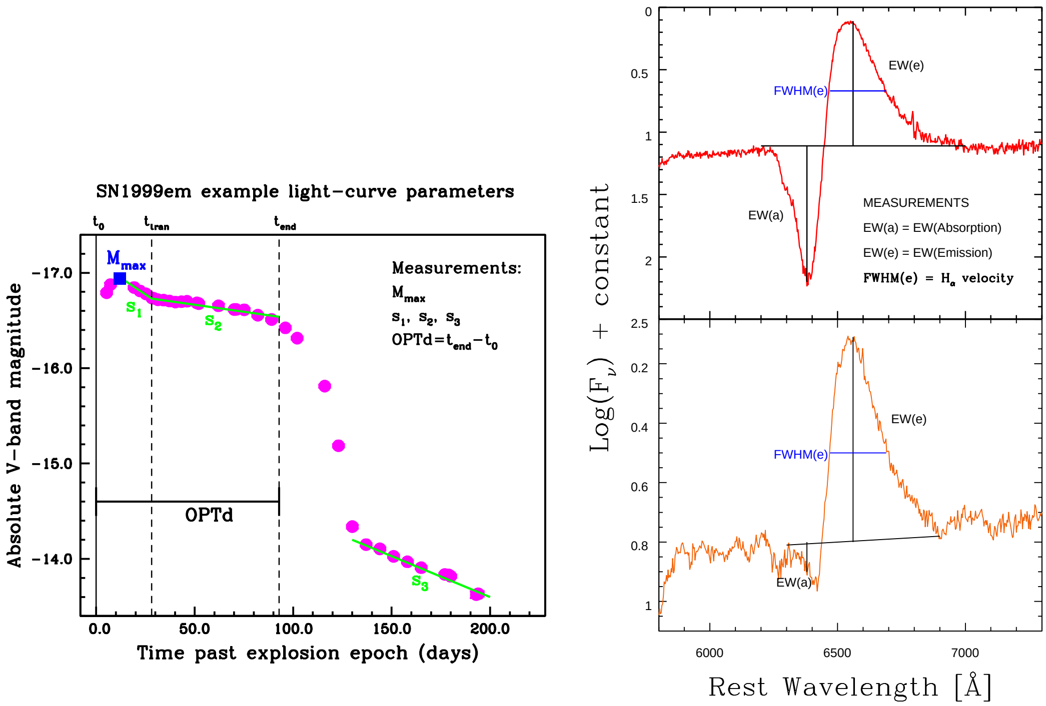

Figure 2.2 *Left:* An example of the light-curve parameters measured for each SN within the sample in the V-band. Observed absolute magnitude at peak, M_{max} is shown in blue, as applied to the sample data points (magenta) of SN 1999em. The positions of the three measured slopes; s_1, s_2, and s_3 are shown in green. The optically thick phase duration, $OPTd$ is indicated in black. Three time epochs are labeled: t_0, the explosion epoch; t_{tran}, the transition from s_1 to s_2; and t_{end}, the end of the optically thick phase. *Right:* Examples of spectral measurements. Top: SN 2009bz shows a normal H_α P-Cygni profile with absorption and emission components well defined. Bottom: SN 2008aw shows a peculiar profile with a extra component on the blue side. In both plots, the blue line represents the FWHM of emission, which is used for the velocities values, and black horizontal line defines the continuum level used to measure the EW of emission and absorption.

were obtained by measuring many times the FWHM and the EW, respectively, changing the trace of the continuum. Using these multiple measurements we calculate a mean and take the standard deviation to be the error on that measurement.

2.4 Results

In Table 2.1 we list the measured spectral and photometric parameters: H_α velocity, a/e, s_1, s_2, s_3, M_{max} and $OPTd$ for each SN, together with the host galaxy and the heliocentric radial velocity and t_{tran}. We searched for correlations between all seven of our defined parameters against each other. Using the Pearson correlation test, a/e was observed to be the dominant measured spectral parameter as it has the highest correlation with all other parameters. The photometric parameter s_1 has the highest mean correlation, however it shows no correlation with the H_α velocity. Table 2.2 shows the strength of the correlations between all our parameters, plus the number of events (within each correlation), and the probability of finding such a correction by chance. The light curve parameters plus the H_α velocity are plotted versus a/e in Figure 3. The plot shows that SNe with smaller a/e have higher H_α velocities, more rapidly declining light curves after maximum, both in the 'plateau' and radioactive tail phases, are brighter and have shorter $OPTd$ values. SNe with higher a/e show opposite behavior. Given that $OPTd$ and s_3 are most likely related to the envelope/ejecta mass (see A14 for detailed discussion), this would appear to imply that a/e is also related to the mass retained by the progenitor before explosion. Indeed, this further points to SNe historically classified as IIL (high s_2) having smaller mass envelopes at the epoch of explosion than their IIP (low s_2) counterparts. Moreover, we see a continuum of events in terms of spectral diversity, thus suggesting a possible continuum in pre-SN envelope masses.

2.5 Discussion

We have presented and analysed the H_α spectral diversity in 58 SNe II and their correlations with photometric parameters. Analyzing the sample we see a variety in the H_α P-Cygni profiles which can be derived from the shape and strength in the emission and absorption, and in the line width. Patat et al. (1994) found that M^B_{max} and $(B-V)_{max}$ correlate with e/a in H_α, concluding that SNe IIL have larger e/a values (i.e. small a/e values). While in our sample we have not made distinctive IIP-IIL classification, our results are consistent with these of Patat et al. (1994), which show that SNe with high s_2 values (faster declining light curves) have small a/e values and are more luminous.

Arcavi et al. (2012) identified a subdivision of SNe II (based on 21 events in the R-band) suggesting that SNe IIL and SNe IIP are not members of one continuous class and may result from different physical progenitor systems. However, A14 with a bigger sample (116 events in the V-band) suggest an observational continuum of events which may be driven by differences of envelope mass at the epoch of explosion, a parameter which is most directly constrained in A14 through observations of the optically thick phase duration ($OPTd$) and the decline rate during the radioactive tail (s_3). This conclusion of an observational continuum is also supported by the spectral analysis presented in this paper (see Figure 3), where differences in the spectral parameters (especially a/e) may also be explained by changes in the hydrogen envelope mass retained.

Schlegel (1996) discussed possible explanations for the behavior of the H_α P-Cygni

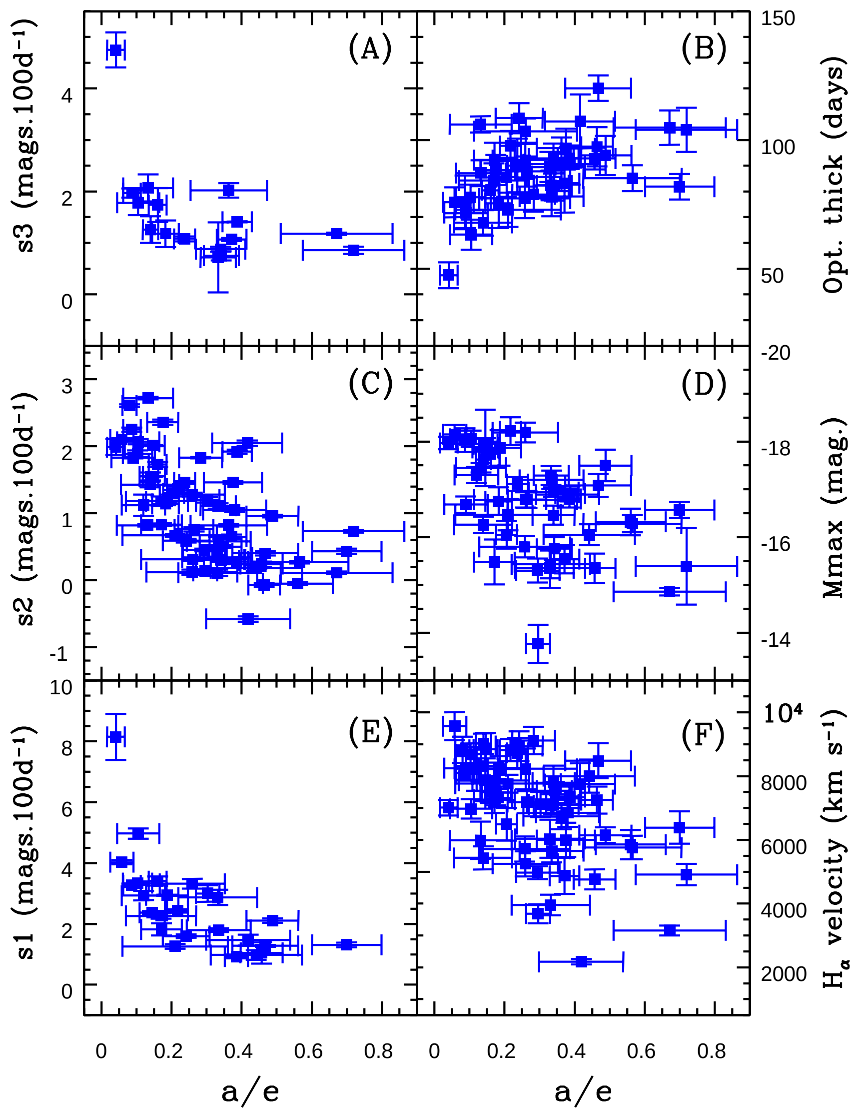

Figure 2.3 Relations between a/e, H_α velocity, s_1, s_2, s_3 and M_{max}. *Panel A:* a/e vs. s_3. *Panel B:* a/e vs. Optically thick phase. *Panel C:* a/e vs. s_2. *Panel D:* a/e vs. M_{max}. *Panel E:* a/e vs. s_1. *Panel F:* a/e vs. H_α velocity.

profile with the most likely being: **(1)** extra emission fills in the absorption component (as can be seen in SN 2008aw, Figure 2, bottom); **(2)** the envelope mass is low; and **(3)** a steep density gradient in the hydrogen envelope. The first explanation invokes scattering of emission off either CSM or the outer envelope (in the case of very extended envelope). The second explanation is described in a low-mass envelope, where there is less absorbing material, so little P-Cygni absorption component will be formed. The third explanation argues that a very steep density gradient implies less absorbing material at high velocities, and so does not produce a well defined P-Cygni profile. Although these considerations could explain the diversity found in our sample, numerous studies discuss other explanations based on the complex P-Cygni line profiles. Baron et al. (2000) granted the term 'complicated P-Cygni profile' to explain the double P-Cygni absorption found in Balmer Series and He I λ5876 in SN 1999em, concluding that these absorption features arise in two velocities regions in the expanding ejecta of the SN at different velocities. Pooley et al. (2002) argue that this extra component might be the signature of weak interaction with a low density CSM, while Chugai et al. (2007) attributes these features to ejecta wind interactions. In conclusion, the change in H_α P-Cygni profile (a/e and FWHM of emission) is most likely related to two parameters: changes in the envelope properties (i.e. its mass and density profile) and the degree of CSM interaction. Although the possible explanations for the behavior of the H_α P-Cygni profile have been exposed, these extra components could be attributed to HV H I features or, absorption lines of other ions (Si II). This issue will be further explored after a full spectral analysis. This will determine if similar features are also present in the blue side of He I λ5876 and H_β.

2.6 Conclusions

We have presented an initial analysis of the spectral diversity H_α of SNe II and how this relates to light curve properties. It has been found that while much diversity and peculiarities exist, spectral and photometric properties do appear to be correlated which can be linked to pre-SN properties. We finally list our main conclusions:

- a/e is an important parameter describing the spectral diversity of SNe II.
- SNe with low a/e values appear to have high H_α velocities and decline rates, are brighter and have a smaller $OPTd$ values.
- While any definitive spectral distinction between IIP and IIL is not clear, SNe with higher s_2 values (i.e. more 'linear' SNe) have smaller a/e values, have higher H_α velocities, and are more luminosity.
- We speculate that the envelope mass retained before explosion and the density gradient play a very important role to determine the differences of H_α P-Cygni profile.
- CSM interaction could also be a cause of the change in the P-Cygni profiles, suggesting that faster declining SNe have more intense interactions

Table 2.1 SNe II spectral and photometric parameters at t_{tran}

SN	Host galaxy	Recession velocity (km s^{-1})	t_{tran} (MJD)	M$_{max}$ (mag)	s_1 (mag 100d^{-1})	s_2 (mag 100d^{-1})	s_3 (mag 100d^{-1})	$Optd$ (days)	a/e	H_α velocity (km s^{-1})
1986L	NGC 1559	1305	46747.4 ± 0.5	−18.19 ± 0.2	3.32 ± 0.16	1.28 ± 0.03	···	92.24 ± 6.71	0.21 ± 0.09	6354 ± 392
1991al	LEDA 140858	4575	48478.1 ± 1.3	−17.62 ± 0.2	···	1.55 ± 0.06	1.26 ± 0.26	···	0.28 ± 0.02	7771 ± 320
1992ba	NGC 2082	1185	48926.3 ± 1.0	−15.39 ± 0.8	···	0.73 ± 0.02	0.86 ± 0.07	103.97 ± 8.54	0.68 ± 0.14	4439 ± 334
1999br	NGC 4900	960	51308.4 ± 0.5	−13.77 ± 0.4	···	0.14 ± 0.02	···	···	0.61 ± 0.03	3566 ± 297
1999cr	ESO 576-G034	6069	51273.6 ± 0.7	−17.20 ± 0.2	1.80 ± 0.06	0.58 ± 0.06	···	78.06 ± 7.62	0.19 ± 0.09	5728 ± 357
1999em	NGC 1637	717	51509.7 ± 0.7	−16.94 ± 0.1	···	0.31 ± 0.02	0.88 ± 0.05	92.86 ± 5.83	0.57 ± 0.07	5915 ± 306
2002gd	NGC 7537	2676	52581.6 ± 0.8	−15.43 ± 0.3	2.87 ± 0.25	0.11 ± 0.05	···	···	0.19 ± 0.11	4023 ± 320
2002gw	NGC 922	3084	52583.1 ± 1.0	−15.76 ± 0.2	···	0.30 ± 0.03	0.75 ± 0.09	82.33 ± 5.83	0.46 ± 0.05	6217 ± 274
2002hj	NPM1G +04.0097	7080	52595.8 ± 3.1	−16.91 ± 0.2	···	1.92 ± 0.03	1.41 ± 0.01	90.24 ± 7.62	0.38 ± 0.04	6857 ± 334
2003B	NGC 1097	1272	52666.2 ± 1.9	−15.54 ± 0.3	···	0.65 ± 0.03	1.07 ± 0.03	83.19 ± 11.4	0.40 ± 0.04	4251 ± 658
2003E	MCG -4-12-004	4470	52661.5 ± 3.5	···	···	−0.07 ± 0.03	···	97.42 ± 7.62	0.40 ± 0.04	5028 ± 424
2003T	UGC 4864	8373	52686.8 ± 1.5	···	···	0.82 ± 0.02	2.02 ± 0.14	90.59 ± 10.44	0.55 ± 0.11	7360 ± 411
2003bl	NGC 5374	4377	52736.7 ± 1.2	−15.35 ± 0.3	1.05 ± 0.35	0.24 ± 0.04	···	92.81 ± 4.24	0.47 ± 0.06	6596 ± 311
2003bn	2MASX J10023529	3831	52729.7 ± 8.6	−16.80 ± 0.2	0.93 ± 0.06	0.28 ± 0.04	···	92.97 ± 4.24	0.60 ± 0.03	6121 ± 352
2003cn	IC 849	5433	52743.6 ± 1.7	−16.26 ± 0.2	···	1.43 ± 0.04	···	67.80 ± 5.00	0.22 ± 0.08	5074 ± 361
2003cx	NEAT J135706.53	11100	52754.7 ± 4.2	−16.79 ± 0.2	···	0.76 ± 0.03	···	87.82 ± 5.83	0.29 ± 0.05	7314 ± 343
2003hd	MCG -04-05-010	11850	52886.9 ± 1.6	−17.29 ± 0.2	···	1.11 ± 0.04	0.72 ± 0.68	82.39 ± 5.83	0.76 ± 0.05	4800 ± 350
2003hg	NGC 7771	4281	52898.3 ± 3.3	···	1.60 ± 0.06	0.59 ± 0.03	···	108.50 ± 5.83	0.38 ± 0.07	7360 ± 466
2003hn	NGC 1448	1170	52900.9 ± 3.9	−17.11 ± 0.1	···	1.46 ± 0.02	1.08 ± 0.05	90.10 ± 10.44	0.29 ± 0.03	7268 ± 375
2004er	MCG -01-7-24	4411	53319.3 ± 0.4	−17.08 ± 0.2	1.28 ± 0.03	0.40 ± 0.03	···	120.15 ± 5.00	0.56 ± 0.09	7680 ± 553
2004fc	NGC 701	1831	53335.7 ± 0.4	···	···	0.82 ± 0.02	···	106.06 ± 3.16	0.37 ± 0.09	5440 ± 585
2005an	SO 506-G11	3206	53466.1 ± 0.3	···	3.34 ± 0.06	1.89 ± 0.05	···	77.71 ± 5.00	0.17 ± 0.04	8548 ± 343
2005dk	C 4882	4708	53638.4 ± 0.9	···	2.26 ± 0.09	1.18 ± 0.07	···	84.22 ± 6.71	0.30 ± 0.10	7008 ± 567
2005dz	GC 12717	5696	53666.7 ± 0.8	−16.57 ± 0.2	1.31 ± 0.08	0.43 ± 0.04	···	81.86 ± 5.00	0.66 ± 0.10	5952 ± 512
2005J	NGC 4012	4183	53421.1 ± 0.4	−17.50 ± 0.3	2.11 ± 0.07	0.96 ± 0.02	···	94.03 ± 7.62	0.54 ± 0.07	6637 ± 245
2005Z	NGC 3363	5766	53432.9 ± 1.0	···	···	1.83 ± 0.01	···	78.84 ± 6.71	0.31 ± 0.06	8512 ± 430
2006Y	anon	10074	53794.7 ± 0.6	−17.97 ± 0.13	8.15 ± 0.76	1.99 ± 0.12	4.75 ± 0.34	47.49 ± 5.00	0.01 ± 0.02	7588 ± 244
2006ai	ESO 005- G 009	4571	53813.7 ± 1.0	−18.06 ± 0.2	4.97 ± 0.17	2.07 ± 0.04	1.78 ± 0.24	63.26 ± 5.83	0.08 ± 0.06	7291 ± 307
2006be	IC 4582	2145	53835.4 ± 0.5	−16.47 ± 0.3	1.26 ± 0.08	0.67 ± 0.02	···	72.89 ± 6.71	0.34 ± 0.15	6308 ± 283
2006ee	NGC 774	4620	53997.2 ± 1.3	−16.28 ± 0.2	···	0.27 ± 0.02	···	85.17 ± 5.00	0.49 ± 0.14	6034 ± 366
2006iw	2MASX J23211915	9226	54049.40 ± 1.9	−16.89 ± 0.1	···	1.05 ± 0.03	···	···	0.46 ± 0.09	6162 ± 448
2006qr	MCG -02-22-023	4350	54098.2 ± 1.2	···	···	1.46 ± 0.02	···	96.85 ± 7.62	0.55 ± 0.08	5440 ± 535
2007aa	NGC 4030	1465	54162.7 ± 0.8	−16.32 ± 0.3	···	−0.05 ± 0.02	···	···	0.70 ± 0.10	5028 ± 462
2007il	IC 1704	6454	54393.4 ± 2.0	−16.78 ± 0.2	···	0.31 ± 0.02	···	103.43 ± 5	0.38 ± 0.15	7634 ± 636
2007ld	SDSS J204929.40	8994	54402 ± 1.9	−17.30 ± 0.2	2.93 ± 0.15	1.12 ± 0.16	···	···	0.14 ± 0.06	8685 ± 690
2007oc	NGC 7418	1450	54419.8 ± 0.4	−16.68 ± 0.2	···	1.83 ± 0.01	···	71.62 ± 5.83	0.11 ± 0.06	7634 ± 386
2007od	UGC 12846	1734	54427.7 ± 0.3	−17.87 ± 0.8	2.37 ± 0.05	1.55 ± 0.04	···	···	0.17 ± 0.04	7314 ± 672
2007P	ESO 566-G36	12224	54154.9 ± 3.2	···	···	2.36 ± 0.04	···	88.33 ± 5.83	0.32 ± 0.04	6880 ± 410
2007U	ESO 552-65	7791	54168.8 ± 1.7	−17.87 ± 0.4	2.94 ± 0.02	1.18 ± 0.01	···	···	0.27 ± 0.06	6994 ± 407
2007W	NGC 5105	2902	54164.3 ± 1.0	−15.80 ± 0.2	···	0.12 ± 0.04	···	77.29 ± 7.62	0.52 ± 0.13	4800 ± 392
2007X	ESO 385-G32	2837	54180.8 ± 0.3	−18.22 ± 0.3	2.43 ± 0.06	1.37 ± 0.03	···	97.71 ± 5.83	0.20 ± 0.03	8091 ± 346
2008aw	NGC 4939	3110	54563.8 ± 0.6	−18.03 ± 0.2	3.27 ± 0.06	2.25 ± 0.03	1.97 ± 0.09	75.83 ± 10.44	0.13 ± 0.02	7817 ± 398
2008bh	NGC 2642	4345	54593.0 ± 2.6	···	3.00 ± 0.27	1.20 ± 0.04	···	···	0.22 ± 0.03	6857 ± 397
2008bk	NGC 7793	227.	54602.3 ± 1.4	−14.86 ± 0.1	···	0.11 ± 0.02	1.18 ± 0.02	104.83 ± 6.71	0.65 ± 0.16	2925 ± 155
2008br	IC 2522	3019	54579.2 ± 1.6	−15.30 ± 0.2	···	0.45 ± 0.02	···	···	0.40 ± 0.06	4571 ± 205
2008gr	IC 1579	6831	54801.8 ± 0.9	−17.95 ± 0.1	···	2.01 ± 0.01	···	···	0.17 ± 0.03	8731 ± 521
2008if	MCG -01-24-10	3440	54850.0 ± 0.4	−18.15 ± 0.2	4.03 ± 0.07	2.10 ± 0.02	···	75.85 ± 5.83	0.08 ± 0.03	8685 ± 441
2008in	NGC 4303	1566	54851.5 ± 0.8	−15.48 ± 0.5	1.82 ± 0.20	0.83 ± 0.02	···	92.20 ± 6.71	0.23 ± 0.06	6903 ± 416
2008K	ESO 504-G5	7997	54513.0 ± 1.2	−17.45 ± 0.1	···	2.72 ± 0.02	2.07 ± 0.26	87.11 ± 5.00	0.16 ± 0.07	7954 ± 511
2008M	ESO 121-26	2267	54508.9 ± 0.6	−16.75 ± 0.3	···	1.14 ± 0.02	1.18 ± 0.26	75.34 ± 9.49	0.22 ± 0.04	6674 ± 290
2009bu	NGC 7408	3494	54940.1 ± 1.0	−16.05 ± 0.2	0.98 ± 0.16	0.18 ± 0.04	···	···	0.50 ± 0.13	5943 ± 516
2009N	NGC 4487	1034	54877.1 ± 0.5	−15.35 ± 0.4	···	0.34 ± 0.01	···	89.50 ± 5.83	0.41 ± 0.10	5348 ± 599

Measurements made of our sample of SNe as mentioned in section 2. The first three columns present the SNe name and the host galaxy information: Host galaxy name and their recession velocities. From column 4 to column 9 the photometric measurements: t_{tran} (in B-band), M_{max}, s_1, s_2, s_3, and $Optd$ (in V-band) are presented. In column 10 we present the a/e, followed by the H_α velocity.

Table 2.2 Pearson's values between all the parameters at t_{tran}

···	a/e	H_α vel.	s_1	s_2	s_3	M_{max}	Opt. thick
a/e	···	−0.51 (58; 3.95×10^{-5})	−0.65 (25; 4.19×10^{-4})	−0.64 (58; 7.54×10^{-8})	−0.52 (16; 0.04)	−0.49 (45; 5.87×10^{-4})	0.52 (43; 3.44×10^{-4})
H_α vel.	−0.51 (58; 3.95×10^{-5})	···	0.12 (25; 0.66)	0.58 (58; 1.85×10^{-6})	−0.13 (16; 0.63)	−0.70 (45; 9.10×10^{-8})	−0.07 (43; 0.67)
s_1	−0.65 (25; 4.19×10^{-4})	0.12 (25; 0.55)	···	0.72 (25; 4.29×10^{-5})	0.93 (4; 0.07)	−0.55 (20; 0.02)	−0.73 (18; 5.14×10^{-4})
s_2	−0.64 (58; 7.54×10^{-8})	0.58 (58; 1.85×10^{-6})	0.72 (25; 4.29×10^{-5})	···	0.53 (16; 0.03)	−0.70 (45; 9.34×10^{-8})	−0.40 (43; 8.60×10^{-3})
s_3	−0.47 (17; 0.06)	−0.03 (17; 0.91)	0.60 (4; 0.39)	0.45 (17; 0.07)	···	−0.57 (16; 0.02)	−0.53 (16; 0.03)
M_{max}	0.49 (45; 9.87×10^{-4})	−0.70 (45; 9.10×10^{-8})	−0.55 (20; 0.02)	−0.70 (45; 9.34×10^{-8})	−0.72 (15; 2.65×10^{-3})	···	0.29 (33; 0.11)
OPTd	0.52 (43; 3.44×10^{-4})	−0.07 (43; 0.67)	−0.73 (18; 5.14×10^{-4})	−0.40 (43; 8.60×10^{-3})	−0.49 (16; 0.05)	0.29 (33; 0.11)	···

We present the Pearson's r-parameter which indicates the strength of the correlation, together with in brackets the number of events, and probability of finding such correlation by chance.

Chapter 3

Type II supernova spectral diversity. Paper I: Observations, sample characterization and spectral line evolution

3.1 Abstract

We present 893 optical wavelength spectra of 123 nearby type II supernovae (SNe II) obtained between 1986 and 2009, and ranging between 3 and 363 days post explosion. Here, we outline our observations and data reductions techniques, together with a characterization of the spectral diversity of SNe II. A statistical analysis of the spectral matching technique is discussed as an alternative to non-detection constraints for estimating SN explosion epochs. The time evolution of spectral lines is presented and analysed in terms of how this differs for SNe of different photometric, spectral, and environmental properties. We conclude that the feature located at $\sim 5700 - 5800$ Å is related to He I in early phases (before 25 days) and associated to Na I D in the recombination phase (later than 30 days). Between 15 and 25 days the transition from He I to Na I D happens. Around of 60% of our sample show the extra absorption component on the blue side of the H_{α} P-Cygni profile (Cachito feature) between 7 and 120 days since explosion. Studying the nature of Cachito, we conclude that these features at early times (before ~ 35 days) are associated with Si II λ6355, while later during the plateau phase they are related to high velocity (HV) features of hydrogen lines. These HV features could imply signs of interaction between the SNe ejecta and the RSG wind. We find a huge range in ejecta expansion velocities at all epochs, which could imply a

large range in explosion energies. We also find a large range in the absolute strength and evolution of various lines. This implies a range in the temperature evolution (radius) and progenitor metallicities in our sample.

3.2 Introduction

Supernovae (SNe) that show strong Balmer lines in their spectra, are known as Type II SNe (SNe II henceforth, Minkowski 1941). They are produced by the final explosion of massive (> 8 $M_\odot$) stars, which retain a significant part of their hydrogen envelope at the time of the explosion. Red supergiant (RSG) stars have been found at the position of SN II explosion sites in pre-explosion images (e.g. Van Dyk et al., 2003, Smartt et al., 2004, 2009, Maund and Smartt, 2005, Smartt, 2015), suggesting that they are the direct progenitors of the vast majority of SNe II.

Initially SNe II were classified according to the shape of the light curve: SNe with faster 'linear' declining light curves are cataloged as SNe IIL, while SNe with a plateau (quasi-constant luminosity for a period of a few months) as SNe IIP (Barbon et al., 1979). More recently, two classes were added within the SNe II group: SNe IIn and SNe IIb. SNe IIn show narrow emission lines in their spectra (Schlegel, 1990), attributed to interaction with circumstellar medium (CSM), while SN IIb are thought to be transitional objects, between SN II and SN Ib (Filippenko et al., 1993). The latter two sub-types (IIn and IIb) are not included in the bulk of the analysis for this chapter, and are not discussed any further.

A large diversity is observed in the spectral and photometric properties of SNe II[1]. This includes: fast declining SNe (e.g. Branch et al., 1981, Buta, 1982, Cappellaro et al., 1995a), intermediate between SNe IIL/IIP (e.g. Clocchiatti et al., 1996), peculiar events (e.g. Menzies et al., 1987, Catchpole et al., 1987, 1988), low luminosity/velocity objects (e.g. Turatto et al., 1998, Pastorello et al., 2006, Zhang et al., 2014), intermediate luminosity SNe (e.g. Roy et al., 2011, Takáts et al., 2014), together with the historical separation between SNe IIL and SNe IIP (Barbon et al., 1979, Arcavi et al., 2012, Faran et al., 2014a,b).

Many individual studies have been published showing spectral line identification, evolution and parameters such as velocities, pseudo-equivalent widths (pEWs) for specific SNe. Examples of very well studied SNe include SN 1979C (e.g. Branch et al., 1981, Immler et al., 2005), SN 1980K (e.g. Buta, 1982, Dwek, 1983, Fesen et al., 1999),

[1]Throughout the rest of the manuscript we use SN II to refer to all SNe which would historically have been classified as SN IIP or SN IIL. In general we will differentiate these events by referring to their specific light-curve or spectral morphology, and we only return to this historical separation if clarification and comparison with previous works is required.

SN 1999em (e.g. Baron et al., 2000, Leonard et al., 2002a, Hamuy et al., 2001), SN 1999gi (e.g. Leonard et al., 2002b), SN 2004dt (e.g. Li et al., 2005, Sahu et al., 2006, Misra et al., 2007, Maguire et al., 2010), SN 2005cs (e.g. Pastorello et al., 2006, 2009). The first two SNe (1979C and 1980K) are the prototypes of SNe IIL according to their linear light curve behaviour. They showed bright luminosities and high expansion velocities. On the other hand, the rest of the objects indicated before belong to the family of SNe IIP. They display longer plateaus and lower velocities compared to SNe IIL. For SN 2005cs, the expansion velocity and luminosity are even lower, probably due to its low energy explosion (see Pastorello et al. 2009). All SNe IIP mentioned here have progenitor mass estimates (Smartt, 2015) in a range between 8 and 15 $M_{\odot}$.

In the recent years, the study of individual SNe have increased significantly, however statistical studies of the diversity of these parameters are to date scarce. Here we attempt to remedy this situation. The purpose of this chapter is to present a statistical characterization of the optical spectra of SNe II, as well as an initial analysis of their spectral features. Only in this way can the full SN II spectral diversity be characterized in order to further understand the diversity in physics which explains the SN II phenomenon. To that aim, we have analyzed more than 900 spectra of 123 SNe II between 3 and 363 days since explosion. We identified 11 features in the photospheric phase and four in the nebular phase with the aim of understanding the overall evolution of optical wavelength spectroscopy of SNe II with time.

The chapter is organized as follows. In section 3.3 we outline the data sample. The spectroscopic observations and data reduction techniques are presented in section 3.4. In section 3.5 the estimation of the explosion epoch and their implementation are presented. In section 3.6 we describe the sample properties, while in section 3.7 we present the spectral feature identification. The spectral measurements are presented in section 3.8 while the line evolution analysis and the conclusions are in section 3.9 and 3.10, respectively.

While here in chapter 3 we concentrate on the overall characterisation of SN II spectral diversity, in a second analysis; chapter 4, we build on this characterisation to present an investigation of correlations between different spectral and photometric parameters, and try to understand these in terms of the diversity of the underlying physics of the explosions and their progenitors.

3.3 Data sample

Our dataset was obtained between 1986 and 2009 from a range of different sources. This sample consists of 898 optical spectra of 123 SNe II[2], of which 4 were provided by the Cerro Tololo Supernova Survey (CTSS), 7 were obtained by the Calán/Tololo survey (CT, Hamuy et al. 1993, PI: Hamuy 1989-1993), 5 by the Supernova Optical and Infrared Survey (SOIRS, PI: Hamuy, 1999-2000), 31 by the Carnegie Type II Supernova Survey (CATS, PI: Hamuy, 2002-2003) and 76 by the Carnegie Supernova Project (CSP, Hamuy et al. 2006 PIs: Phillips & Hamuy, 2004-2009). These follow-up campaigns concentrated on obtaining well sampled and high cadence light curves and spectral sequences of nearby SNe, based mainly on 2 criteria. 1) that SNe were brighter than V$\sim$ 17 mag at discovery, and 2) that those discovered SNe were classified as being relatively young, at maximum one month from explosion. The redshift distribution of our sample is shown in Figure 3.1. The figure shows that the majority of the sample have a redshift ≤ 0.03. SN 2002ig has the highest redshift in the sample with a value of 0.077, while the nearest SN (SN 2008bk) has a redshift of 0.00076. The mean value of the sample is 0.0178 and the median is 0.0152. The redshift information comes from the heliocentric recession velocity of each host galaxy as published in the NASA/IPAC extragalactic Database (NED)[3]. These NED values were compared with those obtained through the measurement of narrow emission lines observed within SN spectra and originating from host H II regions. In case of discrepancy between both sources, we give the priority to our spectral estimations. Two of our SNe (SN 2006Y and SN 2007ld) occur in anonymous host galaxies. Their redshift were obtained from the Asiago supernova catalog[4] and from the narrow emission lines within SN spectra originating from the underlying host galaxy, respectively. Table 3.1 lists the sample of SNe II selected for this work, their host galaxy information, and the campaign to which they belong.

[2]In the data release we include 8 spectra of the SN 1987A-like, 2000cb, which has not been analysed in this work.

[3]http://ned.ipac.caltech.edu

[4]http://graspa.oapd.inaf.it

Table 3.1: SN II sample

SN	Host Galaxy	Recession velocity (km s^{-1})	Hubble type	$E(B-V)_{\rm MW}$ (mag)	Discovery date	Discovery Reference	Explosion Epoch	N of spectra	Campaign
1986L	NGC 1559	1305	SBcd	0.026	46711.1	IAUC 4260	46708.0^{n}(3)	31	CTSS
1988A	NGC 4579	1517	SABb	0.036	47179.0	IAUC 4533	47177.2^{n}(2)	5	CTSS
1990E	NGC 1035	1241	SAc	0.022	47937.7	IAUC 4965	47935.1^{n}(3)	5	CTSS
1990K	NGC 0150	1584	SBbc	0.013	48037.3	IAUC 5022	48001.5^{n}(6)	9	CTSS
1991al	2MASX J19422191–5506275	4575[1]	?	0.054	48453.7	IAUC 5310	48442.5^{s}(8)*	8	CT
1992af	ESO 340-G038	5541	S	0.046	48802.8	IAUC 5554	48798.8^{s}(8)*	5	CT
1992am	MCG -01-04-039	14397[1]	S	0.046	48829.8	IAUC 5570	48813.9^{s}(6)*	2	CT
1992ba	NGC 2082	1185	SABc	0.051	48896.2	IAUC 5625	48884.9^{s}(7)	10	CT
1993A	2MASX J07391822–6203095	8790[1]	?	0.153	49004.6	IAUC 5693	48995.5^{n}(9)	2	CT
1993K	NGC 2223	2724	SBbc	0.056	49075.5	IAUC 5733	49065.5^{n}(9)	17	CT
1993S	2MASX J22522390-4018432	9903	S	0.014	49133.7	IAUC 5812	49130.8^{s}(5)	4	CT
1999br	NGC 4900	960	SBc	0.021	51281.0	IAUC 7141	51276.7^{n}(4)	8	SOIRS
1999ca	NGC 3120	2793	Sc	0.096	51296.0	IAUC 7158	51277.5^{s}(7)*	4	SOIRS
1999cr	ESO 576-G034	6069[1]	S/Irr	0.086	51249.7	IAUC 7210	51246.5^{s}(4)*	5	SOIRS
1999eg	IC 1861	6708	SA0	0.104	51455.5	IAUC 7275	51449.5^{s}(6)*	2	SOIRS
1999em	NGC 1637	717	SABc	0.036	51481.0	IAUC 7294	51476.5^{n}(5)	12	SOIRS
2002ew	NEAT J205430.50-000822.0	8975	?	0.091	52510.8	IAUC 7964	52500.6^{n}(10)	7	CATS
2002fa	NEAT J205221.51+020841.9	17988	?	0.088	52510.8	IAUC 7967	52502.5^{s}(8)*	6	CATS
2002gd	NGC 7537	2676	SAbc	0.059	52552.7	IAUC 7986	52551.5^{s}(4)*	12	CATS
2002gw	NGC 922	3084	SBcd	0.017	52560.7	IAUC 7995	52553.5^{s}(8)*	11	CATS
2002hj	NPM1G +04.0097	7080	?	0.102	52568.0	IAUC 8006	52562.5^{n}(7)	7	CATS
2002hx	PGC 023727	9293	SBb	0.048	52589.7	IAUC 8015	52582.5^{n}(9)	9	CATS
2002ig	SDSS J013637.22+005524.9	23100[2]	?	0.034	52576.7	IAUC 8020	52570.5^{s}(5)*	5	CATS
210	MCG +00-03-054	15420	?	0.033	?	?	52486.5^{s}(6)*	6	CATS
2003B	NGC 1097	1272	SBb	0.024	52645.0	IAUC 8042	52613.5^{s}(11)*	9	CATS
2003E	MCG -4-12-004	4470[3]	Sbc	0.043	52645.0	IAUC 8044	52629.5^{s}(8)*	8	CATS
2003T	UGC 4864	8373	SAab	0.028	52665.0	IAUC 8058	52654.5^{n}(10)	6	CATS
2003bl	NGC 5374	4377[3]	SBbc	0.024	52701.0	IAUC 8086	52696.5^{s}(4)*	8	CATS
2003bn	2MASX J10023529-2110531	3828	?	0.057	52698.0	IAUC 8088	52694.5^{n}(3)	12	CATS
2003ci	UGC 6212	9111	Sb	0.053	52720.0	IAUC 8097	52711.5^{n}(8)	7	CATS
2003cn	IC 849	5433[3]	SABcd	0.019	52728.0	IAUC 8101	52717.5^{s}(4)*	5	CATS
2003cx	NEAT J135706.53-170220.0	11100	?	0.083	52730.0	IAUC 8105	52725.5^{s}(5)*	6	CATS
2003dq	MAPS-NGP O4320786358	13800	?	0.016	52739.7	IAUC 8117	52731.5^{n}(8)	3	CATS
2003ef	NGC 4708	4440[3]	SAab	0.041	52770.7	IAUC 8131	52757.5^{s}(9)*	6	CATS
2003eg	NGC 4727	4388[1]	SABbc	0.046	52776.7	IAUC 8134	52764.5^{s}(5)*	5	CATS
2003ej	UGC 7820	5094	SABcd	0.017	52779.7	IAUC 8134	52775.5^{n}(5)	3	CATS
2003fb	UGC 11522	5262[3]	Sbc	0.162	52796.0	IAUC 8143	52772.5^{s}(10)*	4	CATS
2003gd	M74	657	SAc	0.062	52803.2	IAUC 8150	52755.5^{s}(9)*	3	CATS
2003hd	MCG -04-05-010	11850	Sb	0.011	52861.0	IAUC 8179	52855.9^{s}(5)*	9	CATS
2003hg	NGC 7771	4281	SBa	0.065	52870.0	IAUC 8184	52865.5^{n}(5)	5	CATS
2003hk	NGC 1085	6795	SAbc	0.033	52871.6	CBET 41	52866.8^{s}(4)*	4	CATS
2003hl	NGC 772	2475	SAb	0.064	52872.0	IAUC 8184	52868.5^{n}(5)	6	CATS
2003hn	NGC 1448	1170	SAcd	0.013	52877.2	IAUC 8186	52866.5^{n}(10)	9	CATS
2003ho	ESO 235-G58	4314	SBcd	0.034	52851.9	IAUC 8186	52848.5^{s}(7)*	5	CATS
2003ib	MCG -04-48-15	7446	Sb	0.043	52898.7	IAUC 8201	52891.5^{n}(8)	5	CATS
2003ip	UGC 327	5403	Sbc	0.058	52913.7	IAUC 8214	52896.5^{s}(4)	4	CATS

2003iq	NGC 772	2475	SAb	0.064	52921.5	CBET 48	52919.5^{n}(2)	5	CATS
2004dy	IC 5090	9352	Sa	0.045	53242.5	IAUC 8395	53240.5^{n}(2)	3	CSP
2004ej	NGC 3095	2723	SBc	0.061	53258.5	CBET 78	53223.9^{s}(9)*	9	CSP
2004er	MCG -01-7-24	4411	SAc	0.023	53274.0	CBET 93	3271.8^{n}(2)	10	CSP
2004fb	ESO 340-G7	6100	S	0.056	53286.2	IAUC 8420	53258.6^{s}(7)*	4	CSP
2004fc	NGC 701	1831	SBc	0.023	53295.2	IAUC 8422	53293.5^{n}(1)	10	CSP
2004fx	MCG -02-14-3	2673	SBc	0.090	53307.0	IAUC 8431	53303.5^{n}(4)	10	CSP
2005J	NGC 4012	4183	Sb	0.025	53387.0	IAUC 8467	53379.8^{s}(7)*	11	CSP
2005K	NGC 2923	8204	?	0.035	53386.0	IAUC 8468	53369.8^{s}(8)	2	CSP
2005Z	NGC 3363	5766	S	0.025	53402.0	IAUC 8476	53396.7^{n}(6)	9	CSP
2005af	NGC 4945	563	SBcd	0.156	53409.7	IAUC 8482	53320.8^{s}(17)*	9	CSP
2005an	ESO 506-G11	3206	S0	0.083	53432.7	CBET 113	53431.8^{s}(6)*	7	CSP
2005dk	IC 4882	4708	SBb	0.043	53604.0	IAUC 8586	53601.5^{s}(6)*	7	CSP
2005dn	NGC 6861	2829	SA0	0.048	53609.5	IAUC 8589	53602.6^{s}(6)*	8	CSP
2005dt	MCG -03-59-6	7695	SBb	0.025	53614.7	CBET 213	53605.6^{n}(9)	1	CSP
2005dw	MCG -05-52-49	5269	Sab	0.020	53612.7	CBET 219	53603.6^{n}(9)	3	CSP
2005dx	MCG -03-11-9	8012	S	0.021	53623.0	CBET 220	53611.8^{s}(7)*	1	CSP
2005dz	UGC 12717	5696	Scd	0.072	53623.7	CBET 222	53619.5^{n}(4)	7	CSP
2005es	MCG +01-59-79	11287	S	0.076	53643.7	IAUC 8608	53638.7^{n}(5)	1	CSP
2005gz	MCG -01-53-022	8518	SBbc	0.06	53654.7	IAUC 8616	53650.2^{n}(5)	1	CSP
2005lw	IC 672	7710	?	0.043	53719.0	CBET 318	53716.8^{s}(10)	14	CSP
2005me	ESO 244-31	6726	SAc	0.022	53728.2	CBET 333	53717.9^{s}(10)*	1	CSP
2006Y	anon	10074[2]	?	0.115	53770.0	IAUC 8668	53766.5^{n}(4)	13	CSP
2006ai	ESO 005-G009	4571[1]	SBcd	0.113	53784.0	CBET 406	53781.6^{s}(5)	12	CSP
2006bc	NGC 2397	1363	SABb	0.181	53819.1	CBET 446	53815.5^{n}(4)	3	CSP
2006be	IC 4582	2145	S	0.026	53819.0	CBET 449	53802.8^{s}(9)*	4	CSP
2006bl	MCG +02-40-9	9708	?	0.045	53829.5	CBET 597	53822.7^{s}(10)*	3	CSP
2006ee	NGC 774	4620	S0	0.054	53966.0	cbet 597	53961.9^{n}(4)	13	CSP
2006it	NGC 6956	4650	SBb	0.087	54009.5	CBET 660	54006.5^{n}(3)	6	CSP
2006iw	2MASX J23211915+0015329	9226	?	0.044	54011.5	CBET 663	54010.7^{n}(1)	5	CSP
2006ms	NGC 6935	4543	SAa	0.031	54046.2	CBET 725	54028.5^{s}(6)**	4	CSP
2006qr	MCG -02-22-023	4350	SABbc	0.040	54070.0	CBET 766	54062.8^{n}(7)	8	CSP
2007P	ESO 566-G36	12224	Sa	0.036	54124.0	CBET 819	54118.7^{n}(5)	6	CSP
2007U	ESO 552-65	7791	S	0.046	54136.5	CBET 835	54133.6^{s}(6)*	7	CSP
2007W	NGC 5105	2902	SBc	0.045	54146.5	CBET 844	54130.8^{s}(7)*	7	CSP
2007X	ESO 385-G32	2837	SABc	0.060	54146.5	CBET 844	54143.5^{s}(5)	12	CSP
2007Z	PGC 016993	5277	Sbc	0.525	54148.7	CBET 847	54135.6^{s}(5)	2	CSP
2007aa	NGC 4030	1465	SAbc	0.023	54149.7	CBET 848	54126.7^{s}(8)*	11	CSP
2007ab	MCG -01-43-2	7056	SBbc	0.235	54150.7	CBET 851	54123.9^{s}(10)	5	CSP
2007av	NGC 3279	1394	Scd	0.032	54180.2	CBET 901	54173.8^{s}(5)*	4	CSP
2007bf	UGC 09121	5327	Sbc	0.018	54285.0	CBET 919	54191.5^{n}(7)	4	CSP
2007hm	SDSS J205755.65-072324.9	7540	?	0.059	54343.7	CBET 1050	54336.6^{s}(6)*	7	CSP
2007il	IC 1704	6454	S	0.042	54354.0	CBET 1062	54349.8^{n}(4)	12	CSP
2007it	NGC 5530	1193	SAc	0.103	54357.5	CBET 1065	54348.5^{n}(1)	11	CSP
2007ld	anon	7499[1]	?	0.081	54379.5	CBET 1098	54376.5^{s}(8)*	7	CSP
2007oc	NGC 7418	1450	SABcd	0.014	54396.5	CBET 1114	54388.5^{n}(3)	17	CSP
2007od	UGC 12846	1734	Sm	0.032	54407.2	CBET 1116	54400.6^{s}(5)*	14	CSP
2007sq	MCG -03-23-5	4579	SAbc	0.183	54443.0	CBET 1170	54422.8^{s}(6)*	7	CSP
2008F	MCG -01-8-15	5506	SBa	0.044	54477.5	CBET 1207	54469.6^{s}(6)*	2	CSP
2008H	ESO 499- G 005	4287	SAc	0.057	54481.0	CBET 1210	54432.8^{s}(8)	1	CSP
2008K	ESO 504-G5	7997	Sb	0.035	54481.0	CBET 1211	54475.5^{s}(6)*	12	CSP
2008M	ESO 121-26	2267	SBc	0.040	54480.7	CBET 1214	54471.7^{n}(9)	12	CSP

2008W	MCG -03-22-7	5757	Sc	0.086	54502.7	CBET 1238	54483.8^s(8)*	10	CSP
2008ag	IC 4729	4439	SABbc	0.074	54499.5	CBET 1252	54477.9^s(8)*	18	CSP
2008aw	NGC 4939	3110	SAbc	0.036	54528.0	CBET 1279	54517.8^n(10)	12	CSP
2008bh	NGC 2642	4345	SBbc	0.020	54549.0	CBET 1311	54543.5^n(5)	6	CSP
2008bk	NGC 7793	227	SAd	0.017	54550.7	CBET 1315	54540.9^s(8)*	26	CSP
2008bm	CGCG 071-101	9563	Sc	0.023	54554.7	CBET 1320	54522.8^s(6)	4	CSP
2008bp	NGC 3095	2723	SBc	0.061	54558.7	CBET 1326	54551.7^n(6)	5	CSP
2008br	IC 2522	3019	SAcd	0.083	54564.2	CBET 1332	54555.7^n(9)	4	CSP
2008bu	ESO 586-G2	6630	S	0.376	54574.0	CBET 1341	54566.8^s(7)	5	CSP
2008ga	LCSB L0250N	4639	?	0.582	54734.0	CBET 1526	54711.5^s(7)	3	CSP
2008gi	CGCG 415-004	7328	Sc	0.060	54752.0	CBET 1539	54742.7^n(9)	6	CSP
2008gr	IC 1579	6831	SBbc	0.012	54768.7	CBET 1557	54769.6^s(6)*	5	CSP
2008hg	IC 1720	5684	Sbc	0.016	54785.5	CBET 1571	54779.8^n(5)	6	CSP
2008ho	NGC 922	3082	SBcd	0.017	54796.5	CBET 1587	54792.7^n(5)	3	CSP
2008if	MCG -01-24-10	3440	Sb	0.029	54812.7	CBET 1619	54807.8^n(5)	20	CSP
2008il	ESO 355-G4	6276	SBb	0.015	54827.7	CBET 1634	54825.6^n(3)	3	CSP
2008in	NGC 4303	1566	SABbc	0.020	54827.2	CBET 1636	54825.4^n(2)*	13	CSP
2009A	KUG 0150-036B	5128	S	0.025	54833.5	CBET 1645	54821.5^n(10)	5	CSP
2009N	NGC 4487	1034	SABcd	0.019	54856.3	CBET 1670	54846.8^s(5)	13	CSP
2009W	SDSS J162346.79+114423	5100	?	?	54865.0	CBET 1683	54816.9^s(9)	1	CSP
2009aj	ESO 221- G 018	2883	Sa	0.130	54887.0	CBET 1704	54880.5^n(7)	12	CSP
2009ao	NGC 2939	3339	Sbc	0.034	54895.0	CBET 1711	54890.7^n(4)	7	CSP
2009au	ESO 443-21	2819	Scd	0.081	54902.0	CBET 1719	54897.5^n(4)	10	CSP
2009bu	NGC 7408	3494	SBc	0.022	54916.2	CBET 1740	54901.9^s(8)*	6	CSP
2009bz	UGC 9814	3231	Sdm	0.035	54920.0	CBET 1748	54915.8^n(4)	5	CSP

[1] Measured using our own spectra.
[2] Taken from the Asiago supernova catalog: http://graspa.oapd.inaf.it/ (Barbon et al., 1999).
[3] From our own data (Jones et al., 2009).
^{s} Explosion epoch estimation through spectral matching.
^{n} Explosion epoch estimation from SN non-detection.
Observing campaigns: CTSS=Cerro Tololo Supernova Survey; CT=Calán/Tololo Supernova Program; SOIRS=Supernova Optical and Infrared Survey; CATS=Carnegie Type II Supernova Survey; CSP=Carnegie Supernova Project.

In the first column the SN name, followed by its host galaxy are listed. In column 3 we list the host galaxy heliocentric recession velocity. These are taken from the Nasa Extragalactic Database (NED: http://ned.ipac.caltech.edu/) unless indicated by a superscript (sources in table notes). In columns 4 and 5 we list the host galaxy morphological Hubble types (from NED) and the reddening due to dust in our Galaxy (Schlafly and Finkbeiner, 2011) taken from NED. In column 6, 7 and 8 we list the discovery date, their reference and the explosion epochs. The number of spectra and the the observing campaign from which each SN was taken are given in column 9 and 10, and acronyms are listed in the table notes.
* SNe with explosion epochs different to that published by Anderson et al. (2014b).

From our SNe II sample, SNe IIn, SNe IIb and SN 1897A-like events (SN 2006au and SN 2006V; Taddia et al. 2012) were excluded based on spectral and photometric information. Details of the SNe IIn sample can be found in Taddia et al. (2013), while those of the SNe IIb will be published in an upcoming paper (Stritzinger et al., in prep). The photometry of our sample in the $V-$band was published by Anderson et al. (2014b). More recently, Galbany et al. (2016) released the UBVRIZ photometry of our sample obtained between 1986 and 2003. Around 500 spectra of 80 objects are published here for the first time. Now we briefly discuss each of the surveys providing SNe for our analysis.

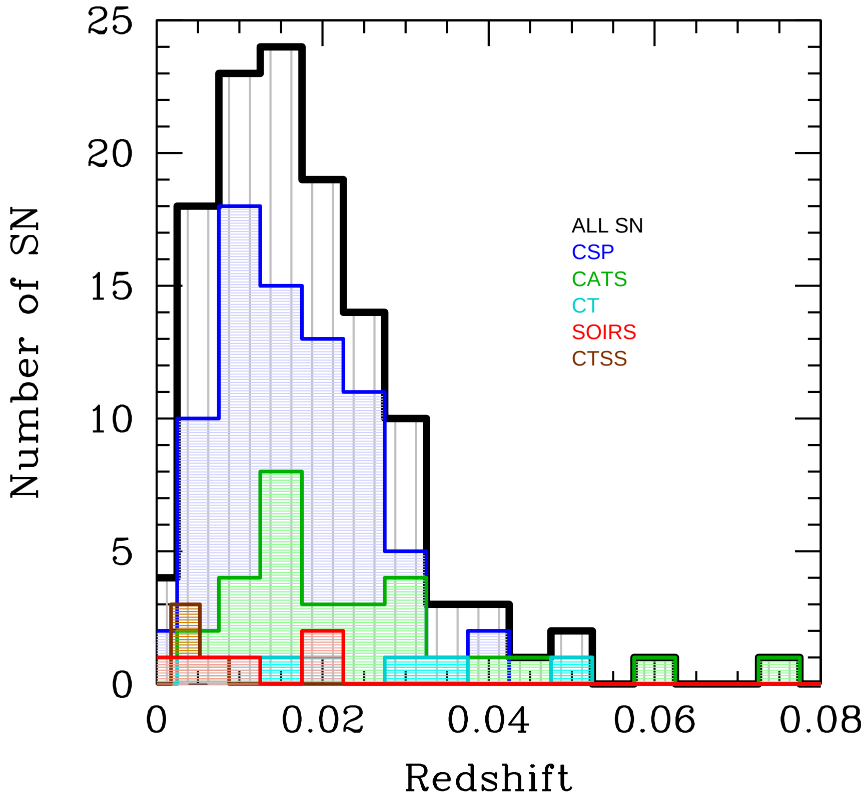

Figure 3.1 Distribution of heliocentric redshifts for the 123 SN II in our sample.

3.3.1 The Cerro Tololo Supernova Survey

A total of 4 SNe II (SN 1986L, SN 1988A, SN 1990E, and SN 1990K) were extensively observed at CTIO by the Cerro Tololo SN program (PIs: Phillips & Suntzeff, 1986-2003). These SNe have been analyzed in previous works (e.g Schmidt et al., 1993, Turatto et al., 1993, Cappellaro et al., 1995a, Hamuy, 2001).

3.3.2 The Calán/Tololo survey (CT)

The Calán/Tololo survey was a project of follow-up campaigns to study the usefulness of SNe as distance indicators. A total of 50 SNe were obtained between 1989 and 1993. The analysis of SNe Ia were published by Hamuy et al. (1996). Spectral and photometric details of six SNe II were presented by Hamuy (2001). In this analysis we include these six SNe II and an additional object, SN 1993K.

3.3.3 The Tololo Supernova program, the Supernova Optical and Infrared Survey (SOIRS)

The Supernova Optical and Infrared Survey carried out a program to obtain optical and IR photometry and spectroscopy of nearby SNe ($z < 0.08$). In the course of 1999-2000, 20 SNe were observed, six of which are SNe II. Details of these SNe were published by Hamuy (2001), Hamuy et al. (2001), Hamuy and Pinto (2002), and Hamuy (2003).

3.3.4 The Carnegie Type II Supernova Survey (CATS)

Between 2002 and 2003 the Carnegie Type II Supernova Survey observed 34 SNe II. Optical spectroscopy and photometry of these SNe have been used to derive distances (Olivares, 2008, Jones et al., 2009), the spectral data have not been released until now.

3.3.5 The Carnegie Supernova Project (CSP)

The Carnegie Supernova Project (CSP) was a five year follow-up program to obtain high quality optical and near infrared light curves and optical spectroscopy. The data obtained by CSP between 2004 and 2009 consist of ~ 250 SNe of all types, of which 76 correspond to SNe II. The first SN Ia photometry data were published in Contreras et al. (2010), while their analysis was done by Folatelli et al. (2010). A second data release was provided by Stritzinger et al. (2011). A spectroscopy analysis of SNe Ia was published by Folatelli et al. (2013). The CSP spectral data for SNe II are published here for the first time, while the complete optical and near-IR photometry will be published by Anderson et al. (in prep.) and de Jaeger et al. (in prep.), respectively.

3.4 Observations and data reduction

In this section we summarize our observations and the data reduction techniques. However, a detailed description of the CT methodology is presented in Hamuy et al. (1993), in the case of SOIRS is described in Hamuy et al. (2001) and for CSP can be found in Hamuy et al. (2006) and Folatelli et al. (2013).

3.4.1 Observations

The data presented here were obtained with a great variety of instruments and telescopes, as shown in Table 3.2. The majority of the spectra were taken in long-slit spectroscopic mode with the slit placed along the paralactic angle. However, when the SN was located close to the host, it was necessary to pick a different and more convenient angle to avoid contamination from the host. The majority of our spectra cover the range of ~ 3800 to ~ 9500 Å. The observations were performed with the Cassegrain spectrographs at 1.5-m and 4.0-m telescopes at Cerro Tololo, with the Wide Field CCD Camera (WFCCD) at the 2.5m du Pont Telescope, the Low Dispersion Survey Spectrograph (LDSS2; Allington-Smith et al. 1994) on the Magellan Clay 6.5-m telescope and the Inamori Magellan Areal Camera and Spectrograph (IMACS; Dressler et al. 2011) on the Magellan Baade 6.5-m telescope at Las Campanas Observatory. At La Silla, the observations were carried out with the ESO Multi-Mode Instrument (EMMI; Dekker et al. 1986) in medium resolution spectroscopy mode (at the NTT) and the ESO Faint Object Spectrograph and Camera (EFOSC; Buzzoni et al. 1984) at the NTT and 3.6-m and NTT telescopes. We also have 3 spectra for SN 2006ee obtained with the Boller & Chivens CCD spectrograph at the Hiltner 2.4 m Telescope of the MDM Observatory. Table 3.2 displays a complete journal of the 898 spectral observations, listing for each spectrum the UT and Julian dates, phases, wavelength range, FWHM resolution, exposure time, airmass, and the telescope and instrument used.

Table 3.2: Spectroscopic observations information

UT Date	JD	Phase (days)	Tel.	Inst.	Wavelength Range (AA)	Resol. (AA)	Exp. (s)	Air-mass
(1)	(2)	(3)	(4)	(5)	(6)	(7)	(8)	(9)
SN 1986L								
3561-6446 1986-10-09	2446712.50	4	···	···	3681-7728	···	1000	1.21
1986-10-11	2446714.50	6	···	···	3730-7168	···	1556	1.20
1986-10-12	2446715.50	7	···	···	3800-7322	···	2000	1.21
1986-10-13	2446716.50	8	···	···	3681-4988	···	1352	1.21⋆
1986-10-14	2446717.50	9	···	···	3681-4988	···	2500	1.19⋆
1986-10-15	2446718.50	10	···	···	3681-4988	···	2500	1.18⋆
1986-10-20	2446723.50	15	···	···	3720-5031	···	3000	1.24⋆
1986-10-26	2446729.50	21	···	···	3830-7330	···	2000	1.20
1986-10-28	2446731.50	23	···	···	3596-5125	···	2000	1.37
1986-10-28	2446731.50	23	···	···	3590-5130	···	···	1.37
1986-10-29	2446732.50	24	···	···	3675-5240	···	1200	1.23
1986-11-01	2446735.50	27	···	···	3270-7205	···	1800	1.21
1986-11-02	2446736.50	28	···	···	3270-7205	···	1200	1.2
1986-11-03	2446737.50	29	···	···	3847-7357	···	2000	1.22
1986-11-03	2446737.50	29	···	···	3270-7205	···	1200	1.21
1986-11-04	2446738.50	30	···	···	4166-7701	···	1800	1.22
1986-11-04	2446738.50	30	···	···	3270-7205	···	1200	1.20
1986-11-05	2446739.50	31	···	···	3270-7205	···	1200	1.20
1986-11-06	2446740.50	32	···	···	3270-7205	···	1200	1.21
1986-11-07	2446741.50	33	···	···	3270-7205	···	1200	1.21
1986-11-10	2446744.50	36	···	···	4166-7701	···	1800	1.23
1986-11-11	2446745.50	37	···	···	3830-7285	···	1000	1.19
1986-11-14	2446748.50	40	···	···	3561-6446	···	···	1.20
1986-11-16	2446750.50	42	···	···	3561-6446	···	···	1.18
1986-11-25	2446759.50	51	···	···	3450-6950	···	2000	1.20⋆
1986-12-09	2446773.50	65	···	···	3680-6670	···	1000	1.44
1986-12-10	2446774.50	66	···	···	3769-7329	···	2262	···
1986-12-23	2446787.50	79	···	···	3991-7548	···	2394	···
1987-01-01	2446796.50	88	···	···	3776-7578	···	2545	···
1987-01-23	2446818.50	110	···	···	3450-6950	···	3000	1.20
1987-01-30	2446825.50	117	···	···	5601-7998	···	···	1.24
SN 1988A								
1988-01-28	2447188.50	11	···	···	3047-7731	···	600	1.37
1988-01-29	2447189.50	12	···	···	3034-7778	···	600	1.35
1988-02-02	2447193.50	16	···	···	5786-10284	···	600	1.34
1988-02-03	2447194.50	17	···	···	2914-7389	···	600	1.34
1988-03-06	2447226.50	49	···	···	7699-10964	···	600	1.48
SN 1990E								
1990-02-23	2447945.50	10	···	···	3172-7910	···	600	1.37
1990-03-04	2447954.50	19	···	···	3147-6412	···	600	1.35
1990-03-04	2447954.50	19	···	···	3147-9083	···	600	1.34
1990-03-19	2447969.50	34	···	···	5794-9082	···	600	5.52
1990-07-03	2448075.50	140	···	···	2979-7726	···	600	1.48
SN 1990K								
1990-05-31	2448042.50	41	···	···	3177-6489	···	240	1.23
1990-05-31	2448042.50	41	···	···	6180-9553	···	360	1.38
1990-06-07	2448049.50	48	···	···	2980-7729	···	900	1.31
1990-06-08	2448050.50	49	···	···	6078-10597	···	900	1.23
1990-06-12	2448054.50	53	···	···	2982-7731	···	900	1.15
1990-06-19	2448061.50	60	···	···	5933-10440	···	600	1.33
1990-07-03	2448075.50	74	···	···	2980-7726	···	1200	1.20
1990-08-13	2448116.50	115	···	···	2994-7733	···	1800	1.01
1990-08-17	2448120.50	119	···	···	2982-7737	···	1800	1.03
SN 1991al								
1991-08-05	2448473.50	31	···	···	3595-9899	···	···	···
1991-08-06	2448474.50	32	···	···	3545-6794	···	···	···
1991-08-10	2448478.50	36	···	···	3545-9793	···	···	···
1991-08-13	2448481.50	39	···	···	4432-7052	···	···	···
1991-09-02	2448501.67	59	···	···	2961-7621	···	3600	1.24
1991-09-14	2448513.68	71	···	···	3218-7417	···	2x600	1.40
1991-10-10	2448538.61	97	···	···	2957-7612	···	1800	1.41
1991-11-07	2448567.54	125	···	···	3157-7384	···	600	1.45
SN 1992af								
1992-07-09	2448812.87	14	···	···	4666-7037	···	1800	1.25
1992-07-10	2448813.81	15	···	···	4667-7038	···	1200	1.07
1992-07-29	2448832.76	34	···	···	3194-7364	···	900	1.08
1992-10-01	2448896.59	98	···	···	3149-7360	···	3x1200	1.08
1992-10-31	2448926.55	128	···	···	3152-7334	···	3x1800	1.21

			SN 1992am					
1992-07-29	2448832.89	19	···	···	3106-7161	···	900	1.10
1992-10-01	2448896.78	84	···	···	3061-7156	···	3X900	1.16
			SN 1992ba					
1992-10-01	2448896.85	12	···	···	3196-7470	···	4X180	1.23
1992-10-01	2448896.90	12	···	···	6159-10112	···	120	1.20
1992-10-05	2448900.88	16	···	···	5968-10447	···	150	1.20
1992-10-05	2448900.82	16	···	···	3119-7367	···	4X900	1.25
1992-10-27	2448922.81	38	···	···	2944-7658	···	2X1200	1.21
1992-11-23	2448949.80	65	···	···	3182-7425	···	500	1.22
1992-12-18	2448974.83	95	···	···	3213-7468	···	2X90	1.45
1993-01-28	2449015.69	131	···	···	3683-6977	···	600	1.34
1993-02-27	2449045.66	161	···	···	3082-8918	···	2X2700	1.67
1993-03-21	2449067.54	183	···	···	5806-9125	···	4X480	1.34
			SN 1993A					
1993-01-28	2449015.72	20	···	···	3591-6803	···	1200	1.22
1993-04-21	2449098.60	103	···	···	3132-7240	···	2X900	1.56
			SN 1993K					
1993-04-01	2449078.50	13	···	···	3171-7610	···	900	1.05
1993-04-21	2449098.55	33	···	···	3180-7386	···	3x600	1.75
1993-04-28	2449105.50	40	···	···	3665-9759	···	2x1200	1.31
1993-05-16	2449123.47	58	···	···	3657-9741	···	2x300	1.61
1993-05-17	2449124.47	59	···	···	6001-9743	···	···	···
1993-05-17	2449124.47	59	···	···	7053-6728	···	···	···
1993-11-17	2449308.83	243	···	···	5789-8357	···	···	1.00
1993-11-18	2449309.78	244	···	···	4453-8357	···	···	1.02
1993-11-18	2449309.82	244	···	···	4453-7053	···	···	1.00
1993-11-18	2449309.50	244	···	···	4453-7053	···	···	1.02
1993-12-15	2449336.78	271	···	···	3660-6825	···	2x1800	1.02
1994-01-14	2449366.65	301	···	···	6355-10282	···	1200	1.10
1994-01-14	2449366.66	301	···	···	6355-10282	···	1800	1.15
1994-01-14	2449366.60	301	···	···	3696-6817	···	1800	1.01
1994-01-14	2449366.62	301	···	···	3657-6827	···	1500	1.04
1994-02-10	2449393.70	328	···	···	5802-8370	···	···	1.29
1994-03-17	2449428.58	363	···	···	4181-7506	···	3600	1.16
			SN 1993S					
1993-06-26	2449164.76	34	···	···	2903-7478	···	2x1800	1.28
1993-06-28	2449166.50	36	···	···	3872-9339	···	···	···
1993-07-23	2449191.92	61	···	···	3111-7448	···	1800	1.21
1993-08-24	2449223.76	93	···	···	3574-9523	···	2x1800	1.02
			SN 1999br					
1999-04-23	2451291.50	15	···	···	3463-9271	···	3x600	1.30
1999-04-26	2451294.50	18	···	···	2990-11961	···	900	1.19
1999-04-29	2451297.50	21	···	···	2990-11961	···	600	1.20
1999-05-03	2451301.50	25	···	···	2990-11961	···	600	1.18
1999-05-11	2451309.50	33	···	···	2990-11961	···	900	1.47
1999-05-19	2451317.50	41	···	···	2990-11961	···	400	1.37
1999-05-21	2451320.02	43	···	···	3339-10249	···	2x1800	1.24
1999-07-21	2451380.45	104	···	···	3113-8757	···	2400	1.29
			SN 1999ca					
1999-05-06	2451303.50	26	···	···	10603-14225	···	4x303	1.20⋆
1999-05-07	2451304.50	27	···	···	3170-10005	···	600	1.04
1999-05-11	2451305.50	31	···	···	3338-10080	···	900	1.10
1999-05-19	2451309.50	39	···	···	3170-10006	···	400	1.11
			SN 1999cr					
1999-03-20	2451257.50	11	DUP	···	3528-9086	···	4x900	1.03
1999-03-30	2451267.50	21	···	···	3430-8821	···	600	1.02
1999-04-23	2451291.50	45	DUP	···	3406-9116	···	2x1200	1.30
1999-05-03	2451301.50	55	···	···	3136-9893	···	600	1.04
1999-05-07	2451305.50	59	···	···	3136-9901	···	600	1.02
			SN 1999eg					
1999-10-16	2451467.50	18	DUP	···	3521-9038	···	1200	1.74
1999-11-19	2451501.50	52	NTT	···	4597-9879	···	200	1.76
			SN 1999em					
1999-11-02	2451484.50	8	···	···	8978-12653	···	3x200	1.59
1999-11-03	2451485.50	9	···	···	3292-10074	···	200	1.40
1999-11-09	2451491.50	15	···	···	3292-10074	···	150	1.32
1999-11-14	2451496.50	20	···	···	3292-10074	···	150	1.23
1999-11-18	2451500.50	24	···	···	2992-26935	···	3x200	1.27
1999-11-19	2451501.50	25	···	···	3292-10074	···	150	1.23
1999-11-28	2451510.50	34	···	···	8978-26935	···	2x200	1.18
1999-12-16	2451528.75	52	···	···	4907-9257	···	2x900	1.23
1999-12-31	2451543.75	67	···	···	3092-7109	···	2x450	1.22
2000-04-09	2451643.50	167	···	···	3292-10074	···	300	2.42
			SN 2002ew					

2002-09-12	2452329.50	29	DUP	WF	3670-7080	···	2x1800	1.43
2002-09-13	2452329.50	30	DUP	WF	3670-7080	···	1800	1.33*
2002-09-28	2452545.50	45	CLA	LD	3496-8740	···	600	1.38
2002-10-08	2452555.50	55	DUP	WF	3709-9060	···	2x900	1.61
2002-10-15	2452562.50	62	CLA	LD	3496-8740	···	600	1.41
2002-10-25	2452572.50	72	CLA	LD	3496-8740	···	600	1.00
2002-10-29	2452576.50	76	CLA	LD	3496-8740	···	600	1.79
			SN 2002fa					
2002-09-12	2452529.50	27	DUP	WF	3565-6875	···	2x1800	1.17
2002-09-28	2452545.50	43	CLA	LD	3395-8489	···	600	1.29
2002-10-08	2452555.50	53	DUP	WF	3603-8800	···	5x900	1.21
2002-10-14	2452561.50	59	CLA	LD	3395-8489	···	600	1.17
2002-10-25	2452572.50	70	CLA	LD	3395-8489	···	900	1.00
2002-10-29	2452576.50	74	CLA	LD	3395-8489	···	900	1.35
			SN 2002gd					
2002-10-08	2452555.50	4	DUP	WF	3786-9247	···	2x300	1.89
2002-10-14	2452561.50	10	CLA	LD	3568-8920	···	300	1.36
2002-10-25	2452572.50	21	CLA	LD	3568-8920	···	300	1.00
2002-10-29	2452576.50	25	CLA	LD	3568-8920	···	300	1.42
2002-10-30	2452577.50	26	DUP	WF	3786-9247	···	450	1.30
2002-11-07	2452585.50	34	DUP	WF	3786-9247	···	450	1.28
2002-11-10	2452588.50	37	CLA	LD	3568-8920	···	180	2.00
2002-11-12	2452590.50	39	CLA	LD	3151-9247	···	300	1.55
2002-11-28	2452606.50	55	CLA	LD	3151-9247	···	300	1.24
2002-12-01	2452609.50	58	DUP	WF	3786-9247	···	600	1.57
2002-12-27	2452635.50	84	DUP	WF	3746-7215	···	3x600	1.86
2003-01-09	2452648.50	97	CLA	LD	3151-9247	···	300	2.42
			SN 2002gw					
2002-10-25	2452572.50	19	CLA	LD	3563-8908	···	300	1.00
2002-10-29	2452576.50	23	CLA	LD	3563-8908	···	300	1.03
2002-10-30	2452577.50	24	DUP	WF	3781-9234	···	450	1.04
2002-11-07	2452585.50	32	DUP	WF	3781-9234	···	450	1.00
2002-11-10	2452588.50	35	CLA	LD	3563-8908	···	200	1.26
2002-11-12	2452590.50	37	CLA	LD	3147-9234	···	300	1.06
2002-11-28	2452606.50	53	CLA	LD	3147-9234	···	300	1.03
2002-12-01	2452609.50	56	DUP	WF	3781-9234	···	600	1.02
2002-12-27	2452635.50	82	DUP	WF	3741-7205	···	3x600	1.53
2003-01-03	2452642.50	89	DUP	WF	3741-7205	···	3x600	1.93
2003-01-10	2452649.50	96	CLA	LD	3147-9234	···	300	1.51
			SN 2002hj					
2002-11-07	2452585.50	23	DUP	WF	3731-9114	···	450	1.21
2002-11-10	2452588.50	26	CLA	LD	3516-8792	···	200	1.59
2002-11-12	2452590.50	28	CLA	LD	3106-9114	···	300	1.25
2002-11-28	2452606.50	44	CLA	LD	3180-9330	···	300	1.22
2002-12-03	2452611.50	49	DUP	WF	3731-9114	···	600	1.22
2002-12-27	2452635.50	73	DUP	WF	3692-7111	···	3x600	1.51
2003-01-08	2452647.50	85	CLA	LD	3106-9114	···	300	1.45
			SN 2002hx					
2002-11-28	2452606.50	24	CLA	LD	3084-9049	···	300	1.22
2002-12-01	2452609.50	27	DUP	WF	3705-9049	···	600	1.11
2002-12-27	2452635.50	53	DUP	WF	3666-7061	···	3x600	1.07
2003-01-03	2452642.50	60	DUP	WF	3666-7061	···	3x600	1.04
2003-01-08	2452647.50	65	CLA	LD	3084-9049	···	300	1.12
2003-01-09	2452648.50	66	CLA	LD	3084-9049	···	600	1.12
2003-01-27	2452666.50	84	DUP	WF	3705-9049	···	1200	1.14
2003-02-03	2452673.50	91	DUP	WF	3705-9049	···	900	1.06
2003-03-04	2452702.50	120	DUP	WF	3685-9044	···	900	1.13
			SN 2002ig					
2002-11-10	2452588.50	18	CLA	LD	3345-8364	···	200	1.17
2002-11-12	2452590.50	20	CLA	LD	2955-8671	···	300	1.16
2002-11-28	2452606.50	36	CLA	LD	2955-8671	···	450	1.18
2002-12-03	2452611.50	41	DUP	WF	3550-8671	···	900	1.17
2002-12-27	2452635.50	65	DUP	WF	3513-6765	···	4x900	1.46
			SN 210					
2002-09-28	2452588.50	59	CLA	LD	3424-8560	···	450	1.21
2002-09-30	2452590.50	60	DUP	WF	3633-8874	···	4x900	1.32
2002-10-08	2452606.50	69	DUP	WF	3633-8874	···	4x900	1.37
2002-10-14	2452611.50	75	CLA	LD	3424-8560	···	600	1.44
2002-10-25	2452635.50	86	CLA	LD	3424-8560	···	900	1.00
2002-10-29	2452635.50	90	CLA	LD	3424-8560	···	900	1.16
			SN 2003B					
2003-01-06	2452645.50	32	···	···	3684-8961	···	···	···
2003-01-08	2452647.50	34	CLA	LD	3166-9290	···	200	1.00
2003-01-09	2452648.50	35	CLA	LD	3166-9290	···	200	1.13
2003-01-10	2452649.50	36	CLA	LD	3166-9290	···	200	1.45

2003-02-03	2452673.50	60	DUP	WF	3783-9285	···	600	2.17
2003-03-02	2452700.50	87	DUP	WF	3803-9290	···	600	1.61
2003-03-31	2452729.50	116	DUP	WF	3764-7249	···	2x700	2.36
2003-06-07	2452797.50	184	DUP	WF	3783-9285	···	2x300	1.60
2003-09-15	2452897.81	284	CLA	LD	3584-8961	···	450	1.01
			SN 2003E					
2003-01-09	2452648.50	18	CLA	LD	3133-9194	···	300	1.06
2003-01-10	2452649.50	19	CLA	LD	3133-9194	···	300	1.12
2003-01-27	2452666.50	36	DUP	WF	3764-9194	···	900	1.57
2003-03-03	2452701.50	71	DUP	WF	3744-9189	···	352	1.41
2003-03-12	2452710.50	80	DUP	WF	3744-9189	···	900	1.67
2003-03-31	2452729.50	99	DUP	WF	3725-7174	···	2x900	1.72
2003-04-10	2452739.50	109	CLA	LD	3547-8869	···	240	1.60
2003-05-05	2452764.50	134	CLA	LD	3547-8869	···	240	2.30
			SN 2003T					
2003-02-03	2452673.50	19	DUP	WF	3716-9076	···	900	1.55
2003-03-03	2452701.50	47	DUP	WF	3696-9071	···	900	1.48
2003-03-12	2452710.50	56	DUP	WF	3696-9071	···	900	1.70
2003-03-31	2452729.50	75	DUP	WF	3677-7082	···	3x900	1.68
2003-04-10	2452739.50	85	CLA	LD	3502-8755	···	300	1.60
2003-05-05	2452764.50	110	CLA	LD	3502-8755	···	300	1.54
			SN 2003bl					
2003-03-03	2452701.50	5	DUP	WF	3746-9193	···	600	1.23
2003-03-04	2452702.50	6	DUP	WF	3746-9193	···	900	1.32
2003-03-31	2452729.50	33	DUP	WF	3726-7177	···	2x900	1.37
2003-04-06	2452735.50	39	DUP	WF	3746-9193	···	900	1.40
2003-04-10	2452739.50	43	CLA	LD	3549-8872	···	200	2.15
2003-05-05	2452764.50	68	CLA	LD	3549-8872	···	300	1.41
2003-05-30	2452789.50	93	DUP	WF	3746-9193	···	2x900	1.88
2003-06-04	2452794.50	98	CLA	LD	3549-8872	···	300	2.10
			SN 2003bn					
2003-03-08	2452706.50	12	DUP	WF	3751-9205	···	300	1.18
2003-03-12	2452710.50	16	DUP	WF	3751-9205	···	900	1.36
2003-03-31	2452729.50	35	DUP	WF	3731-7186	···	2x900	1.16
2003-04-04	2452733.50	39	DUP	WF	88843553-	···	600	1.15
2003-04-07	2452736.50	42	DUP	WF	3751-9205	···	600	1.01
2003-04-10	2452739.50	45	CLA	LD	3553-8884	···	250	1.54
2003-05-05	2452764.50	70	CLA	LD	3553-8884	···	250	1.30
2003-05-30	2452789.50	95	DUP	WF	3751-9205	···	2x600	1.22
2003-06-04	2452794.50	100	CLA	LD	3751-9205	···	300	1.6
2003-06-07	2452797.50	103	DUP	WF	3751-9205	···	2x600	1.18
2003-06-23	2452813.50	119	DUP	WF	3751-9205	···	2x600	1.31
2003-06-30	2452820.50	126	CLA	LD	3553-8884	···	300	2.08
			SN 2003ci					
2003-03-31	2452729.50	18	DUP	WF	3668-7065	···	2x900	1.50
2003-04-04	2452733.50	22	DUP	WF	3688-9050	···	900	1.84
2003-05-05	2452764.50	53	CLA	LD	3494-8735	···	300	1.95
2003-05-30	2452789.50	78	DUP	WF	3688-9050	···	2x600	1.22
2003-06-04	2452794.50	83	CLA	LD	3494-8735	···	450	1.32
2003-06-07	2452797.50	86	DUP	WF	3688-9050	···	3x900	1.38
2003-06-26	2452816.50	105	DUP	WF	3688-9050	···	2x900	1.76
			SN 2003cn					
2003-03-31	2452729.50	12	DUP	WF	3712-7150	···	2x900	1.27
2003-04-04	2452733.50	16	DUP	WF	3732-9159	···	600	2.34
2003-04-10	2452739.50	22	CLA	LD	3535-8839	···	300	1.46
2003-05-05	2452764.50	47	CLA	LD	3535-8839	···	300	1.29
2003-06-07	2452797.50	80	DUP	WF	3732-9159	···	2x900	1.88
			SN 2003cx					
2003-04-10	2452739.50	14	CLA	LD	3472-8681	···	300	1.79
2003-05-05	2452764.50	39	CLA	LD	3472-8681	···	450	1.23
2003-06-04	2452794.50	69	CLA	LD	3472-8681	···	450	1.77
2003-06-07	2452797.50	72	DUP	WF	3665-8994	···	3x600	2.14
2003-06-24	2452814.50	89	DUP	WF	3665-8994	···	2x900	1.21
2003-06-30	2452820.50	95	CLA	LD	3472-8681	···	450	1.41
			SN 2003dq					
2003-05-05	2452764.50	33	CLA	LD	3440-8600	···	300	1.42
2003-05-30	2452789.50	58	DUP	WF	3631-8911	···	2x900	1.74
2003-06-04	2452794.50	63	CLA	LD	3440-8600	···	450	1.46
			SN 2003ef					
2003-05-30	2452789.50	32	DUP	WF	3748-9199	···	2x450	1.33
2003-06-04	2452794.50	37	CLA	LD	3551-8878	···	300	1.37
2003-06-07	2452797.50	40	DUP	WF	3748-9199	···	2x600	1.30
2003-06-24	2452814.50	57	DUP	WF	3748-9199	···	2x450	1.14
2003-06-30	2452820.50	63	CLA	LD	3551-8878	···	300	1.72
2003-08-15	2452866.50	109	CLA	LD	3551-8878	···	450	2.00

			SN 2003eg					
2003-05-30	2452789.50	25	DUP	WF	3745-9191	···	2x300	1.64
2003-06-04	2452794.50	30	CLA	LD	3548-8871	···	200	1.45
2003-06-07	2452797.50	33	DUP	WF	3745-9191	···	2x300	1.49
2003-06-30	2452820.50	56	CLA	LD	3548-8871	···	300	1.45
2003-08-20	2452871.51	107	DUP	WF	3745-9191	···	600	2.39
			SN 2003ej					
2003-05-30	2452789.50	14	DUP	WF	3736-9169	···	2x300	1.41
2003-06-04	2452794.50	19	CLA	LD	3539-8849	···	300	1.33
2003-06-25	2452815.50	40	DUP	WF	3736-9169	···	2x450	1.30
			SN 2003fb					
2003-06-07	2452797.50	25	DUP	WF	3734-9164	···	2x900	1.22
2003-06-30	2452820.50	48	CLA	LD	3537-8844	···	450	1.22
2003-08-15	2452866.50	94	CLA	LD	3537-8844	···	900	1.23
2003-08-20	2452871.62	99	DUP	WF	3734-9164	···	2x900	1.22
			SN 2003gd					
2003-06-27	2452817.50	62	DUP	WF	3791-9304	···	2x300	1.54
2003-06-30	2452820.50	65	CLA	LD	3592-8980	···	75	1.82
2003-09-26	2452908.71	153	DUP	WF	3791-9304	···	2x600	1.47
			SN 2003hd					
2003-08-15	2452866.50	11	CLA	LD	3463-8658	···	450	1.22
2003-08-20	2452871.86	16	DUP	WF	3655-8970	···	2x900	1.01
2003-09-15	2452897.70	42	CLA	LD	3463-8658	···	450	1.15
2003-09-18	2452900.76	45	DUP	WF	3636-7003	···	3x900	1.02
2003-09-26	2452908.67	53	DUP	WF	3655-8970	···	2x900	1.14
2003-10-16	2452928.64	73	DUP	WF	3655-8970	···	900	1.09
2003-11-05	2452948.79	93	CLA	LD	3463-8658	···	450	1.48
2003-11-29	2452972.64	117	DUP	WF	3655-8970	···	2x1200	1.07
2003-12-16	2452989.66	134	DUP	WF	3655-8970	···	2x900	1.33
			SN 2003hg					
2003-09-07	2452889.61	24	CLA	LD	3551-8878	···	410	2.33
2003-09-15	2452897.65	32	CLA	LD	3551-8878	···	600	1.67
2003-09-18	2452900.68	35	DUP	WF	3729-7181	···	3x900	1.55
2003-10-16	2452928.57	63	DUP	WF	3748-9199	···	2x900	1.63
2003-11-29	2452972.54	107	DUP	WF	3748-9199	···	2x900	1.59
			SN 2003hk					
2003-09-18	2452900.84	34	DUP	WF	3696-7118	···	2x900	1.20
2003-09-26	2452908.77	42	DUP	WF	3715-9118	···	2x900	1.22
2003-10-16	2452928.79	62	DUP	WF	3715-9118	···	900	1.25
2003-11-29	2452972.69	106	DUP	WF	3715-9118	···	2x900	1.30
			SN 2003hl					
2003-09-18	2452900.79	32	DUP	WF	3749-7220	···	2x600	1.50
2003-09-26	2452908.73	40	DUP	WF	3768-9248	···	2x900	1.54
2003-10-16	2452928.71	60	DUP	WF	3768-9248	···	2x900	1.50
2003-11-05	2452948.77	80	CLA	LD	3570-8926	···	300	2.22
2003-11-23	2452966.68	98	DUP	WF	3768-9248	···	2x600	1.73
2003-12-23	2452996.59	128	DUP	WF	3768-9248	···	2x900	1.68
			SN 2003hn					
2003-09-15	2452897.85	31	CLA	LD	3586-8965	···	90	1.04
2003-09-18	2452900.87	34	DUP	WF	3765-7251	···	2x300	1.04
2003-09-26	2452908.82	42	DUP	WF	3785-9288	···	2x600	1.04
2003-10-16	2452928.83	62	DUP	WF	3785-9288	···	600	1.07
2003-11-05	2452948.82	82	CLA	LD	3586-8965	···	150	1.18
2003-11-23	2452966.81	100	DUP	WF	3785-9288	···	2x600	1.29
2003-12-16	2452989.74	123	DUP	WF	3785-9288	···	3x600	1.29
2003-12-23	2452996.68	130	DUP	WF	3785-9288	···	2x600	1.13
2004-02-05	2453040.69	174	CLA	LD	3586-8965	···	600	2.03
			SN 2003ho					
2003-09-07	2452889.53	41	CLA	LD	3549-8873	···	900	1.15
2003-09-15	2452897.59	49	CLA	LD	3549-8873	···	900	1.06
2003-09-18	2452900.58	52	DUP	WF	3727-7177	···	3x900	1.06
2003-09-26	2452908.55	60	DUP	WF	3746-9194	···	3x900	1.06
2003-11-23	2452966.58	118	DUP	WF	3746-9194	···	3x900	1.63
			SN 2003ib					
2003-09-18	2452900.65	9	DUP	WF	3900-7100	···	2x900	1.15
2003-09-26	2452908.52	17	DUP	WF	3850-8200	···	2x900	1.01
2003-10-16	2452928.54	37	DUP	WF	3800-9100	···	2x900	1.06
2003-11-16	2452959.52	68	CLA	LD	3800-8800	···	600	1.30
2003-11-23	2452966.54	75	DUP	WF	4100-9000	···	2x900	1.62
			SN 2003ip					
2003-10-16	2352928.61	32	DUP	WF	3700-9150	···	2x900	1.31
2003-11-05	2352948.65	52	CLA	LD	3600-8850	···	450	1.35
2003-11-23	2352966.64	70	DUP	WF	3900-9150	···	2x900	1.49
2003-12-16	2352989.63	93	DUP	WF	4400-9100	···	2x450	2.30
			SN 2003iq					

2003-10-16	2452928.5	9	DUP	WF	4800-9200	· · ·	2x1200	1.53
2003-11-05	2452948.5	29	CLA	LD	3700-9100	· · ·	300	1.86
2003-11-23	2452966.5	47	DUP	WF	3900-9200	· · ·	2x600	1.62
2003-12-16	2452989.5	70	DUP	WF	4000-9200	· · ·	180	3.27
2003-12-23	2452996.5	77	DUP	WF	3900-9200	· · ·	2x900	1.94
				SN 2004dy				
2004-09-07	2453255.61	15	DUP	MS	3663-7097	5.0	3x900	1.12⋆
2004-09-14	2453262.55	22	DUP	WF	3683-8951	8.0	3x900	1.18⋆
2004-09-20	2453268.58	28	DUP	WF	3683-8951	8.0	3x900	1.12⋆
				SN 2004ej				
2004-09-14	2453262.91	39	DUP	WF	3765-9151	8.0	480	2.54
2004-09-19	2453267.89	44	DUP	WF	4489-9531	8.0	600	2.59
2004-09-20	2453268.50	45	DUP	WF	3765-9151	8.0	300	2.32
2004-10-24	2453302.50	79	CLA	LD	3567-8918	14.0	3x300	1.56
2004-11-17	2453326.84	103	DUP	WF	3765-9240	8.0	3x600	1.23
2004-11-26	2453335.74	112	CLA	LD	3567-8918	14.0	3x300	1.93
2004-12-04	2453343.50	120	DUP	WF	3765-9151	8.0	500	1.05
2004-12-13	2453352.79	129	DUP	WF	3765-9151	8.0	3x900	1.13
2004-12-19	2453358.76	135	CLA	LD	3567-8918	14.0	3x450	1.17
				SN 2004er				
2004-10-24	2453302.79	31	CLA	LD	3547-8869	14.0	3x300	1.22
2004-11-17	2453326.73	55	DUP	WF	3744-9189	8.0	3x600	1.25
2004-11-25	2453334.71	63	CLA	LD	3547-8869	14.0	3x300	1.26
2004-12-04	2453343.68	72	DUP	WF	3744-9101	8.0	3x600	1.24
2004-12-09	2453348.66	77	DUP	WF	3744-9101	8.0	3x600	1.21
2004-12-13	2453352.68	81	DUP	WF	3744-9101	8.0	3x600	1.35
2004-12-17	2453356.60	85	T60	CS	3153-9436	14.0	3x160	1.14
2004-12-19	2453358.61	87	CLA	LD	3547-8869	14.0	3x400	1.14
2005-01-11	2453381.56	110	T60	CS	3153-9475	14.0	3x120	1.20
2005-03-17	2453446.50	175	DUP	WF	3744-9101	8.0	900	2.51
				SN 2004fb				
2004-10-24	2453302.58	44	DUP	WF	3723-9048	8.0	3x900	1.96
2004-11-17	2453326.54	68	CLA	LD	3527-8818	14.0	3x300	1.33
2004-11-26	2453335.52	77	CLA	LD	3527-8818	14.0	3x450	1.49
2004-12-04	2453343.54	85	DUP	WF	3723-9137	8.0	3x600	1.47
				SN 2004fc				
2004-10-24	2453302.69	9	CLA	LD	3578-8945	14.0	3x300	1.06
2004-11-17	2453326.71	33	DUP	WF	3776-9268	8.0	3x300	1.25
2004-11-25	2453334.69	41	CLA	LD	3578-8945	14.0	150	1.30
2004-12-04	2453343.62	50	DUP	WF	3776-9178	8.0	3x300	1.12
2004-12-09	2453348.63	55	DUP	WF	3776-9178	8.0	3x300	1.18
2004-12-13	2453352.60	59	DUP	WF	3776-9178	8.0	3x300	1.12
2004-12-17	2453356.54	63	T60	CS	3180-9517	14.0	3x900	1.07
2004-12-19	2453358.57	65	CLA	LD	3578-8945	14.0	3x200	1.09
2004-01-11	2453381.53	88	T60	CS	3180-9555	14.0	3x600	1.17
2004-02-12	2453413.53	120	DUP	WF	3776-9178	8.0	3x300	1.74
				SN 2004fx				
2004-11-17	2453326.81	23	DUP	WF	3766-9242	8.0	3x450	1.13
2004-11-25	2453334.73	31	CLA	LD	3568-8920	14.0	3x300	1.06
2004-12-04	2453343.74	40	DUP	WF	3766-9153	8.0	3x450	1.09
2004-12-09	2453348.81	45	DUP	WF	3766-9153	8.0	3x450	1.42
2004-12-17	2453356.68	53	T60	CS	3171-9491	14.0	3x120	1.07
2004-12-19	2453358.66	55	CLA	LD	3568-8920	14.0	3x300	1.06
2004-01-11	2453381.61	78	T60	CS	3171-9529	14.0	3x120	1.07
2004-02-04	2453405.63	102	DUP	WF	3766-9153	8.0	3x900	1.24
2004-02-08	2453409.61	106	DUP	WF	3766-9153	8.0	3x900	1.21
2004-02-12	2453413.60	110	DUP	WF	3766-9153	8.0	3x900	1.22
				SN 2005J				
2005-02-04	2453405.78	26	DUP	WF	3747-9107	8.0	3x700	1.30
2005-02-08	2453409.79	30	DUP	WF	3747-9107	8.0	3x700	1.30
2005-02-12	2453413.82	34	DUP	WF	3747-9107	8.0	3x700	1.30
2005-03-15	2453444.70	65	DUP	WF	3747-9107	8.0	3x600	1.30
2005-03-19	2453448.67	69	DUP	WF	3747-9107	8.0	3x600	1.30
2005-03-24	2453453.68	74	DUP	MS	3727-7171	5.0	3x900	1.30
2005-04-03	2453462.67	84	DUP	WF	3747-9107	8.0	3x800	1.30
2005-04-07	2453467.66	88	DUP	WF	3747-9107	8.0	3x800	1.30
2005-04-12	2453472.66	93	DUP	WF	3747-9107	8.0	3x600	1.30
2005-04-15	2453475.69	96	DUP	WF	3747-9107	8.0	3x600	1.40
2005-04-19	2453479.56	100	DUP	WF	3747-9107	8.0	3x600	1.40
				SN 2005K				
2005-02-08	2453409.68	40	DUP	WF	3698-8987	8.0	3x900	1.46
2005-02-12	2453413.71	44	DUP	WF	3698-8987	8.0	3x900	1.44
				SN 2005Z				
2005-02-04	2453405.74	9	DUP	WF	3727-9059	8.0	3x700	1.65
2005-02-08	2453409.76	13	DUP	WF	3727-9059	8.0	3x700	1.60

2005-02-12	2453413.78	17	DUP	WF	3727-9059	8.0	3x700	1.64
2005-03-15	2453444.66	48	DUP	WF	3727-9059	8.0	3x600	1.60
2005-03-19	2453448.61	52	DUP	WF	3727-9059	8.0	3x800	1.66
2005-03-24	2453453.50	57	DUP	MS	3707-7134	5.0	3x900	1.64
2005-04-03	2453462.62	67	DUP	WF	3727-9059	8.0	3x900	1.60
2005-04-07	2453467.61	71	DUP	WF	3727-9059	8.0	3x1200	1.60
2005-04-15	2453475.58	79	DUP	WF	3727-9059	8.0	3x900	1.60
			SN 2005af					
2005-02-12	2453413.86	93	DUP	WF	3792-9217	8.0	120	1.07
2005-03-15	2453444.78	124	DUP	WF	3792-9217	8.0	3x200	1.07
2005-03-19	2453448.74	128	DUP	WF	3792-9217	8.0	3x200	1.07
2005-03-24	2453453.75	133	DUP	MS	3772-7258	5.0	3x300	1.07
2005-04-03	2453463.75	143	DUP	WF	3792-9217	8.0	3x200	1.10
2005-04-07	2453467.84	147	DUP	WF	3792-9217	8.0	3x200	1.42
2005-04-12	2453472.76	152	DUP	WF	3792-9217	8.0	3x200	1.14
2005-04-15	2453475.80	155	DUP	WF	3792-9217	8.0	3x200	1.32
2005-04-19	2453479.75	159	DUP	WF	3792-9217	8.0	200	1.18
			SN 2005an					
2005-03-15	2453444.75	13	DUP	WF	3758-9133	8.0	3x600	1.01
2005-03-19	2453448.71	17	DUP	WF	3758-9133	8.0	3x600	1.01
2005-03-24	2453453.72	22	DUP	MS	3738-7193	5.0	3x800	1.00
2005-04-07	2453467.77	36	DUP	WF	3758-9133	8.0	3x600	1.16
2005-04-12	2453472.72	41	DUP	WF	3758-9133	8.0	3x600	1.07
2005-04-15	2453475.73	44	DUP	WF	3758-9133	8.0	3x600	1.11
2005-04-19	2453479.70	48	DUP	WF	3758-9133	8.0	3x600	1.06
			SN 2005dk					
2005-09-26	2453639.50	40	DUP	WF	3740-9090	8.0	3x600	1.11
2005-09-27	2453640.52	41	DUP	WF	3740-9090	8.0	3x600	1.12
2005-10-05	2453648.50	49	DUP	WF	3740-9090	8.0	3x600	1.12
2005-10-18	2453661.54	62	NTT	EM	3150-5217	6.0	3x300	1.18
2005-10-18	2453661.53	62	NTT	EM	5709-10040	9.0	3x300	1.26
2005-10-18	2453661.51	62	NTT	EM	3937-10040	9.0	3x300	1.22
2005-11-25	2453699.54	100	DUP	MS	3720-7176	5.0	3x1200	1.79
			SN 2005dn					
2005-09-26	2453639.55	37	DUP	WF	3759-9137	8.0	3x600	1.07
2005-10-05	2453648.53	46	DUP	WF	3759-9137	8.0	3x600	1.07
2005-10-18	2453661.56	59	NTT	EM	3166-5243	6.0	3x200	1.21
2005-10-18	2453661.59	59	NTT	EM	5738-10092	9.0	3x150	1.30
2005-10-18	2453661.58	59	NTT	EM	3957-10092	9.0	3x150	1.26
2005-11-06	2453680.53	78	T60	CS	3166-9454	14.0	3x900	1.27
2005-11-24	2453698.52	96	DUP	MS	3740-7212	5.0	3x1200	1.48
2005-11-25	2453699.51	97	T60	CS	3166-9483	14.0	3x900	1.45
			SN 2005dt					
2005-09-26	2453639.6	34	DUP	WF	3703-9000	8.0	3x900	1.02
			SN 2005dw					
2005-09-26	2453639.59	36	DUP	WF	3733-9074	8.0	3x900	1.01
2005-10-05	2453648.58	45	DUP	WF	3733-9074	8.0	3x900	1.00
2005-12-20	2453724.56	121	DUP	WF	3733-9074	8.0	1200	1.84
			SN 2005dx					
2005-09-26	2453639.78	24	DUP	WF	3698-8988	8.0	3x900	1.13
			SN 2005dz					
2005-09-26	2453639.70	20	DUP	WF	3728-9061	8.0	3x900	1.25
2005-10-05	2453648.71	29	DUP	WF	3728-9061	8.0	3x700	1.36
2005-10-18	2453661.68	42	NTT	EM	3139-5200	6.0	3x300	1.36*
2005-10-18	2453661.65	42	NTT	EM	3924-10008	9.0	3x300	2.09
2005-10-18	2453661.66	42	NTT	EM	3924-10008	9.0	3x300	1.27
2005-12-21	2453725.54	106	DUP	WF	3728-9061	8.0	3x1200	1.55
2005-12-23	2453727.53	108	DUP	WF	3728-9061	8.0	3x1200	1.57
			SN 2005es					
2005-10-05	2453648.67	10	DUP	WF	3659-8893	8.0	3x900	1.29
			SN 2005gz					
2005-10-18	2453661.63	11	NTT	EM	3887-9914	9.0	3x300	1.55*
			SN 2005lw					
2005-12-18	2453722.80	6	NTT	EM	3899-9944	9.0	3x450	1.33
2005-12-21	2453725.81	9	DUP	WF	3704-9003	8.0	3x900	1.24
2005-12-23	2453727.81	11	DUP	WF	3704-9003	8.0	3x900	1.22$^\clubsuit$
2005-01-26	2453761.84	45	CLA	LD	3696-5982	2.9	900	1.06$^\clubsuit$
2005-01-26	2453761.85	45	CLA	LD	5541-9731	4.7	900	1.08
2005-03-05	2453799.80	83	DUP	WF	3704-9003	8.0	3x900	1.24
2005-03-08	2453802.82	86	DUP	WF	3704-9003	8.0	3x900	1.37$^\clubsuit$
2005-03-15	2453809.71	93	CLA	LD	3800-6130	2.9	900	1.06$^\clubsuit$
2005-03-15	2453809.71	93	CLA	LD	5673-9950	4.7	900	1.05
2005-03-22	2453816.73	100	DUP	WF	3704-9003	8.0	900	1.13$^\clubsuit$
2005-03-24	2453818.78	102	DUP	WF	3704-9003	8.0	3x900	1.43$^\clubsuit$
2005-04-02	2453827.73	111	DUP	WF	3704-9003	8.0	3x900	1.25$^\clubsuit$

2005-04-24	2453849.58	133	DUP	WF	3704-9003	8.0	3x900	1.05$^{\clubsuit}$
2005-04-26	2453851.65	135	DUP	WF	3704-9003	8.0	3x1200	1.17$^{\clubsuit}$
			SN 2005me					
2006-02-28	2453794.52	77	DUP	WF	3715-9030	8.0	1200	1.88
			SN 2006Y					
2006-02-13	2453779.67	13	NTT	EM	3094-5124	6.0	3x300	1.15*
2006-02-13	2453779.70	13	NTT	EM	5608-9862	9.0	3x300	1.22*
2006-02-13	2453779.69	13	NTT	EM	3867-9862	9.0	3x300	1.19*
2006-02-27	2453793.63	27	DUP	WF	3674-8929	8.0	3x900	1.14
2006-03-05	2453799.54	33	DUP	WF	3674-8929	8.0	3x900	1.08
2006-03-08	2453802.60	36	DUP	WF	3674-8929	8.0	3x900	1.14
2006-03-14	2453808.59	42	CLA	LD	3659-5926	2.9	3x600	1.14
2006-03-14	2453808.59	42	CLA	LD	5485-9642	4.7	3x600	1.20
2006-03-22	2453816.55	50	DUP	WF	3674-8929	8.0	3x900	1.12
2006-03-23	2453817.57	51	DUP	WF	3674-8929	8.0	3x900	1.15
2006-03-30	2453824.51	58	DUP	WF	3674-8929	8.0	3x900	1.10
2006-04-23	2453848.48	82	DUP	WF	3674-8929	8.0	3x1200	1.14
2006-04-26	2453851.54	85	DUP	WF	3674-8929	8.0	3x1200	1.38
			SN 2006ai					
2006-03-05	2453799.61	18	DUP	WF	3707-9009	8.0	3x400	1.75
2006-03-08	2453802.68	21	DUP	WF	3707-9009	8.0	3x600	1.83
2006-03-15	2453809.56	28	CLA	LD	3692-6130	2.9	3x300	1.74*
2006-03-15	2453809.56	28	CLA	LD	5700-9725	4.7	3x300	1.75*
2006-03-15	2453809.66	28	NTT	EM	3121-5170	6.0	3x300	1.82*
2006-03-15	2453809.67	28	NTT	EM	3902-9950	9.0	3x300	1.84
2006-03-15	2453809.69	28	NTT	EM	5658-9950	9.0	3x300	1.87
2006-03-22	2453816.59	35	DUP	WF	3707-9009	8.0	3x600	1.78
2006-03-24	2453818.61	37	DUP	WF	3707-9009	8.0	3x600	1.80
2006-03-30	2453824.60	43	DUP	WF	3707-9009	8.0	3x600	1.81
2006-04-16	2453841.61	60	BAA	IM	3842-9670	4.0	3x600	1.91*
2006-04-25	2453850.50	69	DUP	WF	3707-9200	8.0	3x600	1.77
			SN 2006bc					
2006-03-30	2453824.55	9	DUP	WF	3782-9193	8.0	3x400	1.36
2006-04-16	2453841.53	26	BAA	IM	3824-9660	4.0	3x600	1.39
2006-04-21	2453847.49	31	DUP	WF	3782-9193	8.0	3x400	1.35
			SN 2006be					
2006-03-30	2453824.85	22	DUP	WF	3772-9169	8.0	3x200	1.88
2006-04-02	2453827.87	25	DUP	WF	3772-9169	8.0	3x300	1.99
2006-04-24	2453849.79	47	DUP	WF	3772-9169	8.0	4x600	1.88
2006-04-25	2453850.75	48	DUP	WF	3772-9169	8.0	3x400	1.86
			SN 2006bl					
2006-04-16	2453841.82	19	BAA	IM	3842-9500	4.0	3x900	1.42
2006-04-23	2453848.69	26	DUP	WF	3678-8940	8.0	3x600	1.56
2006-04-26	2453851.75	29	DUP	WF	3678-8940	8.0	3x600	1.38
			SN 2006ee					
2006-09-25	2454003.79	42	DUP	WF	3742-9094	8.0	3x900	1.37
2006-09-28	2454006.68	45	DUP	WF	3742-9094	8.0	3x900	1.39
2006-10-05	2454013.70	52	NTT	EM	3151-5219	6.0	3x300	1.37
2006-10-05	2454013.75	52	NTT	EM	5711-10044	9.0	3x300	1.41
2006-10-05	2454013.72	52	NTT	EM	3950-10044	9.0	3x300	1.39
2006-10-06	2454014.72	53	MGH	BC	3950-10044	3.1	3x600	1.05
2006-10-07	2454015.72	54	MGH	BC	3950-10044	3.1	3x600	1.05
2006-10-11	2454019.73	58	DUP	WF	3800-9200	8.0	3x600	1.05
2006-10-21	2454029.73	68	MGH	BC	3800-9200	3.1	3x600	1.09
2006-11-03	2454042.69	81	NTT	EM	4000-10100	9.0	3x900	1.62
2006-11-03	2454042.66	81	NTT	EM	3151-5219	6.0	3x400	1.42
2006-11-03	2454042.68	81	NTT	EM	5800-10100	9.0	3x400	1.38
2006-11-16	2454055.63	94	DUP	WF	3800-9200	8.0	3x900	1.38
			SN 2006it					
2006-10-08	2454016.58	10	CLA	LD	5940-10570	4.0	3x300	1.47
2006-10-10	2454018.53	12	DUP	WF	3800-9200	8.0	3x600	1.36
2006-10-13	2454021.49	15	DUP	WF	3800-9200	8.0	3x900	1.34
2006-11-03	2454042.55	36	NTT	EM	3150-5218	6.0	3x300	1.57
2006-11-03	2454042.54	36	NTT	EM	5710-10042	9.0	3x299	1.85
2006-11-03	2454042.52	36	NTT	EM	3949-10042	9.0	3x300	1.71
			SN 2006iw					
2006-10-08	2454016.61	6	CLA	LD	5849-10410	4.0	2x300	1.15*
2006-10-10	2454018.63	8	DUP	WF	3800-9200	8.0	3x1200	1.15
2006-10-13	2454021.58	11	DUP	WF	3800-9200	8.0	3x1800	1.18
2006-11-16	2454087.58	45	DUP	WF	3800-9200	8.0	3x900	1.16
2006-12-18	2454055.54	77	DUP	WF	3800-9200	8.0	3x900	1.95
			SN 2006ms					
2006-11-09	2454048.67	20	CLA	LD	5800-9826	4.7	2x300	2.71
2006-11-09	2454048.67	20	CLA	LD	3727-6038	2.9	2x300	2.61*
2006-11-16	2454055.51	27	DUP	WF	3800-9200	8.0	3x500	1.25

2006-11-22	2454061.56	33	DUP	WF	3800-9200	8.0	3x500	1.57
			SN 2006qr					
2006-12-13	2454082.76	20	DUP	BC	3627-9800	8.0	3x900	1.17
2006-12-18	2454087.85	25	DUP	WF	3745-9101	8.0	900	1.08
2007-01-01	2454101.82	39	CLA	LD	3651-6049	2.9	3x700	1.06
2007-01-01	2454101.78	39	CLA	LD	5690-9842	4.7	3x700	1.09
2007-01-13	2454113.82	51	DUP	BC	3960-10000	8.0	900	1.18
2007-01-14	2454114.80	52	DUP	BC	5075-9693	8.0	1200	1.11
2007-01-29	2454129.68	67	BAA	IM	4217-9500	4.0	3x1200	1.07
2007-02-25	2454156.66	94	DUP	WF	3800-9200	8.0	3x900	1.08
			SN 2007P					
2007-01-29	2454129.80	11	BAA	IM	4279-9525	4.0	3x900	1.01
2007-01-31	2454131.71	13	NTT	EM	3223-5280	6.0	3x400	1.03
2007-02-12	2454143.76	25	DUP	WF	3800-9200	8.0	3x1200	1.04
2007-02-13	2454144.85	26	DUP	WF	3800-9200	8.0	1200	1.38
2007-02-19	2454150.66	32	DUP	WF	3800-9200	8.0	3x1200	1.05
2007-04-18	2454208.64	90	DUP	WF	3800-9200	8.0	3x1000	1.21
			SN 2007U					
2007-02-11	2454142.56	9	DUP	WF	3800-9200	8.0	3x900	1.04
2007-02-12	2454143.53	10	DUP	WF	3800-9200	8.0	3x1200	1.00
2007-02-13	2454144.58	11	DUP	WF	3800-9200	8.0	3x1200	1.10
2007-02-19	2454150.61	17	DUP	WF	3800-9200	8.0	3x900	1.29
2007-03-04	2454163.60	30	NTT	EM	4000-10100	9.0	4x400	1.47
2007-03-14	2454173.54	40	DUP	BC	3429-9600	8.0	3x1200	1.22
2007-04-19	2454209.47	76	DUP	WF	3800-9200	8.0	3x900	1.41
			SN 2007W					
2007-02-19	2454150.81	20	DUP	WF	3800-9200	8.0	3x600	1.06
2007-02-25	2454156.88	26	DUP	WF	3800-9200	8.0	600	1.10
2007-03-04	2454163.80	33	NTT	EM	3961-10101	9.0	3x300	1.04
2007-03-14	2454173.76	43	DUP	BC	3430-9552	8.0	3x600	1.04
2007-04-12	2454202.77	72	DUP	WF	3800-9200	8.0	3x600	1.15
2007-04-18	2454208.79	78	DUP	WF	3800-9200	8.0	3x600	1.31
2007-05-11	2454231.77	101	DUP	BC	3344-9458	8.0	900	1.64
			SN 2007X					
2007-02-19	2454150.78	7	DUP	WF	3764-9148	8.0	3x300	1.18
2007-02-25	2454156.90	14	DUP	WF	3764-9148	8.0	300	1.02
2007-03-04	2454163.87	20	NTT	EM	3962-10100	9.0	3x300	1.01
2007-03-10	2454169.90	26	BAA	IM	3800-10180	6.0	300	1.08
2007-03-14	2454173.82	30	DUP	BC	3430-9626	8.0	3x400	1.01
2007-03-19	2454178.82	35	DUP	BC	3419-9600	8.0	3x400	1.01
2007-03-26	2454185.88	42	DUP	BC	3400-9600	8.0	3x400	1.15
2007-04-12	2454202.85	59	DUP	WF	3800-9200	8.0	300	1.20
2007-04-17	2454207.87	64	DUP	WF	3800-9200	8.0	3x300	1.35
2007-04-25	2454215.78	72	DUP	BC	3564-9714	8.0	3x500	1.09
2007-05-11	2454231.71	88	DUP	BC	3344-9460	8.0	3x400	1.05
			SN 2007Z					
2007-02-19	2454150.58	15	DUP	WF	3800-9200	8.0	3x900	1.74
2007-02-25	2454156.56	21	DUP	WF	3800-9200	8.0	3x900	1.73
			SN 2007aa					
2007-02-19	2454150.74	24	DUP	WF	3800-9200	8.0	3x300	1.17
2007-02-25	2454156.77	30	DUP	WF	3800-9200	8.0	3x500	1.13
2007-03-04	2454163.69	37	NTT	EM	3300-5274	6.0	3x300	1.26
2007-03-04	2454163.67	37	NTT	EM	5771-10150	9.0	3x300	1.17
2007-03-04	2454163.70	37	NTT	EM	3980-10150	9.0	3x300	1.20
2007-03-14	2454173.73	47	DUP	BC	3440-9630	8.0	3x600	1.13
2007-03-19	2454178.69	52	DUP	BC	3402-9580	8.0	3x600	1.14
2007-03-26	2454185.74	59	DUP	BC	3383-9600	8.0	3x600	1.20
2007-04-12	2454202.67	76	DUP	WF	3800-9200	8.0	3x500	1.15
2007-04-18	2454208.72	82	DUP	WF	3800-9200	8.0	3x400	1.38
2007-05-11	2454231.54	105	DUP	BC	3344-9550	8.0	3x900	1.13
			SN 2007ab					
2007-03-04	2454163.89	40	NTT	EM	4000-10180	9.0	3x400	1.18
2007-03-14	2454173.90	50	DUP	BC	3429-9600	8.0	600	1.12
2007-03-19	2454178.89	55	DUP	BC	3419-9530	8.0	3x900	1.12
2007-03-26	2454185.84	62	DUP	BC	3400-9550	8.0	3x1200	1.17
2007-04-17	2454207.90	84	DUP	WF	3800-9200	8.0	3x900	1.21
			SN 2007av					
2007-03-26	2454185.69	12	DUP	BC	3400-9600	8.0	3x600	1.42
2007-04-12	2454202.61	29	DUP	WF	3800-9200	8.0	3x400	1.34
2007-04-18	2454208.61	35	DUP	WF	3800-9200	8.0	3x400	1.38
2007-05-11	2454231.48	58	DUP	BC	3343-9530	8.0	3x400	1.32
			SN 2007bf					
2007-04-12	2454202.73	11	DUP	WF	3800-9200	8.0	3x900	1.41
2007-04-17	2454207.75	16	DUP	WF	3800-9200	8.0	3x900	1.44
2007-04-25	2454215.72	24	DUP	BC	3600-9650	8.0	3x900	1.42

2007-05-11	2454231.65	40	DUP	BC	3344-9500	8.0	3x900	1.41
			SN 2007hm					
2007-09-12	2454355.69	19	DUP	BC	3506-9600	8.0	3x900	1.29
2007-09-18	2454361.65	25	DUP	BC	3408-9550	8.0	3x900	1.18
2007-10-03	2454376.55	40	3P6	EF	5220-9260	4.0	3x900	1.08
2007-10-03	2454376.52	40	3P6	EF	3300-6075	2.7	3x900	1.09
2007-10-16	2454389.60	53	DUP	BC	3412-9500	8.0	3x1200	1.28
2007-11-05	2454409.54	73	DUP	WF	3800-9200	8.0	3x900	1.28
2007-11-17	2454421.53	85	BAA	IM	3900-10600	6.0	900	1.39
			SN 2007il					
2007-09-18	2454361.88	12	DUP	BC	3408-9500	8.0	3x1200	1.88
2007-10-03	2454376.74	27	3P6	EF	3300-6065	2.7	3x900	1.40
2007-10-03	2454376.78	27	3P6	EF	5108-9250	4.0	3x900	1.48
2007-10-16	2454389.72	40	DUP	BC	3412-9600	8.0	3x1200	1.40
2007-10-21	2454394.69	45	DUP	BC	3352-9530	8.0	3x900	1.39
2007-10-28	2454401.65	52	CLA	LD	4076-9250	7.0	3x900	1.38
2007-11-05	2454409.63	60	3P6	EF	3300-6060	20.0	3x900	1.44
2007-11-05	2454409.60	60	3P6	EF	5539-9240	30.0	3x900	1.39
2007-11-11	2454415.64	66	DUP	WF	3800-9200	8.0	3x900	1.41
2007-12-01	2454435.62	86	3P6	EF	5108-9262	30.0	3x900	1.51
2007-12-01	2454435.59	86	3P6	EF	3300-6060	20.0	3x900	1.41
2007-12-10	2454444.62	95	DUP	WF	3800-9200	8.0	1200	1.61
			SN 2007it					
2007-09-15	2454358.48	10	DUP	BC	3668-6822	8.0	2x150	1.58
2008-02-24	2454520.87	172	BAA	IM	3743-10700	7.0	600	1.03
2008-03-14	2454539.88	191	3P6	EF	3286-6006	20.0	3x300	1.09
2008-03-14	2454539.87	191	3P6	EF	5199-9203	30.0	400	1.07
2008-04-07	2454563.83	215	DUP	WF	3800-9200	8.0	3x600	1.14
2008-04-12	2454568.86	220	DUP	WF	3800-9200	8.0	3x600	1.29
2008-04-13	2454569.80	221	DUP	WF	3800-9200	8.0	3x900	1.10
2008-04-26	2454582.75	234	BAA	IM	3879-10370	6.0	600	1.07
2008-04-29	2454585.76	237	DUP	WF	3800-9200	8.0	3x600	1.10
2008-05-12	2454598.72	250	DUP	WF	3800-9200	8.0	3x600	1.09
2008-05-30	2454616.74	268	DUP	BC	3476-9660	8.0	3x600	1.34
			SN 2007ld					
2007-10-08	2454381.5	5	BAA	IM	3900-9950	4.0	900	1.14
2007-10-16	2454389.5	13	DUP	BC	3412-9500	8.0	1200	1.19
2007-10-21	2454394.5	18	DUP	BC	3352-9400	8.0	900	1.16
2007-10-28	2454401.5	25	CLA	LD	4076-9278	7.0	970	1.22
2007-11-04	2454408.5	32	3P6	EF	3300-6060	20.0	600	1.22
2007-11-04	2454408.5	32	3P6	EF	5660-9250	30.0	600	1.30
2007-11-11	2454415.5	39	DUP	WF	3800-9200	8.0	900	1.48
			SN 2007oc					
2007-11-04	2454408.56	20	3P6	EF	3300-6017	20.0	3x300	1.01
2007-11-04	2454408.55	20	3P6	EF	5660-9195	30.0	3x300	1.02
2007-11-05	2454409.64	21	DUP	WF	3800-9200	8.0	3x300	1.23
2007-11-11	2454415.60	27	DUP	WF	3800-9200	8.0	3x300	1.12
2007-11-17	2454421.56	33	BAA	IM	3809-10670	6.0	3x100	1.08
2007-11-19	2454423.61	35	NTT	EM	3200-5300	6.0	3x200	1.27
2007-11-19	2454423.63	35	NTT	EM	5800-10180	9.0	3x200	1.44
2007-11-19	2454423.64	35	NTT	EM	4000-10180	9.0	3x199	1.36
2007-11-26	2454430.57	42	CLA	MA	3100-9450	0.5	2x600	1.15
2007-11-30	2454434.53	46	3P6	EF	3300-6065	20.0	3x300	1.05
2007-11-30	2454434.52	46	3P6	EF	5660-9240	30.0	3x300	1.08
2007-12-03	2454437.54	49	DUP	WF	3800-9200	8.0	3x300	1.13
2007-12-09	2454443.62	55	DUP	WF	3800-9200	8.0	3x400	1.71
2007-12-17	2454451.55	63	BAA	IM	3873-10670	6.0	3x200	1.36
2007-12-18	2454452.54	64	NTT	EM	3200-5262	6.0	3x300	1.31
2007-12-18	2454452.57	64	NTT	EM	5790-10190	9.0	3x300	1.53
2007-12-18	2454452.56	64	NTT	EM	3980-10190	9.0	3x300	1.42
			SN 2007od					
2007-11-04	2454408.60	8	3P6	EF	3300-6045	20.0	3x300	1.49
2007-11-04	2454408.59	8	3P6	EF	5660-9243	30.0	3x300	1.51
2007-11-05	2454409.59	9	DUP	WF	3300-9200	8.0	3x300	1.50
2007-11-11	2454415.57	15	DUP	WF	3800-9200	8.0	3x300	1.50
2007-11-17	2454421.55	21	BAA	IM	3809-10670	6.0	3x100	1.48
2007-11-19	2454423.52	23	NTT	EM	3200-5269	6.0	3x200	1.49
2007-11-19	2454423.55	23	NTT	EM	5800-10180	9.0	3x200	1.49
2007-11-19	2454423.54	23	NTT	EM	4000-10180	9.0	3x200	1.49
2007-12-01	2454435.53	35	3P6	EF	3300-6074	20.0	3x300	1.50
2007-12-01	2454435.52	35	3P6	EF	5220-9257	30.0	3x300	1.53
2007-12-03	2454437.57	37	DUP	WF	3800-9200	8.0	3x400	1.71
2007-12-10	2454444.58	44	DUP	WF	3800-9200	8.0	3x400	1.97
2007-12-17	2454451.53	51	BAA	IM	3809-10670	6.0	3x200	1.74
2008-01-04	2454469.54	69	3P6	EF	3300-6073	20.0	3x400	2.52

			SN 2007sq					
2007-12-18	2454452.77	30	NTT	EM	4000-10100	9.0	4x1800	1.07
2007-12-27	2454461.81	39	BAA	IM	3800-9450	6.0	1200	1.01⋆
2007-12-28	2454462.79	40	BAA	IM	3800-9450	6.0	3x1200	1.02
2008-01-03	2454468.70	46	3P6	EF	3300-6070	20.0	3x1200	1.13
2008-01-03	2454468.74	46	3P6	EF	5220-9257	30.0	3x1200	1.03
2008-01-05	2454470.73	48	DUP	BC	4166-10200	8.0	3x1200	1.05
2008-02-25	2454521.68	99	CLA	LD	3650-9420	7.0	3x1200	1.04
			SN 2008F					
2008-01-17	2454482.61	13	NTT	EM	4000-10180	9.0	3x1200	1.41
2008-01-26	2454491.61	22	DUP	BC	4859-9500	8.0	3x900	1.58⋆
			SN 2008H					
2008-01.17	2454482.82	50	NTT	EM	4000-10180	9.0	3x600	1.03
			SN 2008K					
2008-01-17	2454482.78	7	NTT	EM	4000-10200	9.0	3x900	1.11
2008-01-26	2454491.74	16	DUP	BC	4859-9500	8.0	3x900	1.17
2008-02-01	2454497.75	22	DUP	BC	3510-9650	8.0	3x1200	1.08
2008-02-14	2454510.75	35	NTT	EM	4000-10200	9.0	900	1.02
2008-02-19	2454515.74	40	CLA	MA	3102-9470	0.5	1200	1.02
2008-02-24	2454520.77	45	BAA	IM	6390-10700	7.0	3x200	1.78
2008-03-09	2454534.80	59	BAA	IM	4500-10700	6.0	900	1.11
2008-03-14	2454539.70	64	3P6	EF	3300-6030	20.0	3x900	1.00
2008-03-14	2454539.73	64	3P6	EF	5220-9220	30.0	3x900	1.02
2008-03-31	2454556.70	81	DUP	WF	3800-9200	8.0	3x900	1.04
2008-04-12	2454568.69	93	DUP	WF	3800-9200	8.0	3x900	1.07
2008-04-26	2454582.63	107	BAA	IM	4300-10360	6.0	3x900	1.03
			SN 2008M					
2008-01-26	2454491.66	20	DUP	BC	4859-9700	8.0	3x300	1.18
2008-01-27	2454492.75	21	3P6	EF	3300-6073	20.0	3x300	1.44
2008-01-27	2454492.76	21	3P6	EF	5230-9260	30.0	3x300	1.49
2008-02-01	2454497.65	26	DUP	BC	3510-9685	8.0	3x300	1.20
2008-02-13	2454509.68	38	NTT	EM	4000-10220	9.0	3x600	1.33
2008-02-25	2454521.63	50	CLA	LD	3620-9422	7.0	3x600	1.28
2008-03-13	2454538.53	67	3P6	EF	3300-6073	20.0	3x400	1.16
2008-03-13	2454538.51	67	3P6	EF	5230-9260	30.0	3x400	1.18
2008-03-19	2454544.50	73	CLA	MA	3327-9465	0.5	1200	1.17
2008-03-20	2454545.56	74	CLA	LD	3601-9430	7.0	3x600	1.28
2008-03-31	2454556.52	85	DUP	WF	3800-9200	8.0	3x900	1.24
2008-04-13	2454569.48	98	DUP	WF	3800-9200	8.0	3x1200	1.24
			SN 2008W					
2008-02-13	2454509.71	26	NTT	EM	4000-10130	9.0	3x600	1.05
2008-02-19	2454515.69	32	CLA	MA	3150-9470	0.5	1200	1.04
2008-02-24	2454520.72	32	BAA	IM	4000-10715	7.0	3x900	1.16
2008-03-14	2454539.62	56	3P6	EF	3300-6075	20.0	3x900	1.04
2008-03-14	2454539.66	56	3P6	EF	5220-9260	30.0	3x900	1.12
2008-03-20	2454545.61	62	CLA	LD	3630-9430	7.0	3x900	1.05
2008-04-07	2454563.59	80	DUP	WF	3800-9200	8.0	3x600	1.14
2008-04-13	2454569.59	86	DUP	WF	3800-9200	8.0	3x900	1.18
2008-05-12	2454598.54	115	DUP	WF	3800-9200	8.0	1200	1.30
2008-05-22	2454608.50	125	BAA	IM	4500-10700	7.0	3x900	1.25
			SN 2008ag					
2008-02-13	2454509.88	32	NTT	EM	3500-5295	6.0	3x600	1.80
2008-02-13	2454509.85	32	NTT	EM	4000-10150	9.0	3x600	1.98
2008-02-24	2454520.90	43	BAA	IM	3743-10716	7.0	600	1.54
2008-02-25	2454521.87	44	CLA	LD	3620-9405	7.0	3x900	1.67
2008-03-13	2454538.85	61	3P6	EF	3300-6030	20.0	3x600	1.54
2008-03-13	2454538.85	61	3P6	EF	5230-9240	30.0	3x600	1.45
2008-03-19	2454544.87	67	CLA	MA	3303-9450	0.5	1200	1.41
2008-03-20	2454545.91	68	CLA	LD	3630-9430	7.0	900	1.33
2008-03-28	2454553.86	76	NTT	EM	3500-5300	6.0	3x300	1.36
2008-03-28	2454553.88	76	NTT	EM	4000-10150	9.0	3x200	1.32
2008-04-07	2454563.87	86	DUP	WF	3800-9200	8.0	3x600	1.32
2008-04-12	2454568.90	91	DUP	WF	3800-9200	8.0	600	1.28
2008-04-13	2454569.86	92	DUP	WF	3800-9200	8.0	3x1200	1.31
2008-04-25	2454581.87	104	BAA	IM	4200-10370	6.0	3x600	1.27
2008-05-12	2454598.80	121	DUP	WF	3800-9200	8.0	3x600	1.28
2008-05-16	2454602.81	125	BAA	IM	4200-10570	7.0	3x900	1.27
2008-05-22	2454608.77	131	BAA	IM	4500-10700	7.0	3x600	1.29
2008-05-30	2454616.77	139	DUP	BC	3480-9660	8.0	3x900	1.27
			SN 2008aw					
2008-03-13	2454538.81	21	3P6	EF	3300-6030	20.0	3x400	1.07
2008-03-13	2454538.81	21	3P6	EF	5230-9220	30.0	3x400	1.10
2008-03-19	2454544.76	27	CLA	MA	3240-9460	0.5	900	1.05
2008-03-20	2454545.84	28	CLA	LD	3650-9400	7.0	3x600	1.26
2008-03-28	2454553.79	36	NTT	EM	3330-6030	6.0	3x200	1.12

2008-03-28	2454556.81	36	NTT	EM	4000-10170	9.0	3x200	1.16
2008-03-31	2454569.75	39	DUP	WF	3800-9200	8.0	3x400	1.28
2008-04-13	2454582.75	52	DUP	WF	3800-9200	8.0	3x700	1.17
2008-04-26	2454585.72	65	CLA	LD	3650-9450	7.0	3x600	1.30
2008-04-29	2454597.68	68	DUP	WF	3800-9200	8.0	3x600	1.20
2008-05-11	2454616.70	80	DUP	WF	3800-9200	8.0	3x500	1.18
2008-05-30		99	DUP	BC	3480-9640	8.0	3x900	1.70
			SN 2008bh					
2008-03-28	2454553.66	10	NTT	EM	4000-10000	9.0	3x299	1.50
2008-03-31	2454556.59	13	DUP	WF	3800-9200	8.0	3x600	1.19
2008-04-13	2454569.65	26	DUP	WF	3800-9200	8.0	1200	1.87
2008-04-26	2454582.52	39	CLA	LD	3650-9400	7.0	3x900	1.16
2008-05-05	2454591.51	48	DUP	WF	3800-9200	8.0	3x900	1.21
2008-05-12	2454598.49	55	DUP	WF	3800-9200	8.0	3x900	1.21
			SN 2008bk					
2008-04-12	2454568.92	28	DUP	WF	3797-9228	8.0	120	2.36
2008-04-13	2454569.91	29	DUP	WF	3797-9228	8.0	120	2.50
2008-04-25	2454581.92	41	BAA	IM	3876-10367	6.0	3x60	1.74
2008-04-26	2454582.91	42	BAA	IM	3875-10367	6.0	6x60	1.73
2008-04-26	2454582.90	42	CLA	LD	3623-9425	7.0	3x120	1.88
2008-05-05	2454591.93	51	DUP	WF	3797-9228	8.0	3x120	1.40
2008-05-11	2454597.88	57	DUP	WF	3797-9228	8.0	120	1.69
2008-05-12	2454598.90	58	DUP	WF	3797-9228	8.0	3x120	1.46
2008-05-16	2454602.91	62	BAA	IM	3923-10580	6.0	100	1.28
2008-05-22	2454608.91	68	BAA	IM	3878-10858	7.0	3x60	1.21
2008-05-30	2454616.84	76	DUP	BC	3473-9672	8.0	4x120	1.49
2008-06-04	2454621.81	81	DUP	BC	3572-9768	8.0	3x600	1.72
2008-06-16	2454633.88	93	BAA	IM	3455-9479	2.0	3x200	1.09
2008-09-15	2454724.64	184	BAA	IM	4024-10717	7.0	4x600	1.06
2008-09-17	2454726.59	186	CLA	LD	3643-9452	7.0	4x600	1.23
2008-09-21	2454730.76	190	DUP	WF	3797-9228	8.0	3x600	1.08
2008-09-28	2454737.73	197	DUP	WF	3797-9228	8.0	3x600	1.05
2008-09-29	2454738.63	198	DUP	WF	3797-9228	8.0	3x600	1.03
2008-10-14	2454753.59	213	NTT	EF	3398-6015	27.0	3x900	1.02
2008-10-14	2454753.66	213	NTT	EF	5236-9203	39.0	3x900	1.01
2008-11-05	2455505.61	235	BAA	IM	3973-10049	7.0	4x180	1.01
2008-11-20	2454790.65	250	NTT	EF	3297-5999	27.0	3x400	1.27
2008-11-20	2454790.68	250	NTT	EF	5236-9203	39.0	3x400	1.47
2008-11-25	2454795.66	255	DUP	WF	3797-9228	8.0	900	1.40
2008-12-10	2454810.57	270	NTT	EF	3297-5999	27.0	3x400	1.10
2008-12-10	2454810.55	270	NTT	EF	5236-9203	39.0	3x400	1.17
			SN 2008bm					
2008-04-07	2454563.76	41	DUP	WF	3800-9200	8.0	3x900	1.44
2008-04-13	2454569.70	47	DUP	WF	3800-9200	8.0	3x900	1.32
2008-04-26	2454582.72	60	CLA	LD	3512-9137	7.0	3x900	1.46
2008-05-15	2454601.65	74	BAA	IM	4064-10245	7.0	3x700	1.41
			SN 2008bp					
2008-04-07	2454563.72	12	DUP	WF	3765-9151	8.0	3x1200	1.42
2008-04-26	2454582.57	31	BAA	IM	4207-10670	7.0	3x900	1.07
2008-05-05	2454591.65	40	DUP	WF	3765-9151	8.0	3x900	1.48
2008-05-12	2454598.60	47	DUP	WF	3765-9151	8.0	3x1200	1.3
2008-05-22	2454608.55	57	BAA	IM	4390-10670	7.0	3x900	1.19
			SN 2008br					
2008-04-12	2454568.50	13	DUP	WF	3761-9142	8.0	3x900	1.01
2008-04-26	2454582.50	27	CLA	LD	3590-9338	7.0	3x900	1.05
2008-05-05	2454591.50	36	DUP	WF	3761-9142	8.0	3x900	1.07
2008-05-12	2454598.50	43	DUP	WF	3761-9142	8.0	3x900	1.13
			SN 2008bu					
2008-04-22	2454578.74	12	CLA	LD	3619-10502	7.0	900	1.11
2008-04-25	2454581.84	12	BAA	IM	4153-10148	6.0	3x900	1.03
2008-04-26	2454582.82	12	BAA	IM	4163-10161	6.0	3x1200	1.01
2008-05-12	2454598.75	32	DUP	WF	3716-9032	8.0	3x1200	1.01
2008-05-16	2454602.75	36	BAA	IM	4105-10354	6.0	3x1200	1.01
			SN 2008ga					
2008-10-27	2454766.81	55	DUP	WF	3800-9235	8.0	3x1800	1.48
2008-11-20	2454790.79	79	NTT	EF	3300-6003	27.0	3x600	1.65*
2008-12-21	2454821.65	110	DUP	WF	3800-9235	8.0	3x1200	1.49
			SN 2008gi					
2008-10-14	2454753.70	11	NTT	EF	3319-5874	27.0	3x900	1.27*
2008-10-14	2454753.73	11	NTT	EF	5113-8987	39.0	3x600	1.21*
2008-10-20	2454759.77	17	DUP	WF	3708-9011	8.0	900	1.26
2008-10-27	2454766.75	24	DUP	WF	3708-9011	8.0	3x1200	1.24
2008-11-04	2454774.62	32	CLA	LD	3548-9209	7.0	3x900	1.35
2008-12-22	2454822.62	80	DUP	WF	3708-9011	8.0	4x1200	1.30
			SN 2008gr					

2008-11-02	2454772.59	3	BAA	IM	3934-10470	6.0	800	1.00
2008-11-19	2454789.61	20	NTT	EF	3225-5868	27.0	3x600	1.02
2008-11-23	2454793.67	24	DUP	WF	3714-9026	8.0	3x700	1.24
2008-12-15	2454815.60	46	CLA	LD	3538-9217	7.0	3x400	1.22
2008-12-29	2454829.60	60	DUP	WF	3714-9026	8.0	3x900	1.39
			SN 2008hg					
2008-11-19	2454789.57	10	NTT	EF	3238 5891	27.0	5x600	1.02
2008-11-20	2454790.71	11	NTT	EF	5141 9037	39.0	3x600	1.21
2008-11-23	2454793.73	14	DUP	WF	3728 9061	8.0	3x800	1.34
2008-12-08	2454808.62	29	BAA	IM	3947 10522	6.0	4x900	1.07
2008-12-10	2454810.61	31	NTT	EF	3238 5891	27.0	3x400	1.08
2008-12-10	2454810.64	31	NTT	EF	5141 9037	39.0	3x400	1.14
			SN 2008ho					
2008-12-10	2454810.67	18	NTT	EF	3266-5942	27.0	3x400	1.18
2008-12-10	2454810.70	18	NTT	EF	5186-9115	39.0	3x400	1.29
2008-12-15	2454815.63	23	CLA	LD	3582-9333	7.0	600	1.07
			SN 2008if					
2008-12-18	2454818.79	11	CLA	LD	3588-9322	7.0	3x600	1.12
2008-12-20	2454820.79	13	DUP	WF	3757-9130	8.0	3x600	1.11
2008-12-21	2454821.74	14	DUP	WF	3757-9130	8.0	3x600	1.28
2008-12-22	2454822.74	15	DUP	WF	3757-9130	8.0	3x600	1.27
2008-12-23	2454823.78	16	DUP	WF	3757-9130	8.0	3x600	1.11
2008-12-24	2454824.78	17	DUP	WF	3757-9130	8.0	3x600	1.12
2008-12-27	2454827.50	20	DUP	WF	3757-9130	8.0	3x600	1.09
2008-12-29	2454829.81	22	DUP	WF	6478-10007	8.0	600	1.07
2009-01-05	2454836.71	29	CLA	LD	3579-9322	7.0	900	1.23
2009-01-17	2454848.76	41	CLA	LD	3587-9332	7.0	100	1.07
2009-01-22	2454853.81	46	CLA	LD	3579-9321	7.0	300	1.17
2009-02-11	2454873.73	66	BAA	IM	3987-10007	5.0	3x400	1.09
2009-02-16	2454878.66	71	BAA	IM	3975-9997	5.0	400	1.07
2009-02-23	2454885.67	78	DUP	WF	3757-9130	8.0	3x400	1.08
2009-02-25	2454887.70	80	DUP	WF	3757-9130	8.0	3x600	1.11
2009-03-16	2454906.62	99	BAA	IM	3980-10111	11.0	3x500	1.07
2009-03-28	2454918.60	111	DUP	WF	3757-9130	8.0	3x900	1.09
2009-04-03	2454924.54	117	DUP	WF	3757-9130	8.0	3x900	1.07
2009-04-17	2454938.54	131	CLA	LD	3672-9328	7.0	900	1.08
2009-04-22	2454943.54	136	DUP	BC	3322-9462	8.0	3x900	1.09
			SN 2008il					
2008-12-28	2454888.51	3	DUP	WF	3721-9044	8.0	3x600	1.04
2008-12-29	2454828.57	4	DUP	WF	3721-9044	8.0	3x600	1.33
2009-02-26	2454829.65	63	DUP	WF	3721-9044	8.0	3x900	1.47
			SN 2008in					
2008-12-29	2454829.83	4	DUP	WF	3780-9186	8.0	500	1.53
2009-01-09	2454840.83	15	NTT	EF	3282-5972	20.0	300	1.33
2009-01-09	2454840.80	15	NTT	EF	5212-9162	30.0	3x300	1.52
2009-01-22	2454853.82	28	CLA	LD	3601-9379	7.0	3x300	1.20
2009-02-08	2454870.79	45	CLA	LD	3696-9389	7.0	300	1.22
2009-02-11	2454873.78	48	BAA	IM	4011-10066	5.0	3x300	1.22
2009-02-25	2454887.77	62	DUP	WF	3780-9186	8.0	3x400	1.21
2009-03-16	2454990.20	81	NTT	EF	3282-5972	27.0	3x400	1.21
2009-03-16	2454990.20	81	NTT	EF	5212-9162	39.0	3x400	1.22
2009-03-29	2454919.76	94	DUP	WF	3780-9186	8.0	3x900	1.31
2009-04-03	2454924.70	99	DUP	WF	3780-9186	8.0	900	1.23
2009-04-17	2454938.63	113	CLA	LD	3694-9385	7.0	3x700	1.22
2009-04-23	2454944.71	119	DUP	BC	3343-9517	8.0	3x900	1.41
			SN 2009A					
2009-01-05	2454836.56	15	CLA	LD	3558-9268	7.0	600	1.23□
2009-01-09	2454840.56	19	NTT	EF	3244-5901	27.0	3x400	1.44□
2009-01-09	2454840.58	19	NTT	EF	5151-9053	39.0	3x400	1.29□
2009-02-08	2454870.56	49	CLA	LD	3652-9265	7.0	600	2.24□
2009-02-09	2454871.55	50	CLA	LD	3652-9276	7.0	3x600	2.17□
			SN 2009N					
2009-02-08	2454870.80	24	CLA	LD	3703-9406	7.0	3x300	1.08
2009-02-09	2454871.77	25	CLA	LD	3703-9405	7.0	3x600	1.15
2009-02-11	2454873.81	27	BAA	IM	4018-10084	5.0	3x300	1.07
2009-02-24	2454886.81	40	DUP	WF	3786-9203	8.0	3x300	1.09
2009-02-25	2454887.84	41	DUP	WF	3786-9203	8.0	3x400	1.15
2009-02-26	2454888.83	42	DUP	WF	3786-9203	8.0	3x400	1.12
2009-03-15	2454905.84	59	BAA	IM	4012-10078	5.0	400	1.32
2009-03-29	2454919.80	73	DUP	WF	3786-9203	8.0	3x700	1.29
2009-04-03	2454924.73	78	DUP	WF	3786-9203	8.0	700	1.11
2009-04-18	2454939.66	93	DUP	BC	3438-9625	8.0	3x900	1.07
2009-04-23	2454944.76	98	DUP	BC	3349-9534	8.0	3x900	1.46
2009-05-01	2454952.66	106	CLA	LD	3708-9412	7.0	3x700	1.11
2009-05-23	2454974.61	128	DUP	BC	3348-9532	8.0	3x900	1.14

			SN 2009W					
2009-08-02	2454870.87	54	CLA	LD	3654-9283	7.0	600	1.90
			SN 2009aj					
2009-02-26	2454888.72	8	DUP	WF	3763-9146	8.0	3x300	1.27
2009-03-11	2454901.89	21	BAA	IM	3988-10025	5.0	3x400	1.16
2009-03-16	2454990.20	26	NTT	EF	3268-5946	27.0	3x400	1.06
2009-03-16	2454990.20	26	NTT	EF	5189-9121	39.0	3x400	1.07
2009-03-28	2454918.83	38	DUP	WF	3763-9146	8.0	3x600	1.13
2009-04-03	2454924.79	44	DUP	WF	3763-9146	8.0	3x600	1.09
2009-04-17	2454938.77	58	CLA	LD	3678-9344	7.0	3x600	1.11
2009-04-18	2454939.70	59	DUP	BC	3416-9564	8.0	3x900	1.06
2009-04-22	2454943.69	63	DUP	BC	3327-9475	8.0	3x900	1.06
2009-04-23	2454944.84	64	DUP	BC	3329-9475	8.0	3x900	1.40
2009-04-30	2454951.79	71	CLA	LD	3666-9354	7.0	3x600	1.29
2009-05-14	2454965.64	85	BAA	IM	3935-10035	5.0	3x600	1.06
			SN 2009ao					
2009-03-15	2454905.54	15	BAA	IM	3981-10001	5.0	3x600	1.46
2009-03-16	2454906.66	16	BAA	IM	3981-10001	11.0	3x900	1.32
2009-03-28	2454918.64	28	DUP	WF	3757-9132	8.0	3x600	1.40
2009-04-03	2454924.59	34	DUP	WF	3757-9132	8.0	3x900	1.30
2009-04-18	2454939.54	49	DUP	BC	3411-9551	8.0	3x900	1.28
2009-04-23	2454944.56	54	DUP	BC	3324-9462	8.0	3x1000	1.36
2009-05-01	2454952.49	62	CLA	LD	3679-9340	7.0	3x800	1.27
			SN 2009au					
2009-03-15	2454905.80	8	BAA	IM	3988-10017	5.0	3x500	1.03
2009-03-16	2454990.20	9	NTT	EF	3269-5947	27.0	3x500	1.01
2009-03-16	2454990.20	9	NTT	EF	5190-9123	39.0	3x500	1.04
2009-03-28	2454918.80	21	DUP	WF	3764-9148	8.0	3x500	1.10
2009-03-29	2454919.87	22	DUP	WF	3764-9148	8.0	3x900	1.45
2009-04-03	2454924.75	27	DUP	WF	3764-9148	8.0	3x700	1.03
2009-04-17	2454938.73	41	CLA	LD	3679-9346	7.0	3x700	1.07
2009-04-22	2454943.65	46	DUP	BC	3328-9477	8.0	3x900	1.00
2009-05-01	2454952.74	55	CLA	LD	3686-9356	7.0	3x900	1.23
2009-05-23	2454974.65	77	DUP	BC	3328-9475	8.0	3x900	1.11
			SN 2009bu					
2009-03-29	2454919.91	18	DUP	WF	3755-9127	8.0	600	1.98
2009-04-03	2454924.90	23	DUP	WF	3321-9454	8.0	3x900	1.43
2009-04-18	2454939.87	38	DUP	BC	3678-9335	8.0	3x600	1.47
2009-04-23	2454944.88	43	DUP	BC	3410-9544	8.0	4x700	1.85
2009-05-01	2454952.90	51	CLA	LD	3410-9544	7.0	4x700	1.85
2009-05-23	2454974.85	73	DUP	BC	3322-9455	8.0	3x900	1.69
			SN 2009bz					
2009-04-03	2454924.85	9	DUP	WF	3759-9136	8.0	3x700	1.37
2009-04-18	2454939.75	24	DUP	BC	3413-9553	8.0	3x900	1.31
2009-04-22	2454943.73	28	DUP	BC	3323-9465	8.0	3x900	1.31
2009-05-01	2454952.71	37	CLA	LD	3681-9343	7.0	3x600	1.31
2009-05-14	2454965.72	50	BAA	IM	3931-10025	5.0	3x600	1.33

Columns: (1) UT date of the observation; (2) Julian date of the observation; (3) Phase in days since explosion; (4) Telescope code – 3P6: ESO 3.6-m Telescope; BAA: Las Campanas Magellan I 6.5-m Baade Telescope; CLA: Las Campanas Magellan II 6.5-m Clay Telescope; DUP: Las Campanas 2.5-m du Pont Telescope Telescope; NTT: New Technology Telescope; (5) Instrument code – BC: Boller & Chivens spectrograph; EF: ESO Faint Object Spectrograph and Camera (EFOSC-2); EM: ESO Multi-Mode Instrument (EMMI); IM: Inamori Magellan Areal Camera and Spectrograph (IMACS), LD: Low Dispersion Survey Spectrograph (LDSS); WF: Wide Field Reimaging CCD Camera (WFCCD); (6) Wavelength range covered; (7) Spectral resolution in Å as estimated from arc-lamp lines; (8) Total exposure time; (9) Airmass at the middle of the observation.

⋆ Spectra with low S/N

□ Peculiar SN

♣ Spectra with defects resulting from the observing procedure or data reduction.

The distribution of the number of spectra per object for our sample is shown in Figure 3.2. Seven SNe (SN 1993A, SN 2005dt, SN 2005dx, SN 2005es, SN 2005gz, SN2005me, SN 2008H) only have one spectrum, while 90% of the sample have between two and twelve spectra. SN 1986L is the object with the most spectra (31), followed by SN 2008bk with 26. On average we have 7 spectra per SNe and a median of 6. There are 88 SNe II for which we have five or more spectra, 32 that have ten or more, and 6 objects with over 15 spectra (SN 2007oc, SN 2008ag, SN 2008if, SN 1993K, SN 2008bk and SN 1986L). In the current work, 3% of our obtained spectra are not used for analysis. This is due to low S/N that does not allow useful extraction of our defined parameters. However, these spectra are still included in the data release, and are noted in Table 3.2.

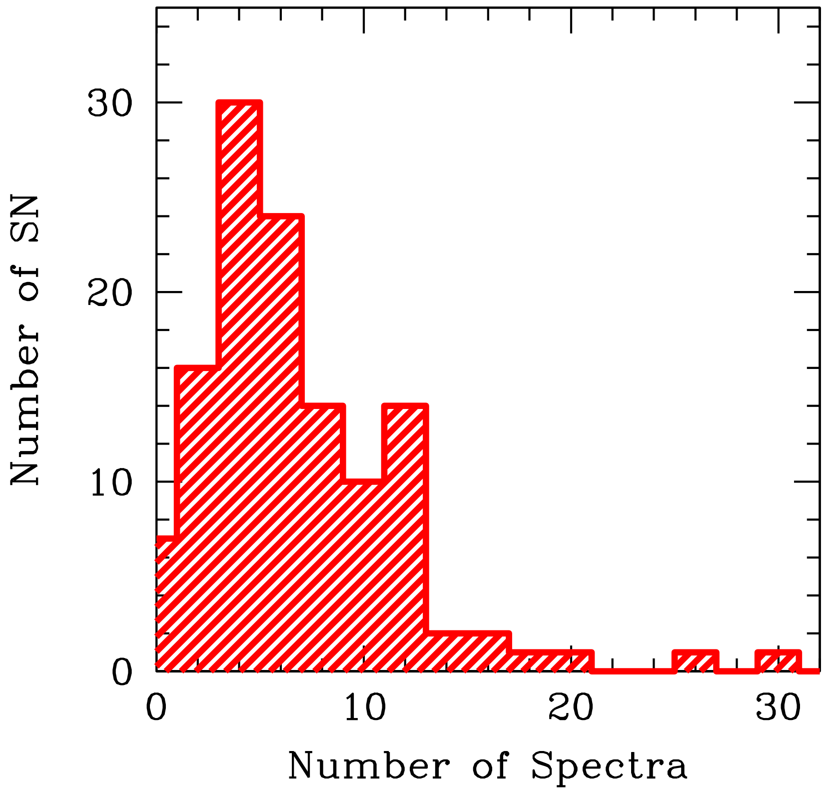

Figure 3.2 Histogram of the number of spectra per SN. The distribution peaks at 4 spectra.

3.4.2 Data reduction

Spectral reduction were achieved in the same manner for all data, using IRAF[5] and employing standard routines, including: bias subtraction, flat-fielding correction, one-dimensional (1D) spectral extraction and sky subtraction, wavelength correction, and flux calibration. Telluric corrections have only been applied to data obtained after October 2004.

In Appendix A we show plots with the spectral series for all SNe of our sample.

[5]IRAF is distributed by the National Optical Astronomy Observatories (NOAO), which are operated by the Association of Universities for Research in Astronomy (AURA), Inc., under cooperative agreement with the National Science Foundation.

3.5 Explosion epoch estimations

Before discussing the properties of our sample, in this section we outline our methods for estimating explosion epochs. The non-detections of SNe on pre-discovery images is the most accurate method for determining the explosion epoch for any given SN. Explosion epochs with non-detections are estimated using the mid-point between SN discovery and non-detection. The error on this epoch is then $(\mathrm{MJD}_{disc} - \mathrm{MJD}_{non-det})/2$. However within our sample (and for many other current SN search campaigns) many SNe do not have such accurate constrains from this method.

Over the last decade several tools have been published that enable explosion epoch estimations through matching of observed SN spectra to libraries of spectral templates. Programs such as the Supernova Identification (SNID) code (Blondin and Tonry, 2007), the GEneric cLAssification TOol (Gelato) (Harutyunyan et al., 2008), and superfit (Howell et al., 2005) allow the user to estimate the type of supernova and its epoch by providing an observed spectrum. In SNID, the code classifies SN spectra using the cross correlation method, which relies on the comparison of an input spectrum with a database of template spectra, which have been deredshifted to the rest frame. It is very efficient when the redshift of the SN host galaxy is unknown. On the other hand, Gelato performs the quantitative classification of SN spectra by comparison (best match) with a large set of template spectra of various SN types at different phase. Meanwhile, Superfit uses χ^2 fitting techniques. In our analysis we used only the first two methods: SNID and Gelato. Comparing them, we find that Gelato gives a large percentage of their quality of fit to H_α P-Cygni profile. However, based on our analysis (see Section 3.9), the most significant changes with time are observed in the blue part of the spectra (i.e. between 4000 and 6000 Å). Besides, according to Gutiérrez et al. (2014), the H_α P-Cygni profile shows a wide diversity and there is no clear, consistent evolution with time, so we decided to implement the use of SNID. In addition, SNID provides the possibility of adding additional templates to improve the accuracy of explosion epoch determinations. We take advantage of this attribute in the following sections adding new templates, so we decide to do our analysis with SNID.

While for many SNe this spectral matching is required in order to obtain a reliable explosion epoch, a significant fraction of our sample do have explosion epoch constraining SN non-detections before discovery. In cases where the non-detection is < 20 days before discovery, we use that information to estimate our final values. In cases where this difference is larger than 20 days, we use the spectral matching technique. However, as a test of our methodology, for non-detection SNe we also estimate explosion epochs using spectral matching to check the latter's validity (more details below).

3.5.1 SNID implementation

As we want to constrain the explosion epoch for our sample, we compare the first spectrum of each SN II within our sample with a library of spectral templates provided by SNID and

Table 3.3 Reference SNe II

SN	Explosion date	V-Maximum date	Reference
1999em	2451475.6 (5)	2451485.5	Leonard et al. 2002a
1999gi	2451518.3 (3)	2451530.0	Leonard et al. 2002b
2004et	2453270.5 (3)	2453286.6	Li et al. 2005, Sahu et al. 2006
2005cs	2453547.6 (1)	2453553.6	Pastorello et al. 2006
2006bp	2453833.4 (1)	2453842.0	Dessart et al. 2008
1988A	2447177.2 (2)	···	This work
1990E	2447935.1 (3)	···	This work
1999br	2451276.7 (4)	···	This work
2003bn	2452694.5 (3)	···	This work
2003iq	2452919.5 (2)	···	This work
2004er	2453271.8 (2)	···	This work
2004fc	2453293.5 (1)	···	This work
2004fx	2453303.5 (4)	···	This work
2005dz	2453619.5 (4)	···	This work
2006bc	2453815.5 (4)	···	This work
2006ee	2453961.9 (4)	···	This work
2006it	2454006.5 (3)	···	This work
2006iw	2454010.7 (1)	···	This work
2006Y	2453766.5 (4)	···	This work
2007il	2454349.8 (4)	···	This work
2007it	2454348.5 (1)	···	This work
2007oc	2454388.5 (3)	···	This work
2008il	2454825.6 (3)	···	This work
2008in	2454825.4 (2)	···	This work
2009ao	2454890.7 (4)	···	This work
2009au	2454897.5 (4)	···	This work
2009bz	2454915.8 (4)	···	This work

Columns: (1) SN name; (2) Julian date of the explosion epoch; (3) Julian date of the V-band maximum; (4) References. The first five SNe are included in SNID and are used as templates in this work. Their respective references are presented in the column 4. The rest of SNe showed after the line are included as template during this work.

then, we choose the best match. For each SN we choose different matches with emphasis on the blue part (4000-6000 Å), that present the most significant changes with time. Explosion epoch errors from this spectral matching are obtained by taking the standard deviation of several good matches of the observed spectrum from our sample with those from the SNID library. H_α is the dominant feature in SN II spectra, however its overall diversity and evolution in time varies greatly between SNe in a manner that does not aid in the spectral matching technique. We therefore ignore the comparison between observed and template spectra at this wavelength region.

From the SNID library we use those template SNe that have well constrained explosion epochs, meaning SNe II with explosion epoch errors of less than five days (see Table 3.3). Therefore, we use SNe 1999em (Leonard et al., 2002a), SNe 1999gi (Leonard et al., 2002b), SNe 2004et (Li et al., 2005), SNe 2005cs (Pastorello et al., 2006), and SNe 2006bp (Dessart et al., 2008). In the database of SNID there are a total of 166 spectra. However, these templates do not provide a good coverage of the overall diversity of SNe II within our sample/the literature. Most of the SNe in the library are relatively 'normal', with only one sub-luminous event (SN 2005cs). This means that any non-normal event within our sample will probably have poor constraints on its explosion epoch using these templates. For this reason we decided to use some of our own well-observed SNe II to compliment the SNID database.

3.5.2 New SNID templates

Table 3.4: Explosion epoch estimations comparison

SN	Spect. date JD	Best Match	Days from maximum	Days from explosion	Average (Using match)	Explosion date (MJD)	Non Detection date (MJD)	Discovery date (MJD)	Explosion date (MJD)	Difference (days)
1968L	46715.5	2006bp	−2	7	7	46708.5 (5)	46705.5	46710.5	46708.0 (3)	0
		1999em	−4	6						
1988A	47188.5	1999em	+5	15	17	47171.5 (6)	47175.5	47179.0	47177.2 (2)	−6
		2006bp	+7	16						
		2004et	+4	20						
1990E	47945.5	1999em	−3	7	9	47936.5 (6)	47932.5	47937.7	47935.1 (3)	1
		2004et	−3	13						
		1999gi	−4	8						
		2006bp	0	9						
1990K	48049.5	2004et	+33	49	48	48001.5 (6)	···	48037.3	···	···
		2006bp	+49	58						
		1999em	+27	37						
1991al	48473.5	2006bp	+25	34	31	48442.5 (8)	···	48453.7	···	···
		2004et	+20	36						
		1999em	+16	26						
		2003iq	···	29						
1992af	48832.8	2003bn	···	35	34	48798.8 (8)	···	48802.8	···	···
		2007il	···	45						
		1999gi	+19	31						
		2006bp	+20	29						
		2003iq	···	29						
		2004et	+20	36						
1992am	48832.9	2004et	+6	21	19	48813.9 (6)	···	48829.8	···	···
		1999em	+7	17						
1992ba	48896.9	1999em	+1	11	12	48884.9 (7)	···	48896.2	···	···
		2006it	···	12						
1993A	49015.7	1999em	+11	21	23	48992.7 (6)	48985.5	49004.6	48995.5 (9)	−3
		2004et	+10	26						
		2006bp	+14	23						
1993K	49098.6	2006bp	+15	24	26	49072.6 (6)	49057.5	49075.5	49065.5 (9)	7
		1999em	+11	21						
		2004et	+12	28						
		2004fc	···	33						
1993S	49164.8	2006bp	+20	29	34	49130.8 (5)	···	49133.7	···	···
		2004et	+23	39						

1999br	51291.5	2005cs	+7	13	13	51278.5 (4)	51273.0	51280.5	51276.7 (4)	2
1999ca	51304.5	2006bp	+20	29	27	51277.5 (7)	51271.0	51296.0	51283.5 (13)	−6
		2003iq	···	29						
		1999em	+16	26						
		1999gi	+19	31						
		2007oc	···	21						
1999cr	51257.5	2005cs	+5	11	11	51246.5 (4)	···	51249.7	···	···
1999eg	51467.5	2005cs	+7	13	18	51449.5 (6)	···	51455.5	···	···
		1999br	···	18						
		2004et	+6	22						
			···							
1999em	51485.5	2004et	−2	13	12	51473.5 (5)	51472.0	51481.0	51476.5 (5)	−3
		2006bp	+3	12						
2002ew	···	···	···	···	···	···	52490.5	52510.8	52500.6 (10)	···
2002fa	52529.5	2004et	+15	31	28	52501.5 (8)	52489.5	52510.8	52500.0 (11)	1
		1992H	+25	30						
		1999em	+11	21						
		2006bp	+20	29						
		1999gi	+19	31						
2002gd	52555.5	2005cs	-2	4	4	52551.5 (4)	52508.5	52552.7	52530.6 (22)	21
2002gw	52572.5	2009bz	···	24	19	52553.5 (8)	52529.5	52560.7	52545.1 (16)	8
		2005dz	···	20						
		1999em	+6	16						
		2003bn		16						
2002hj	52585.5	2004et	+12	28	27	52558.5 (10)	52556.5	52568.0	52562.5 (7)	−4
		2009bz	···	28						
		2005dz	···	29						
		1999em	+11	21						
		2006bp	+16	25						
		1999gi	+19	31						
		2003iq	···	29						
2002hx	52606.5	2007il	···	45	27	52575.5 (9)	52574.0	52589.7	52582.5 (9)	−7
		2009bz	···	37						
		2004fx	···	31						
		1999em	+16	26						
		2005cs	+10	16						
		2006bp	+20	29						
		2003bn	···	39						
		1999br	···	25						
2002ig	52588.5	2004et	+6	22	18	52570.5 (5)	···	52576.7	···	···
		2006bp	+7	16						
		1999em	+5	15						

SN210	52545.5	2004et	+40	56	59	52486.5 (6)	· · ·	· · ·	· · ·	· · ·
		2004er	· · ·	63						
		2006bp	+49	58						
2003B	52645.5	2007il		45	32	52613.5 (11)	· · ·	52645.0	· · ·	· · ·
		1999em	+16	26						
		2005cs	+10	16						
		2003bn	· · ·	39						
		2006bp	+25	34						
2003E	52648.5	2009bz	· · ·	24	19	52629.5 (8)	52605.7	52645.0	52625.3 (20)	4
		2004et	+6	22						
		1999em	+5	15						
		2006bp	+7	16						
		2003bn	· · ·	16						
2003T	52673.5	1999em	+9	19	22	52651.5 (6)	52645.0	52665.0	52654.5 (10)	−3
		2004et	+10	26						
		2006bp	+13	22						
2003bl	52702.5	2005cs	−2	4	6	52696.5(4)	52438.7	52701.0	· · ·	· · ·
		1999em	−4	6						
		1999gi	−4	8						
2003bn	52706.5	2004et	−2	14	12	52694.5 (5)	52691.5	52698.0	52694.5 (3)	0
		2006bp	+4	13						
		1999em	0	10						
2003ci	52729.5	2006bp	+16	25	26	52703.5 (5)	52704.0	52720.0	52711.5 (8)	−8
		1999em	+11	21						
		2004et	+15	31						
2003cn	52729.5	2005cs	+4	10	12	52717.5 (4)	52706.0	52728.0	52717.0 (11)	0
		1999br	· · ·	15						
2003cx	52739.5	2009bz	· · ·	24	14	52725.5 (5)	52683.0	52730.0	52706.5 (24)	19
		2006bp	+7	16						
		1999em	+5	15						
		2005cs	+4	10						
2003dq	52764.5	2006bp	+7	16	25	52739.5 (8)	52724.7	52739.7	52731.5 (8)	8
		2004et	+4	20						
		1999em	+5	15						
		2006Y	· · ·	51						
2003ef	52789.5	2004et	+23	39	32	52757.5 (9)	52720.7	52770.7	52745.7 (25)	12
		1999em	+16	26						
		2006bp	+20	29						
		1999gi	+19	31						
		2003bn	· · ·	39						
		2004fc	· · ·	33						
		2003iq	· · ·	29						

2003eg	52789.5	2004et	+6	22	25	52764.5 (5)	52743.7	52776.7	52759.5 (17)	5
		2009ao	· · ·	28						
2003ej	52789.5	2004et	+4	20	15	52775.5 (5)	52770.7	52779.7	52775.5 (5)	0
		2005cs	+2	8						
		2006bp	+7	16						
2003fb	52797.5	1999em	+11	21	25	52772.5 (10)	52591.7	52796.0	· · ·	· · ·
		2005dz	· · ·	29						
		2004et	+9	25						
		2006bp	+13	22						
		2003iq		29						
2003gd	52817.5	2005cs	+57	63	62	52755.5 (9)	· · ·	52803.2	· · ·	· · ·
		1999em	+62	72						
		2006ee	· · ·	52						
2003hd	52871.9	2004et	+2	18	16	52855.9 (5)	52640.7	52861.0	· · ·	· · ·
		2006bp	+4	13						
2003hg	52897.6	2006bp	+20	29	30	52867.6 (9)	52861.0	52870.0	52865.5 (5)	2
		2004et	+15	31						
		1999em	+16	26						
		1999gi	+19	31						
		2004fc	· · ·	33						
		2003iq	· · ·	29						
2003hk	52908.8	2004et	+25	41	42	52866.8 (4)	52687.5	52871.6	52679.6 (92)	· · ·
		1999gi	+24	41						
		1999em	+34	44						
2003hl	52900.8	2006bp	+25	34	33	52869.8 (5)	52863.0	52872.0	52868.5 (5)	1
		1999em	+35	45						
		2005cs	+14	20						
2003hn	52897.9	2006bp	+20	29	30	52867.9 (8)	52856.5	52877.2	52866.5 (10)	1
		2003iq		29						
		1999em	+16	26						
		2004et	+20	36						
2003ho	52889.5	2006bp	+34	43	41	52848.5 (7)	52830.5	52851.9	52841.2 (11)	7
		2004et	+25	41						
		2003bn	· · ·	39						
2003ib	52900.6	2005cs	+3	9	12	52888.6 (5)	52883.7	52898.7	52891.5 (8)	−3
		2006it	· · ·	12						
		2004et	−1	15						
		1999em	+2	12						
2003ip	52928.6	2004et	+20	36	32	52896.6 (4)	52637.5	52913.7	· · ·	· · ·
		2006bp	+25	34						
		1999em	+16	26						

2003iq	52928.5	2006bp	+3	12	10	52918.5 (7)	52918.5	52921.5	52919.5 (2)	−1
		2004et	−3	13						
		1999em	−3	7						
		2004fc	· · ·	9						
2004dy	· · ·	· · ·	· · ·	· · ·	· · ·	· · ·	53238.5	53242.5	53240.5 (2)	· · ·
2004ej	53262.9	1999em	+27	37	39	53223.9 (9)	53221.2	53258.5	53239.9 (19)	−16
		2006bp	+34	43						
		1999gi	+24	36						
		2004et	+23	39						
2004er	53302.8	2006bp	+16	25	31	53271.8 (6)	53270.0	53274.0	53271.8 (2)	0
		1999em	+16	36						
		2004et	+15	31						
2004fb	53302.6	2004et	+35	51	44	53258.6 (7)	53250.2	53286.2	53268.2 (18)	−10
		2006bp	+34	43						
		1999gi	+24	36						
		1999em	+33	43						
		2003iq	· · ·	47						
2004fc	53302.7	1999em	−3	7	10	53292.7 (5)	53285.2	53295.2	53293.5 (1)	−1
		2004et	−3	13						
		2006bp	+2	11						
		2003iq	· · ·	9						
2004fx	53326.8	2005dz		29	26	53300.8 (8)	53301.0	53307.0	53303.5 (4)	−3
		1999em	+11	21						
		1999gi	+19	31						
		2006bp	+14	23						
2005J	53405.8	2004er	· · ·	31	26	53379.8 (7)	53026.0	53387.0	· · ·	· · ·
		2004et	+15	31						
		1999em	+11	21						
		2006bp	+13	22						
2005K	53409.8	2006bp	+34	43	40	53369.8 (8)	53261.0	53386.0	53323.5 (63)	46
		2003bn	· · ·	39						
		1999gi	+24	36						
		2006it	· · ·	36						
		2007il	· · ·	45						
2005Z	53405.7	2004fc	· · ·	9	10	53395.7 (4)	53391.0	53402.0	53396.7 (6)	−1
		2006bp	+2	11						
		1999em	−2	8						
		2004et	−3	13						
2005af	53413.8	1999em	+101	111	93	53320.8 (17)	53177.5	53409.7	· · ·	· · ·
		2006ee	· · ·	94						
		1999gi	+78	90						
		1987A	−7	78						

2005an	53444.8	2004et	−1	15	13	53431.8 (6)	53391.0	53432.7	53411.9 (21)	20
		2006bp	+4	13						
		1999em	+0	10						
		2006it		12						
2005dk	53639.5	2004et	+23	39	38	53601.5 (6)	53562.0	53604.0	53583.0 (21)	18
		2006bp	+25	34						
		1999gi	+24	36						
		2003bn	· · ·	42						
2005dn	53639.6	2004et	+23	39	37	53602.6 (6)	53465.7	53609.5	53537.6 (72)	65
		2006bp	+25	34						
2005dt	53639.6	1999em	+33	43	41	53598.6 (4)	53596.7	53614.7	53605.6 (9)	−7
		2006bp	+34	43						
		1999gi	+24	36						
2005dw	53648.6	2006bp	+25	34	38	53610.6 (8)	53594.7	53612.7	53603.6 (9)	7
		2003bn	· · ·	42						
		1999em	+16	36						
		2004et	+23	39						
		1999gi	+24	36						
		2004fc	· · ·	33						
		2006iw	· · ·	45						
2005dx	53639.8	2007il	· · ·	40	28	53611.8 (7)	53424.7	53623.0	53523.9 (99)	· · ·
		1999em	+16	26						
		2005cs	+10	16						
		2003iq	· · ·	29						
2005dz	53639.7	1999em	+5	15	16	53623.7 (6)	53615.7	53623.7	53619.5 (4)	4
		2003bn	· · ·	16						
2005es	53648.7	1999em	−2	8	10	53638.7 (6)	53634.7	53643.7	53638.7 (5)	0
		2006bp	+3	12						
		2004et	−3	13						
		2004fc	· · ·	9						
		2006iw	· · ·	11						
		1999gi	−4	8						
2005gz	· · ·	· · ·	· · ·	· · ·	· · ·	· · ·	53645.7	53654.7	53650.2 (5)	· · ·
2005lw	53722.8	1999em	−4	6	6	53716.8 (10)	53696.0	53719.0	53707.5 (12)	9
		1999gi*	· · ·	6						
2005me	53794.5	2004et	+58	74	70	53724.5 (9)	53707.5	53728.2	53717.9 (10)	7
		2006bp	+65	74						
		2008il	· · ·	63						
		2003bn	· · ·	70						
		2003iq	· · ·	70						
2006Y	· · ·	· · ·	· · ·	· · ·	· · ·	53766.5 (4)	53763.0	53770.0	53766.5 (4)	· · ·

2006ai	53799.6	2004et	+6	22	18	53781.6 (5)	53721.2	53784.0	53752.6 (31)	29
		2003bn	· · ·	16						
		2006bp	+7	16						
2006bc	53846.5	1999br	· · ·	25	33	53813.5 (6)	53811.0	53819.1	53815.5 (4)	−2
		2009au	· · ·	41						
2006be	53824.8	2009bz	· · ·	24	22	53802.8 (9)	53789.0	53819.0	53804.0 (15)	−2
		2005dz	· · ·	29						
		1999em	+11	21						
		2006bp	+13	22						
		2003bn		16						
2006bl	53848.7	2004et	+10	26	26	53822.7 (10)	53763.5	53829.5	53796.5 (33)	26
		1999em	+11	21						
		2006bp	+13	22						
		1999gi	+19	31						
		2004er	· · ·	31						
		2003iq	· · ·	29						
		1990E	· · ·	19						
2006ee	54003.8	1999em	+35	45	41	53962.8 (7)	53958.0	53966.0	53961.9 (4)	1
		2005cs	+30	36						
		1999br	· · ·	43						
2006it	54016.6	1999em	+2	12	12	54005.6 (5)	54004.7	54009.5	54006.5 (3)	−1
		2004et	+1	17						
		2006bp	+4	13						
		2005cs	+1	7						
2006iw	54016.6	1990E	· · ·	10	9	54007.6 (7)	54009.5	54011.5	54010.7 (1)	−3
		1999em	−3	7						
		2004et	−3	13						
		1999gi	−5	7						
2006ms	54055.5	1999em	+16	26	27	54028.5 (6)	54021.2	54046.2	54034.0 (13)	−6
		2006bp	+25	34						
		2005cs	+13	19						
		1999gi	+19	31						
2006qr	54082.8	2005cs	+10	16	22	54061.8 (5)	54056.2	54070.0	54062.8 (7)	−1
		2004et	+10	26						
		2006bp	+15	24						
2007P	54143.7	2004et	+6	22	19	54124.7 (5)	54114.0	54124.0	54118.7 (5)	6
		2006bp	+8	17						
		2005dz	· · ·	20						
		2006it	· · ·	15						
2007U	54143.6	2006iw	· · ·	11	10	54133.6 (6)	54111.5	54136.5	54124.0 (13)	9
		2004fc	· · ·	9						
		1990E	· · ·	10						

2007W	54150.8	2005cs	+5	11	20	54130.58 (7)	54103.5	54146.5	54125.0 (22)	5
		2005dz	···	29						
		1999em	+11	21						
2007X	54150.8	1999em	−4	6	9	54143.8 (5)	53961.2	54146.5	54053.8 (93)	···
		1999gi	−4	8						
		2004et	−3	13						
		2006bp	−2	7						
2007Z	54150.6	2006bp	+7	16	15	54135.6 (5)	54125.5	54148.7	54137.1 (12)	−2
		2004et	+1	17						
		2003bn	···	16						
		2006it	···	12						
2007aa	54150.7	1999em	+11	21	24	54126.7 (8)	53441.7	54149.7	···	···
		1999gi	+19	31						
		2005cs	+9	15						
		2006bp	+20	29						
2007ab	54163.9	2006bp	+34	43	42	54123.9 (10)	···	54150.7	···	···
		1999em	+33	43						
		2004et	+23	39						
		2006it	···	36						
		2003iq	···	47						
2007av	54185.8	1999em	0	10	12	54173.8 (5)	···	54180.2	···	···
		2004et	−3	13						
		2006bp	+3	12						
		2003it	···	12						
2007bf	54202.7	1999em	−1	9	11	54191.7 (5)	54184.5	54198.5	54191.5 (7)	0
		2004et	−3	13						
		2006bp	+3	12						
2007hm	54355.6	2004et	+9	25	19	54336.6 (6)	···	54343.7	···	···
		1999em	+6	16						
		2006bp	+8	17						
2007il	54361.9	1999em	−2	8	10	54351.9 (7)	54346.0	54354.0	54349.8 (4)	2
		1990E	···	10						
		2004fc	···	9						
		1999gi	−4	8						
		2004et	−2	14						
		2009bz	···	9						
2007it	54358.5	2004et	−3	13	10	54348.5 (4)	54347.5	54349.5	54348.5 (1)	0
		2009bz	···	9						
		2004fc	···	9						
		2003iq	···	9						
		2006bp	+3	12						
			···							
2007ld	54389.5	2004et	+1	17	13	54376.5 (8)	···	54379.5	···	···

		1999em	+1	11						
		2006bp	+4	13						
		2006it	· · ·	12						
2007oc	54408.6	2004et	+15	31	29	54379.6 (6)	54381.5	54396.5	54388.5 (3)	−9
		2003iq	· · ·	29						
		1999em	+16	26						
		2006bp	+20	29						
2007od	54409.6	2004et	−3	13	9	54400.6 (5)	54026.5	54407.2	· · ·	· · ·
		2004fc	· · ·	9						
		1999em	−2	8						
		2005cs	0	6						
2007sq	54452.8	2004et	+15	31	30	54422.8 (6)	54413.0	54443.0	54428.0 (15)	−6
		2006bp	+20	29						
		2003iq	· · ·	29						
		2004er	· · ·	31						
2008F	54482.6	1999em	+1	11	13	54469.6 (6)	54413.5	54477.5	54445.5 (32)	24
		2004et	+1	17						
		2006bp	+4	13						
		2006it	· · ·	12						
2008H	54482.8	2006ee	· · ·	42	50	54432.8 (8)	54408.0	54481.0	54444.5 (37)	−12
		2004fc	· · ·	59						
		2004et	+47	63						
		2005cs	+30	36						
		1999em	+39	49						
2008K	54482.8	2005cs	−1	5	7	54475.8 (6)	54447.7	54481.0	54464.4 (17)	11
		2004fc	· · ·	9						
		1999gi	−4	8						
		1999em	−3	7						
2008M	54497.7	2009bz	· · ·	28	25	54472.7 (9)	54462.5	54480.7	54471.7 (9)	1
		1999em	+11	21						
		2005dz	· · ·	24						
		2004et	+10	26						
2008W	54509.8	2009ao	· · ·	28	26	54483.8 (8)	54450.7	54502.7	54476.7 (26)	7
		2005cs	+7	17						
		2004et	+15	31						
		1999em	+16	26						
		2006bp	+17	26						
		1999gi	+19	31						
2008ag	54509.9	1999em	+16	26	32	54477.9 (8)	54408.5	54499.5	54454.0 (46)	23
		2003bn	· · ·	39						
		2006bp	+25	34						
		2004et	+25	41						
		2005cs	+13	19						

		1999gi	+19	31						
2008aw	54545.8	2006Y	···	27	24	54522.8 (5)	54508.0	54528.0	54517.8 (10)	5
		2004et	+4	20						
2008bh	54553.7	2004et	−3	13	12	54541.7 (3)	54538.6	54549.0	54543.5 (5)	−2
		2006bp	+3	12						
2008bk	54568.9	1999br	···	25	28	54540.9 (8)	54468.2	54550.7	54509.4 (41)	31
		2005cs	+14	20						
		2004fx		40						
2008bm	54563.8	2009au	···	41	41	54522.8 (6)	54497.0	54554.7	54522.5 (26)	0
2008bp	54563.7	2005cs	+1	7	10	54553.7 (10)	54546.5	54558.7	54551.7 (6)	2
		2004et	−3	13						
		2004fc	···	9						
		2003iq	···	9						
		2006it	···	12						
		1999em	+2	12						
2008br	54568.5	2005cs	+10	16	17	54551.5 (7)	54546.5	54564.2	54555.7 (9)	−4
		1999br	···	18						
2008bu	54578.8	2004et	−2	14	12	54566.8 (7)	54297.7	54574.0	···	···
		2005cs	+2	8						
		2006it	···	12						
		1999em	+2	12						
		2006bp	+4	13						
2008ga	54766.5	2006bp	+49	58	55	54711.5 (7)	54534.7	54734.0	···	···
		2007oc	···	64						
		1999em	+33	43						
2008gi	54759.7	2004et	+9	25	20	54739.7 (7)	54734.0	54752.0	54742.7 (9)	−3
		1999em	+6	16						
			···							
2008gr	54793.6	1999em	+11	21	24	54769.6 (6)	54303.5	54768.7	···	···
		2004et	+12	28						
		2006bp	+15	24						
2008hg	54790.7	2004et	+1	17	12	54778.7 (5)	54774.5	54785.5	54779.8 (5)	−1
		2004fc	···	9						
		2006bp	+4	13						
		1999em	+0	10						
		2006iw		11						
2008ho	54815.6	2004fx	···	31	27	54788.6 (7)	54787.7	54796.5	54792.7 (5)	−4
		2009bz	···	37						
		2005cs	+10	16						
		1999em	+16	26						
2008if	54822.7	1999em	−4	6	8	54814.7 (3)	54802.7	54812.7	54807.8 (5)	7

		2004fc	···	9						
		2008il	···	3						
		1990E	···	10						
		1999gi	−4	8						
		2006iw	···	11						
2008il	54828.6	1999em	−4	6	7	54821.6 (7)	54822.7	54827.7	54825.6 (3)	−4
		1999gi	−4	8						
		2006iw	···	8						
2008in	54829.8	2005cs	0	6	9	54820.8 (8)	54823.5	54827.2	54825.4 (2)	−5
		1999em	−3	7						
		2004fc	···	9						
		2004et	−3	13						
2009A	54836.5	···	···	···	···	···	54813.5	54833.5	54821.5 (10)	···
2009N	54870.8	2005cs	+10	16	24	54846.8 (5)	54834.5	54856.3	54845.4 (11)	1
		1999em	+16	22						
		1999br	···	25						
		1999gi	+19	31						
2009W	54870.9	2004fx	···	55	54	54816.9 (9)	54737.5	54865.0	54801.3 (64)	15
		1999br	···	43						
		2008il	···	63						
2009aj	···	···	···	···	···	···	54874.0	54887.0	54880.5 (7)	···
2009ao	54918.5	2004et	+12	22	24	54894.5 (7)	54887.0	54895.0	54890.7 (4)	4
		1999em	+16	26						
		2006bp	+15	24						
2009au	54918.8	2006bc	···	9	9	54909.8 (6)	54894.0	54902.0	54897.5 (4)	12
2009bu	54919.9	2003bn	···	16	18	54901.9 (8)	54827.5	54916.2	54871.8 (44)	30
		2006bp	+8	17						
		2005dz	···	20						
		2006it	···	15						
		1999em	+6	16						
		2004et	+6	22						
2009bz	54924.8	2004et	−3	13	10	54914.8 (7)	54909.5	54920.0	54915.8 (4)	−1
		1999em	−2	8						
		2006bp	+2	11						
		2005cs	+1	7						

Columns: (1) SN name; (2) Reduced Julian date of the spectrum used to the match (JD − 2400000); (3) Best match obtained with SNID; (4) Days from maximum of the template used to the match; (5) Days from explosion of the template used to the match; (6) Average obtained from the days from explosion; (7) Explosion date obtained with the matching technique; (8) Non-detection date of the SN; (9) Discovery date of the SN; (10) Explosion date obtained from non-detection and discovery date; (11) Difference in days between the explosion date from matching technique and non-detection.

We created a new set of spectral templates using our own SNe II that have well constrained explosion epochs from non-detections. Well constrained is defined as events that have errors smaller than 5 days. Given this error constraint, we included 22 SNe, which show a large spectral and photometric diversity. In this manner, the new SNID templates were constructed using ~ 150 spectra and employing the *logwave* program included in the SNID packages. Adding our own template SNe to the SNID database we can now therefore use a total of 27 template SNe II for further explosion epoch constraints. Table 3.3 shows the explosion and maximum dates for the reference SNe, as well as the explosion epoch for our new templates. We note an important difference between our templates and those older events in SNID: for the newer templates explosion epochs are defined with respect to the explosion epoch, while for the older templates epochs are defined with respect to maximum light (meaning that one then has to add the "rise time" to obtain the actual explosion date).

With the inclusion of these 22 SNe to SNID we estimated the explosion epoch for our full sample. An example of the best match is shown in Figure 3.3. We can see that first spectrum of SN 2003iq (October 16th) presents similarities with SN 2006bp, SN 2004et, SN 1999em and SN 2004fc, at 3, −3, −3 days with respect to maximum (SN 2004fc does not show the maximum date) and 12, 13, 7 and 9 days from explosion, respectively. Taking the average, we conclude that the spectrum was obtained at 10 ± 7 days since explosion. Table 3.1 shows the explosion epoch for each SN as well as the method employed to derive it, while Table 3.5.2 shows all the details of spectral matching and non-detection techniques. The Appendix B shows the plots with the best matches for each SN of our sample.

To check the validity of spectral matching we compare the explosion epoch estimated with this technique and those with non-detections. While this analysis was done in Anderson et al. (2014b) with very good agreement, now with the use of new templates we improve that. Figure 3.4 shows a comparison between both methods. We can see that the mean absolute error between them diminishes from 4.2 (Anderson et al., 2014b) to 3.9 days. Also the mean offset decreases from 1.5 in Anderson et al. (2014b) to 0.5 in this work. Cases where explosion epochs have changed between Anderson et al. (2014b) and the current work are noted in Table 3.1. Nevertheless, although this method works well as a substitute for non-detections, exact constraints for any particular object are affected by any peculiarities that the observed (or indeed template) SN has. For example, differences in the colour (and therefore temperature) evolution of events can mimic differences in time evolution, while progenitor metallicity differences can delay/hasten the onset of line formation. To solve these drawbacks the inclusion of more SNe to SNID is the best option.
To obtain the new SNe II templates you can access to http://csp1.lco.cl/ and download the .tar file.

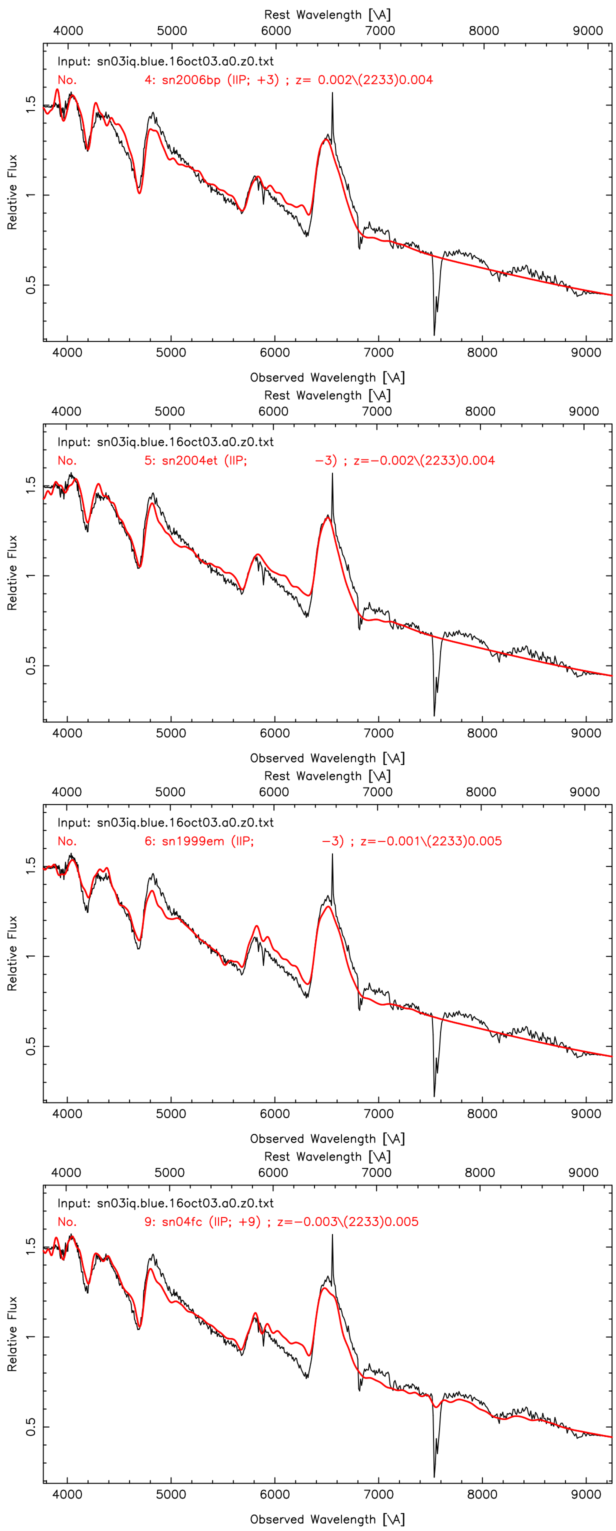

Figure 3.3 Best spectral matching of SNe 2003iq using SNID. The plots show SN 2003iq compared with SN 2006bp, SN 2004et, SN 1999em and SN 2004fc at 3, −3 and −3 around maximum and 9 days from explosion, respectively. Taking the average, this means that this spectrum is at 10 days from explosion.

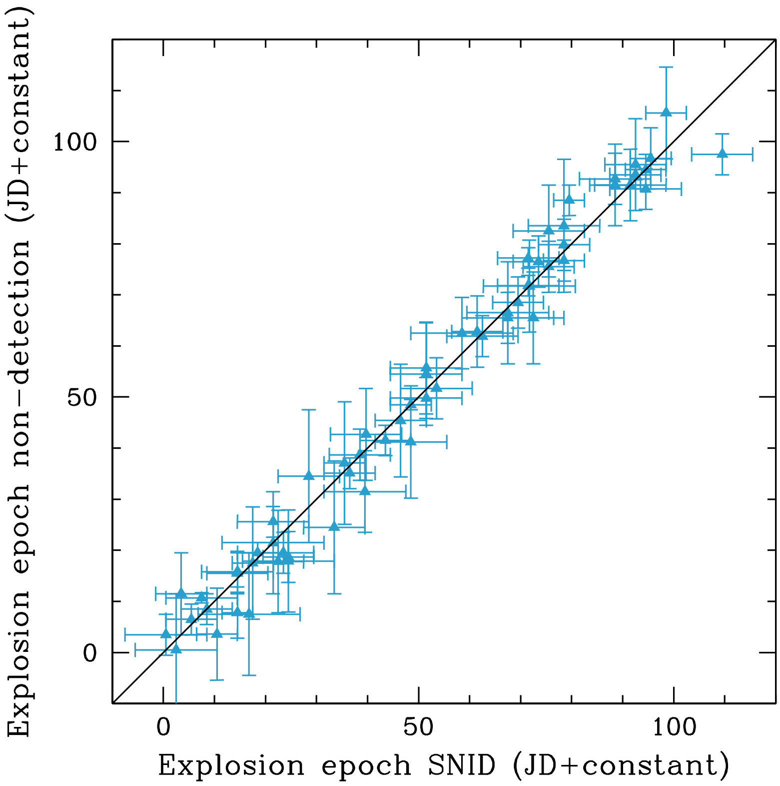

Figure 3.4 Comparison between spectral matching and non-detection methods.

3.6 Sample properties

As mentioned in Section 3.3 we have 893 optical spectra of 123 SNe II, however due to low signal-to-noise (S/N) we remove around 25 spectra of 12 SNe for our analysis. We also remove one spectrum of SN 1999ca because it is in a range of 11000 to 13000 Å (and therefore of no use for our study of the diversity of optical wavelength spectra); nine spectra of SN 2005lw because they contain peculiarities that we expect are not intrinsic to the SN (most probably defects resulting from the observing procedure or data reduction); five of SN 2009A, which shows peculiar properties making comparison to the rest of our sample not useful. In total, we remove 40 spectra ($\sim 4.5\%$). Figure 3.5 shows the epoch distribution of our spectra since explosion to 370 days. One can see that the majority of the spectra were observed between 0 and 100 days since explosion, with a total of 738 spectra. Our earliest spectrum corresponds to SN 2008il at 3 ± 3 and SN 2008gr at 3 ± 6 days from explosion, while the oldest spectrum is at 363 ± 9 days for SN 1993K. Before 50 days there are 53% of the spectra, 3.8% of which were observed before 10 days for 23 SNe. Between ~ 30 to 84 days there are 441 spectra of 114 SNe. There are 115 spectra older than 100 days and 27 older than 200 days, corresponding to 45 and 4 SNe, respectively. The average of this distribution is 60 days, while its median is 46 days.

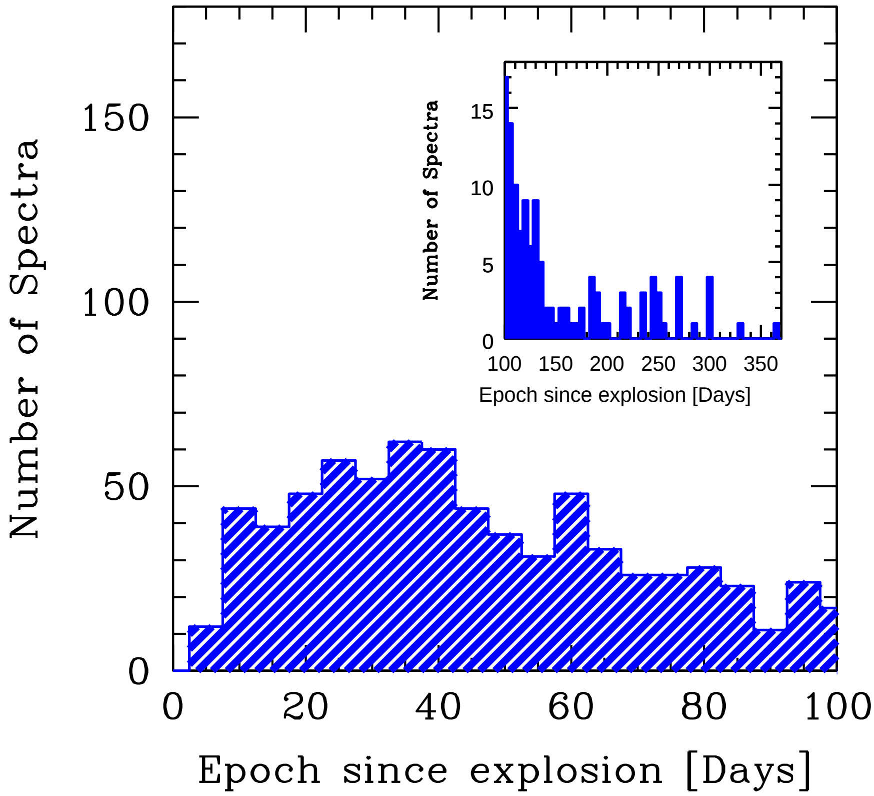

Figure 3.5 Distribution of the number of spectra as a function of epoch from explosion. The inset on the right shows the same distribution between 100 and 370 days.

Figure 3.6 shows the epoch distribution of the first and last spectrum for each SN in our sample. The majority of SNe have their first spectra before 40 days since explosion. There are 31 SNe with their first spectra around 10 days (the peak of the distribution). On the other hand, the peak of the distribution of the last spectrum is around 100 days. Almost all SNe have their last spectra between 30 and 120 days, i.e., in the photospheric phase. There are 11 SNe with their last spectra after 140 days, while only 4 SNe (SN 1993K, 2003B, SN 2007it, SN 2008bk) have their last spectrum in the nebular phase ($\geq$ 200 days).

The photometric behaviour of our sample in terms of their plateau decline rate (s_2) in the V band is shown in Figure 3.7. For 116 SNe we have a s_2 value between -0.58 and 3.39, however there are two outliers, SN 2004dy and SN 2008H with a value of 6.55 and -1.67, respectively. Smaller s_2 values mean that the SN light curve has a more pronounced plateau, meanwhile fast declining SNe II display higher s_2 values. We can see a continuum in the s_2 distribution, which shows that the majority of the SNe (85) have a s_2 value between 0 and 2. There are 9 objects with s_2 values smaller than 0, while 6 SNe show a value larger than 3. The average of s_2 in our sample

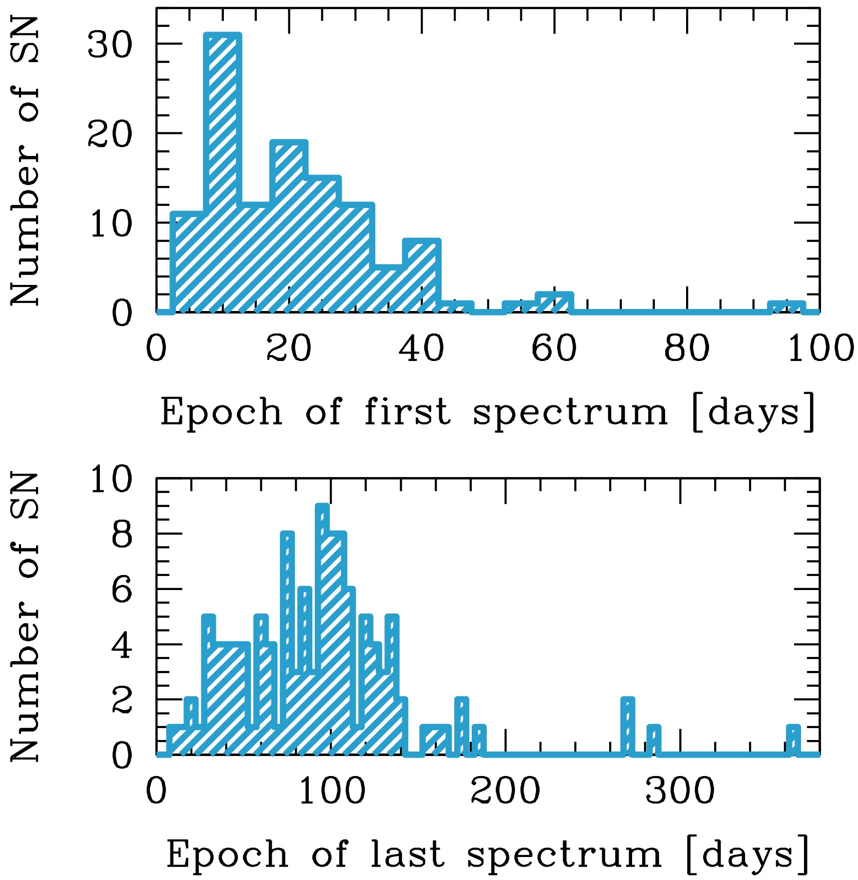

Figure 3.6 *Top:* Epoch from explosion of first spectrum. *Bottom:* Epoch from explosion of last spectrum.

is 1.22. We are unable to estimate the s_2 value for 5 SNe as there is insufficient information from their light-curves. The photometric information in the V-band and its analysis can be found in Anderson et al. (2014b), Galbany et al. (2016). However, the complete photometric information will be published in upcoming paper by Anderson et al. (in prep).

3.7 Spectral line identification

We identified 20 absorption features within our photospheric spectra, within the observed wavelength range of 3800 to 9500 Å. Early spectra exhibit lines of H_α λ6563, H_β λ4861, H_γ λ4341, H_δ λ4102, and He I λ5876, with the latter disappearing at $\sim 20-25$ days from explosion. An extra absorption component on the blue side of H_α (hereafter "Cachito"[6] is present in many SNe). That line has previously been attributed to high velocity (HV) features of hydrogen or Si II λ6533. Figure 3.8 shows the main lines in early spectra of SNe II at 3 and 7 days from explosion. We can see that SN 2008il shows the Balmer lines and He I, while SN 2007X, in

[6]Cachito is a Latin American word that means small piece of something. We use this name to refer to the small absorption components blue ward of H_α, giving its (until now) previously ambiguous nature.

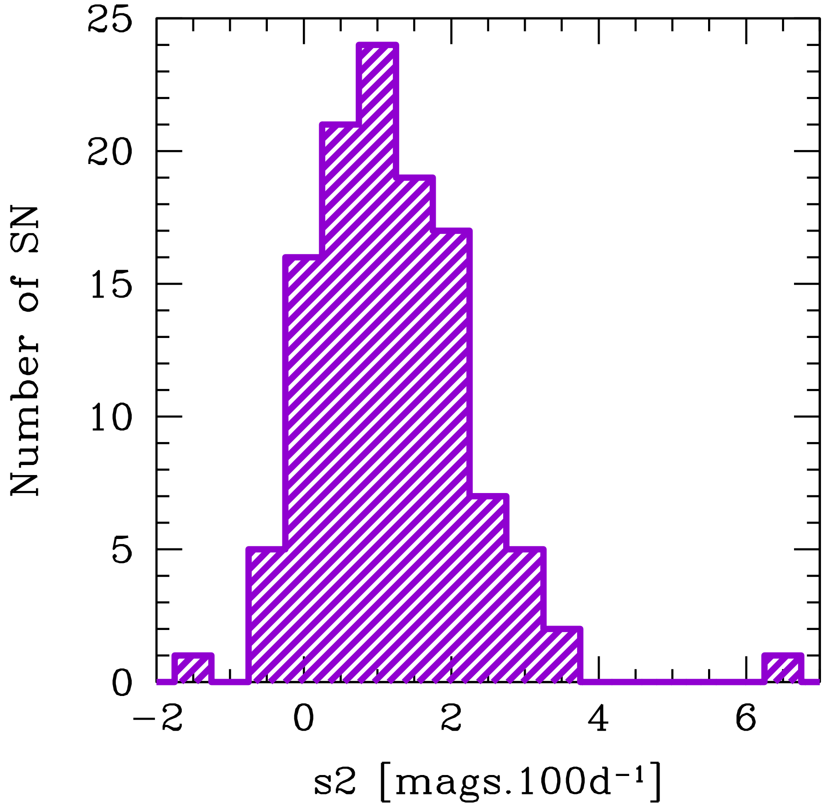

Figure 3.7 Distribution of the plateau decline "s_2" for 111 SNe of our sample.

addition to these lines, also shows the Cachito on the blue side of H_α.

In Figures 3.9 and 3.10 we label the lines present in the spectra of SNe II during the photospheric phase at 31, 70 and 72 days from explosion. Later than $\sim$ 15 days the iron group lines start to appear and to dominate the region between 4000 and 6000 Å. We can see Fe-group blends near λ4554, and between 5200 and 5450 Å (hereafter "Fe II blend"). Strong features such as Fe II λ4924, Fe II λ5018, Fe II λ5169, Sc II/Fe II λ5531, Sc II multiplet λ5663 (hereafter "Sc II M"), Ba II λ6142, Sc II λ6247, O I λ7774, O I λ9263 and the Ca II triplet λ8498, 8662 (λ8579) are also present from $\sim$ 20 days to the end of the plateau. At 31 days, SN 2003hn shows all these lines, except Ba II, while at 70 and 72 days, SN 2003bn and SN 2007W show all the lines. Unlike SN 2003bn, SN 2007W shows Cachito and the "Fe line forest"[7]. The Fe lines forest is visible in a small fraction of SNe from 25-30 days (see the analysis in section 3.9). As we can see there are big differences between two different SNe at almost the same epoch. These differences can be due to the explosion mechanism and/or the progenitor properties.

[7]We label "Fe line forest" to that region around H_β where a series of Fe-group (e.g. Fe II λ4629, Sc II λ4670, Fe II λ4924) absorption lines emerge.

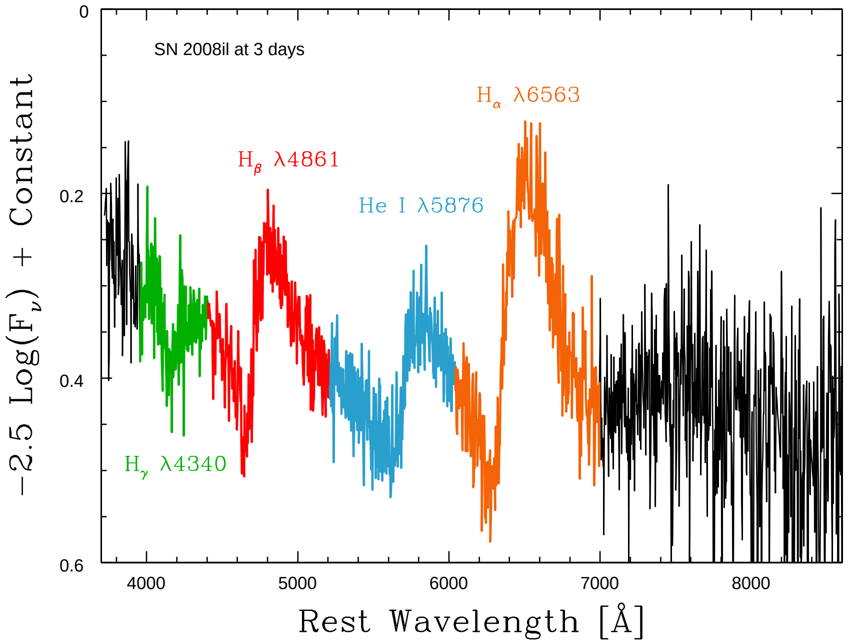

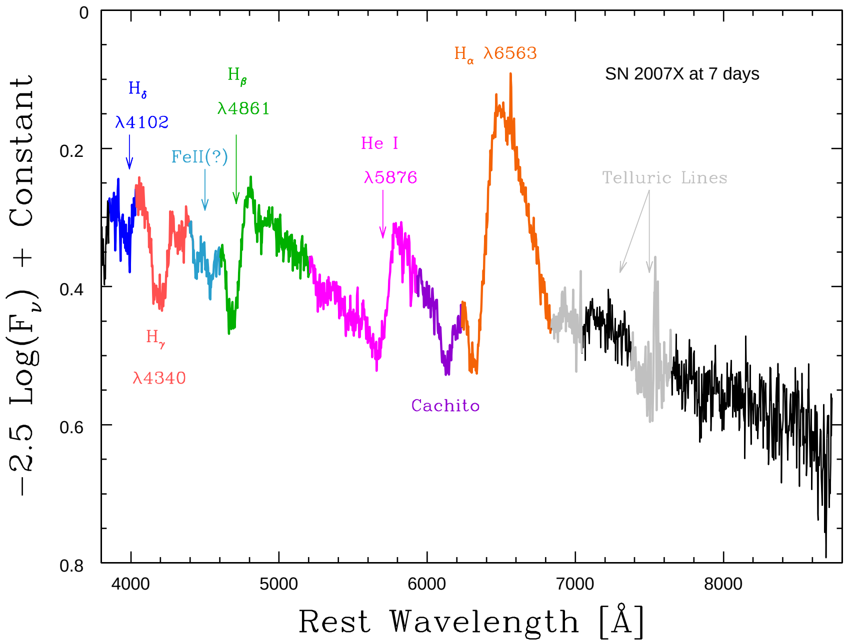

Figure 3.8 Line identification in the early spectra of SN 2008il (top) and SN 2007X (bottom).

The identification of photospheric lines was performed using the Atomic Spectra Database[8]

[8]http://physics.nist.gov/asd3

and theoretical models (e.g. Dessart and Hillier, 2005, 2006).

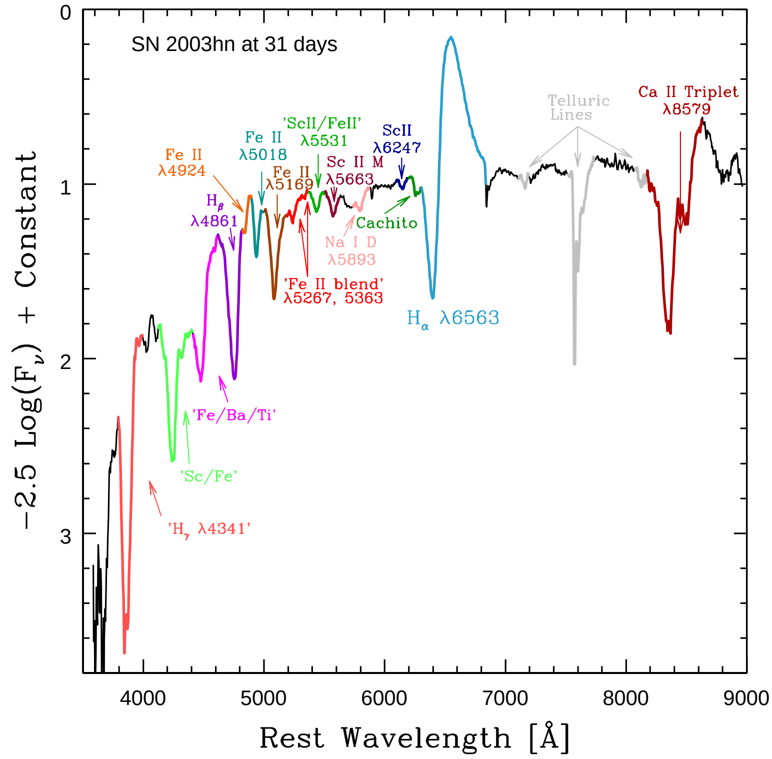

Figure 3.9 Line identification in the photospheric phase for SNe II 2003hn at 31 days.

In the nebular phase, later than 200 days post explosion, the forbidden lines [Ca II] λλ7291, 7323, [O I] λλ6300, 6364 and [Fe II] λ7155 emerge in the spectra. At this epoch H_α, H_β, Na I D, the Ca II triplet, O I and the Fe group lines between 4800 and 5500, and 6000-6500 Å are also present. Figure 3.11 shows a nebular spectrum of SN 2007it at 250 days from explosion.

3.7.1 The H_α P-Cygni profile

H_α λ6563 is the dominant spectral feature in SNe II. It is usually used to distinguish different SN types at the discovery moment. This line is present in the 100% of SNe II from explosion until nebular phases, showing, in the majority of cases, a P-Cygni profile. Although the P-Cygni profile has an absorption and emission characteristic, SNe display a huge diversity in the absorption component.

Gutiérrez et al. (2014) showed that SNe with little absorption of H_α (smaller absorption to emission (a/e) values) appear to have higher velocities, faster declining light-curves and are

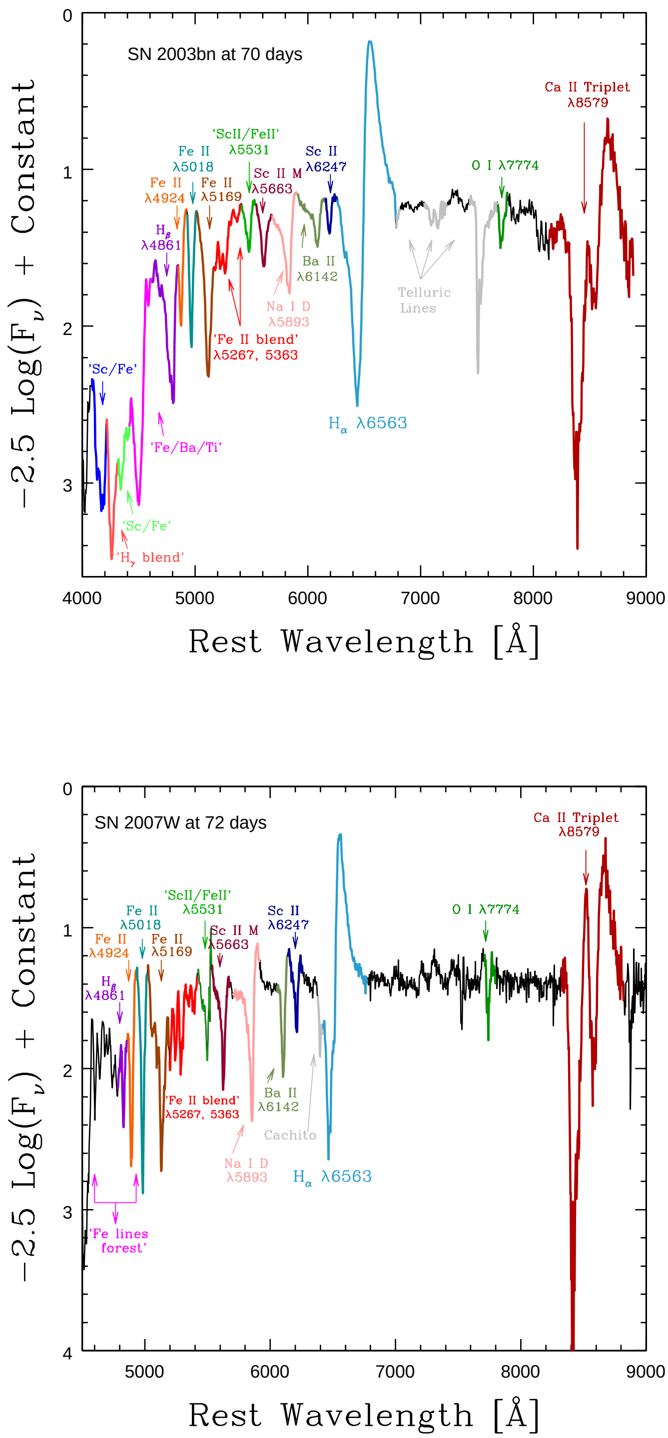

Figure 3.10 Line identification in the photospheric phase for SN 2003bn at 70 days (top) and 2007W at 72 days (bottom).

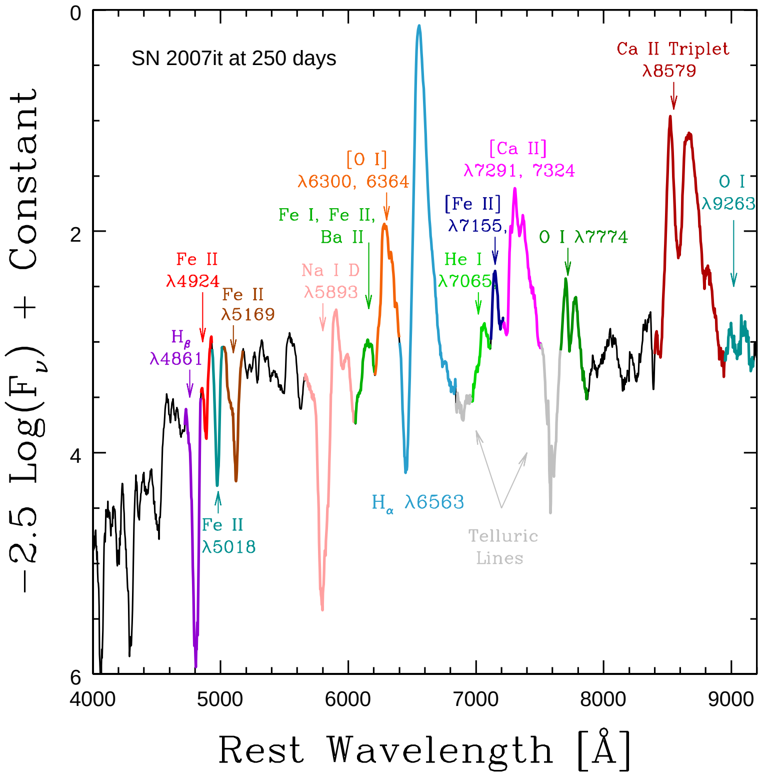

Figure 3.11 Line identification in the nebular spectrum of SN II 2007it at 250 days from explosion.

brighter. They also showed that H_α displays a large range of velocities in the photospheric phase, from 9500 km s^{-1} to 1500 km s^{-1} at 50 days (see the first two panels in Figure 3.19, which correspond to the H_α velocity derived from the FWHM and from the minimum flux absorption).

The diversity of H_α in the photospheric phase is also observed through the blueshifted offset in the emission peaks in early times (Dessart and Hillier, 2008, Anderson et al., 2014a) and the boxy profile (Inserra et al., 2011, 2012). The former is associated with differing density distributions of the ejecta, while the latter with an interaction of the ejecta with a dense CSM. In the nebular phase this shift in H_α emission peak and the boxy profile have been interpreted as evidence of dust production in the SN ejecta. Despite the fact that this is an important issue in SNe II, only a few studies (e.g Sahu et al., 2006, Kotak et al., 2009, Fabbri et al., 2011) have focussed on these features.

In Figure 3.12 we show an example of the evolution of H_α P-Cygni profile in SN 1992ba. We can see in early phases a normal profile which evolves to a complicated profile around 65 days. Cachito on the blue side of H_α is present from 65 to 183 days.

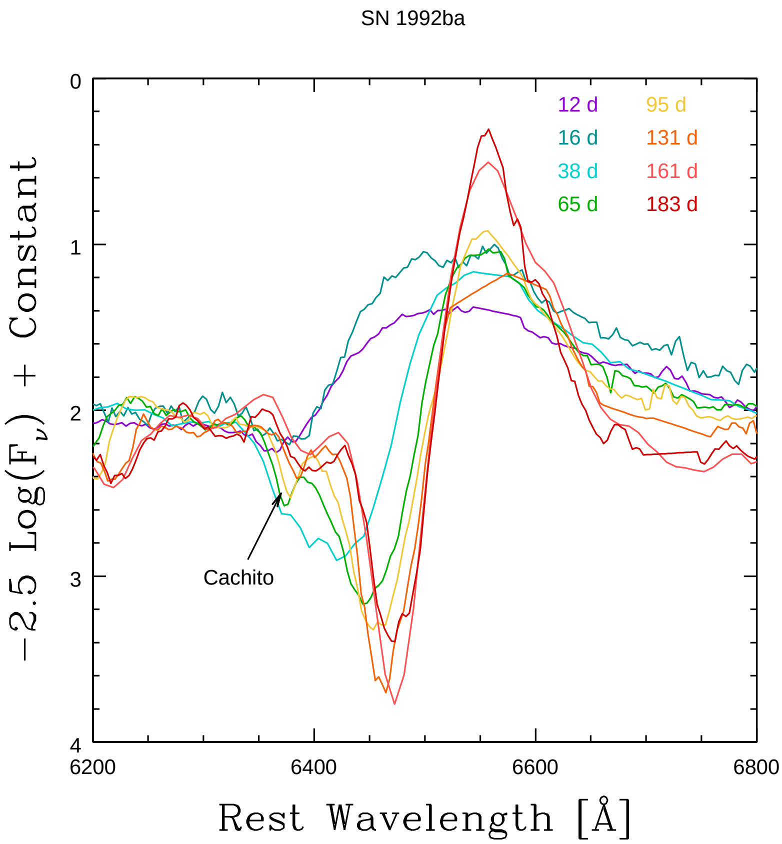

Figure 3.12 H_α P-Cygni profile evolution in SN 1992ba. The epochs are labeled on the right.

3.7.2 H_β, H_γ and H_δ absorption features

H_β λ4861, H_γ λ4341 and H_δ λ4102 like H_α are present from the first epochs. In earlier phases, these lines show a visible P-Cygni profile, however, from $\sim$ 15 days the spectra only display the absorption component, giving space to Fe group lines. The range of velocities of H_β, H_γ and H_δ at 50 days post explosion vary from 8000 to 1000 km s^{-1} (see Figure 3.19), which is similar to those found in H_α, although offset to lower values (in general by around $\sim$ 1500 km s^{-1}).

Although H_δ is a common line in SNe II, we do not include a detailed analysis of this line because in many cases the spectra are noisy where the line is placed. Besides, like other lines on the blue part of the spectrum, this line is blended with Fe-group lines later than 30 days.

Around 30 days from explosion H_γ starts to blend with other lines, such as Ti II, Fe II. Meanwhile in a few SNe, the H_β absorption feature is surrounded by the Fe lines forest. Our later analysis shows that SNe displaying this behaviour are generally dimmer and lower velocity events (see Section 3.9 for more details).

3.7.3 He I λ5876 and Na I D λ5893

He I λ5876 is present in very early phases when the temperature of the ejecta is high enough. As the temperature decreases, the He I line starts to disappear due to the recombination of He I ions (around 15 days; Roy et al. 2011). At $\sim$ 30 days the Na I D λ5893 absorption feature arises in the spectrum at a similar position where He I was located. This new line evolves with time to a strong P-Cygni profile, displaying velocities between 8000 km s^{-1} to 1500 km s^{-1} at 50 days from explosion (Figure 3.19).

In many SNe II (or indeed SNe of all types), at these wavelengths one often also observes narrow absorption features arising from slow-moving line of sight material from the ISM (or possibly from CSM material). Such material can constrain the amount of foreground reddening suffered by SNe, however we do not discuss this in any detail here.

3.7.4 Fe-group lines

When the SN ejecta has cooled sufficiently, Fe II features start to dominate SNe II spectra between 4000 to 6500 Å. The first line that appears is Fe II λ5169 on the emission component of H_β. With time Fe II λ5018 and λ4924 emerge between H_β and Fe II λ5169. Fe II λ5169 can to be affected by a Fe II blend later than $\sim 30-40$ days. At $\sim$ 50 days the 4000-5500 Å region is completely filled with these lines and the continuum is diminished due to Fe II line-blanketing. The H_γ and H_δ absorption features are blended with Fe-group lines, such as, Fe II, Ti II, Sc II and Sr II. Between $\sim$ 5400 and 6500 Å other metal lines appear in the spectra. Lines such as Sc II/Fe II λ5531, Sc II M, Ba II λ6142 and Sc II λ6247 begin to get strong with time.

As we can see in Figure 3.19, the Fe-group lines show a range of velocities between 7000 km s^{-1} to 500 km s^{-1} at 50 days. The peak of the Fe II group lines velocities is around 4000 km s^{-1}. In the case of Ba II, the peak is lower (around 3000 km s^{-1}).

Although Fe II lines affect H_β in late phases, a few SNe show the iron lines forest at 30 days. This behaviour happens earlier in low velocity/luminosity SNe (See section 3.9).

3.7.5 The Ca II IR triplet

The Ca II IR triplet is a strong feature in the spectra of SNe II. This line appears at $\sim 20-30$ days as an absorption feature, but with time it starts to show an emission component, obtaining the appearance of a P-Cygni profile. The Ca II IR triplet is composed of two members, a blend of λ8498 and λ8542 in the bluer part and a separate component in λ8662. In SNe II with higher velocities these lines are merged and we can see in the spectra a broad absorption and emission profile, however in low velocity SNe we can see two absorption components and one emission in the red part. The range of velocities of the Ca II IR triplet is between 9000 to 1000 km s^{-1} at 50 days. In the nebular phase the Ca II IR triplet is also present, however at this epoch it only exhibits the emission component which comes from both the inner and outer ejecta (Dessart and Hillier, 2011).

Although in the majority of our spectra we can not see Ca II H & K λ3945, due to the bad signal to noise in this region, this line is present in the photospheric phase of SNe II.

While the Ca II IR triplet is a prominent feature in SNe II, we do not include its analysis in the subsequent discussion, given that the overlap of lines make a consistent comparison of velocities and pseudo-equivalent widths (pEWs) difficult.

3.7.6 O I lines

The O I $\lambda\lambda$7772, 7775 doublet (hereafter O I λ7774) and O I λ9263 are the most evident oxygen lines in the optical spectra of SNe II. These lines are mainly driven by recombination and they appear when the temperature decreases sufficiently. The O I λ7774 line is relatively strong and emerges around 20 days from explosion, however in the majority of cases it is contaminated by the telluric A-band absorption ($\sim 7600 - 7630$ Å), which hinders detailed analysis. Meanwhile, O I λ9263 is weaker and appears one month later than O I λ7774. These lines are present until the nebular phase and their expansion velocity at 50 days post explosion goes from $\sim$ 7000 km s^{-1} to 500 km s^{-1}, as can be seen in Figure 3.19.

3.7.7 Cachito: Hydrogen High Velocity (HV) Features or the Si II λ6355 line?

The extra absorption component on the blue side of H_α P-Cygni profile, called here "Cachito", is normally seen in early phases in some SNe (e.g. SN 2005cs Pastorello et al. 2006) as well as in the plateau phase (e.g. SN 1999em Leonard et al. 2002a). However, its shape and strength is completely different in both epochs and its evolution is not permanent with time. Baron et al. (2000) assigned the term "complicated P-Cygni profle" to explain the presence of this component on the blue side of He I λ5876 and the Balmer series. They concluded that these features are due to two velocity regions in the expanding ejecta of the SNe II. A few years later, Pooley et al. (2002) and Chugai et al. (2007) argued that this extra component might originate from ejecta – circumstellar (CS) interactions, meanwhile Pastorello et al. (2006) earmark this feature as Si II λ6355.

In early phases Cachito appears at around 5-7 days between 6100 and 6300 Å, and disappears at $\sim$ 35 days. Later than 40 days the Cachito feature emerges closer to H_α (between 6250-6450 Å) and it can be seen until 100-120 days. Figure 3.13 shows this component in SN 2007X. In early phases this feature is marked with letter A and later with letter B. As we can see, both components have different velocities with respect to H_α, 18000 to 12000 km s^{-1} and 10000 km s^{-1}, respectively. A detailed analysis of this feature is presented in 3.9.4.

3.7.8 Nebular Features

As we mentioned above, H_α, H_β, the Ca II IR triplet, Na I D , O I and Fe II are also present in the nebular phase (later than 200 days since explosion), however in the case of the Ca II IR triplet,

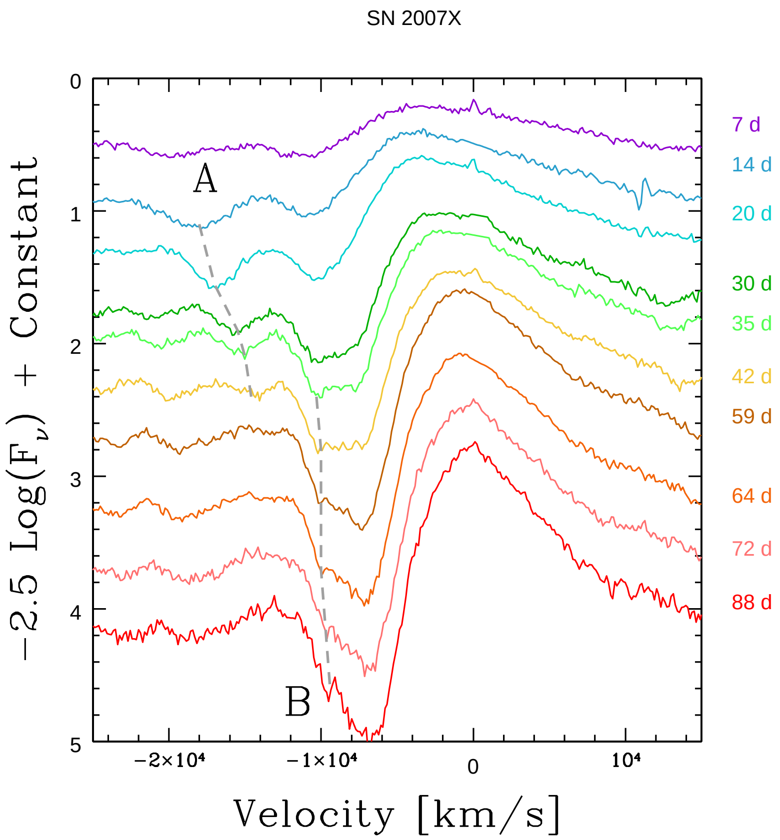

Figure 3.13 H_α P-Cygni profile of the SN 2007X. The epochs are labeled on the right. The dashed lines indicate the velocities for the A and B features.

its appearance changes, passing from absorption and emission components to only emission components when the nebular phase starts. The rest of the lines have the same behaviour but at much later epochs. The emergence of forbidden emission lines in this phase is a clear evidence that the outer ejecta has become transparent and we can see in deeper. Lines such as [Ca II] $\lambda\lambda$7291, 7323, [O I] $\lambda\lambda$6300, 6364 and [Fe II] λ7155, 7172 are the strongest features visible in the spectra.

[O I] $\lambda\lambda$6300, 6364 are the most important diagnostic lines of the helium-core mass, due to most of the oxygen is synthesized during hydrostatic helium and carbon burning, with little creation or destruction in the explosive process (Jerkstrand et al., 2014). Usually they are blended, however in SNe with low velocities these lines can be resolved (see SN 2008bk). Meanwhile, [Fe II] λ7155 is easily detectable, but in most cases it is blended with [Ca II] $\lambda\lambda$7291, 7323 and He I λ7065, which may hinder their analysis. In Figure 3.14 we can see the diversity found in transitional spectra (from photospheric to nebular phase) and the nebular spectra in our sample.

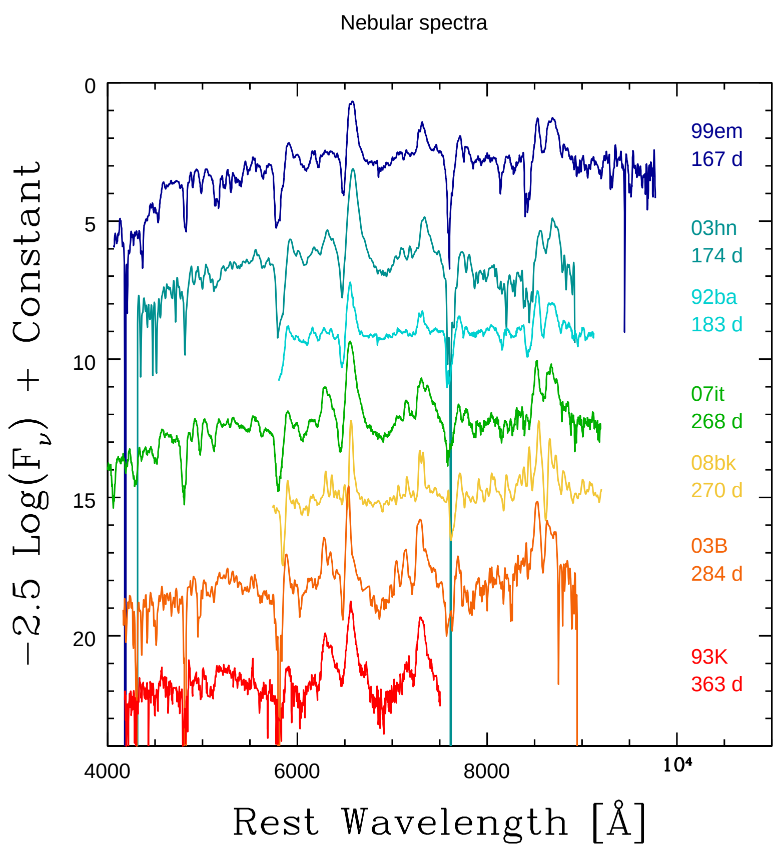

Figure 3.14 Nebular spectral of seven different SNe of our sample. The spectra are organized according to epoch.

3.8 Spectral measurements

As discussed previously, SNe II spectra evolve from having a blue continuum with a few lines (Balmer series and He I) to redder spectra with many lines: Fe II, Ca II, Na I D, Sc II, Ba II, and O I. To analyse the spectral properties of SNe II, we measure the expansion velocities and pEWs of eleven features in the photospheric phase and four in the nebular epochs (see in Table 3.5 the features used), the ratio of absorption to emission (a/e) of H_α P-Cygni profile before 120 days, and the velocity decline rate of H_β.

3.8.1 Expansion velocities

The expansion velocities of the ejecta are commonly derived from the minimum flux of the absorption component of the P-Cygni line profile. Using the Doppler equation[9] and the rest wavelength of each line, we can derive the velocity. To obtain the minimum flux line

[9]We use in our analysis the non-relativistic equation, however we compared both relativistic and non-relativistic results and the maximum difference is of ~ 500 km s−1.

Table 3.5 Spectral features used to the statistical analysis in the photospheric and nebular phases

Feature name	Rest wavelength⋆ [Å]	Blue-ward limit range♣ [Å]	Red-ward limit range♣ [Å]
H_α	6563	6000 - 6300	6900 - 7100
H_β	4861	4400 - 4700	4800 - 4900
Fe II	4924	4800 - 4900	4900 - 4950
Fe II	5018	4900 - 4500	5000 - 5050
Fe II	5169	5000 - 5050	5100 - 5300
Na I	5893	5500 - 6000	5800 - 6000
Sc II	5531	5400 - 5450	5500- 5550
Sc II/Fe II	5663	5500 - 5550	5600 - 5700
Ba II	6142	6000 - 6050	6100 - 6150
Sc II	6247	6150 - 6170	6250 - 6270
O I	7774	7630 - 7650	7750 - 7780
[O] I] doublet	6300, 6364	6100 - 6250	6350 - 6400
[Fe II] doublet	7155, 7172	6350 - 6450	6750 - 6800
[Ca II] doublet	7291, 7323	7200 - 6230	7500 - 7600
Ca II IR triplet	8498, 8662	8400 - 8430	8750 - 8850

⋆ The rest wavelengths are weighted averages of the strongest spectral lines that give rise to each absorption feature.
♣ These limits are necessary in order to account for variations in spectral feature width and expansion velocity among SNe.

position, a Gaussian fitting was employed, which was performed with IRAF[10] using the *splot* package. As the absorption component presents a wide diversity (e.g. asymmetries, flat shape, extra absorption components) we reproduce the process many times, and the mean of the measurements were take as the minimum flux. As our measurement error we take the standard deviation on the mean. This error is added in quadrature to errors arising from the spectral resolution of our observations and from peculiar velocities of host galaxies with respect to the Hubble flow (200 km s^{-1}). This means that, in addition to the standard deviation error, which realizes the width of the line and signal-to-noise, we take into account the spectral resolution, which in our case is the most dominant parameter to determine the error.

The particular case of the H_α velocity was explored as part of this thesis. As few SNe have little or extremely weak absorption component that complicates measuring the minimum, we also employ the full width at half maximum (FWHM) of emission line for its estimation. In this analysis we derive the expansion velocity of H_α using both techniques: the minimum flux of the absorption component and the FWHM of the emission component.

The case of O I 7174 where the telluric lines can affect its absorption, and, of course, the measurements, we only use the SNe with a clear separation between both components. This

[10]IRAF is distributed by the National Optical Astronomy Observatories (NOAO), which are operated by the Association of Universities for Research in Astronomy (AURA), Inc., under cooperative agreement with the National Science Foundation.

means that the amount of SNe with O I measurements in significantly less (only 47 SNe).

3.8.2 Velocity decline rate

To calculate the rate of change of the expansion velocity in SNe II, we select the H_β absorption line. Its presence from the first days since explosion, its easy identification and its relatively isolated position in the spectra, make it the ideal line to quantify this property. To analyze quantitatively our sample, we introduce the $\Delta v(H_\beta)$ as the the mean velocity decline rate in a fixed phase range [t_0,t_1]:

$$\Delta v(\mathrm{H}_\beta) = \frac{\Delta v_{abs}}{\Delta t} = \frac{v_{abs}(t_1) - v_{abs}(t_0)}{t_1 - t_0}.$$

We measure this parameter over the interval $15 \leq t \leq 30$d, $15 \leq t \leq 50$d, $30 \leq t \leq 50$d, $30 \leq t \leq 80$ d, and $50 \leq t \leq 80$ days.

3.8.3 Pseudo-equivalent widths

To quantify the spectral properties of SNe II, another avenue for investigation is the measurement and characterization of spectral line pEWs. The prefix "pseudo" is used to indicate that the reference continuum level adopted is generally not the actual continuum emission. The pEW basically defines the strength of any given line (with respect to the continuum), at any given time. The most simple and used method is to trace a straight line along the absorption feature to mimic the continuum flux. Figure 3.15 shows an example of this technique applied to SN 2003bn. We do not include analysis of spectra where it is difficult to define the continuum level, due to complicated line morphology, such as significant blending between lines. For example, later than 20 - 25 days, all absorption features on the blue part of H_β are produced by blends of Fe-group lines plus other strong lines, such as Ca II H & K and H_γ. Meanwhile, the Ca II IR triplet λ8498, 8662 shows a profile that depends on the SN velocity (higher velocity SNe show a single broad absorption, while low velocity SNe show two absorption characteristics). These attributes make a consistent analysis between SNe difficult, and therefore we do not include the analysis of this line in this work.

Grounded on the study of Gutiérrez et al. (2014), we measure the ratio of absorption to emission (a/e) in H_α. Unlike Gutiérrez et al. (2014), here, we estimate a/e in all available phases until 120 days. In the same way that we estimate the pEWs of the absorption lines, we evaluate the pEWs for the emission in H_α, thus we have:

$$a/e = \frac{pEW(H_{\alpha(abs)})}{pEW(H_{\alpha(emis)})}.$$

3.9 Line Evolution analysis

Here, we present an analysis of when different lines form within different SNe, and make a comparison of those SNe with/without specific lines at different epochs. For all lines included

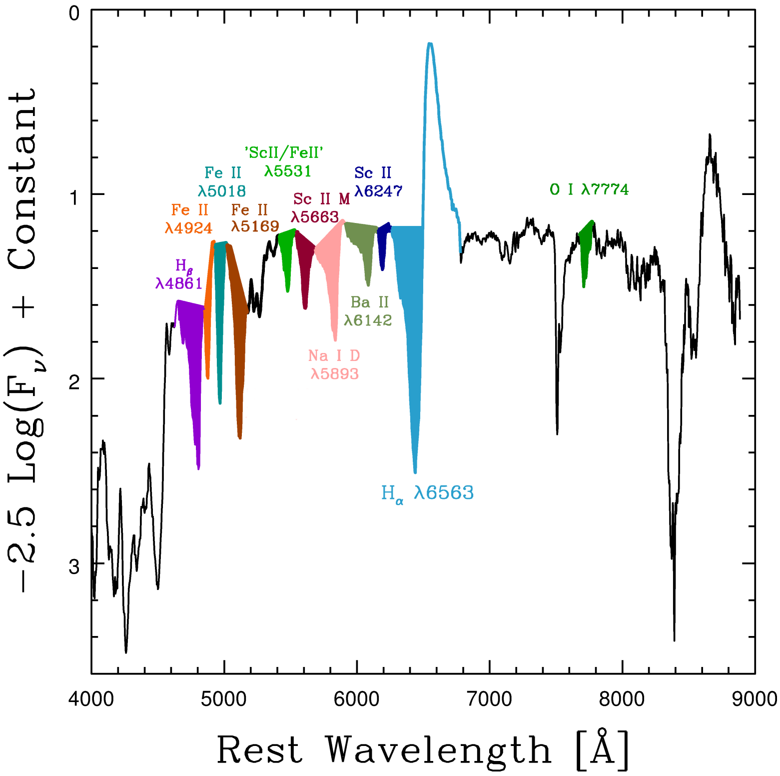

Figure 3.15 Examples of pEWs used in this work for eleven features in the photospheric phase.

in our analysis, we search for their presence in each observed spectrum. Then, at any given epoch we obtain the percentage of SNe that display each line. This enables an analysis of the overall line evolution of our sample, affording an analysis of whether the speed of this evolution changes between different SNe of different light-curve, spectral, and environment (metallicity) characteristics. In Figure 3.16 we show the percentage of SNe displaying all measured spectral parameters as a function of time. In Table 3.6 are presented all the results obtained with the Kolmogorov-Smirnov (KS) test used to analyze the SNe with/without each line (Fe II line forest, H_γ blended, He I, Ca II, Fe II 4924, Fe II 5018, Fe II λ5169, Fe II blended, Sc II/Fe II, Sc II multiplet, Ba II, and Sc II) as a function of a/e and H_α velocity at $t_{tran+10}$, M_{max}, s_2, and metallicity (M13 N2 diagnostic; Marino et al. 2013) in a particular epoch. The values of the first four parameters can be found in Table 2.1, while the metallicity information was obtained of Anderson et al. (2016).

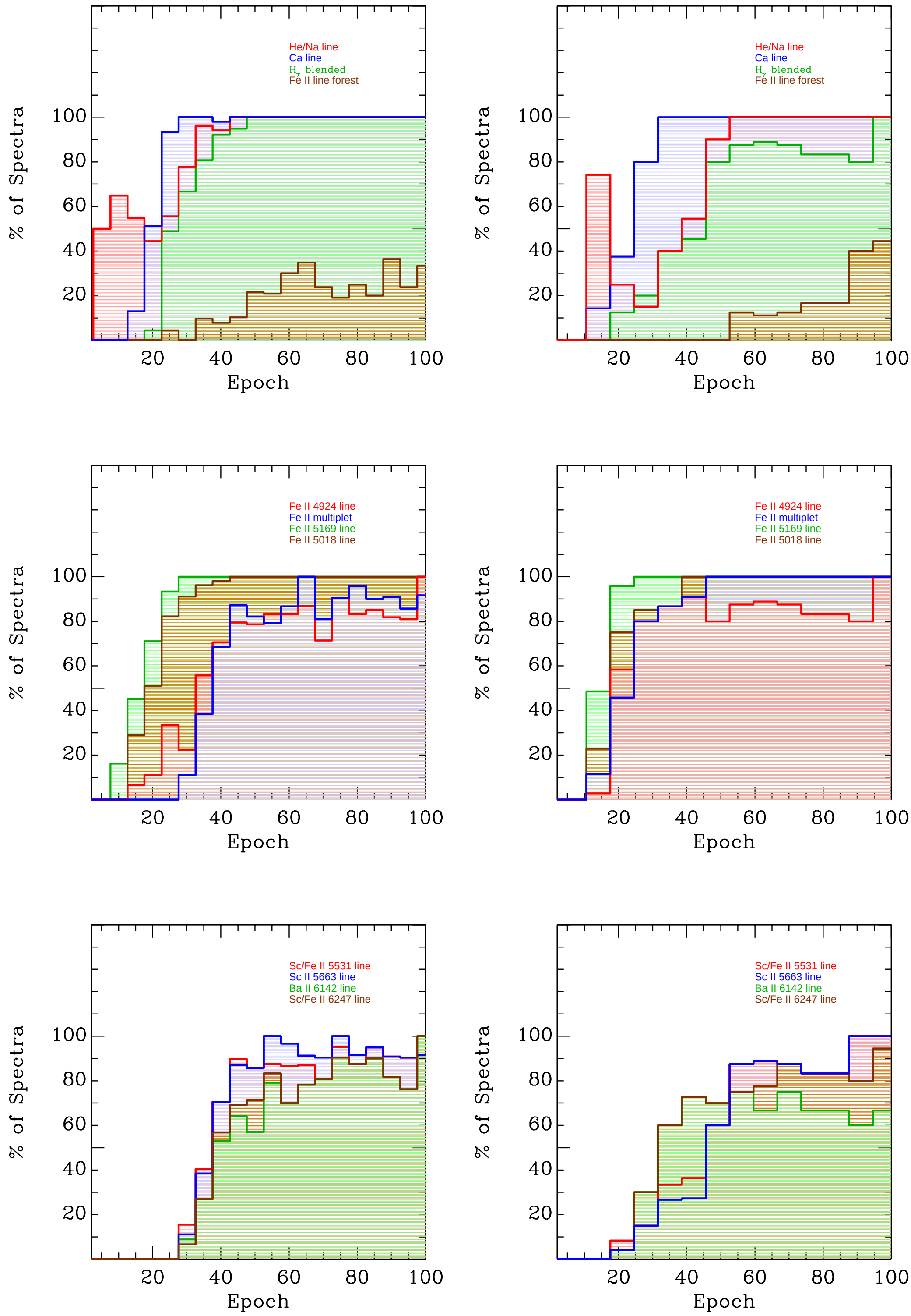

Figure 3.16 Appearance of different lines in SNe II between explosion and 100 days. **Left:** from the observed spectra. **Right:** from synthetic spectra.

Table 3.6 KS-Test values

Feature name	$v(H_\alpha)$	a/e	M_{max}	s_2	M13N2	Epoch [days]
Fe II line forest	5.19	9.80	2.17	3.73×10^{-4}	4.38	0 - 100
H_γ blended	29.75	58.33	31.21	55.32	16.10	23 - 27
He I 5876	18.62	1.91	30.94	25.73	46.18	18 - 22
Ca II IR triplet	87.73	91.97	94.47	53.30	98.82	18 - 22
Fe II 4924	2.82	16.84	1.09	4.80	99.40	28 - 32
Fe II 5018	15.68	90.80	99.02	68.84	61.53	18 - 22
Fe II 5169	60.76	35.15	74.88	50.83	20.30	13 - 17
Fe II multiplet	21.38	26.75	1.00	0.25	99.28	33 - 37
Sc II/Fe II 5531	75.60	89.60	30.34	45.20	1.84	38 - 42
Sc II multiplet 5663	63.54	63.54	30.34	80.10	0.79	38 - 42
Ba II 6142	45.75	83.58	1.90	57.43	1.29	38 - 42
Sc II 6247	45.76	83.58	1.89	57.42	0.52	38 - 42

Percentage obtained using a KS Test to verify if two distributions (with and without each line) are drawn from the same parent population as a function of $v(H_\alpha)$, a/e, M_{max}, s_2, and M13N2 in an particular epoch. This epoch is shown in the last column of the table.

As we said in previous sections, H_α and H_β are present in the SNe II spectra from the first days, so we do not include them in the plot. We can see that:

- He I/Na I D are present in all epochs, however around 15-25 days less SNe show the line. We suggest that in this epoch the transition from He I to Na I D happens. Therefore, after 30 days we refer to this line as Na I D. It is present in the 96% of the spectra from $\sim$ 35 days. Later than 43 days it is present in all spectra. Using a KS test, we analyze the SNe with and without the He I line between 18 and 22 days. We find that the line is present in SNe with smaller a/e values. No significant differences were found with other spectral and photometric parameters.

- The Ca II IR triplet is present in 50% of the sample at $\sim$ 20 days. Before 20 days it is present in $\sim$ 12% of the sample, while later than 25 days is visible in all the sample, however at 38 days only one spectrum does not show the line. The spectrum corresponds to SN 2009aj, which shows signs of CS interaction in the early phases. With the KS test between 18 and 22 days we find that there are no significant difference between SNe with the Ca II IR triplet and without it.

- The H_γ line starts to be blended with Fe-group lines from $\sim$ 20 days, growing dramatically at 35-45 days. Only one spectrum at $\sim$ 46 days does not have the blend (SN 2008bp). Meanwhile, a few spectra show H_β surrounded by the Fe II line forest. Using a KS test to find the difference between the distributions with/without the Fe II line forest, we find that faster declining (larger s_2 values) SNe do not show it. There is only $\sim 3.73 \times 10^{-4}$% chance that they are drawn from the same parent distribution. In general, the Fe II line forest is present in dimmer SNe (low velocities) and/or SNe in higher metallicity environments.

- The Fe-group lines start to appear around 10 days (see Figure 3.16). The first line that emerges is Fe II λ5169. We can see that few SNe exhibit the absorption feature before 15 days, however later at 15 days around 50% of SNe show the line and at 30 days all spectra have it. The next line that arises is Fe II 5018. This line is seen from 15 days, being present in all SNe later than 40 days. Meanwhile, Fe II 4924 is seen in one spectrum at 13 days (SN 2008br). From 30 days it is visible in more than 50% of the spectra. The Sc II/Fe II 5531, Sc II multiplet 5668, Ba II 6142 and Sc II 6246 are detectable later than 30 days. The emergence of the Sc II/Fe II 5531 and Sc II multiplet 5668 happens at similar epochs, as well as Ba II 6142 and Sc II 6246. Using a KS test between 38 and 42 days, we find less than 2% chance probability that SNe with Sc II and Ba II lines are drawn from the same metallicity environments as those SNe without them. This suggest the possibility to use these lines as metallicity indicators. Ba II 6142 and Sc II 6246 are also present in low luminosity SNe.

Table 3.7 Model properties

Model	Z $[Z_\odot]$	M_{final} $[M_\odot]$	R_* $[R_\odot]$	E_{kin} [B]
m15z2m3	0.1	14.92	524	1.35
m15z8m3	0.4	14.76	611	1.27
m15z8m3	1.0	14.09	768	1.27
m15z4m2	2.0	12.60	804	1.24
m15mlt1	1.0	14.01	1107	1.24
m15mlt3	1.0	14.08	501	1.34
m12mlt3	1.0	10.50	500	0.25

Summary of model properties used in this work.
Columns: (1) Model name; (2) Metallicity; (3) Progenitor mass; (4) Progenitor radius; (5) Kinetic energy

This analysis was also performed with synthetic spectra for seven different models, which have been presented by Dessart and Hillier (2005), Dessart et al. (2013a). The synthetic spectra used here present the characteristics showing in Table 3.7. In general, the synthetic spectra show the same behaviour that observed spectra. The transition between He I to Na I D is more evident, and it happens between 18 and 40 days. This implies that the transition in synthetic spectra is a little bit later than in observed ones. This could be due to the models only present limited variations in some parameters such as the explosion energy, the radius of the progenitor or the hydrogen envelope mass at the explosion. In the nature a big range of these parameters may cause a huge diversity, as we can see in our sample and its analysis. The Na I D is visible 100% of the sample after 50 days, only 5 days later than the observed spectra. Ca II shows the same behaviour in both synthetic and observed spectra, however H_γ is blended in all of the sample later than 90 days, unlike the observed spectra that show it from 45 days. On the other hand, the Fe II line forest is visible from 55 days, in contradiction to the observed spectra that show this characteristic from 30 days. This behaviour is only present in the spectra of higher metallicity model (2 times solar) and in the lower explosion energy model. The iron lines (Fe II λ4924, Fe II λ5018, Fe II λ5169, and the Fe II blended) are present from $\sim$ 15 days, however Fe II λ5169 is visible in 50% of the spectra, while Fe II λ4924 is only visible in less than 10%. From 30 days Fe II λ5169 is present in all the synthetic spectra, which is also seen in the observed ones. The behaviour of Fe II λ5018 and Fe II λ4924 is similar in both synthetic and observed spectra. We can see differences in the Fe II blend, which is visible in 100% of the sample from 50 days in the models, however in the observed spectra that never happens. More differences are also appreciable between models and observation in Sc II/Fe II λ5531, the Sc II multiplet λ5668, Ba II λ6142 and Sc II λ6246. These lines in models arise from 20 days, but in the observations it occurs from 38-40 days. Nevertheless, the evolution of the distribution is similar from 50 days. Although the observed and synthetic spectra have a similar behaviour, we can observe small differences, thus suggesting that the explosion mechanism is related with many different parameters which are not reproduced by the current models.

3.9.1 Expansion velocity evolution

Figure 3.17 shows the velocity evolution of eleven spectral features as a function of time. The first two panels of the plot show the expansion velocity of the H_α feature: on the left the velocity derived from the FWHM and on the right that derived from the minimum absorption flux. As we can see, the behaviour is similar, however the velocity obtained from the minimum absorption flux is offset between 1000 and 2000 km s^{-1} to higher velocities. Figure 3.18 shows this shift at 50 days. Velocities obtained from the minimum absorption flux are higher, with a peak in 8000 km s^{-1}, while the velocity derived from the FWHM shows its peak in 7000 km s^{-1}, and two outliers (extreme cases, the lowest and highest value). Figure 3.19 shows the velocity distribution for the eleven features at 50 days post explosion. We can see that H_α shows higher velocities than the other lines, followed by H_β. The lowest velocities are presented by the iron-group lines. In Figure 3.17 is possible to see that the H_β expansion velocity shows the typical evolution for a homologous expansion and like H_α, is possible to see it from early phases. The iron lines display lower velocities than the Balmer lines. According to that, the highest velocity in SNe II is found in H_α, which implies that it is formed in the outer layers of the SN ejecta. Meanwhile, based on the lower velocities, the iron-group lines form in the inner part, closer to the photosphere. The O I line does not show a strong evolution. As we can see, its velocity evolution is almost flat.

The lowest velocities are found in SN 2008bm, SN 2009aj and SN 2009au. However, these SNe are distinct from the rest of the population. Unlike sub-luminous SNe II (such as SN 2008bk

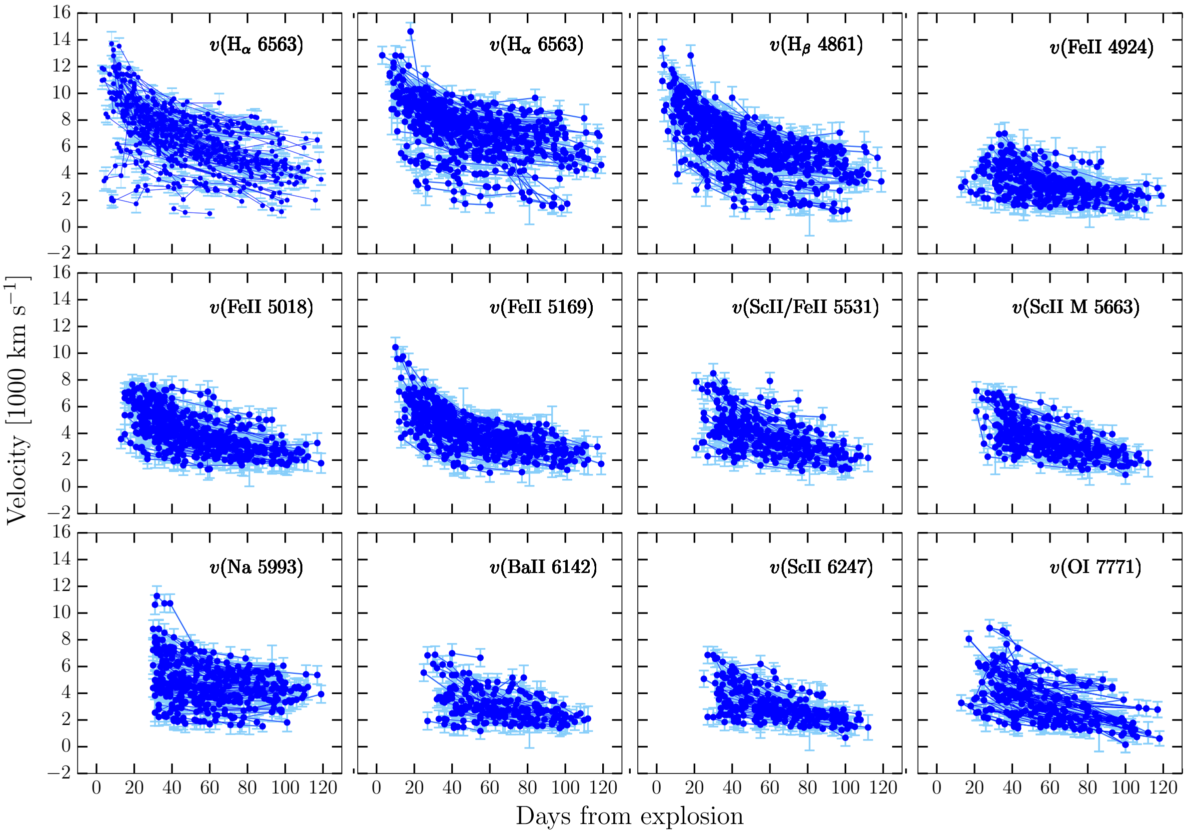

Figure 3.17 Expansion velocity evolution for H_α (from minimum flux absorption and the FWHM of emission), H_β, Fe II λ4924, Fe II λ5018, Fe II λ5169, Sc II/Fe II, Sc II multiplet, Na I D, Ba II, Sc II and O I from explosion to 120 days.

and SN 1999br) – that also display low expansion velocities – these events are relatively bright. They also show early signs of CS interactions, e.g., narrow emission lines. SNe showing the highest velocity depend on which line is being studied. However, in general terms SN 2007ab, SN 2008if, SN 2005Z have larger velocities.

3.9.2 Velocity decline rate of H_β analysis

The velocity decline rate of SNe II with time has not been previously analyzed. We estimate the $\Delta v(H_\beta)$ in five different epochs (which was detailed before) in order to understand their behaviour. We compare them against each other and they show a very strong correlation with each other. This correlation shows that SNe with a higher decline rate at early times keep this conduct at later epochs.

3.9.3 pEWs evolution

The temporal evolution of pEWs for each of the eleven spectral features is shown in Figure 3.20. In general the pEWs increase faster at early times but later, their evolution starts to be quasi-constant. The first two panels show the pEW evolution of H_α. On the left is displayed the

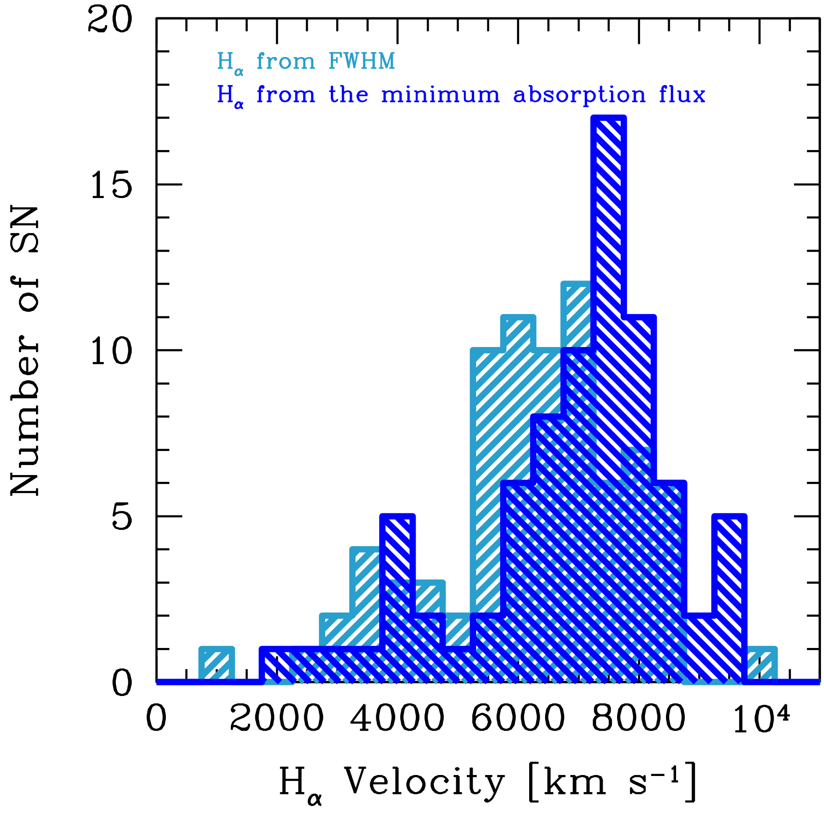

Figure 3.18 Distribution of the H$_\alpha$ velocity at at 50 days post explosion, obtained form the FWHM of the emission and from the minimum of the absorption.

absorption, while on the right the emission component. The absorption component has values from 0 increasing to ~ 120, however in a few SNe its evolution is different: from 70 days the pEW decreases significantly. This behaviour is observed in low and intermediate velocity SNe (e.g., SN 2003bl, SN 2006ee, SN 2007W, SN 2008bk, SN 2008in, SN 2009N). Generally, these SNe show a very narrow H$_\alpha$ P-cygni profile, and at around 70 days from explosion Ba II 6497 appears in the spectra as a dominant feature (see Roy et al. 2011 for more details). As H$_\alpha$ and Ba II 6497 are located almost at the same place in the spectrum, and at later time we see more deeper in the ejecta, Ba II grows up. In Figure 3.21 we can see the H$_\alpha$ P-Cygni profile with the presence of Ba II 6497, and the HV feature of hydrogen line (see section 3.9.4 for more details) on the blue side of Ba II.

Figure 3.20 also shows the H$_\alpha$ emission component evolution. An increment in the majority of SNe is appreciable. There are a couple cases (e.g. SN 2006Y) that display a quasi-constant evolution. The range of pEW of H$_\alpha$ emission goes up 400. In the case of H$_\beta$, we can see that from 60 days there are few SNe with lower pEW values, which show a quasi-constant evolution. SNe with this behaviour are those that show the Fe II line forest. The remaining SNe shows

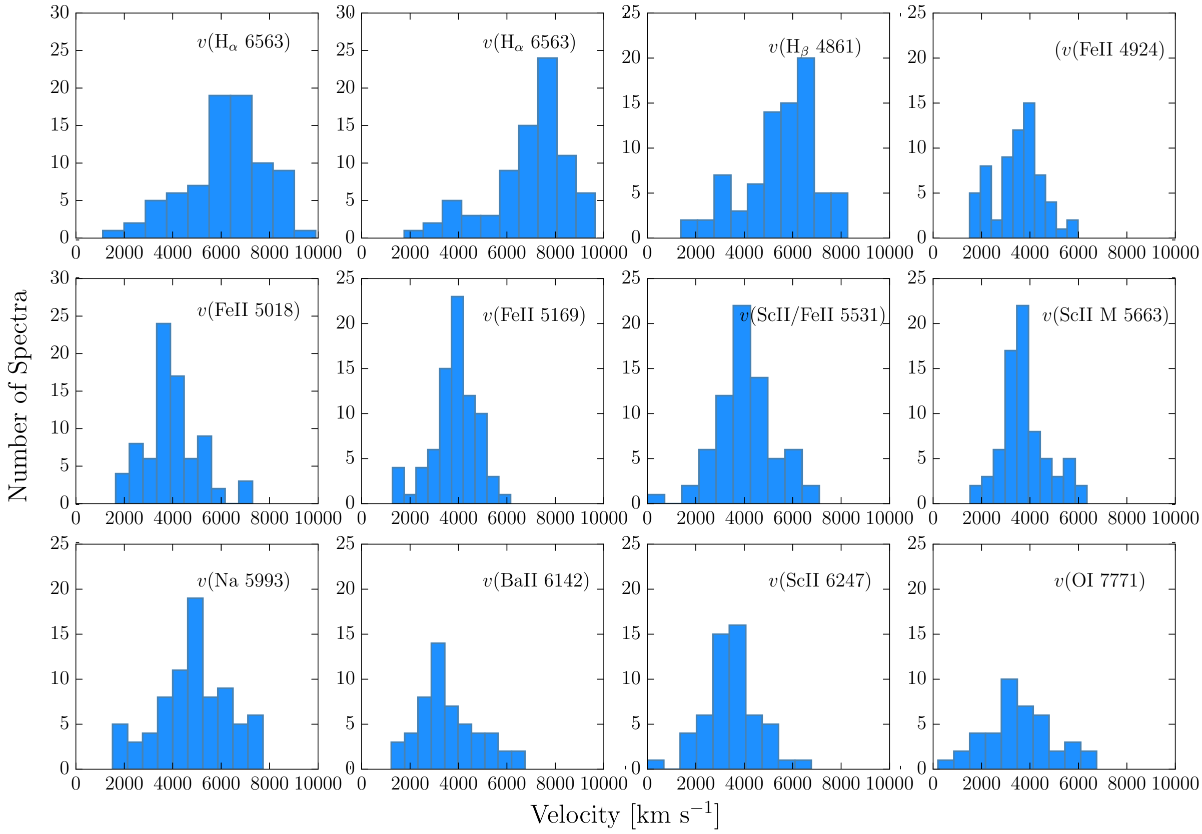

Figure 3.19 Distribution of the expansion ejecta velocities for 11 optical features at 50 days. The first two panels show the H_α velocity obtained from the FWHM and from the minimum absorption flux.

an increase. The pEWs of iron-group lines grow with time, however there is an evident number of SNe with pEW= 0. This indicates that one specific SN does not have the line yet. For Sc II/Fe II, the Sc II multiplet, Ba II, and Sc II this is more obvious. On the other hand, the O I shows an almost constant behaviour and Na I D a steady increase. Comparing the values, we can see that the absorption of H_α, H_β and Na I D have the highest values (from 0 to ~ 120), while Fe II 4924, Fe II 5018, Sc II/Fe II, the Sc II multiplet, Ba II, Sc II and O I have the lowest ones (from 0 to ~ 50).

The a/e evolution is displayed in Figure 3.22. One can see an increase until ~ 60 days and then, a constant or decreasing behaviour.

3.9.4 Cachito: Hydrogen HV features or the Si II λ6355 line?

The nature of Cachito has been studied in the last years. Its presence on the blue side of H_α has given rise to multiple interpretations, such as HV features of hydrogen (e.g. Leonard et al., 2002a, Baron et al., 2000, Chugai et al., 2007) or Si II 6355 (e.g. Pastorello et al., 2006). Seventy-two SNe from our sample show the Cachito in the photospheric phase, between 7 and 120 days post-explosion, however its behaviour, shape and evolution is different according to the epoch.

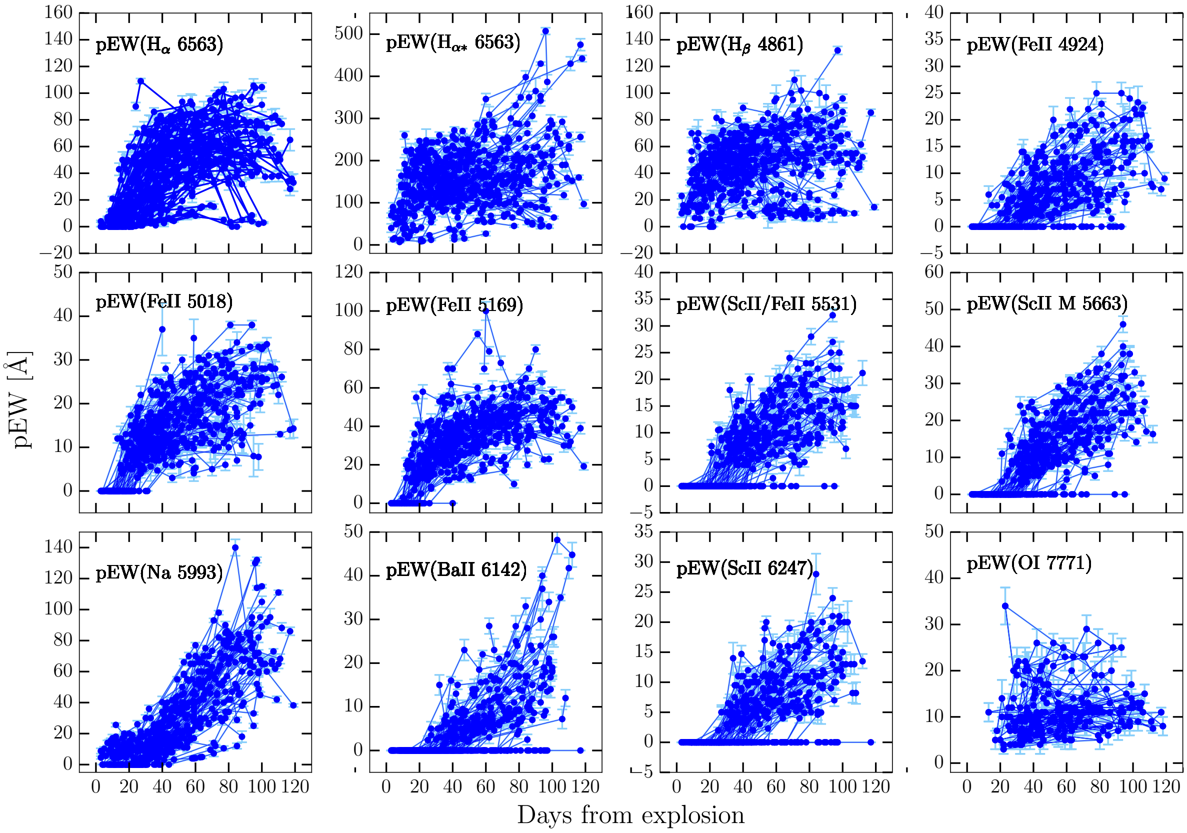

Figure 3.20 pEWs evolution for H_α absorption, H_α emission, H_β, Fe II λ4924, Fe II λ5018, Fe II λ5169, Sc II/Fe II, Sc II multiplet, Na I D, Ba II, Sc II and O I from explosion to 120 days.

In early phases (before 40 days) we detect the line in 55 SNe, while later than 40 days it is visible in 34 SNe. As we said, the Cachito could be due to HV features, Si II λ6355, or Ba II λ6497. However, in early phases the presence of Ba II is discarded because the temperature is too hot to produce the line. If Cachito is produced by Si II, its velocity should be similar to those presented by the metal lines. Comparing the Cachito velocities with those obtained by Fe II λ5018 and Fe II λ5169, we find that 24% of SNe present a good match, which could favour the Si II interpretation. However, 28 SNe have the Cachito velocity much higher than Fe II lines[11]. This suggests the presence of HV hydrogen features. In Figure 3.23 we present the velocity comparison, where a good agreement is found between Cachito, assumed as Si II λ6355 (blue), and the iron lines, Fe II λ5018 (green) and Fe II λ5169 (red). SNe with Cachito related to Si II show the line before 35 days, only 3 SNe display it later. Using a KS test we analyze the a/e parameter in SNe II with/without Si II and we find that there is only 4% chance that these SNe II are drawn from the same underlying population. SNe II with Si II have smaller a/e values in comparison with those SNe that do not have the line.

[11]Four SNe show a good match with Si II in very early phases, but later than 30 days they do not show it. They also show a different shape between both characteristics (Si II and HV features of hydrogen).

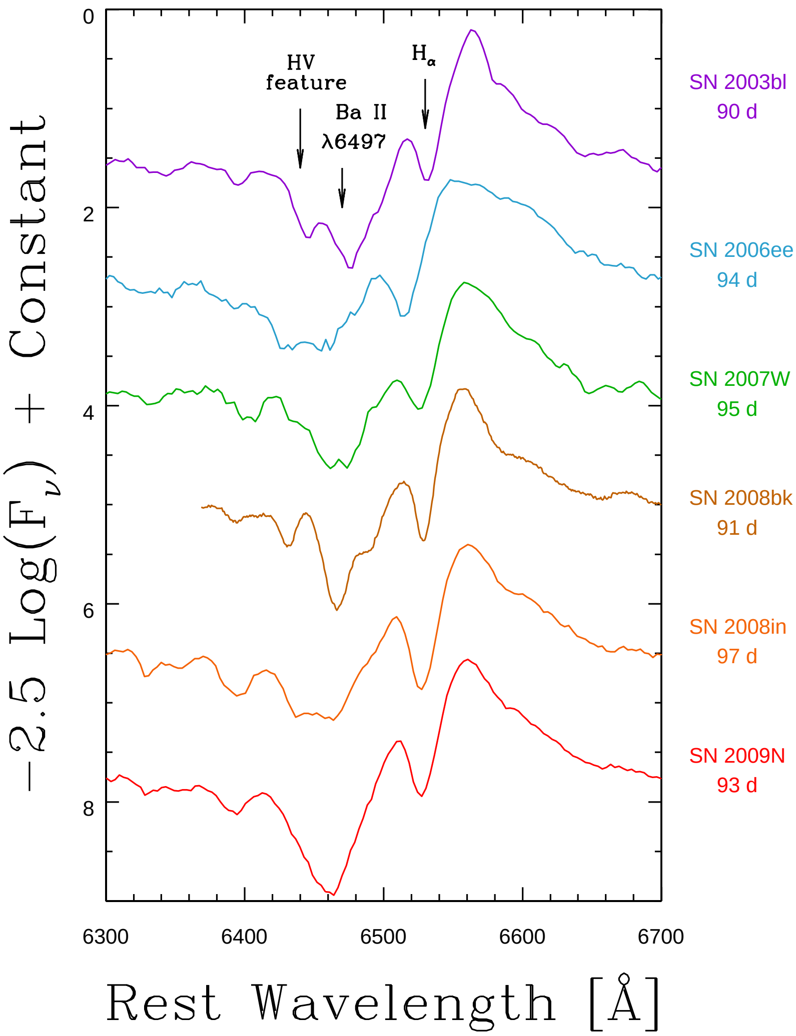

Figure 3.21 H_α P-Cygni profile of low and intermediate velocity SNe II: 2003bl, 2006ee, 2007W, 2008bk, 2008in and 2009N around 95 days post-explosion.

According to Chugai et al. (2007), the interaction between the SN ejecta and the RSG wind should result in the emergence of these HV absorption features on the blue side of H_α and He I λ10830. They argue that the existence of a shallow absorption feature is the result of the enhanced excitation of the outer unshocked ejecta. As in the H_β line the optical depth is low, the HV feature is not expected in this line, however in H_α it could increase with the wind density. Analyzing the Cachito as a HV feature of hydrogen for these 28 SNe (before 40 days), we find a velocity range between 8500 and 15800 km s^{-1}. Investigating the full sample in detail, we have 37 SNe with this shallow feature, between 20 and 80 days. Our result is consistent with those

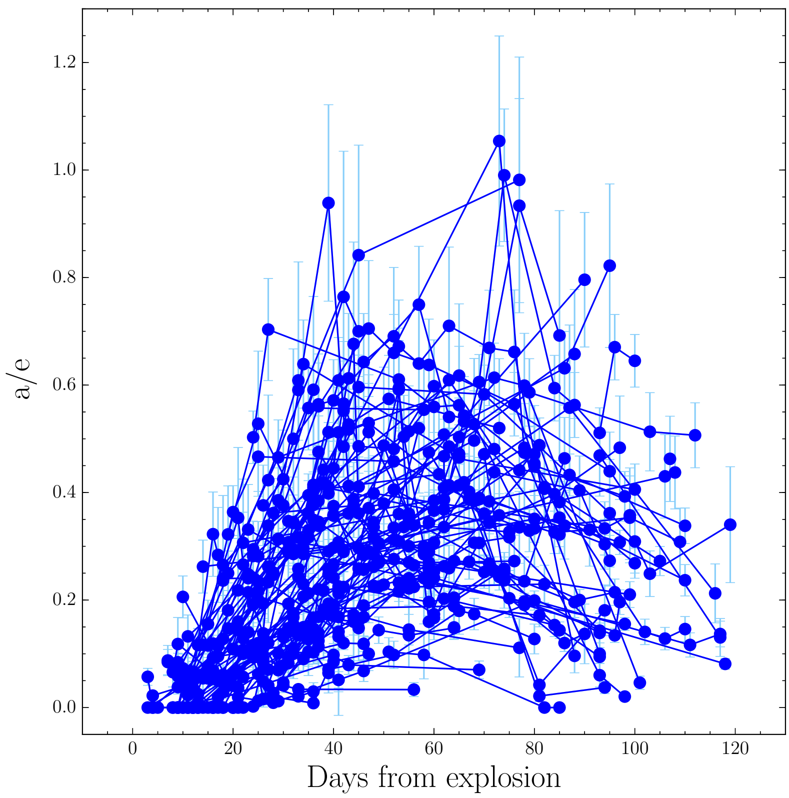

Figure 3.22 Evolution of a/e between explosion and 120 days.

presented by Chugai et al. (2007) for SN 1999em.

Later than 40 days we detect the presence of Cachito as a narrow and deeper absorption, both on the blue side of H_α and H_β (see an example in Figure 3.25, where both features are shown). Chugai et al. (2007) argue that in addition to the HV shallow absorption (explained above), a HV notch is formed in the cool dense shell (CDS) behind the reverse shock (similar to the one we detected). We measure the velocities for the Cachito as HV features, both in H_α and H_β. We find that the HV H_α and HV H_β are consistent, which favours the hypothesis of CS interaction. The HV H I is found in 30 SNe, however in the low velocity/luminosity SNe, it is only present in H_α. This may be because after 50 days the blue part of the spectrum (<5000 Å) is dominated by the metal lines (see the previous analysis), which may hinder its detection in H_β. Nonetheless, we argue that these are HV features because the low velocity/luminosity SN, e.g. SN 2006ee shows in spectra at around 50 days both components, in H_α and H_β at similar velocities. As we do not have sufficient data for the other low velocity/luminosity SNe at similar epochs, we only see the feature in H_α. This analysis is displayed in Figure 3.24, where the H_α (red), HV H_α (blue), H_β (cyan), and HV H_β (green) velocity evolution is presented for 20 SNe.

Summarizing, Cachito is originated by two different effects: Si II before 40 days, and HV

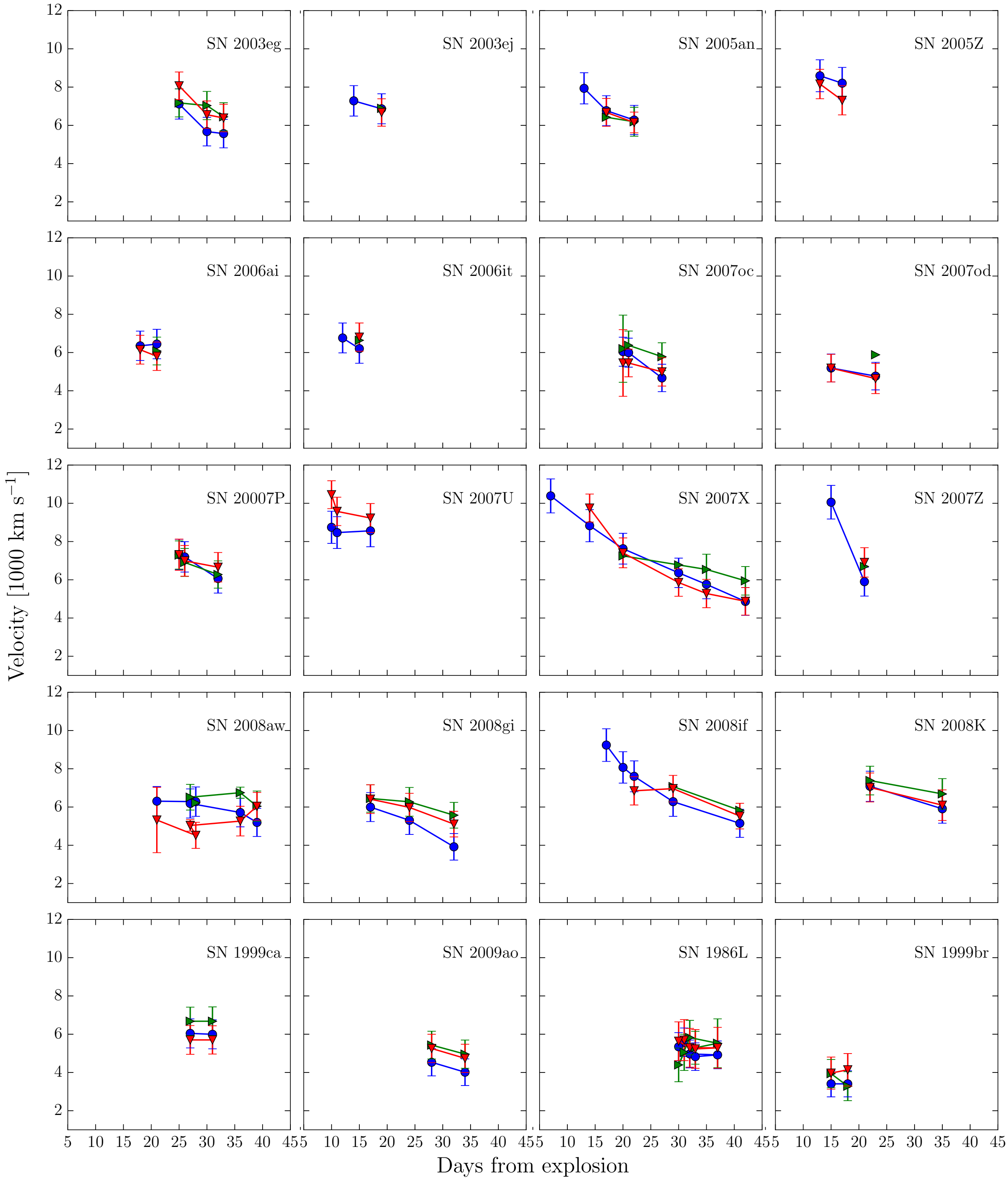

Figure 3.23 Velocity evolution of Cachito (blue) at early phases compared with Fe II λ5018 (green) and Fe II λ5169 (red).

hydrogen features, as shallow absorption later than 30 days, and as deeper and narrow absorption after 40 days.

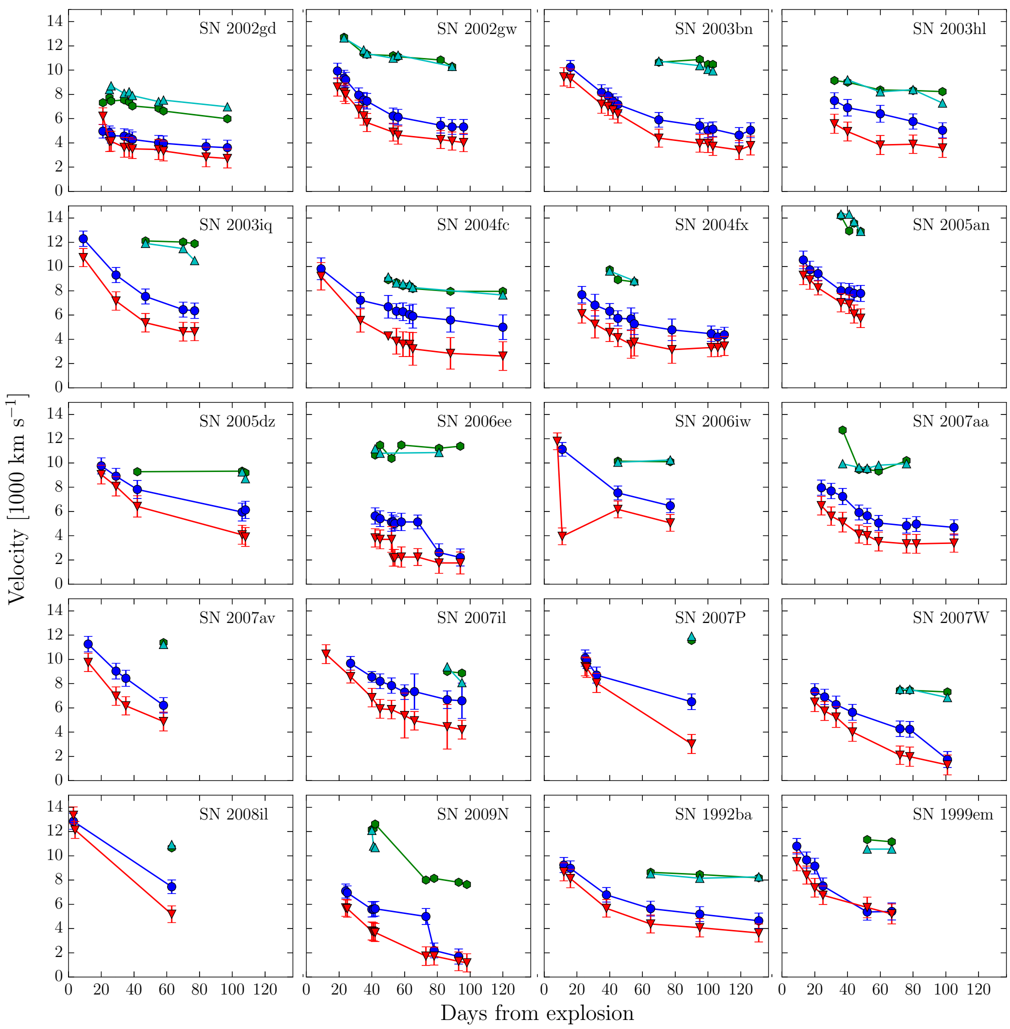

Figure 3.24 Velocity evolution of Cachito in the plateau phase compared with the Balmer lines. In green: HV of H_α, in cyan: HV of H_β, in blue: the H_α velocity and in red the H_β velocity.

3.9.5 O I λ7774

Faran et al. (2014b) suggested that O I λ7774 can be used as proxy for a helium rich ejecta. They argue that fast declining SNe are more helium rich, and hence hydrogen poor. This conclusion is based on the higher pEW values of O I relative to H_α. As we said in previous sections (see section 3.7.6), O I is contaminated by the telluric A-band absorption, and its analysis is more complicated by this fact. In spite of this, we analyse the line in those SNe where the telluric line is clearly separated from O I. Thus, the analysis was possible in 49 SNe II ($\sim$ 40% of our sample).

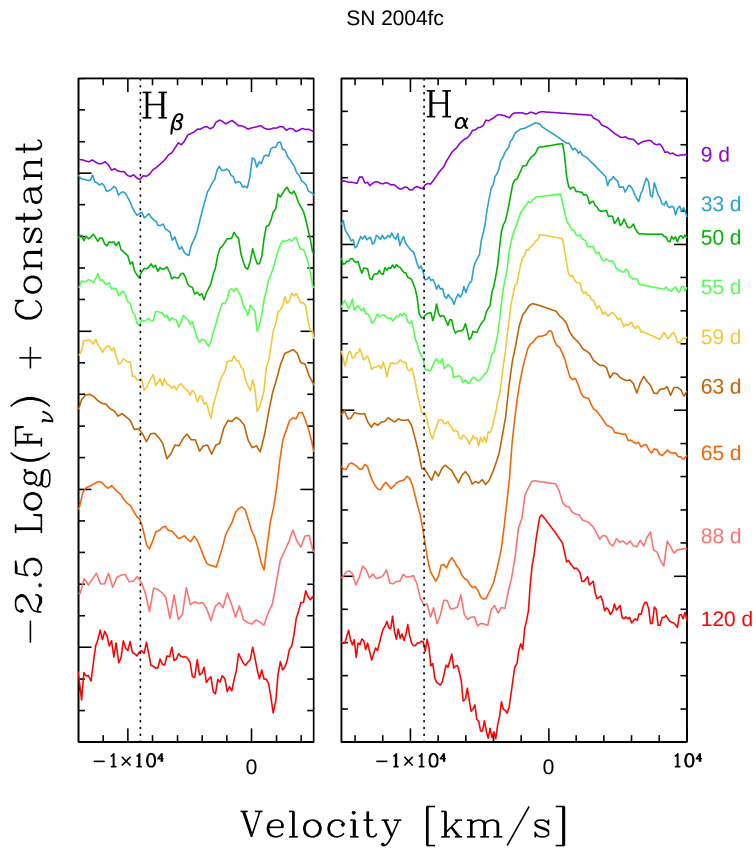

Figure 3.25 Spectral evolution of H_α and H_β lines of SN 2004fc. The dotted lines correspond to the HV features seen on the blue side of H_α and H_β from 50 to 120 days. We can see that the HV features show a velocity evolution from $\sim$ 9000 to $\sim$ 8000 km s^{-1}.

Reproducing Figure 14 from Faran et al. (2014b), but at 35 days since explosion, we find the same behaviour. Faster declining SNe show higher pEW(O I)/pEW(H_α abs). Figure 3.26 shows this relation. Using the Pearson Correlation test, we find a moderate correlation of 0.52. However, we note that this correlation is biased by H_α absorption measurement. According to Gutiérrez et al. (2014), fast declining SNe show smaller pEW of the H_α absorption component, thus, this parameter that could control the ratio. Despite this, we check the relation between the pEW of O I and s_2 and we find a weak correlation (0.39). In order to analyze if faster declining SNe have the O I line stronger than plateau ones, we divide our sample in fast declining SNe (s_2 >1.5) and plateau SNe. A KS-test gives 35.4% probability that the two distribution are drawn from the same parent population, which implies that the oxygen abundance does no affect the light curve behaviour. In fact, according to the radiative-transfer simulations, when the main sequence mass increases, the atmosphere should be more nitrogen rich and more oxygen poor, so O I is not a diagnostic of He I abundance (private communication with Luc Dessart) . This result contradicts the conclusions of Faran et al. (2014b).

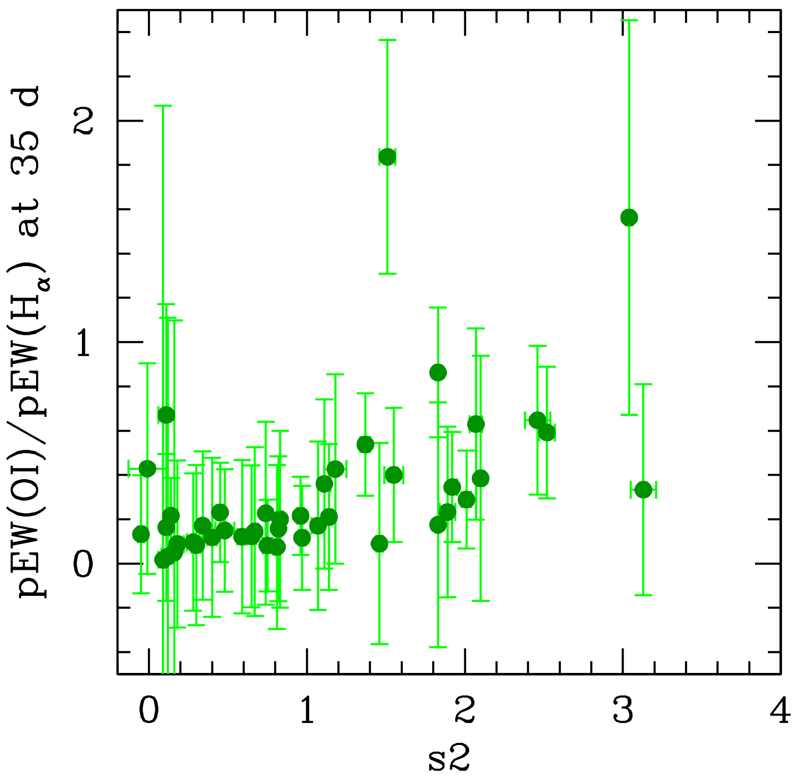

Figure 3.26 Correlation between pEW(O I)/pEW(H_α abs) and s_2 at 35 days since explosion.

3.10 Conclusions

In this work we have presented the optical spectra of 123 nearby SNe II observed between 1986 and 2009. A total of 893 spectra ranging between 3 and 363 days post explosion have been analysed. A statistical analysis of the spectral matching technique was discussed as an alternative to non-detection constraints for estimating SN explosion epochs.

In order to quantify the diversity of the spectra we analyse the appearance of the photospheric lines and their time evolution in terms of the a/e and H_α velocity at $t_{tran+10}$, M_{max}, s_2, and metallicity (M13 N2). We analysed the velocity decline rate of H_β, the a/e evolution, the expansion ejecta velocities and the pEWs for eleven features: H_α, H_β, He I/Na I D, Fe II λ4924, Fe II λ5018, Fe II λ5169, Fe II blended, Sc II/Fe II, Sc II multiplet, Ba II, Sc II, and O I. We find a large range in velocities and pEWs, which can be related with a diversity in the explosion energy, radius of the progenitor, and metallicity. In addition, we analysed the nature of Cachito during the photospheric phase. We used and analysed 7 spectral models with different explosion properties with the aim of understanding the spectral evolution with time. The evolution in both, observed and synthetic spectra shows few differences, probability due to the lack of more diverse models.

The main results obtained with our analysis are summarizing as follows:

- The H I lines are present in the SNe II spectra from the first days until the nebular phase. However, at around 20 days, H_γ and H_δ start to be blended with the Fe II-group lines.

- In early phases (before than 20 days), SNe II show the He I 5876 feature. Between 15 and 25 days the transition between He I and Na I D happens. Therefore, later than 30 days the feature presented in the spectra is associated to Na I D.

- Around of 18% of our sample display the Fe II line forest. These absorption features around H_β emerge at ~ 30 days post-explosion. Using KS test we find that fast declining SNe do not show the forest. The Fe II line forest is present in dimmer SNe II with low velocities and/or in high metallicity environments. Comparing this result with the synthetic spectra, we find that the forest is visible from 55 days and it is only present in higher metallicity (2 times solar) and lower explosion energy models, which is consistent with our observed results.

- The Ca II IR triplet is present in the SNe II spectra from 20 days. Its appearance happens almost at the same time that Fe II 5018.

- The Fe II-group lines start to appear at around 10 days. The first line that emerges is Fe II λ5169, followed by Fe II λ5018 and Fe II λ4924. Fe II blend, Sc II/Fe II, Sc II multiplet, Ba II, Sc II are visible from 30 days post-explosion. A KS test shows that the Sc II and Ba II lines are more sensitive to metallicity than Fe II lines.

- Around of 60% of our SNe II show the Cachito feature between 7 and 120 days since explosion. Cachito at early phases is associated with Si II λ6355 and it could be related with higher temperatures. This feature shows similar velocities to those presented by metal lines, such as Fe II λ5169 and Fe II λ5018 (between 10000 and 2000 km s^{-1}). SNe with Si II show, in general, a weak H_α absorption component. In the recombination phase, Cachito is associated with the HV features of hydrogen lines. Its presence later than ~ 25 days could imply signs of interaction between the SNe ejecta and the RSG wind. Fifty-three SNe of our sample display the line, however based on their shape we divided them into two groups: SNe with a shallow absorption and SNe with a notch absorption.

- In early phases (before 25 days), SNe II with a weak H_α absorption component present the He I λ5876 and the Si II λ6355 features. We speculate that these SNe have higher temperatures at this epoch.

- SNe II display a huge variety of velocities. The H_α line shows the highest velocity, followed by H_β, while the lowest velocities are presented by the Fe II-group. The velocities evolution are well fitted with power laws, however for O I line its velocity evolution is almost constant.

- The H_α velocities derived from the minimum absorption flux show a shift to higher velocities of $\sim$ 1000 km s^{-1} compared to those obtained from the FWHM of the emission component. However, their behaviour and evolution with time are similar.

- O I λ7774 absorption relative to H_α shows stronger values in fast declining SNe II, as Faran et al. (2014b) showed. However, we conclude that O I is not a good proxy for a helium-rich envelope.

- Three SNe in our sample (SN 2008bm, SN 2009aj and SN 2009au) show the lowest velocities, nevertheless unlike sub-luminous SNe II that also present low velocities, they are relatively bright. We found that these SNe have early signs of CS interactions.

- SNe II with a higher velocity decline rate at early times present the same behaviour at late epochs.

- In SNe II, the pEWs temporal evolution presents an increase faster in the early times but later, their evolution start to be quasi-constant. This behaviour is seen in H I and Fe II-group lines, however in Na I D, it is steady increase.

- We find that six low and intermediate velocity SNe (e.g., SN 2003bl, SN 2006ee, SN 2007W, SN 2008bk, SN 2008in, SN 2009N) show a complex H_α P-cygni profile: a small and narrow absorption associated to H_α feature and an extra broad and strong absorption component corresponding to Ba II λ6497.

All data analysed in this work are available on http://csp1.lco.cl/, as well as the additional SNID templates (22 SNe), for the SNe II comparison.

Chapter 4

Type II supernova spectral diversity. Paper II: Spectroscopic and photometric correlations

4.1 Abstract

We present an analysis of correlations between various of spectral and photometric parameters of more than 100 type II supernovae. Looking for correlations at three different epochs (30, 50 and 80 days from explosion), we find that they are stronger at 50 days. We speculate that this happens because at this epoch all the SNe II are in the recombination phase and probably they have similar physical conditions. Analyzing these correlations, we find that supernovae with higher velocities are brighter, have more rapidly declining light curves, shorter optically thick duration phases and shorter plateau durations, and higher ^{56}Ni mass. Trying to relate the observed parameters of the SN with the physical properties of the progenitor star and explosion, we conclude that the plateau duration (Pd) is the best hydrogen mass indicator. We also find that the hydrogen mass does not affect the expansion velocities observed, while neither does the explosion energy significantly affect the plateau duration. A relation between SNe II with the Si II λ6355 line and the decline rates in the light curve are found. We suggest that these SNe have progenitor stars with larger radius.

4.2 Introduction

It is commonly accepted that Core-Collapse Supernovae (CC-SNe) are produced by the explosion of massive (> 8 M$_\odot$) stars, which collapse when they have spent their nuclear fuel. CC-SNe display a wide spectral and photometric variety that leads to their classification. One of the most commonly applied SN type classifications is based on the presence or absence of hydrogen within SN spectra. SNe where hydrogen is clearly visible are called SNe II, while those without these features correspond to SNe Ib/c (Minkowski, 1941, Filippenko, 1997).

Initially, SNe II were classified according to the shape of the light curve: SNe with a faster decline rate are called SNe IIL, while SNe with almost constant luminosity for several months were called SNe IIP (Barbon et al., 1979). However, years later, two new classes of SNe II emerged: SNe IIn and SNe IIb. SNe IIn show narrow emission lines in their spectra, possibly due to interaction with a circumstellar medium (CSM) (Schlegel, 1990), while SNe IIb are thought to be transitional events between SNe II and SNe Ib (Filippenko et al., 1993). The overall properties of SNe IIn and SNe IIb are sufficiently distinct from 'normal' SNe II, that we do not include them for study, and they are no longer discussed in this paper.

With ever increasing numbers of SNe, new sub-classes have appeared. Menzies et al. (1987), Catchpole et al. (1987, 1988) presented the analysis of SN 1987A, an object that exhibited typical characteristics of the SN II spectra, but a peculiar light curve. With this SN the 87A-like objects were introduced. Examples of these SNe can be found in Pastorello et al. (2005), and Taddia et al. (2013)[1]. Later, Pastorello et al. (2004) and more recently Spiro et al. (2014) studied the properties of low luminosity SNe II, which have narrow spectral lines (indicating low expansion velocities) and low luminosities. On the other hand, Inserra et al. (2013) analyzed a group of luminous SNe II. Lately, intermediate luminosity SNe (e.g. Roy et al., 2011, Takáts et al., 2014) have been also studied, supporting the wide diversity in SNe II.

Red Super-Giant (RSG) stars with zero-age main-sequence mass $\geq 8\ M_\odot$ have generally been assumed as the progenitors of SNe II, with hydrodynamical modelling supporting this hypothesis (Chevalier, 1976). In recent years, a significant number of direct identifications of the progenitor stars of nearby SNe IIP (e.g. Van Dyk et al., 2003, Smartt et al., 2004, 2009, Maund and Smartt, 2005, Smartt, 2015) suggest that Red Supergiant (RSG) stars with masses of 8 - 20 $M_\odot$ are their progenitors, supporting initial assumptions. There is weak evidence of the range of mass of SNe IIL because only two direct identifications have been obtained (Elias-Rosa et al. 2010, 2011, but see Maund et al. 2015), however these do give some evidence in favor of higher mass progenitors. However, a recent analysis by Valenti et al. (2016) did not find any evidence for progenitor mass differences between SNe II of different decline rates.

While direct detections of progenitors have constrained a relatively narrow mass range for SNe II, the same SNe show significant differences in their final explosive displays (e.g. SN 2008bk, a low luminosity event, and SN 2004et, a normal SNe II). It must therefore be the case that differences in stellar evolutionary processes leave the progenitors in different final states (e.g. the extent of the hydrogen envelope, the progenitor radius at explosion) or explode with e.g. different energies, in order to produce the diversity we observe.

Theoretical studies have suggested that progenitors that explode with smaller hydrogen envelope masses produce faster declining light curves (SNe IIL), together with shorter or non-existent 'plateaus' (Litvinova and Nadezhin, 1983, Popov, 1993, Moriya et al., 2016). An

[1] As the SN 87A-like objects have different progenitor properties than 'normal' SNe II, we also exclude them from our analysis.

alternative study presented by Kasen and Woosley (2009) shows that a change in the explosion energy leads to a range of luminosities, velocities, and light curve durations. That is to say, higher explosion energies result in brighter events with higher expansion velocities and shorter plateaus. They also found that an increasing synthesised ^{56}Ni mass extends the length of the plateau (see also Bersten 2013). Meanwhile, Dessart et al. (2013b) using radiative-transfer models explored the properties of SNe II changing the physical parameters (e.g. metallicity, explosion energy, radius). They found that the radius has an influence in the temperature evolution (more compact objects evolve faster) and in the plateau brightness, while a variation in the explosion energy leads in a variation of the plateau brightness and the plateau duration, which is consistent with the Kasen and Woosley (2009) predictions.

To quantify the spectral and photometric diversity, a few statistical studies of SNe II have been published. Patat et al. (1994) characterized the properties of 57 SNe II using the maximum B-band magnitude, the color at maximum and the ratio of emission to absorption (e/a) in H_α. They concluded that faster declining events are more luminous, have shallower P-Cygni profiles (larger e/a values) and are bluer than SNe IIP. After this work, the majority of more recent studies are focused on SNe IIP. Hamuy et al. (2002) analyzed 17 SNe IIP and found that SNe with brighter plateaus have higher expansion velocities. Hamuy (2003) concluded that more massive SNe IIP progenitors produce more energetic explosions and in turn produce more nickel. Similar results were found by Pastorello et al. (2003) and more recently by Faran et al. (2014a). The only exception to these works about SNe IIP was published by Faran et al. (2014b), whom analyzed a sample of SNe IIL.

Most recently Gutiérrez et al. (2014), Anderson et al. (2014a) with large samples analyzed the dominant line in SNe II, the H_α P-Cygni profile. Gutiérrez et al. (2014) working with 52 SNe II concluded that the differences in the ratio of absorption to emission (a/e) on H_α are mainly related with the mass of the H envelope at the moment of the explosion. This shows that SNe with less pronounced absorption are brighter and have fast declining light curves. Meanwhile, Anderson et al. (2014a) analyzed the blueshifted offset in the emission peaks of H_α of 95 SNe II. Through comparison to spectral modelling (Dessart et al., 2013a), they argue that this behaviour is a natural consequence of the distinct density distribution found in SN ejecta.

With the analysis of 117 SNe II, Anderson et al. (2014b) studied the light curve diversity of these objects. They found that SNe II with shorter plateau duration (Pd) exhibit faster decline rates (s_2 in their nomenclature). They concluded that the envelope mass at the epoch of explosion is the dominant physical parameter that explains this observed diversity. Similar results were found by Sanders et al. (2014) and Valenti et al. (2016). They also found that SNe IIP and SNe IIL show a continuum in their photometric properties and it is not possible separate into two different types.

In addition to these results, Anderson et al. (2014b) found relatively high radioactive decline rates (s_3) values for a significant number of SNe. As s_3 is related with ^{56}Co decay, and the expected decline rate value for full trapping of gamma-ray photons is 0.98 mag per 100 days, a higher decline rate implies lower ejecta mass where full trapping is not achieved. As we can see, the relation between observed parameters and physical properties are limited only to few parameters (e.g. hydrogen envelope mass, explosion energy), however, more links between observed and physical properties have not been established until now, which encourages us to further investigate them.

While there is now an abundance of literature on individual SNe II, together with much recent work on photometric diversity within this class, large scale studies focussing on the spectral diversity of SNe II are still lacking. This motivates our current work where we study a sample of almost 1000 optical-wavelength spectra of $>$ 100 SNe II. To that aim, we divide the analysis into two chapters. In chapter 3 we present the full description of the observations, data reduction techniques, and the spectral properties. We discuss also the spectral matching technique to estimate the explosion epochs, the analysis of the spectral line evolution and the nature of the extra absorption component on the blue side of H_{α}.

Here, in chapter 4 we present an analysis of correlations between different spectral parameters defined to explore the diversity of SNe II, together with their correlation with previously defined photometric parameters. Expansion velocities, pseudo-equivalent widths (pEWs), the ratio of absorption to emission (a/e) of the H_{α} P-Cygni profile, and velocity decline rates are used to search for correlations with photometric parameters and between other spectral properties. We analyze the spectral correlations and we determine the most important properties to compare them with the photometric parameters. Our overall aim is to search for trends between different measured parameters, and then attempt to link these to the underlying physical properties of SN II progenitors.

The chapter is organized as follows. Section 4.3 briefly describes the data employed to this analysis. In Section 4.4 we describe the measurements techniques. The observed parameters and their physical implications are explained in Section 4.5. The full analysis is presented in Section 4.6, while the discussion is in Section 4.7 and conclusions in Section 4.8.

4.3 Data

The data used in this analysis were published in Gutiérrez et al. (2016) and Anderson et al. (2014b). The details of the spectroscopic and photometric observations and reductions can be found in the mentioned studies. On average we have 7 spectra per SN and their $V-$band light-curve evolution. Details of these SNe are available in Anderson et al. (2014b), Anderson et al. (2014a), Gutiérrez et al. (2014), Galbany et al. (2016), Gutiérrez et al. (2016).

A small number of SNe presented in Gutiérrez et al. (2016) are excluded from this work: SN 2009A shows atypical spectra and weird behavior that complicates their analysis. SNe 1988A, 1990E, 1992ad, 1992am, 1993A, 1999eg, 2002ew, 2003dq, 2004dy, 2005dw, 2005es, 2005K, 2005me, 2006bc, 2007Z, 2008F, 2009W are not used in the current analysis as they have insufficient spectral and/or photometric data to be useful.

4.4 Measurements

SN II evolution with time can be studied according to both spectral and photometric behaviour. At early phases the spectra exhibit the Balmer lines (H_α, H_β, H_γ, H_δ), and He I λ5876 Å. With time, the iron group lines start to appear and to dominate the region between 4000 and 6000 Å. The Ca II triplet, Na I D, and O I also emerge. The light curve at the beginning shows a slight decline, which is powered by the shock wave. Around $\sim$ 30 days post-explosion a plateau arises. It is powered by the recombination of hydrogen in the SN ejecta. When the recombination phase ends (around 80-120 days post explosion), the transition to the nebular phase starts and the light curve drops. Once this happens, the radioactive tail phase starts. This phase is powered by the radioactive decay of ^{56}Co to ^{56}Fe. Later than $\sim$ 200 days, the spectra are dominated by forbidden lines, which are formed in the inner part of the ejecta. Both spectral and photometric diversity have been observed, which suggest differences in the explosion and progenitor star.

To study the diversity within SNe II we use the spectral and photometric parameters defined in Gutiérrez et al. (2014) and Anderson et al. (2014b). We also define a number of additional parameters below. These measurements are chosen to enable a full characterisation of the diversity of SN II V-band light-curve and optical wavelength spectra.

4.4.1 Spectral measurements

Before proceeding with our spectral analysis, below we summarise the parameters we will use, as defined in Gutiérrez et al. (2016):

- *vel*: corresponds to the expansion ejecta velocity. It is derived from the minimum flux of the absorption component of P-Cygni line profile. In this analysis we measure this parameter for eleven features in the photospheric phase: H_α, H_β, Fe II 4924, Fe II 5018, Fe II 5169, Sc II/Fe II 5531, Sc II M, Na I D, Ba II 6142, Sc II 6247, and O I 7774. In the case of H_α, the velocity was also derived using the full width at half maximum (FWHM) of the emission component.

- $\Delta v(H_\beta)$: defined as the rate of change of the expansion velocity of the H_β feature. This parameter was measured at 5 distinct intervals (see Gutiérrez et al. 2016), however here we only use the interval $50 \leq t \leq 80$ days, as this shows the highest correlation with other parameters.

- Δvel: defined as the velocity difference between H_α and Fe II 5018, and Na I D and Fe II 5018.

- pEW: corresponds to the absorption/emission strength of a particular line. Here, we measure the absolute value of pEW for the same features shown above.

- a/e: defined as the flux ratio of the emission to absorption component of H_α P-Cygni profile.

Although the spectroscopic measurements (velocities and pEWs) were done in all phases where data were available, to characterize our sample we choose a common epoch with respect to the explosion date. Thus, we use values at 30, 50 and 80 days from explosion. Interpolation and extrapolation is used to obtain parameter values at these epochs. The values obtained by the interpolation are used when two available spectra are present ±15 days around the common epoch, while the values from the extrapolation are used at ±10 days. These intervals were chosen as they increase the strength of observed correlations. Using bigger intervals causes a drop of correlations because the polynomial does not produce reliable results in some cases (particularly for the pEW). At ±15 and ±10 days for interpolation and extrapolation, respectively, the results do not show a significant change comparing with those obtained using a smaller interval. Hence, our choice intervals is justified. To estimate the velocity at a common epoch, we do an interpolation/extrapolation using a power law fit, while for the pEW we use a low order (first or second) polynomial fit. Power law fits were found to produce satisfactory results in the case of velocity measurements, however for pEWs we found that low-order polynomials were required. For this parameter we used a low order polynomial and the best fit was determined by the lower normalized rms. The errors of each measurement were obtained with the rms error fit. In summary, we are able to use spectral parameter values in in 88, 78, and 59 SNe at 30, 50 and 80 days, respectively.

4.4.2 Photometric measurements

Historical separation of SNe II into distinct classes has been achieved through photometric differences in e.g. decline rates and absolute magnitudes. Hence it is essential to include photometric parameters in our analysis for a full understanding of observed correlations and their implications for SN II physics. Here, we use the V-band photometric parameters already defined (and measured) in Anderson et al. (2014b), which we now summarise:

- t_0: corresponds to the explosion epoch (see Gutiérrez et al. 2016 for more details of their estimation.)
- t_{tran}: determined as the transition between the initial decline (s_1) and the plateau decline (s_2).
- t_{end}: corresponds to the end of the optically thick phase.
- t_{PT}: is the mid point of the transition from 'plateau' to radioactive tail.
- $OPTd$: is the optically thick duration phase, defined between t_0 and t_{end}.
- Pd: is the plateau duration, defined between t_{tran} and t_{end}.
- M_{max}: defined as the initial peak in the $V-$band light-curve.
- M_{end}: defined as the absolute $V-$band magnitude measured 30 days before t_{PT}.

- M_{tail}: defined as the absolute $V-$band magnitude measured 30 days after t_{PT}.
- s_1: defined as the decline rate in magnitudes per 100 days of the initial, steeper slope of the light-curve.
- s_2: defined as the decline rate ($V-$band magnitudes per 100 days) of the second, shallower slope in the light curve.
- s_3: defined as the linear decline rate ($V-$band magnitudes per 100 days) of the slope reached after its transition from the previous 'plateau' phase.
- ^{56}Ni mass: corresponds to the mass of nickel synthesised in the explosion (see Anderson et al. 2014b for exact details of how this was estimated).

Values for these parameters can be found in Table 5 in Anderson et al. (2014b). However, it should be noted that in this work some of these parameters were updated: t_{tran}, Pd, M_{max}, M_{end}, M_{tail}, s_1 and s_2. In the case of the magnitudes, we found that ignoring host galaxy extinction corrections actually produced higher correlations than including them. This suggests that a) in the vast majority of cases host galaxy extinction is relatively small, and b) when we do make extinction corrections (using the absorption Na I D in Anderson et al. 2014b), such corrections are not particularly accurate. Therefore, all magnitudes are being used without host galaxy extinction corrections. For t_{tran} we used the F-test to decide whether the fit was better or not (Anderson et al. 2014b used the BIC criterion. For more details about the F-test, see Galbany et al., in prep.). This method increases the number of SNe with t_{tran} available. This then increases the number of SNe for which we can define s_1 and Pd. All values used in the current analysis are listed in Table 4.2.

Besides the parameters defined by Anderson et al. (2014b) we include two more parameters:

- $\Delta E(B-V)$: defined as the color gradient. We defined this parameter in three different range: $10 \leq t \leq 20$d, $10 \leq t \leq 30$d, and $20 \leq t \leq 50$d.
- Cd: corresponds to the cooling phase durations (Cd), defined between t_0 and t_{tran}.

4.5 Observed parameters and their physical implications

The basic properties of the progenitor stars and explosion that have a significant influence on SN II diversity are the explosion energy (E), ejecta mass (M_{ej}), pre-supernova radius (R_0), the ^{56}Ni mass, and metallicity. Theoretical works (e.g. Young, 2004, Kasen and Woosley, 2009, Dessart et al., 2013a) have studied how variations of these parameters influence their light-curves and spectra. They found that luminosity, expansion velocities and plateau duration depend on these parameters.

The most commonly used parameter to link observed SN properties to progenitor characteristics has been the duration of the plateau. It has been associated to the hydrogen envelope mass of the progenitor at the moment of the explosion. Theoretical models (e.g. Litvinova and Nadezhin, 1983, Popov, 1993) have shown that the plateau duration is more sensitive to the H envelope mass, which implies that the mass of the envelopes are higher in SNe with extended plateaus. Anderson et al. (2014b) compared the $OPTd$ and Pd parameters with the decline rates of the light curves and concluded that faster declining SNe II display shorter Pd and $OPTd$ values. However, Anderson et al. (2014b) and more recently Valenti et al. (2016) have used the $OPTd$ parameter as the indicator of the H envelope mass. Although there is a close relationship between $OPTd$ and Pd, they are associated with different physical parameters. Pd is directly related with the H envelope mass, while $OPTd$ mixes physics from the radius and the amount of hydrogen mass. As we explained before, $OPTd$ is defined between the explosion and the end of the plateau. In this range of time, the light curve shows different behaviours: an initial rise to peak brightness and a steeper decline powered by the shock cooling. Later, when the temperature at the photosphere decreases to ~ 5500 K, the hydrogen recombination phase starts and the light curve displays a plateau. According to Young (2004), the progenitor radius has the largest effect on the early light curve, when the shock wave hits the surface. On the other hand, the hydrogen envelope mass has a more significant impact in the length of the plateau. All this suggests that the association of $OPTd$ with the H mass has been misinterpreted.

Another observational parameter that has a direct association to the ejecta mass is the radioactive tail decline, s_3. Based on (Woosley et al., 1989), the expected decay rate of s_3 is 0.98 mag per 100 days, assuming full trapping of gamma-ray photons from the decay of ^{56}Co. However, Anderson et al. (2014b) found that 10 SNe in their sample have values higher values for s_3, which suggests that in these cases, the ejecta mass is too low for full trapping of the gamma-ray emission. Although they found this relation, the low amount of SNe with Pd and s_3 did not allow to confirm this relationship.

The expansion velocity and luminosity of SNe II are both set by the explosion energy (Kasen and Woosley, 2009): more energetic explosions produce higher photospheric velocities, and in turn, brighter events. These results have been showed in an observational way by Hamuy and Pinto (2002), Hamuy (2003).

More recently, Dessart et al. (2010); Dessart et al. (2013a) showed that in SNe with small radii, the recombination phase starts faster. This would imply that the phase between the explosion and t_{tran} (cooling duration phase, Cd) is shorter in these SNe. Based on that, we could suggest that Cd would have a relationship with the radius of the progenitor.

In summary we have that **the hydrogen envelope mass** is directly related with Pd, s_3; **the explosion energy** with the expansion ejecta velocities (vel), and the luminosities (M_{max}, M_{end}); **the radius of the progenitor** would have some influence in Cd.

4.6 Results

In this section we investigate the spectral and photometric diversity of SNe II through correlations. Here we present the statistics of these correlations and their respective figures. As stated above, the spectral measurements were performed in the phases where the data were available, however to characterize this diversity, the analysis is done at 30, 50 and 80 days with respect the explosion epoch. In Table 4.1 we can see the average of the correlations for each parameter at 30, 50 and 80 days. The mean of these correlations shows a value of 0.299, 0.357 and 0.362 for each epoch, which implies that the correlations are a little stronger at 80 days. As at 80 days there are fewer spectral measurements available (59) compared to those at 50 days (78), and the mean is similar, the following analysis is performed at 50 days. In Table 4.3, and 4.4 are listed the measured spectral parameters, while in Table 4.2 is presented the photometric ones.

Table 4.1 Average of correlations

Parameter	Average at 30 days	Average at 50 days	Average at 80 days
Pd	0.267	0.305	0.289
OPTd	0.249	0.297	0.312
Cd	0.196	0.197	0.233
M_{max}	0.399	0.418	0.381
M_{end}	0.331	0.357	0.378
M_{tail}	0.396	0.454	0.519
s_1	0.321	0.392	0.373
s_2	0.317	0.345	0.324
s_3	0.341	0.360	0.365
^{56}Ni	0.355	0.505	0.549
$\Delta C_(10-30)$	0.204	0.218	0.190
V(H_α	0.363	0.477	0.489
V(H_β	0.419	0.482	0.469
V(Fe II 5018)	0.398	0.447	0.427
V(Fe II 5169)	0.401	0.472	0.463
V(Na I D)	0.401	0.521	0.530
pEW$(H_\alpha)_a$	0.271	0.274	0.281
pEW$(H_\alpha)_e$	0.166	0.347	0.423
pEW(Fe II 5018)	0.321	0.348	0.257
pEW(Fe II 5169)	0.198	0.215	0.180
pEW(Na I D)	0.198	0.238	0.316
a/e	0.291	0.304	0.317
Δvel(H_α - Fe II 5018)	0.152	0.313	0.423
Δvel(Na I D - Fe II 5018)	0.283	0.424	0.421
$\Delta v(H_\beta)$	0.244	0.211	0.163

In the first column the SN II parameter is listed (described in 4.4, measurements by the average of the correlations at 30, 50 and 80 days since explosion.

4.6.1 Spectral correlations in the photospheric phase

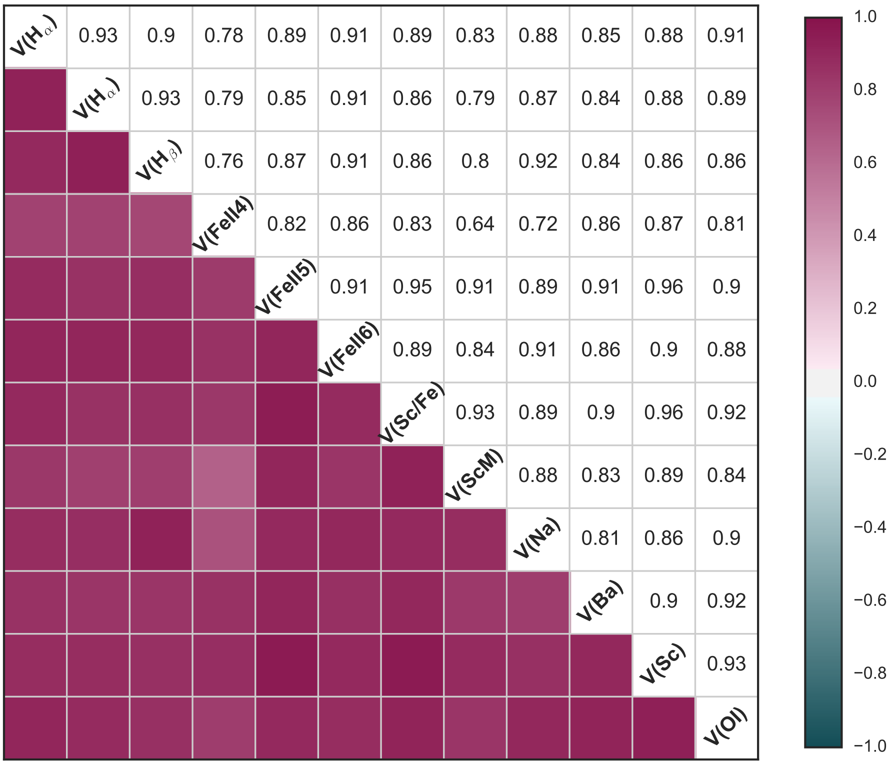

Figure 4.1 Correlation matrix of the individual velocity measurements at 50 days. Colors indicate the absolute Pearson correlation coefficient ρ. The diagonal middle line shows the name of the parameter: H_α from FWHM and from the minimum absorption flux, H_β, Fe II 4924, Fe II 5018, Fe II 5169, Sc II/Fe II 5531, Sc II M, Na I D, Ba II 6142, Sc II 6247, and O I) 7774 velocities.

We analyze the spectral properties of SNe II, focusing on correlations between pEWs, expansion velocities, velocity decline rate, and velocity differences. Figure 4.1 shows the correlation matrix of the velocity measurements at 50 days obtained by estimating the Pearson correlation. Correlation coefficients are displayed in colors: darkest colors (green and purple) represent the highest correlation found with the Pearson correlation test (-1 and 1, respectively), while white colors (0) mean no correlations. These colors are presented in the lower triangle, while the upper triangle shows the Pearson correlation value (ρ). It is generally considered that correlation coefficients between 0 and 0.19 represent close to zero correlation, 2-0.39 weak, 0.4-0.59 moderate, 0.6-0.89 strong, and 0.8-1 very strong. We will use these descriptions for the following discussion. As shown in Figure 4.1, all velocities strongly correlate positively with each other, as we would expect for an homologous expansion ($v \propto r$). Taking an average, v(Sc II) 6247, v(O I) 7774 and v(Fe II) 5018 show the highest correlations with the other parameters, with a value of 0.892, 0.887 and 0.887, respectively, while Fe II 4924 shows the lowest (0.794). The Sc II 6247 line velocities correlate strongly with Fe II 5018 and Sc II/Fe II 5531, with a value of $\rho = 0.95$. It is important to note that while the velocities all correlate, they are offset. In general, the differences in the velocities are related with the optical depth for each line and the proximity to the photosphere. As H_α displays the highest velocities, it is mostly formed in the outer shell of the ejecta and its optical depth is much larger than the Fe II lines, which are forming near to the photosphere. More details about that, can be found in Gutiérrez et al. (2016).

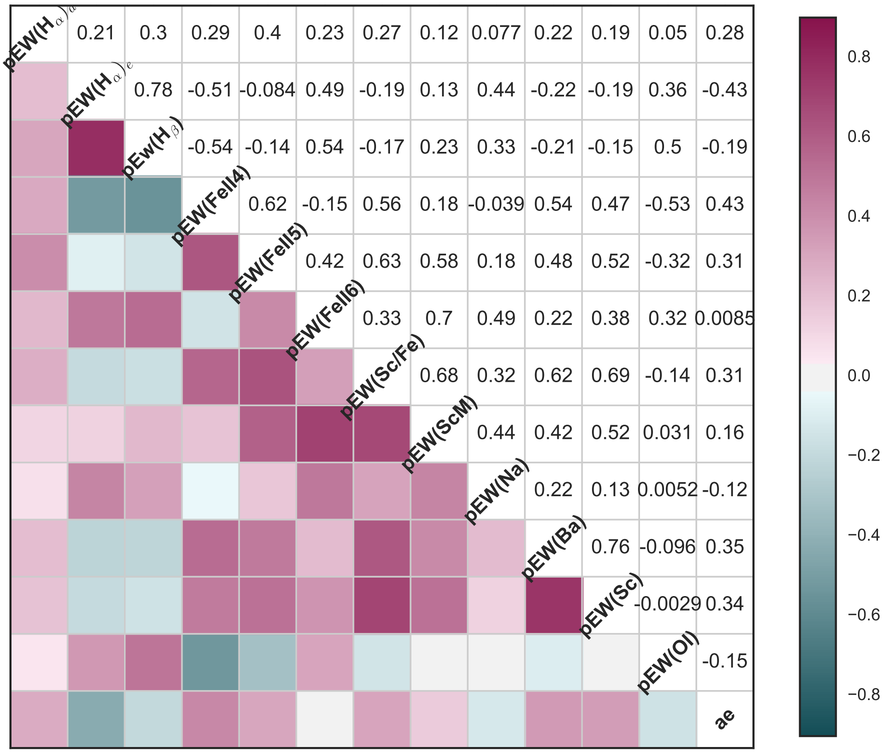

Figure 4.2 Correlation matrix of the individual pEW measurements at 50 days. Colors indicate the absolute Pearson correlation coefficient ρ. The diagonal middle line shows the name of the parameter: pEW(H_α) of absorption component, pEW(H_α) of emission component, pEW(H_β), pEW(Fe II 4924), pEW(Fe II 5018), pEW(Fe II 5169), pEW(Sc II/Fe II 5531), pEW(Sc II M), pEW(Na I D), pEW(Ba II 6142), pEW(Sc II 6247), pEW(O I 7774) and a/e.

Figure 4.2 shows the correlation matrix of the pEWs measurements at 50 days. Searching for correlations of pEWs with each other, we find that Sc II/Fe II 5531 seems to be the dominant parameter to correlate with all the other pEWs (on average 0.404), while the pEW of H_α absorption component shows very weak correlations with other pEWs. The strongest correlations are displayed by the iron-group lines with each other. We can see moderate correlations between the pEW of O I 7774 and H_β. In the case of a/e we find a moderate correlation only with Fe II 4924 ($\rho = 0.43$) and anticorrelation with pEW of H_α emission ($\rho = -0.43$). While H_β shows a weak correlation with H_α absorption component ($\rho = 0.3$), the correlation with H_α emission component is strong, with a $\rho = 0.78$. This could be due to the optical depth of H_α is much larger, and/or H_β is overlapping with Fe II, Sc II, Ba II lines.

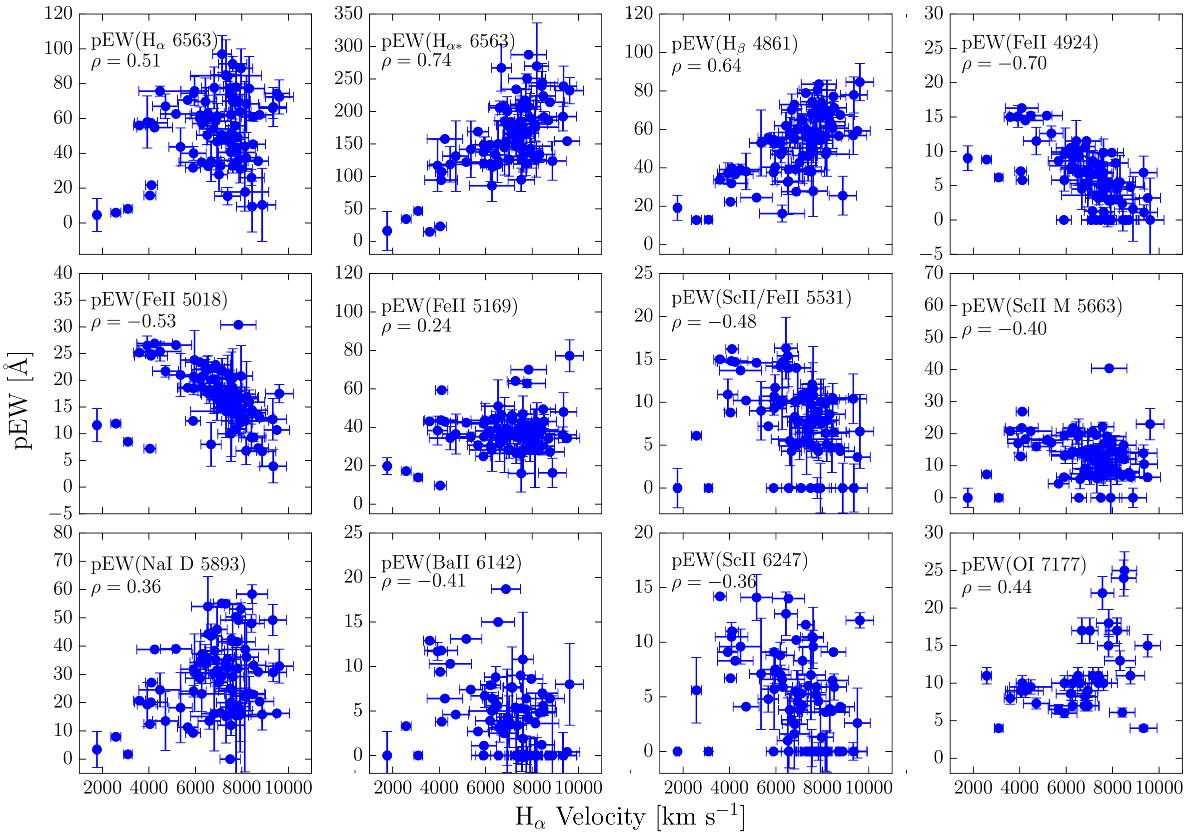

Figure 4.3 Relations between H_α velocities and the pEWs of H_α of absorption and emission component, H_β, Fe II 4924, Fe II 5018, Fe II 5169, Sc II/Fe II 5531, Sc II multiplet, Na I D, Ba II 6142, Sc II 6247, and O I 7774. On the top left of each panel the spectral feature name is displayed, together with the Pearson correlation value.

Figures 4.3, 4.4, and 4.5, show the relations between the H_α, Fe II 5169, and Na I D velocities and the pEWs for the 11 features explained above. Checking these correlations we see that velocities correlate positively with Balmer and Na I D lines, but negatively with Fe II lines. For H_α we present the pEW of the absorption and emission component. In the three figures are shown that there are five objects with the lowest velocities and smallest pEW values. Three of these SNe show signs of interaction at early phases (SN 2008bm, 2009au and 2009bu). The other two SNe are SN 2008br and SN 2002gd. In those panels plotting pEWs of Fe II 4924, Sc II/Fe II 5531, Sc II M, Ba II 6142, and Sc II 6247, one can see that there are many SNe with $pEW = 0$. In these spectra we do not detect these lines.

In Figure 4.3 we can see that the H_α velocities do not show correlation with pEW(Fe II 5169), pEW(Na I D), and pEW(Sc II 6247). The strongest correlations are shown with pEW of H_α (emission component), H_β, and anticorrelations with Fe II 4924, and Fe II 5018. Figures 4.4 and 4.5 show that Fe II 5169 and Na I D velocities present more scatter in their relations than those shown by H_α velocities. Both Fe II 5169 and Na I D velocities have correlations with pEW of H_α (emission component), H_β, and anticorrelations with Fe II 4924, and Fe II 5018. There are no correlations with the rest of the pEWs (except for pEW(Na I D) with Na I D velocities).

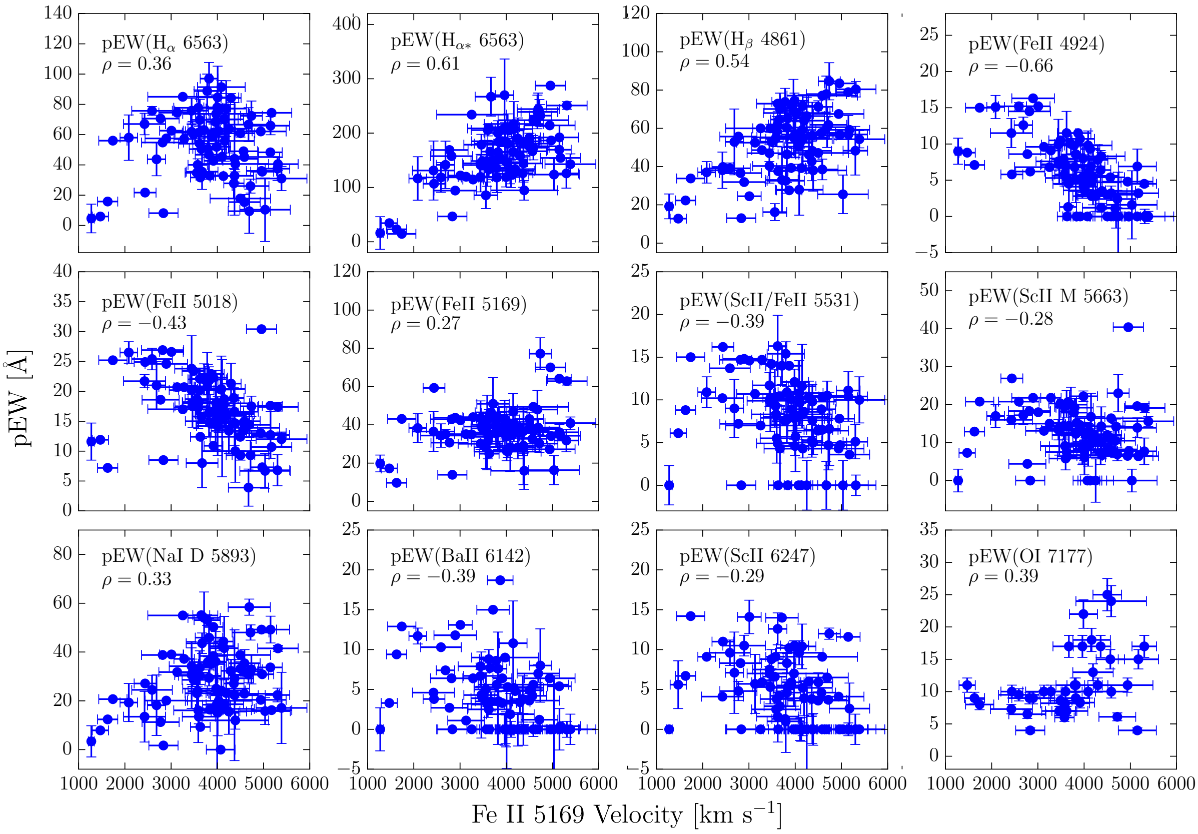

Figure 4.4 Same as Figure 4.3 but for Fe II 5169 velocities.

The expansion ejecta velocities with $\Delta v(H_\beta)$ show anticorrelations, which are stronger at late epochs (between 50 and 80 days) than at early phases (15 to 30 days, 15 to 50 days, and 30 to 50 days). Meanwhile, $\Delta vel(H_\alpha{-}$Fe II 5018) and Δvel(Na I D−Fe II 5018) show correlations with the expansion velocities at 50 days (see Figure 4.6).

4.6.2 Spectroscopic and photometric properties

Here we present a comparison of spectroscopic and photometric properties of SNe II. While we have defined and measured 31 spectroscopic and 13 photometric parameters, here we choose a smaller number of parameters to focus on and search for correlations between them. Thus, we employ 14 spectral and the 11 photometric parameters: $v(H_\alpha)$ obtained from the FWHM of the emission component, $v(H_\beta)$, v(Fe II 5018), v(Fe II 5169), v(Na I D), pEW($H_{\alpha(abs)}$), pEW($H_{\alpha(emis)}$), pEW(H_β)), pEW(Fe II 5018), pEW(Fe II 5169), pEW(Na I D), a/e, $\Delta v(H_\beta)$ in a range of $50 \leq t \leq 80$d, $\Delta vel(H_\alpha{-}$Fe II 5018), Δvel(Na I D−Fe II 5018), $OPTd$, Pd, Cd,

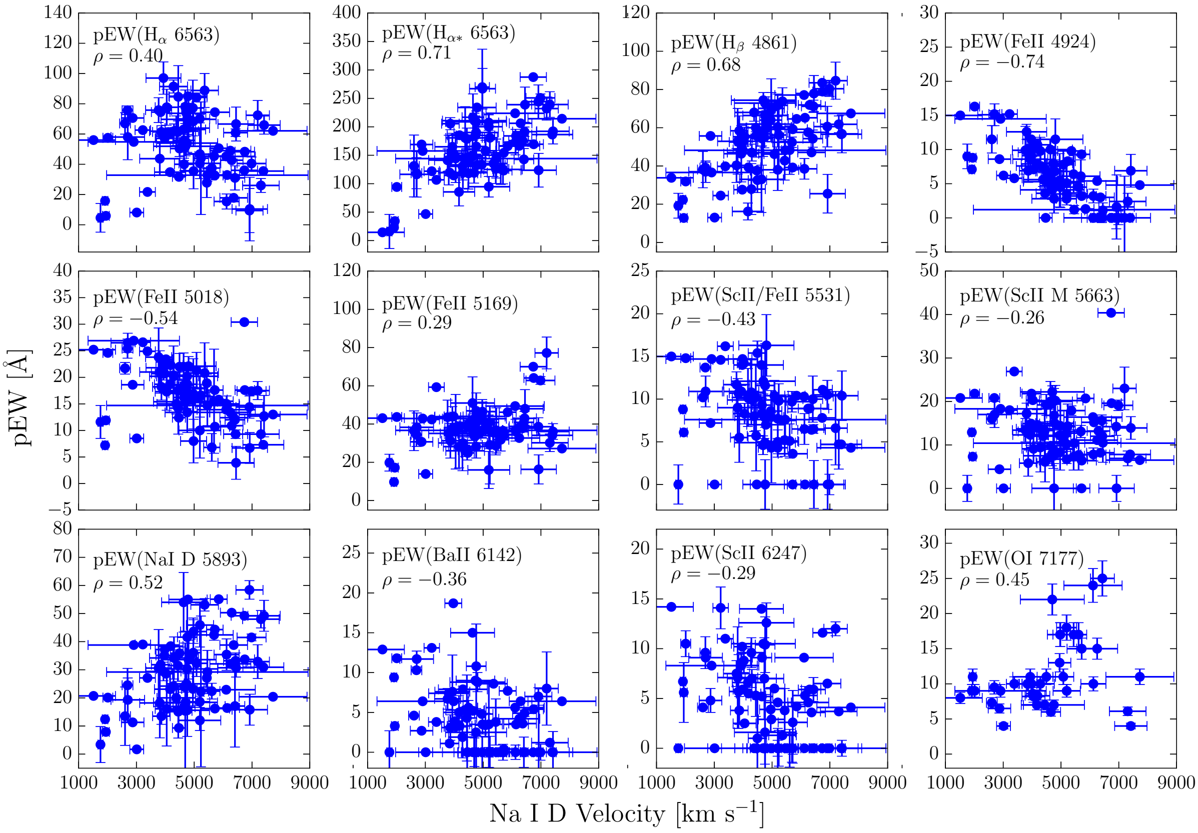

Figure 4.5 Same as Figure 4.3 but for Na I D velocities.

M_{max}, M_{end}, M_{tail}, s_1, s_2, s_3, $\Delta C_{(B-V)}$ in a range of $10 \leq t \leq 30$ d, and the ^{56}Ni.

Figure 4.6 shows the correlation matrix of the spectroscopic and photometric parameters obtained at 50 days from explosion. Although photometric correlations have been shown in previous works (e.g. Anderson et al., 2014b, Valenti et al., 2016), the incorporation of numerous spectral parameters can aid in furthering our understanding of the link between observed parameters and underlying SN II physics. As in the previous matrix of correlation, darkest color indicate higher correlation and white colors, no correlation.

Focusing on the photometric correlations, one can see that many of these correlations are stronger than in Anderson et al. (2014b). As discussed previously, this is because some parameters have been remeasured with new techniques. Interestingly, Pd and s_3 shows an increase in the available points, from 4 in Anderson et al. (2014b) to 11 in this work. As we explained above, both parameters can give us an idea of the amount of hydrogen envelope mass at the moment of the explosion, thus some relation is expected. Figure 4.7 shows an evident trend between both parameters, with a correlation coefficient of $\rho = -0.71$. This results in that SNe with shorter Pd values have higher s_3 slopes, which shows that the variations in the hydrogen envelope mass could derive in the observed diversity in the light curve. The strong correlation found here supports the hypothesis that both Pd and s_3 are related to the hydrogen

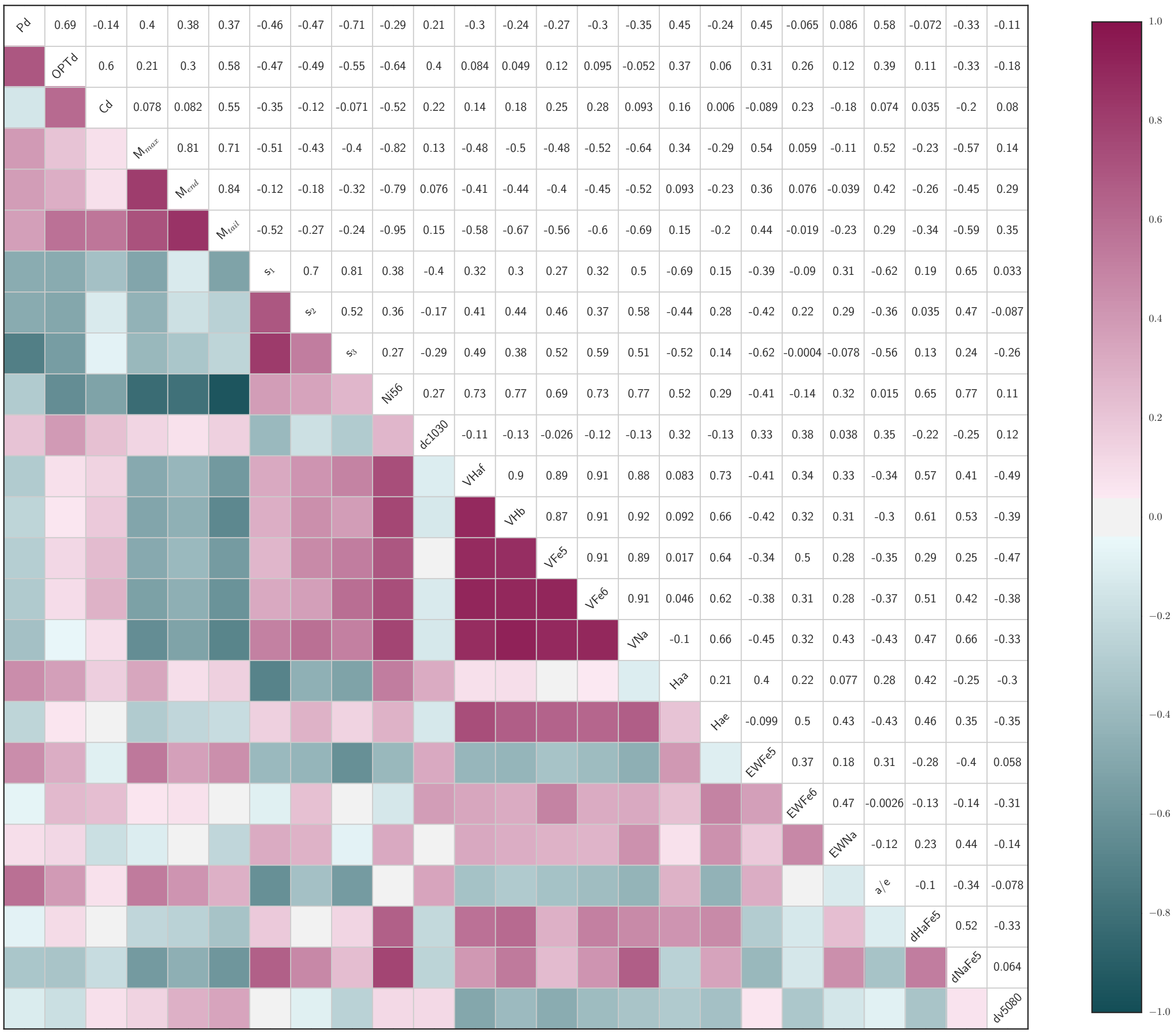

Figure 4.6 Correlation matrix of the individual spectral and photometric parameters at 50 days. Colors indicate the absolute Pearson correlation coefficient ρ.

envelope mass at the epoch of explosion.

From Figure 4.6 we also can see that Pd has a weak correlation with velocities. This suggests that the explosion energy of SNe II does not significantly affect the plateau duration, and hence that the two parameters, explosion energy and H envelope mass, change somewhat independently from SN to SN. In addition, Pd does not show any significant correlation with the synthesised ^{56}Ni mass.

On the other hand, Pd has a moderate correlation with pEW(H_α) emission component and a/e. The correlation coefficients are $\rho = 0.45$ and $\rho = 0.58$, respectively. In Figure 4.8 we present these correlations. The trend shows that SNe with longer Pd values have longer $OPTd$ phases, higher pEW($H_{\alpha(abs)}$) and a/e values. In the last two relations, we can see more scatter, however, they are consistent with the idea of SNe with shorter Pd values have a weaker absorption component of H_α P-Cygni profile.

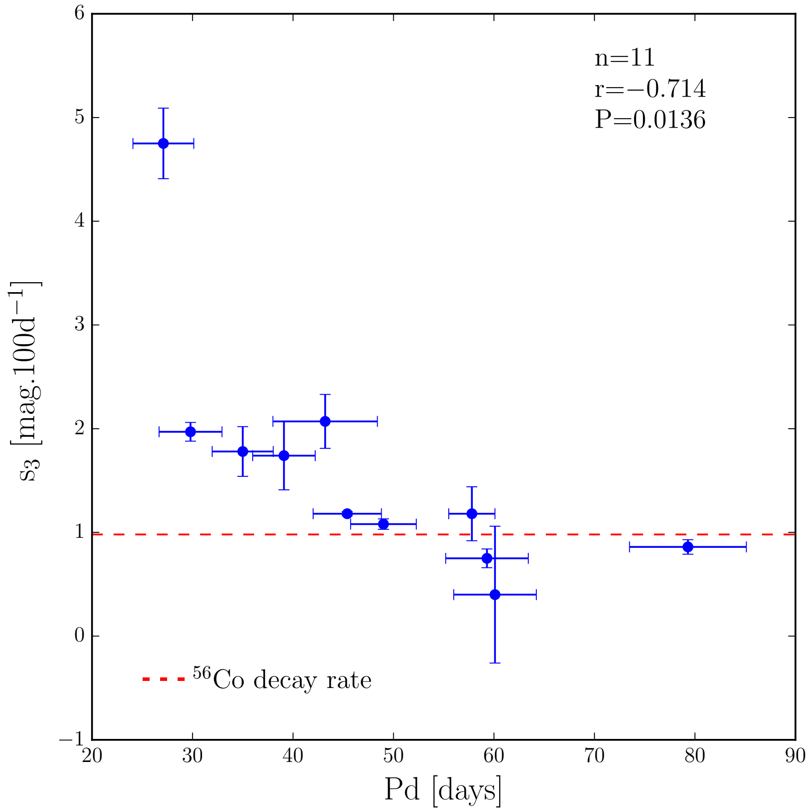

Figure 4.7 Correlations between *Pd* vs. s_3. The dashed horizontal red line shows the expected decline rate on the radioactive tail, assuming full trapping of gamma-rays from ^{56}Co to ^{56}Fe decay.

Figure 4.9 shows how s_3 correlates with other parameters. As we can see, s_3 presents a strong and moderate with s_1 and s_2, respectively, suggesting that a fast decliner at one epoch is usually a fast decliner at other epochs. Although the correlation of s_3 and M_{max} is moderate, it is driven by an outlier event, SNe 2006Y. As Anderson et al. (2014b) noted, this SN presents an atypical behaviour in photometry, but here we confirm their strange behaviour in the spectra. If we remove this SN from the analysis, the correlations decrease significantly. The correlations between s_3 and the velocities are moderate. This shows that faster declining SNe II have higher expansion ejecta velocities. In the last panel of Figure 4.9 is presented the correlation between s_3 and the pEW(Fe II 5018) which, like M_{max} is driven by SN 2006Y. Summarizing, s_3 has weak correlations with the pEWs and the magnitudes.

The expansion ejecta velocities show a strong correlation with ^{56}Ni mass (see Figure 4.10). This suggests that more energetic explosions produce more ^{56}Ni, which supports the results obtained by Hamuy (2003). The correlations between the velocities and the luminosities are moderate, but they are a little bit stronger with Na I D velocity. As we said previously, they

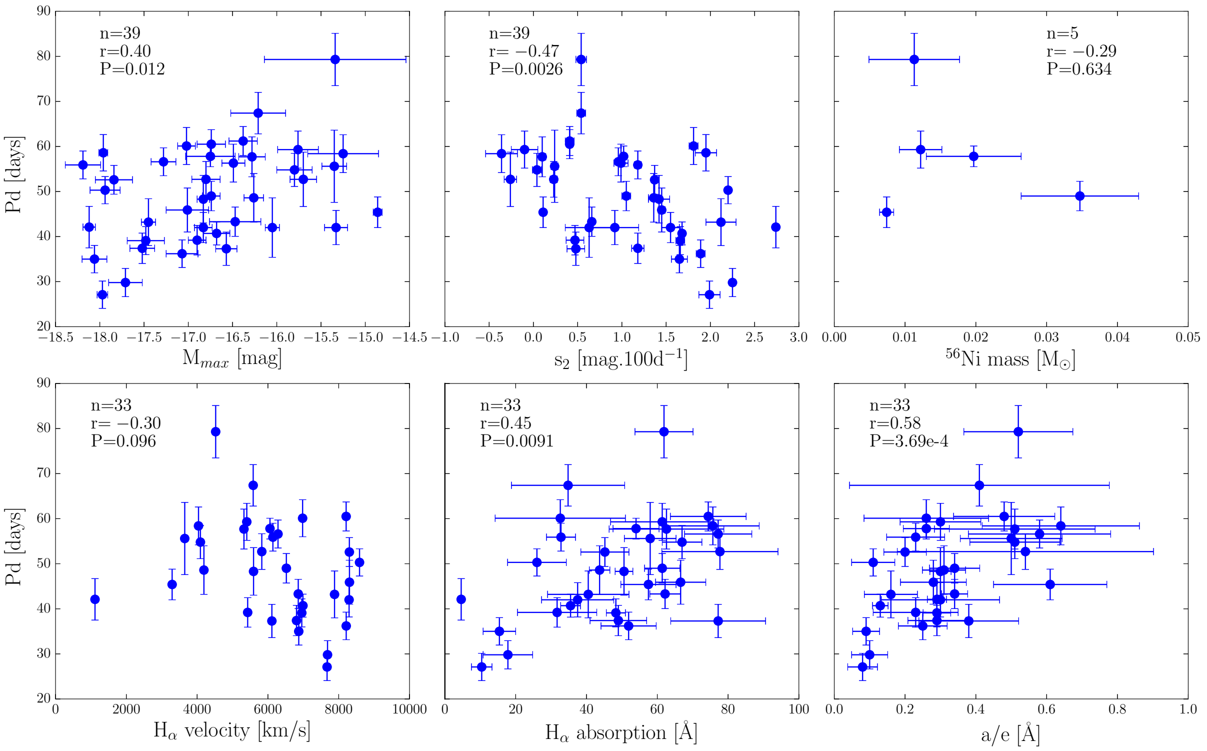

Figure 4.8 Correlations between Pd and six different parameters: M_{max}, s_2, ^{56}Ni mass, H_α velocity, pEW of H_α absorption component, a/e.

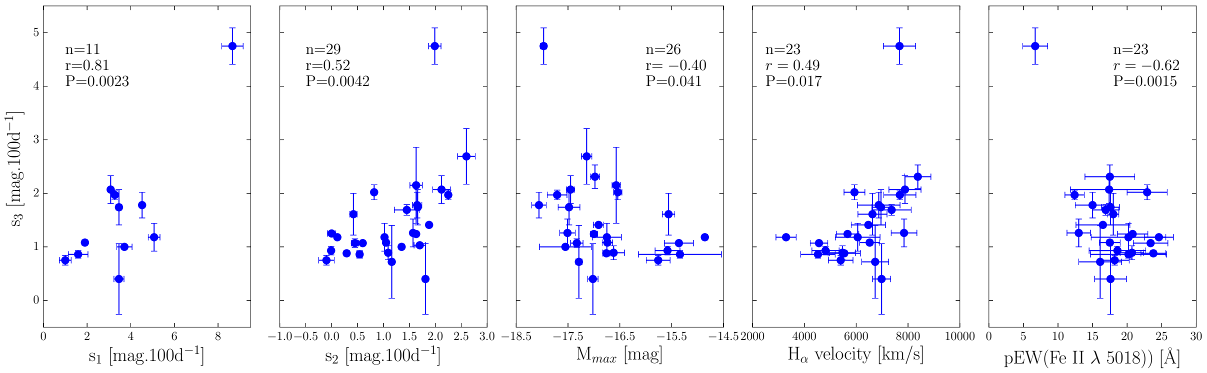

Figure 4.9 Correlations between s_3 and five different parameters: s_1, s_2, M_{max}, H_α velocity, pEW(Fe II λ 5018).

are associated with the explosion energy, and these correlations support it. Figure 4.11 (top) shows the correlation between M_{max} and the expansion velocities of H_α, Fe II 5018, and Na I D. In the three plots it is possible to see that two brightest objects present very low velocities, (the opposite to the rest of the sample). Analysing their spectra, we note that they are SNe with signs of circumstellar interaction at the early phases. We also remark that their spectral evolution is different, since the appearance of the lines is much later (see Gutiérrez et al. 2016).

Looking at the correlations with the luminosities, we find a very strong correlation with the

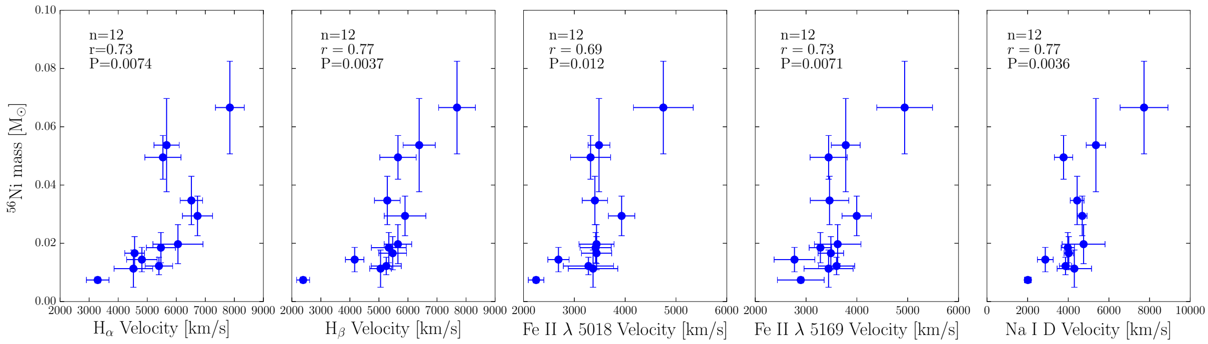

Figure 4.10 Correlations between ^{56}Ni and the expansion velocities.

^{56}Ni mass, as we expected. The remaining correlations can be seen in Figure 4.6.

Figure 4.11 (bottom) presents the correlations between M_{max} and the pEWs of H_α, Fe II 5018, and Na I D. We can observe a weak correlation with the pEW(H_α) absorption component, a moderate ($\rho = 0.54$) correlation with pEW(Fe II 5018), and no correlations with pEW(Na I D).

4.7 Discussion

Using numerous defined spectral and photometric parameters we have searched for correlations between different observed properties of SNe II. We have argued that *Pd* is a better parameter than *OPTd* for constraining the H envelope mass at the epoch of explosion, given that the latter includes information from the early-time light curve, which is more likely associated with progenitor radii differences. Our analysis shows a strong correlation between *Pd* and s_3, arguing that both of these parameters are strongly linked to the H envelope mass/ejecta mass. Assuming that the explosion energy is related to the expansion ejecta velocities and the luminosities, we find moderate correlations between these parameters. However, the velocities and luminosities show weak correlations with *Pd*, suggesting that they do not influence the plateau duration, as well as the H envelope mass do not influence the expansion ejecta velocities and luminosities.

Here we compare our results with those found in previous studies, both observational and theoretical. Finally we discuss the results in terms of the physical properties to explain the diversity of SNe II.

4.7.1 H_α P-Cygni diversity

A large diversity in the H_α P-Cygni profile had been shown by Patat et al. (1994), Gutiérrez et al. (2014). They found that SNe II with smaller a/e values are brighter, and have higher velocities and steeper decline rates. With our analysis at 50 days, we confirm these results, however the correlations presented here are weaker than Gutiérrez et al. (2014). They performed the measurements in different epochs around t_{tran} and they found that the

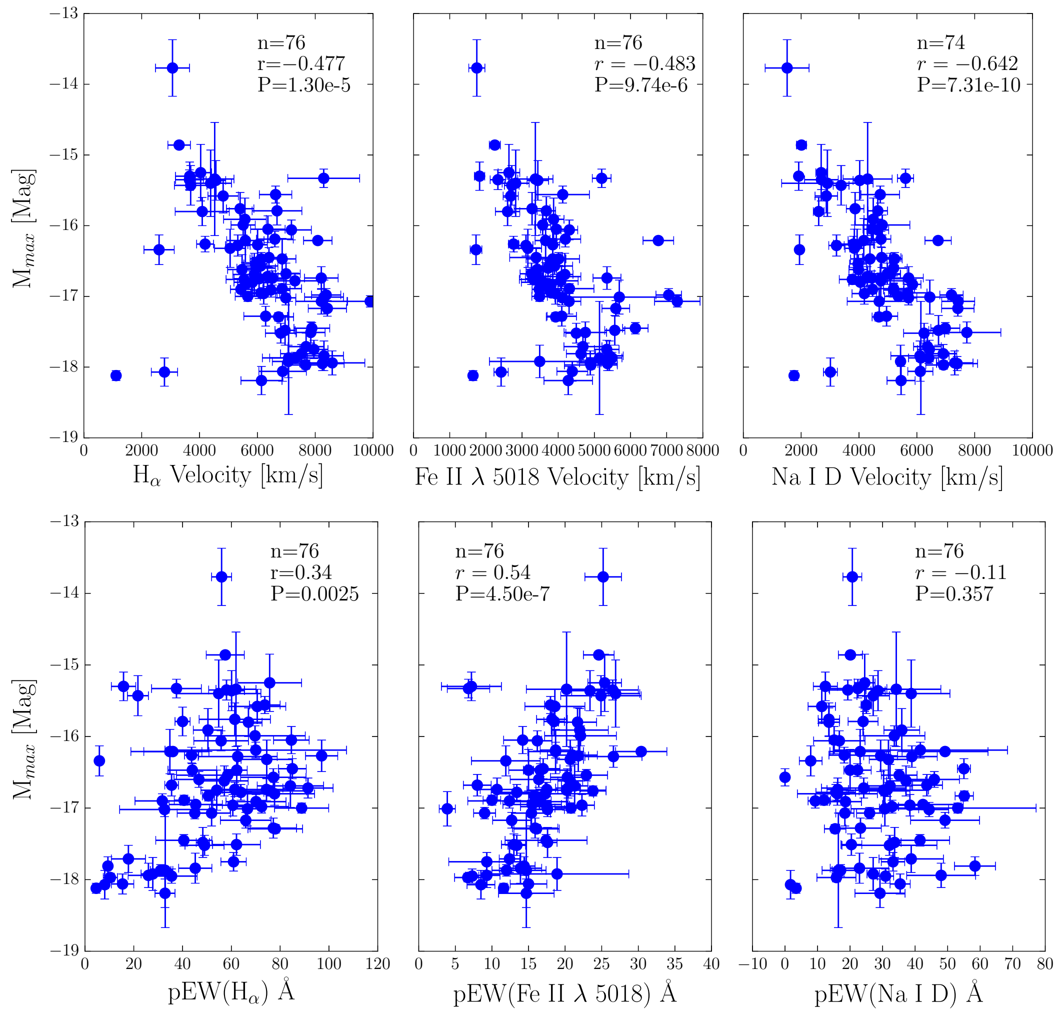

Figure 4.11 **Top panel:** Correlations between M_{max} and the expansion velocities. **Bottom panel:** Correlations between M_{max} and the pEWs

correlations are stronger at $t_{tran+10}$. Comparing the results, the magnitude is almost the same, however for the H_α velocity the correlation decreases from −0.60 to −0.34, and for the slope declines, the correlation decreases significantly with s_2, from −0.65 to −0.36. This could be due to some SNe (e.g. SN 1992af, SN 2006Y, SN 2008bu, SN 2009ao) at 50 days are finishing the recombination phase, so their physical conditions are different. This behaviour also affects to s_1 and s_3, so their correlations also decrease. Gutiérrez et al. (2014) also compared a/e with $OPTd$ and found a correlation value of 0.56. Here we find 0.39, however, the correlation with Pd is 0.58.

A moderate correlation is found between the absorption component of H_α and Pd. SNe II displaying longer Pd values in general have stronger H_α absorption, suggesting that the latter may also be related to the extent of the hydrogen envelope (as discussed in Gutiérrez et al. 2016.) Based on the results by Schlegel (1996), one of the possible explanations for this behaviour in the H_α P-Cygni profile is related with the low hydrogen mass envelope. If this possibility is true, three different observed parameters (Pd, s_3 and the H_α absorption component) could give us an idea of the amount of hydrogen envelope mass at the moment of the explosion.

4.7.2 The Si II λ 6355 line

As we show in Gutiérrez et al. (2016), Cachito at early phase is related to Si II 6355, which is present in SNe II with a weak H_α absorption component. The Si II 6355 line emerges at higher temperatures and all SNe II should show this line. However, as the radius has an influence in the temperature evolution (compact objects evolve faster; Dessart et al. 2013a), the possibility to detect the Si II line in compact objects is lower. Using a KS test to find the difference between the distributions with/without Si II 6355, we find that there is no influence of Pd (i.e. with the H envelope mass) or vel (i.e. the explosion energy) in the appearance of this line. However, we found that faster declining SNe II have Si II 6355 in their spectra. According to (Blinnikov and Bartunov, 1993), faster declining SNe II (known as SNe IIL) should have larger radii. Our results on the SN types where the Si II 6355 line is observed, suggests that faster declining SNe also arise from SNe with larger radii that stay bluer for longer, hence increasing the possibility of detecting Si II.

Pd as hydrogen envelope mass indicator

According to theoretical models (e.g Popov, 1993, Litvinova and Nadezhin, 1983, Moriya et al., 2016) faster declining SNe II can be explained by the explosion of stars with low hydrogen envelope mass, which would have an influence in the plateau duration. This is because the plateau is powered by the recombination of hydrogen in the ejecta, shorter plateau durations imply less mass to travel back through. Recent observational works (e.g. Anderson et al., 2014b, Valenti et al., 2016) have concluded that the phase between the explosion date and the end of the plateau (usually known as the optically thick duration phase, $OPTd$) give us an idea of hydrogen mass. However, as we explained above, besides the H mass, $OPTd$ is also related with the radius, hence, it would not be a primary indicator of that parameter. Here we argue that instead of $OPTd$ we must use Pd. Pd shows correlations with the decline rates, indicating that faster declining SNe II have shorter plateaus. These correlations are stronger with s_3 (Figure 4.7). The simpler explanation leads to think that the full trapping of gamma-ray emission in SNe II with low H mass is inefficient, and therefore the slope in the radioactive tail is steeper.

4.7.3 Other comparisons

As Patat et al. (1994), Anderson et al. (2014b) and more recently Valenti et al. (2016), we find that faster declining SNe II are brighter events (see Figure 4.8). In addition, we also find that

SNe II with brighter luminosities have greater expansion velocities and produce more ^{56}Ni. In Figure 4.10 and 4.11 we show a few examples of these correlations. Similar results were found by several authors in observational (e.g. Hamuy, 2003, Spiro et al., 2014, Valenti et al., 2016) and theoretical (e.g. Kasen and Woosley, 2009) works.

While theoretical models (e.g. Kasen and Woosley, 2009, Nakar et al., 2016) show that the presence of ^{56}Ni mass extends the plateau duration, we do not find such correlation. In fact, there is an opposite behaviour, but not very strong. Many authors have claimed (e.g. Dessart and Hillier, 2011) that the color evolution could be related with the radius of the progenitor star. Although we include the color gradient (ΔE($B-V$)) between 10–30 days post-explosion in our analysis, we do not find significant correlations associated to this parameter. Like ΔE($B-V$), Cd does not show an important relation with any parameter. In previous sections we linked this parameter with the radius as some models predict it (e.g. Dessart et al., 2013a), however we can not prove its influence.

Dessart et al. (2014) showed that differences in metallicity can be evident in the SN II spectra, more precisely in the strength of the iron lines. Anderson et al. (2016) supported this result showing a correlation between the strength of Fe II λ5018 with the oxygen abundance of the host H II regions. They showed that SNe II exploding in lower metallicity regions have less iron absorption. Looking for relations with the pEW(Fe II 5018), we find a correlation of 0.45 with the Pd (See Figure 4.12). Assuming that the pEW(Fe II 5018) gives an idea of the metallicity where the SN explode, this correlation would mean that higher metallicity produce SNe with a longer plateau, which is in the opposite direction of the predictions (e.g. Dessart et al., 2013a). However, when we correlate Pd with the oxygen abundance determined by Anderson et al. (2016), we do not find any relation. This could suggest that pEW(Fe II 5018) also can give us information about other physical parameters, such as the temperature, and it is not the same for all SNe in the recombination phase.

4.8 Conclusions

In this work we have presented an analysis of correlations between a range of spectral and photometric parameters of 123 SNe II, with the purpose of understanding their diversity. To study this diversity, we use the expansion ejecta velocities and pseudo-equivalent widths for eleven features in the photospheric phase (from explosion to $\sim$ 120 days): H_α, H_β, Fe II 4924, Fe II 5018, Fe II 5169, Sc II/Fe II 5531, Sc II M, Na I D, Ba II 6142, Sc II 6247, and O I 7774; the ratio absorption to emission (a/e) of the H_α P-Cigni profile; the velocity decline rate of H_β ($\Delta v(H_\beta)$) and the velocity difference between H_α and Fe II 5018, and Na I D and Fe II 5018 (Δvel). From the light curves we employed three magnitude measurements at different epochs (M_{max}, M_{end}, M_{tail}); three decline rates (s_1, s_2, s_3); three time durations ($OPTd$, Pd, Cd); the ^{56}Ni mass, and the color gradient, $\Delta E(B-V)$. We searched for correlations at 30, 50 and 80 days and we found that the correlations are stronger at 50 days post-explosion. We speculate that this happens because at 50 days all the SNe II are in the recombination phase and probably

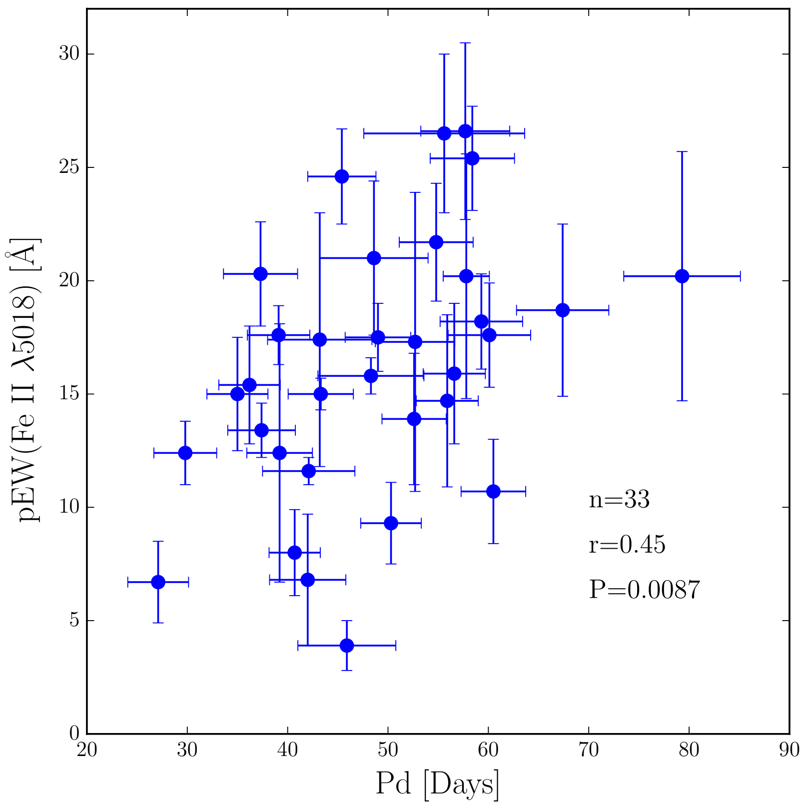

Figure 4.12 Correlations between pEW(Fe II λ5018) and Pd.

they have the same physical conditions. At 30 and 80 days not all SNe II are in the same stage, some are in the cooling (at early phases) and some are in the transition to the nebular phase (at the end of the plateau).

The main results obtained with our analysis are summarized as follows:

- The spectral and photometric diversity in SNe II can not be explained with only one observed/physical property. Although there are observed parameters that dominate the correlations, this diversity is not explained for only one parameter. The differences in SNe II could be due to the masses of their pre-explosion hydrogen envelopes, radius and explosion energy.
- We find that Pd is the best hydrogen mass indicator in SNe II. We rule out the use of $OPTd$ (Anderson et al., 2014b) and t_{PT} (Valenti et al., 2016) due to the fact that both parameters are affected by physical properties in addition to the the amount of hydrogen mass, such as the radius.
- We suggest that SNe II showing the Si II line in the early phases, have progenitor stars

with larger radii.

- We found that the H envelope mass does not significantly affect the expansion velocities observed, while neither does the explosion energy significantly affect the plateau duration.
- As expected, expansion velocities measured from different spectral lines all strongly correlate with each other, although different lines are offset to different velocities.
- Contrary to the theoretical works, we find that the mass of ^{56}Ni has no influence in the plateau duration.

Table 4.2: Photometric parameters

SN	Pd	$OPTd$	Cd	M_{max}	M_{end}	M_{tail}	s_1	s_2	s_3	^{56}Ni mass	ΔC_{10-30}
1986L	54.4 ± 3.09	92.24 ± 6.71	37.9 ± 0.87	-18.19 ± 0.20	-14.37 ± 0.20	2.97 ± 0.11	1.18 ± 0.04	3.79 ± 0.08	···	0.0598 ± 0.009*	26
1988A	···	···	···	···	···	···	0.11 ± 0.45	1.15 ± 0.4	···	···	···
1990E	···	···	···	···	···	···	-0.57 ± 0.12	0.96 ± 0.06	···	···	···
1990K	···	···	···	···	···	···	2.35 ± 0.1	1.33 ± 0.02	···	···	···
1991al	···	···	···	-17.51 ± 0.15	-14.71 ± 0.15	···	1.57 ± 0.04	1.37 ± 0.2	0.0666 ± 0.0159	0.0666 ± 0.0159	37
1992ad	···	···	···	-16.98 ± 0.80	···	···	2.23 ± 0.04	···	···	···	···
1992af	···	54.03 ± 6.71	···	-17.33 ± 0.12	-15.06 ± 0.12	···	0.45 ± 0.07	1.1 ± 0.06	0.0789 ± 0.0184	0.0789 ± 0.0184	19
1992am	···	···	···	-18.06 ± 0.05	···	···	1.14 ± 0.02	···	···	···	···
1992ba	76.3 ± 6.5	103.97 ± 8.54	27.7 ± 3.81	-15.34 ± 0.80	-12.34 ± 0.80	1.59 ± 0.45	0.54 ± 0.06	0.9 ± 0.04	0.0113 ± 0.0064	0.0113 ± 0.0064	28
1993A	···	···	···	-16.44 ± 0.07	···	···	0.74 ± 0.04	···	···	···	30
1993K	···	···	···	-17.92 ± 0.23	···	···	2.26 ± 0.25	···	···	···	18
1993S	···	···	39.5 ± 2.9	-17.52 ± 0.07	···	3.3 ± 0.18	2.02 ± 0.19	···	···	···	36
1999br	···	···	···	-13.77 ± 0.40	···	···	0.15 ± 0.01	1.13 ± 2.39	···	0.0021 ± 0.001*	36
1999ca	40.1 ± 3.11	80.48 ± 7.62	40.4 ± 0.74	-17.48 ± 0.21	-13.78 ± 0.21	3.46 ± 0.13	1.66 ± 0.05	1.69 ± 0.3	···	0.0474 ± 0.003*	···
1999cr	38.2 ± 3.27	78.06 ± 7.62	39.8 ± 1.71	-16.90 ± 0.10	···	1.76 ± 0.07	0.47 ± 0.1	···	···	···	18
1999eg	···	···	···	-16.86 ± 0.10	···	···	1.93 ± 0.07	···	···	···	···
1999em	···	92.86 ± 5.83	···	-16.76 ± 0.07	-13.93 ± 0.07	···	0.29 ± 0.02	0.97 ± 0.01	0.0495 ± 0.0075	0.0495 ± 0.0075	31
S0210	···	90.57 ± 9.49	···	-16.21 ± 0.04	···	···	1.78 ± 0.15	···	···	···	···
2002ew	···	···	32 ± 1.07	-17.42 ± 0.08	···	9.42 ± 1.65	2.9 ± 0.24	···	···	···	···
2002fa	···	67.29 ± 7.62	···	-16.95 ± 0.04	···	···	1.62 ± 0.08	···	···	0.0657 ± 0.004*	···
2002gd	···	···	27.2 ± 0.54	-15.43 ± 0.28	···	3.21 ± 0.3	0.46 ± 0.03	···	···	···	32
2002gw	53.30 ± 3.9	82.33 ± 5.83	29.1 ± 2.11	-15.76 ± 0.23	-13.07 ± 0.23	1 ± 0.27	-0.1 ± 0.15	0.73 ± 0.04	0.0122 ± 0.003	0.0122 ± 0.003	25
2002hj	···	90.24 ± 7.62	···	-16.91 ± 0.10	-13.59 ± 0.10	···	1.88 ± 0.03	0.89 ± 0.42	···	0.0257 ± 0.004*	···
2002hx	···	68.03 ± 9.49	···	-17.00 ± 0.07	-14.60 ± 0.07	···	1.63 ± 0.03	1.29 ± 0.04	0.0537 ± 0.016	0.0537 ± 0.016	23
2002ig	···	···	···	-17.66 ± 0.03	···	···	2.72 ± 0.1	···	···	···	24
2003B	···	83.19 ± 11.40	···	-15.36 ± 0.28	-12.77 ± 0.28	···	0.6 ± 0.04	1.06 ± 0.01	0.0166 ± 0.0057	0.0166 ± 0.0057	···
2003bl	52.6 ± 8.01	92.81 ± 4.24	40.2 ± 1.22	-15.35 ± 0.14	···	1.05 ± 0.35	0.24 ± 0.04	···	···	···	28
2003bn	52.7 ± 3.96	92.97 ± 4.24	40.2 ± 2.54	-16.80 ± 0.16	-13.72 ± 0.16	0.91 ± 0.06	0.23 ± 0.04	···	···	0.0413 ± 0.002*	29
2003ci	48.3 ± 4.00	92.53 ± 8.54	44.2 ± 3.28	-16.83 ± 0.07	···	2.42 ± 0.16	1.42 ± 0.12	···	···	···	···
2003cn	46.6 ± 5.20	67.80 ± 5.00	21.2 ± 3.39	-16.26 ± 0.11	···	3.03 ± 1.22	1.36 ± 0.06	···	···	···	27
2003cx	···	87.82 ± 5.83	···	-16.79 ± 0.06	-14.32 ± 0.06	···	0.66 ± 0.05	1.75 ± 0.62	···	0.0512 ± 0.007*	19
2003dq	···	···	···	-16.69 ± 0.06	···	···	2.86 ± 0.11	···	···	···	···
2003E	48.7 ± 4.8	97.42 ± 7.62	48.7 ± 5.02	-15.70 ± 0.15	···	0.41 ± 0.29	-0.26 ± 0.07	···	···	···	15
2003ef	···	90.93 ± 9.49	···	-16.72 ± 0.14	···	···	0.82 ± 0.02	···	···	···	28
2003eg	···	···	29.2 ± 0.85	-17.81 ± 0.13	···	6.76 ± 0.37	2.3 ± 0.06	···	···	···	14
2003ej	···	68.97 ± 5.83	···	-17.66 ± 0.12	···	···	3.39 ± 0.04	···	···	···	30
2003fb	···	84.27 ± 6.71	···	-15.56 ± 0.12	-13.10 ± 0.12	···	0.42 ± 0.07	1.52 ± 0.22	···	0.0166 ± 0.005*	···
2003gd	···	···	···	···	-12.58 ± 0.40	···	1.7 ± 0.11	1.01 ± 0.01	0.0122 ± 0.006	0.0122 ± 0.006	···
2003hd	···	82.39 ± 5.83	···	-17.29 ± 0.06	-13.85 ± 0.06	···	1.16 ± 0.05	0.65 ± 0.44	0.0294 ± 0.0068	0.0294 ± 0.0068	28
2003hg	61.2 ± 3.22	108.50 ± 5.83	47.3 ± 1.33	-16.38 ± 0.16	···	1.46 ± 0.04	0.41 ± 0.05	···	···	···	30
2003hk	59.1 ± 4.6	86.00 ± 5.00	26.9 ± 2.11	-17.02 ± 0.10	-13.14 ± 0.10	3.46 ± 0.23	1.81 ± 0.05	0.58 ± 0.84	···	0.0166 ± 0.007*	···
2003hl	···	108.92 ± 5.83	···	-15.91 ± 0.30	···	···	0.75 ± 0.01	···	···	···	29
2003hn	49 ± 5.2	90.10 ± 10.44	41.1 ± 1.27	-16.74 ± 0.10	-13.27 ± 0.10	1.9 ± 0.06	1.05 ± 0.05	1.1 ± 0.05	0.0347 ± 0.0083	0.0347 ± 0.0083	29
2003ho	···	···	···	···	-12.00 ± 0.16	···	1.45 ± 0.24	1.75 ± 0.3	···	0.0049 ± 0.003*	···
2003ib	···	···	···	-17.10 ± 0.09	···	···	1.71 ± 0.04	···	···	···	12
2003ip	···	80.74 ± 5.00	···	-17.75 ± 0.13	···	···	2.07 ± 0.03	···	···	···	23
2003iq	···	84.91 ± 3.61	···	-16.69 ± 0.30	···	···	0.84 ± 0.01	···	···	···	24

2003T	···	90.59 ± 10.44	···	−16.54 ± 0.08	−13.67 ± 0.08	···	0.82 ± 0.02	2.07 ± 0.21	···	0.0295 ± 0.01*	27
2004dy	···	···	···	−16.03 ± 0.07	···	···	6.55 ± 0.17	···	···	···	···
2004ej	···	96.14 ± 8.54	···	−16.62 ± 0.21	−12.92 ± 0.21	···	1.09 ± 0.04	0.97 ± 0.04	0.0185 ± 0.0052	0.0185 ± 0.0052	···
2004er	60.6 ± 3.22	120.15 ± 5.00	59.6 ± 1.12	−16.74 ± 0.16	···	1.31 ± 0.03	0.41 ± 0.03	···	···	···	21
2004fb	···	···	···	−16.19 ± 0.11	···	···	1.24 ± 0.07	···	···	···	···
2004fc	67.4 ± 6.3	106.06 ± 3.16	38.6 ± 2.64	−16.21 ± 0.31	···	1.12 ± 0.03	0.54 ± 0.05	···	···	···	29
2004fx	···	68.41 ± 5.00	···	−15.58 ± 0.24	−12.87 ± 0.24	···	−0.01 ± 0.03	0.95 ± 0.06	0.0144 ± 0.0042	0.0144 ± 0.0042	15
2005af	···	104.01 ± 15.30	···	···	−13.41 ± 0.36	···	0 ± 0.08	1.24 ± 0.02	0.0264 ± 0.0116	0.0264 ± 0.0116	···
2005an	39.2 ± 3.06	77.71 ± 5.00	38.5 ± 0.6	−17.07 ± 0.18	···	3.32 ± 0.05	1.89 ± 0.05	···	···	···	29
2005dk	39.4 ± 3.37	84.22 ± 6.71	44.8 ± 1.54	−17.52 ± 0.14	···	2.26 ± 0.08	1.18 ± 0.07	···	···	···	···
2005dn	47 ± 3.5	79.76 ± 6.71	32.8 ± 2.88	−17.01 ± 0.24	···	2.04 ± 0.23	1.45 ± 0.04	···	···	···	···
2005dt	···	112.86 ± 9.49	···	−16.39 ± 0.09	···	···	0.73 ± 0.06	···	···	···	···
2005dw	56.2 ± 3.3	92.59 ± 9.49	36.4 ± 2.24	−16.49 ± 0.13	−13.21 ± 0.13	2.31 ± 0.22	0.99 ± 0.08	···	···	0.0211 ± 0.009*	···
2005dx	37.6 ± 3.6	85.59 ± 7.62	48 ± 5.58	−16.05 ± 0.08	−12.12 ± 0.08	1.8 ± 0.12	0.63 ± 0.27	1.24 ± 2.15	···	0.007 ± 0.005*	32
2005dz	37.3 ± 3.69	81.86 ± 5.00	44.6 ± 2.22	−16.57 ± 0.12	−13.42 ± 0.12	1.28 ± 0.07	0.48 ± 0.1	···	···	0.0213 ± 0.01*	23
2005es	···	···	···	−16.98 ± 0.06	···	···	1.23 ± 0.05	···	···	···	40
2005J	53.7 ± 3.10	94.03 ± 7.62	40.4 ± 0.78	−17.28 ± 0.14	···	2.1 ± 0.06	0.96 ± 0.02	···	···	···	29
2005K	···	···	···	−16.57 ± 0.08	−13.22 ± 0.08	···	1.63 ± 0.12	1.51 ± 0.83	···	0.0155 ± 0.006*	22
2005lw	···	107.23 ± 10.44	···	−17.07 ± 0.08	···	···	2.11 ± 0.04	···	···	···	29
2005me	38.3 ± 3.36	76.91 ± 6.71	38.6 ± 1.52	−16.83 ± 0.10	···	2.98 ± 0.11	1.55 ± 0.1	···	···	···	28
2005Z	···	78.84 ± 6.71	···	−17.17 ± 0.11	···	···	1.82 ± 0.01	···	···	···	30
2006ai	35 ± 3.04	63.26 ± 5.83	28.3 ± 0.52	−18.06 ± 0.14	−14.53 ± 0.14	4.52 ± 0.08	1.65 ± 0.09	1.86 ± 0.32	···	0.05 ± 0.01*	20
2006bc	···	···	23.3 ± 0.74	−15.18 ± 0.26	···	1.78 ± 0.13	−0.58 ± 0.04	···	···	···	22
2006be	40 ± 3.25	72.89 ± 6.71	32.9 ± 1.26	−16.47 ± 0.29	···	1.26 ± 0.08	0.66 ± 0.02	···	···	···	30
2006bl	···	···	15.7 ± 1.91	−18.23 ± 0.07	···	3.42 ± 0.38	2.55 ± 0.02	···	···	···	22
2006ee	57.7 ± 4.2	85.17 ± 5.00	27.4 ± 2.43	−16.28 ± 0.15	···	1.2 ± 0.3	0.1 ± 0.04	···	···	···	25
2006it	···	···	···	−16.20 ± 0.15	···	···	1.25 ± 0.1	···	···	···	40
2006iw	···	···	···	−16.89 ± 0.07	···	···	1.2 ± 0.06	···	···	···	22
2006ms	···	···	31.8 ± 3.17	−16.18 ± 0.15	···	1.95 ± 0.2	0.11 ± 0.48	···	···	0.0564 ± 0.013*	41
2006qr	···	96.85 ± 7.62	···	−15.99 ± 0.14	···	···	1.46 ± 0.01	···	···	···	29
2006Y	27.1 ± 3.03	47.49 ± 5.00	20.4 ± 0.35	−17.97 ± 0.06	−14.26 ± 0.06	8.66 ± 0.49	1.99 ± 0.12	3.26 ± 1.5	···	0.0338 ± 0.02*	15
2007aa	···	···	···	−16.32 ± 0.27	···	···	−0.03 ± 0.01	···	···	···	···
2007ab	···	71.30 ± 10.44	···	−16.98 ± 0.09	−14.22 ± 0.09	···	3.39 ± 0.07	1.56 ± 0.63	···	0.0397 ± 0.01*	···
2007av	···	···	23.4 ± 8.86	−16.27 ± 0.22	···	1.29 ± 0.4	0.96 ± 0.06	···	···	0.0149 ± 0.01*	22
2007bf	···	···	···	···	···	···	···	···	···	···	···
2007hm	···	···	···	−16.47 ± 0.09	···	···	1.44 ± 0.03	···	···	0.045 ± 0.011*	14
2007il	···	103.43 ± 5.00	···	−16.78 ± 0.11	···	···	0.36 ± 0.01	···	···	···	22
2007it	···	···	14 ± 0.77	−17.55 ± 0.50	−14.83 ± 0.50	3.71 ± 0.35	1.35 ± 0.05	1 ± 0	0.0721 ± 0.021	0.0721 ± 0.031	27
2007ld	···	···	25.7 ± 1.45	−17.30 ± 0.09	···	3.19 ± 0.17	1.12 ± 0.16	···	···	···	21
2007oc	40.7 ± 3.8	71.62 ± 5.83	30.9 ± 0.55	−16.68 ± 0.15	···	2.91 ± 0.08	1.68 ± 0.02	···	···	···	···
2007od	···	···	22.9 ± 0.69	−17.87 ± 0.80	···	2.37 ± 0.05	1.55 ± 0.01	···	···	···	24
2007P	58.6 ± 6.2	88.33 ± 5.83	29.8 ± 2.04	−17.96 ± 0.05	···	3.48 ± 0.22	1.95 ± 0.12	···	···	···	23
2007sq	42.7 ± 5.7	88.34 ± 5.00	45.6 ± 1.82	−15.33 ± 0.13	···	2.5 ± 0.29	0.92 ± 0.27	···	···	···	···
2007U	···	···	48.8 ± 1.81	−17.87 ± 0.08	···	2.97 ± 0.15	1.18 ± 0.13	···	···	···	26
2007W	48.5 ± 5.4	77.29 ± 7.62	28.8 ± 1.68	−15.80 ± 0.20	···	0.82 ± 0.13	0.04 ± 0.05	···	···	···	24
2007X	52.3 ± 3.20	97.71 ± 5.83	45.4 ± 1.11	−17.84 ± 0.21	···	2.43 ± 0.06	1.37 ± 0.03	···	···	0.082 ± 0.021*	36
2007Z	···	···	···	···	···	···	···	···	···	···	···
2008ag	···	102.95 ± 6.71	···	−16.96 ± 0.15	···	···	0.16 ± 0.01	···	···	···	···
2008aw	29.8 ± 3.13	75.83 ± 10.44	46 ± 0.585	−17.71 ± 0.19	−14.04 ± 0.19	3.27 ± 0.06	2.25 ± 0.03	1.97 ± 0.09	···	0.0491 ± 0.015*	29
2008bh	···	···	49.5 ± 2.61	−16.06 ± 0.14	···	3 ± 0.27	1.2 ± 0.04	···	···	···	22
2008bk	43 ± 3.9	104.83 ± 6.71	61.8 ± 1.4	−14.86 ± 0.05	−11.98 ± 0.05	···	0.11 ± 0.02	1.18 ± 0.02	0.0074 ± 0.001	0.0074 ± 0.001	···
2008bm	42.1 ± 3.4	87.04 ± 26.17	45 ± 2.55	−18.12 ± 0.07	−12.67 ± 0.07	···	2.74 ± 0.03	···	···	0.014 ± 0.005*	···

2008bp	···	58.62 ± 9.49	···	−14.00 ± 0.21	···	···	3.17 ± 0.18	···	···	···	18
2008br	···	···	17.5 ± 0.51	−15.30 ± 0.20	···	4.25 ± 1.26	0.08 ± 0.11	···	···	0.0261 ± 0.012*	22
2008bu	···	44.75 ± 7.62	···	−17.14 ± 0.10	−13.71 ± 0.10	···	2.6 ± 0.17	2.31 ± 0.53	···	0.0197 ± 0.008*	30
2008F	···	···	40 ± 3.1	−15.67 ± 0.12	···	1.21 ± 0.16	−1.67 ± 1	···	···	···	30
2008ga	···	72.79 ± 5.00	···	−16.45 ± 0.14	···	···	0.86 ± 0.09	···	···	···	···
2008gi	···	···	···	−17.31 ± 0.09	···	···	3.13 ± 0.07	···	···	···	25
2008gr	···	···	···	−17.95 ± 0.10	···	···	2.01 ± 0.01	···	···	···	25
2008H	···	···	···	···	···	···	···	···	···	···	···
2008hg	···	···	···	−15.43 ± 0.12	···	···	−0.44 ± 0.05	···	···	···	33
2008ho	···	···	···	−15.11 ± 0.23	···	···	0.3 ± 0.05	···	···	···	24
2008if	50.3 ± 3.02	75.85 ± 5.83	25.6 ± 0.35	−17.94 ± 0.17	−14.46 ± 0.17	4.03 ± 0.07	2.2 ± 0.02	2.92 ± 0.16	···	0.0625 ± 0.02*	18
2008il	···	···	···	−16.61 ± 0.11	···	···	1.03 ± 0.04	···	···	···	24
2008in	67.19 ± 3.40	92.20 ± 6.71	25 ± 4	−15.40 ± 0.47	···	···	0.74 ± 0.01	0.88 ± 0.01	···	···	30
2008K	41 ± 3.9	87.11 ± 5.00	46.1 ± 3.23	−17.45 ± 0.08	−13.40 ± 0.08	3.08 ± 0.06	2.12 ± 0.17	1.71 ± 0.3	···	0.0123 ± 0.01*	26
2008M	57.8 ± 0.5	75.34 ± 9.49	17.6 ± 0.28	−16.75 ± 0.28	−13.41 ± 0.28	5.07 ± 0.27	1.02 ± 0.02	1.14 ± 0.12	0.0197 ± 0.0067	0.0197 ± 0.0067	18
2008W	···	83.86 ± 6.71	···	−16.60 ± 0.11	···	···	1.12 ± 0.04	···	···	···	···
2009aj	···	···	···	−18.07 ± 0.20	···	2.44 ± 0.09	0.75 ± 0.04	···	···	···	···
2009ao	···	41.71 ± 5.00	···	−15.79 ± 0.20	···	···	2.15 ± 0.09	···	···	···	17
2009au	···	···	···	−16.34 ± 0.21	···	···	3.04 ± 0.02	···	···	···	20
2009bu	···	···	37.8 ± 1.79	−16.05 ± 0.19	···	1.03 ± 0.14	0.18 ± 0.04	···	···	···	···
2009bz	···	···	36.1 ± 1.72	−16.46 ± 0.19	···	1.04 ± 0.1	0.21 ± 0.05	···	···	···	21
2009N	58.2 ± 2.25	89.50 ± 5.83	31.3 ± 2.25	−15.25 ± 0.40	···	0.45 ± 0.11	−0.36 ± 0.18	0.9 ± 0.14	···	···	35
2009W	···	···	···	···	···	···	···	···	···	···	···

* SNe with explosion epochs different to that published.

Table 4.3: Velocity values at 50 days

SN	$vel(H_\alpha)$	$vel(H_\alpha)$	$vel(H_\beta)$	vel(Fe II 4924)	vel(Fe II 5018)	vel(Fe II 5169)	vel(Fe II/Sc II)	vel(Sc II Mult.)	vel(Na I D)	vel(Ba II)	vel(ScII)
1986L	6141 ± 710	7610 ± 476	6647 ± 434	4907 ± 245	4278 ± 672	4373 ± 411	4739 ± 456	4283 ± 336	5455 ± 486	...	...
1988A	...	...	...	...	...	...	...	...	...	...	...
1990E	...	...	...	...	...	...	...	...	...	...	...
1990K	6879 ± 432	7741 ± 426	6492 ± 381	...	4406 ± 298	3916 ± 204	4844 ± 450	4568 ± 239	6297 ± 391	4434 ± 312	4109 ± 238
1991al	7846 ± 496	8768 ± 615	7689 ± 634	4880 ± 244	4751 ± 588	4940 ± 548	5214 ± 261	4540 ± 227	7728 ± 1176	5643 ± 282	4120 ± 206
1992ad	...	...	...	...	...	...	...	...	...	...	...
1992af	...	...	...	...	...	...	...	...	...	...	...
1992am	...	...	...	...	...	...	...	...	...	...	...
1992ba	4524 ± 665	6209 ± 439	5056 ± 374	3143 ± 157	3368 ± 487	3443 ± 483	3458 ± 173	3304 ± 165	4299 ± 847	3026 ± 151	3044 ± 152
1993A	...	...	...	...	...	...	...	...	...	...	...
1993K	7067 ± 551	7016 ± 358	6260 ± 444	4863 ± 269	3488 ± 1390	4358 ± 218	4445 ± 222	3742 ± 270	5437 ± 520	3971 ± 199	4024 ± 420
1993S	...	...	...	...	...	...	...	...	...	...	...
1999br	3065 ± 588	3590 ± 265	3175 ± 243	1507 ± 258	1749 ± 223	1740 ± 305	2092 ± 272	1527 ± 443	1515 ± 759	1225 ± 61	1885 ± 94
1999ca	6957 ± 348	7285 ± 364	6763 ± 338	...	5565 ± 278	5147 ± 257	6042 ± 302	5673 ± 284	6749 ± 337	5778 ± 289	5001 ± 250
1999cr	5428 ± 361	5901 ± 323	4892 ± 478	...	3474 ± 195	3632 ± 212	...	3883 ± 194	4470 ± 224	...	...
1999eg	...	...	...	...	...	...	...	...	...	...	...
1999em	5540 ± 622	5963 ± 595	5656 ± 626	3744 ± 187	3319 ± 394	3444 ± 365	3362 ± 168	2977 ± 149	3769 ± 451	3032 ± 152	3089 ± 154
S0210	8088 ± 492	7851 ± 762	6970 ± 619	...	6770 ± 424	4956 ± 326	6210 ± 311	5325 ± 550	6735 ± 455	...	...
2002ew	...	...	...	...	...	...	...	...	...	...	...
2002fa	6121 ± 649	7553 ± 435	6292 ± 410	3545 ± 268	3807 ± 337	4104 ± 260	4134 ± 207	3581 ± 179	5687 ± 663	...	...
2002gd	3693 ± 563	4109 ± 266	3394 ± 703	2248 ± 196	2716 ± 204	2437 ± 236	3147 ± 297	2988 ± 409	3382 ± 273	2097 ± 177	2404 ± 325
2002gw	5403 ± 474	6600 ± 487	5252 ± 518	3234 ± 329	3277 ± 494	3600 ± 357	3203 ± 345	3215 ± 247	3865 ± 304	3021 ± 211	2961 ± 185
2002hj	6469 ± 661	7830 ± 532	6377 ± 451	3411 ± 579	3762 ± 338	4162 ± 405	4609 ± 230	3571 ± 220	5193 ± 345	...	...
2002hx	5667 ± 434	7964 ± 504	6386 ± 554	3237 ± 337	3485 ± 215	3781 ± 284	3005 ± 157	3600 ± 200	5360 ± 477	2522 ± 160	3197 ± 302
2002ig	...	...	...	...	...	...	...	...	...	...	...
2003B	4565 ± 339	6190 ± 622	5474 ± 478	3186 ± 575	3437 ± 297	3488 ± 251	3621 ± 260	3502 ± 307	4024 ± 228	3323 ± 265	3104 ± 188
2003bl	3650 ± 481	3928 ± 435	3825 ± 326	2050 ± 255	2332 ± 213	2085 ± 190	2440 ± 263	2445 ± 207	2700 ± 582	2766 ± 426	2256 ± 184
2003bn	5827 ± 638	6812 ± 545	5630 ± 471	3616 ± 265	3588 ± 607	3588 ± 530	3437 ± 302	3236 ± 327	4048 ± 397	3278 ± 300	3118 ± 178
2003ci	5594 ± 280	7133 ± 357	5857 ± 293	2991 ± 150	3806 ± 190	3653 ± 183	4724 ± 236	4416 ± 483	5849 ± 292	3125 ± 156	4222 ± 211
2003cn	4192 ± 293	5361 ± 501	4488 ± 946	2388 ± 119	2764 ± 138	2685 ± 197	2947 ± 147	2522 ± 126	3809 ± 695	2804 ± 140	2965 ± 148
2003cx	...	...	...	...	...	...	...	...	...	...	...
2003dq	...	...	...	...	...	...	...	...	...	...	...
2003E	...	...	...	...	...	...	...	...	...	...	...
2003ef	6349 ± 367	7606 ± 610	4230 ± 494	3904 ± 364	4092 ± 534	4087 ± 516	4016 ± 575	3714 ± 395	4284 ± 484	3561 ± 299	3615 ± 181
2003eg	7525 ± 725	8440 ± 675	6632 ± 418	...	4630 ± 405	4691 ± 456	4137 ± 207	4204 ± 210	6912 ± 468	3100 ± 320	3390 ± 410
2003ej	...	...	...	...	...	...	...	...	...	...	...
2003fb	6628 ± 561	7507 ± 625	5535 ± 854	4021 ± 754	4125 ± 738	3974 ± 722	4122 ± 704	3655 ± 677	4734 ± 668	4547 ± 649	3566 ± 627
2003gd	...	...	...	...	...	...	...	...	...	...	...
2003hd	6732 ± 519	7750 ± 539	5899 ± 717	3838 ± 192	3930 ± 260	3997 ± 289	3754 ± 188	3373 ± 169	4688 ± 234	...	...
2003hg	...	...	...	...	...	...	...	...	...	...	...
2003hk	6980 ± 349	6550 ± 328	5628 ± 281	4026 ± 201	4114 ± 206	4131 ± 207	...	...	5712 ± 286	...	...
2003hl	5569 ± 738	6508 ± 462	4515 ± 439	3934 ± 382	3873 ± 287	3795 ± 402	3762 ± 329	3758 ± 283	4492 ± 318	3257 ± 252	3480 ± 244
2003hn	6521 ± 387	6935 ± 462	5288 ± 442	3433 ± 281	3404 ± 249	3462 ± 379	3445 ± 286	3129 ± 293	4437 ± 339	3573 ± 189	3020 ± 375
2003ho	7367 ± 755	8200 ± 520	6041 ± 302	3442 ± 172	3715 ± 186	3963 ± 198	4278 ± 214	3943 ± 197	4969 ± 248	...	...
2003ib	...	...	...	...	...	...	...	...	...	...	...
2003ip	7953 ± 486	8508 ± 533	6736 ± 388	...	5342 ± 341	4501 ± 309	5717 ± 286	5015 ± 251	6432 ± 413	4818 ± 241	5289 ± 264
2003iq	5893 ± 741	7389 ± 386	5432 ± 350	4223 ± 211	4183 ± 225	4297 ± 216	4142 ± 207	3909 ± 195	5080 ± 360	3720 ± 186	3894 ± 195

2003T	5933 ± 403	6873 ± 634	4010 ± 226	3941 ± 341	3783 ± 218	3870 ± 276	3754 ± 190	3370 ± 222	3968 ± 292	4193 ± 257	4012 ± 240
2004dy	...	...	...	...	...	...	...	...	...	...	...
2004ej	5471 ± 501	6291 ± 429	5340 ± 600	3513 ± 505	3419 ± 307	3282 ± 221	3534 ± 536	3272 ± 319	3978 ± 326	2866 ± 191	3160 ± 223
2004er	8210 ± 582	9508 ± 549	7774 ± 600	5980 ± 427	5349 ± 386	5174 ± 436	5451 ± 311	3353 ± 470	5716 ± 506	5243 ± 634	5259 ± 475
2004fb	6604 ± 636	7602 ± 444	5827 ± 435	3900 ± 283	4198 ± 425	4149 ± 300	4335 ± 217	3726 ± 186	4760 ± 340	5217 ± 261	3780 ± 410
2004fc	5584 ± 645	6269 ± 976	4027 ± 329	3667 ± 236	3652 ± 291	3559 ± 256	3736 ± 270	3569 ± 261	4165 ± 541	3178 ± 229	3373 ± 266
2004fx	4816 ± 525	5671 ± 446	4164 ± 318	2375 ± 206	2687 ± 209	2772 ± 401	2986 ± 177	3367 ± 168	2870 ± 389	3162 ± 158	2449 ± 133
2005af	...	...	...	...	...	...	...	...	...	...	...
2005an	8212 ± 888	7561 ± 494	5295 ± 1497	4324 ± 219	4301 ± 325	3985 ± 303	4716 ± 289	4517 ± 293	4698 ± 1106	...	3563 ± 178
2005dk	6808 ± 531	7823 ± 470	6805 ± 359	4506 ± 312	4500 ± 289	4567 ± 306	4384 ± 311	3911 ± 329	6251 ± 709	5067 ± 457	4012 ± 256
2005dn	8304 ± 672	9353 ± 576	7518 ± 484	2351 ± 118	5690 ± 1511	4674 ± 434	...	4818 ± 241	6448 ± 627	...	...
2005dt	...	...	...	...	...	...	...	...	...	...	...
2005dw	...	...	...	...	...	...	...	...	...	...	...
2005dx	...	...	...	...	...	...	...	...	...	...	...
2005dz	6112 ± 595	7496 ± 434	5873 ± 430	...	3901 ± 499	4072 ± 310	...	...	...	...	...
2005es	...	...	...	...	...	...	...	...	...	...	...
2005J	6285 ± 755	8317 ± 668	6311 ± 404	4204 ± 273	4099 ± 406	4192 ± 437	4122 ± 402	4159 ± 265	4953 ± 386	4069 ± 297	4548 ± 272
2005K	...	...	...	...	...	...	...	...	...	...	...
2005lw	9900 ± 785	9645 ± 830	8270 ± 750	...	7294 ± 630	6150 ± 700	7100 ± 520	5985 ± 540	7430 ± 570	6200 ± 550	6770 ± 710
2005me	...	...	...	...	...	...	...	...	...	...	...
2005Z	8419 ± 661	9332 ± 582	7777 ± 843	5620 ± 281	5593 ± 384	5151 ± 411	5581 ± 489	5387 ± 359	7417 ± 560	...	...
2006ai	6871 ± 821	7388 ± 559	6235 ± 560	4104 ± 353	4390 ± 427	4587 ± 340	4363 ± 258	3358 ± 526	6120 ± 434	...	...
2006bc	...	...	...	...	...	...	...	...	...	...	...
2006be	6857 ± 474	7531 ± 625	5925 ± 755	3763 ± 742	3851 ± 738	4031 ± 722	3907 ± 694	3337 ± 677	4378 ± 668	4933 ± 620	...
2006bl	...	...	...	...	...	...	...	...	...	...	...
2006ee	5323 ± 426	5164 ± 675	3004 ± 619	3195 ± 254	3108 ± 194	3008 ± 255	3085 ± 299	2695 ± 316	3221 ± 267	2721 ± 262	2725 ± 202
2006it	...	...	...	...	...	...	...	...	...	...	...
2006iw	6857 ± 671	7531 ± 566	6172694	4630 ± 687	4310 ± 678	4389 ± 722	3898 ± 688	3451 ± 682	5196 ± 724	...	...
2006ms	...	...	...	...	...	...	...	...	...	...	...
2006qr	5507 ± 419	6432 ± 487	5060285	3147 ± 872	3571 ± 221	3621 ± 200	3756 ± 188	3508 ± 175	4804 ± 954	3770 ± 188	2917 ± 146
2006Y	7671 ± 619	8876 ± 589	6879464	3724 ± 186	4904 ± 731	5033 ± 546	...	...	6922 ± 613	...	...
2007aa	5057 ± 539	5925 ± 550	4233374	3131 ± 398	3161 ± 378	3131 ± 396	3082 ± 324	2865 ± 266	3839 ± 321	2685 ± 187	2893 ± 267
2007ab	8378 ± 505	9614 ± 600	8094405	...	7056 ± 353	4737 ± 237	6878 ± 344	6350 ± 318	7198 ± 404	6743 ± 337	5949 ± 614
2007av	6007 ± 338	7146 ± 402	5320311	3641 ± 182	3849 ± 192	3821 ± 191	3822 ± 191	3691 ± 185	3935 ± 605	3638 ± 182	3432 ± 172
2007bf	...	...	...	...	...	...	...	...	...	...	...
2007hm	6132 ± 383	8126 ± 544	6336432	4258 ± 213	4012 ± 201	4371 ± 515	4796 ± 240	3322 ± 166	5232 ± 262	...	...
2007il	7298 ± 809	7917 ± 482	5855505	4189 ± 281	4071 ± 481	4250 ± 383	...	...	4759 ± 769	...	...
2007it	...	...	...	...	...	...	...	...	...	...	...
2007ld	...	...	...	...	...	...	...	...	...	...	...
2007oc	6990 ± 492	6675 ± 435	5193 ± 436	2265 ± 198	3262 ± 315	3670 ± 343	4158 ± 480	3832 ± 378	4977 ± 450	2872 ± 218	3247 ± 291
2007od	7080 ± 655	7087 ± 428	6623 ± 545	...	5143 ± 363	3838 ± 300	...	3851 ± 193	6139 ± 427	5100 ± 525	4806 ± 240
2007P	...	...	...	...	...	...	...	...	...	...	...
2007sq	8293 ± 1243	8186 ± 437	7319 ± 366	5270 ± 390	5203 ± 260	5301 ± 265	4937 ± 247	4107 ± 205	5609 ± 280	...	...
2007U	7308 ± 1137	7932 ± 516	6831 ± 721	...	5489 ± 274	5388 ± 550	5864 ± 293	5379 ± 269	6410 ± 340	...	...
2007W	4093 ± 935	4712 ± 558	3182 ± 269	2333 ± 182	2600 ± 337	2426 ± 454	2531 ± 156	2494 ± 164	2606 ± 186	2078 ± 104	2473 ± 124
2007X	8301 ± 675	8476 ± 537	6609 ± 601	...	5416 ± 383	4585 ± 762	6272 ± 399	5503 ± 354	6107 ± 1008	5115 ± 427	4978 ± 496
2007Z	...	...	...	...	...	...	...	...	...	...	...
2008ag	6218 ± 463	6826 ± 426	4546 ± 473	4017 ± 292	3924 ± 324	3912 ± 311	3837 ± 326	3500 ± 283	4185 ± 426	3205 ± 230	3478 ± 233
2008aw	7684 ± 621	8145 ± 1011	6567 ± 530	4689 ± 376	4684 ± 526	4497 ± 654	4983 ± 458	4395 ± 372	6366 ± 478	4508 ± 394	4424 ± 271
2008bh	7177 ± 688	7724 ± 430	6232 ± 375	4205 ± 210	4308 ± 232	4163 ± 637	4295 ± 215	4150 ± 207	4648 ± 378	4433 ± 222	3963 ± 198
2008bk	3294 ± 390	4086 ± 707	2390 ± 224	1860 ± 133	2247 ± 153	2896 ± 460	2256 ± 276	2426 ± 310	2011 ± 171	1840 ± 137	1991 ± 180
2008bm	1115 ± 56	1760 ± 88	1382 ± 69	1555 ± 78	1644 ± 82	1274 ± 64	...	...	1756 ± 88	...	...

2008bp	...	...	...	...	...	...	...	...	...	...	...
2008br	3659 ± 491	4043 ± 258	2474 ± 169	1659 ± 178	1826 ± 142	1628 ± 218	2152 ± 108	2535 ± 127	1915 ± 96	1382 ± 69	1666 ± 83
2008bu	...	...	...	...	...	...	...	...	...	...	...
2008F	...	...	...	...	...	...	...	...	...	...	...
2008ga	6400 ± 589	7313 ± 653	5357 ± 768	3307 ± 754	3390 ± 732	3253 ± 757	4665 ± 694	3179 ± 677	4785 ± 663	...	...
2008gi	...	...	...	...	...	...	...	...	...	...	...
2008gr	8247 ± 752	8705 ± 435	7454 ± 385	...	5364 ± 268	4971 ± 249	5860 ± 293	5521 ± 276	7393 ± 708	...	...
2008H	6811 ± 790	6537 ± 703	5308 ± 941	3838 ± 420	3766 ± 360	3714 ± 350	3797 ± 400	3655 ± 783	4633 ± 760	3370 ± 325	3410 ± 410
2008hg	...	...	...	...	...	...	...	...	...	...	...
2008ho	...	...	...	...	...	...	...	...	...	...	...
2008if	8588 ± 1126	8415 ± 549	7137 ± 642	3182 ± 200	4887 ± 298	4718 ± 398	5018 ± 272	4745 ± 251	7309 ± 633	3789 ± 189	4582 ± 234
2008il	...	...	...	...	...	...	...	...	...	...	...
2008in	4384 ± 721	4245 ± 768	3210 ± 310	2754 ± 259	2824 ± 373	2817 ± 455	2666 ± 283	2667 ± 251	2907 ± 1581	2368 ± 203	2562 ± 227
2008K	7882 ± 619	7784 ± 793	6791 ± 701	...	6134 ± 352	5311 ± 437	...	5491 ± 301	6984 ± 501	...	...
2008M	6058 ± 862	6793 ± 631	5654 ± 474	3487 ± 214	3436 ± 345	3622 ± 458	3748 ± 271	3593 ± 198	4754 ± 1056	3368 ± 217	3486 ± 275
2008W	5955 ± 665	6932 ± 435	5815 ± 435	3435 ± 335	3719 ± 233	3820 ± 297	3710 ± 224	3487 ± 278	5197 ± 470	3078 ± 255	3296 ± 185
2009aj	2787 ± 455	3095 ± 183	2800 ± 470	2082 ± 161	2421 ± 197	2834 ± 315	...	...	3011 ± 240	...	...
2009ao	6678 ± 859	5920 ± 544	5194 ± 471	3767 ± 334	3672 ± 256	3575 ± 210	4126 ± 206	3745 ± 230	4650 ± 335	...	3396 ± 170
2009au	2601 ± 524	2575 ± 215	1978 ± 165	1613 ± 113	1727 ± 161	1470 ± 175	1769 ± 237	1912 ± 296	1943 ± 118	1285 ± 64	1698 ± 85
2009bu	6363 ± 596	7316 ± 1521	5522 ± 1304	3969 ± 267	3948 ± 436	4007 ± 456	4204 ± 210	3440 ± 172	4448 ± 308	...	...
2009bz	...	...	...	...	...	...	...	...	...	...	...
2009N	4039 ± 377	4475 ± 909	2799 ± 259	2515 ± 282	2638 ± 299	2588 ± 439	2537 ± 238	2489 ± 195	2692 ± 186	2289 ± 206	2387 ± 156
2009W	...	...	...	...	...	...	...	...	...	...	...

Columns: (1) SN name; (2) Velocity of H_α absorption component; (3) Velocity of H_α emission component; (4) Velocity of H_β; (5) Velocity of Fe II 4924; (6) Velocity of Fe II 5018; (7) Velocity of Fe II 5169; (8) Velocity of Fe II/Sc II; (9) Velocity of Sc II Multiplet; (10) Velocity of Na I D; (11) Velocity of Ba II; (12) Velocity of ScII

Table 4.4: pEW values at 50 days

SN	(H_α)	(H_α)	(H_β)	(Fe II 4924)	(Fe II 5018)	(Fe II 5169)	(Fe II/Sc II)	(Sc II Mult.)	(Na I D)	(Ba II)	(ScII)	a/e
1986L	32.8 ± 4.1	144.2 ± 34.2	48.2 ± 5.6	1.2 ± 0.6	14.7 ± 3.8	36.7 ± 11.8	7.6 ± 2.9	10.4 ± 3.1	29.2 ± 7.7	0.0 ± 0.0	0.0 ± 0.0	0.23 ± 0.08
1988A	···	···	···	···	···	···	···	···	···	···	···	···
1990E	···	···	···	···	···	···	···	···	···	···	···	···
1990K	42.7 ± 4.8	206.2 ± 27.4	71.9 ± 4.4	0.0 ± 0.0	10.9 ± 0.7	38.8 ± 3.1	8.9 ± 0.7	13.2 ± 1.6	50.3 ± 7.5	6.4 ± 0.4	5.9 ± 0.9	0.21 ± 0.05
1991al	62.1 ± 9.8	214.2 ± 25.8	67.5 ± 10.2	4.8 ± 2.7	13.0 ± 1.7	27.2 ± 4.8	4.3 ± 1.9	6.5 ± 3.1	20.4 ± 3.2	6.4 ± 2.9	4.1 ± 2.2	0.29 ± 0.08
1992ad	···	···	···	···	···	···	···	···	···	···	···	···
1992af	···	···	···	···	···	···	···	···	···	···	···	···
1992am	···	···	···	···	···	···	···	···	···	···	···	···
1992ba	61.9 ± 8.2	119.3 ± 19.7	47.0 ± 8.9	7.6 ± 3.5	20.2 ± 5.5	30.1 ± 8.9	9.9 ± 1.5	13.7 ± 2.7	34.2 ± 13.7	7.9 ± 1.3	7.1 ± 1.3	0.52 ± 0.15
1993A	···	···	···	···	···	···	···	···	···	···	···	···
1993K	27.8 ± 4.8	126.1 ± 25.3	42.8 ± 2.7	6.4 ± 2.4	18.9 ± 9.8	28.7 ± 1.9	5.2 ± 1.2	7.3 ± 1.4	27.1 ± 1.9	3.8 ± 1	3.8 ± 1.4	0.22 ± 0.08
1993S	···	···	···	···	···	···	···	···	···	···	···	···
1999br	56.0 ± 4.1	14.6 ± 10.6	33.8 ± 7.8	15.0 ± 1.7	25.2 ± 2.5	43.1 ± 9.1	15.1 ± 2.9	20.8 ± 3	20.7 ± 2.9	12.9 ± 1.6	14.2 ± 1.4	3.84 ± 3.06
1999ca	48.3 ± 2.7	169.4 ± 13.6	78.9 ± 5.9	0.0 ± 0.0	17.6 ± 1.3	64.1 ± 3.9	11.1 ± 1.1	19.6 ± 1.7	33.7 ± 2.1	5.4 ± 0.4	11.6 ± 0.8	0.29 ± 0.03
1999cr	31.7 ± 11.2	137.5 ± 22.9	37.6 ± 7.1	0.0 ± 0.0	12.4 ± 5.7	24.9 ± 6.8	0.0 ± 0.0	6.4 ± 1.1	9.3 ± 2.2	0.0 ± 0.0	0.0 ± 0.0	0.23 ± 0.12
1999eg	···	···	···	···	···	···	···	···	···	···	···	···
1999em	75.8 ± 15	141.2 ± 40.2	40.3 ± 5.6	9.9 ± 1.6	23.8 ± 1.8	43.6 ± 7.5	11.7 ± 1.8	13.4 ± 3	30.6 ± 7.8	6.7 ± 1.0	7.5 ± 1.2	0.54 ± 0.25
S0210	36 ± 11.9	287.4 ± 42.3	83.5 ± 4.9	0.0 ± 0.0	30.4 ± 3.5	70.1 ± 19.5	7.8 ± 1.2	40.4 ± 3.3	49.2 ± 13.2	0.0 ± 0.0	0.0 ± 0.0	0.13 ± 0.06
2002ew	···	···	···	···	···	···	···	···	···	···	···	···
2002fa	45.4 ± 10.9	125.1 ± 43.6	52.4 ± 17.2	6.1 ± 1.1	15.5 ± 4.1	36.5 ± 2.4	9.7 ± 3.4	13.1 ± 2.4	42.4 ± 12.4	0.0 ± 0.0	0.0 ± 0.0	0.36 ± 0.21
2002gd	21.7 ± 4.3	106.8 ± 23.8	39.8 ± 13.3	5.8 ± 2.2	24.9 ± 5.5	59.3 ± 12.7	16.2 ± 3.8	26.9 ± 5.6	27.1 ± 5.1	3.8 ± 2.6	11.0 ± 5.1	0.20 ± 0.08
2002gw	61.4 ± 14.6	205.5 ± 29.5	58.4 ± 10.6	6.9 ± 1.6	18.2 ± 2.1	31.3 ± 4.7	5.5 ± 1.7	5.8 ± 2.0	13.5 ± 3.3	3.1 ± 1.1	3.8 ± 1.5	0.30 ± 0.11
2002hj	70.1 ± 12.3	207.5 ± 34.1	71.7 ± 5.5	2.8 ± 1.6	16.5 ± 3.9	40.8 ± 4.2	4.3 ± 2.5	10.2 ± 4.4	18.6 ± 4.9	0.0 ± 0.0	0.0 ± 0.0	0.34 ± 0.11
2002hx	88.8 ± 11.1	135.6 ± 18.1	73.8 ± 11.8	9.8 ± 2.2	20.8 ± 2.2	35.5 ± 6.0	7.5 ± 1.1	17.9 ± 2.7	53.1 ± 24.1	8.6 ± 2.2	1.3 ± 4.1	0.65 ± 0.16
2002ig	···	···	···	···	···	···	···	···	···	···	0.0 ± 0.0	···
2003B	60.1 ± 5.3	148.6 ± 27.6	53.0 ± 6.5	10.5 ± 1.8	23.4 ± 2.5	38.1 ± 3.3	14.2 ± 1.4	20.3 ± 2.4	28.6 ± 2.2	3.9 ± 0.9	8.8 ± 1.5	0.40 ± 0.11
2003bl	58.0 ± 7.3	116.5 ± 19.1	37.1 ± 2.1	15.1 ± 2.8	26.5 ± 3.5	38.3 ± 3.8	10.9 ± 3.9	17.0 ± 6.6	19.3 ± 5.6	11.7 ± 5.4	9.1 ± 3.9	0.51 ± 0.14
2003bn	77.7 ± 16.4	144.4 ± 66.6	55.3 ± 16.5	7.1 ± 2.9	17.3 ± 6.6	36.0 ± 10.1	8.3 ± 3.1	9.1 ± 4.1	16.1 ± 12.3	3.2 ± 2.0	2.5 ± 2.1	0.54 ± 0.36
2003ci	50.6 ± 2.5	166.2 ± 8.3	64.6 ± 3.2	1.3 ± 0.1	15.8 ± 0.8	46.2 ± 3.6	10.4 ± 0.5	20.7 ± 1.0	55.1 ± 2.8	7.7 ± 0.4	4.2 ± 0.2	0.31 ± 0.03
2003cn	43.7 ± 2.9	141.6 ± 18.4	52.9 ± 9.7	12.6 ± 2.1	21.1 ± 3.4	35.1 ± 3.9	9.2 ± 1.8	17.2 ± 3.1	18.2 ± 4.7	7.4 ± 1.5	7.1 ± 1.2	0.31 ± 0.06
2003cx	···	···	···	···	···	···	···	···	···	···	···	···
2003dq	···	···	···	···	···	···	···	···	···	···	···	···
2003E	···	···	···	···	···	···	···	···	···	···	···	···
2003ef	91.4 ± 10.3	130.5 ± 14.3	27.9 ± 6.2	9.8 ± 1.3	20.4 ± 1.7	28.3 ± 9.4	10.8 ± 4.9	9.4 ± 6.2	24.2 ± 13	1.9 ± 5.3	9.6 ± 3.2	0.70 ± 0.15
2003eg	9.4 ± 1.1	244.2 ± 24.5	60.6 ± 4.4	0.0 ± 0.0	14.4 ± 1.5	38.6 ± 11.1	10.5 ± 3.4	14.2 ± 3.7	58.4 ± 6.3	7.1 ± 2.1	6.5 ± 2.8	0.04 ± 0.01
2003ej	···	···	···	···	···	···	···	···	···	···	···	···
2003fb	73.7 ± 6.3	185.1 ± 13.4	55.1 ± 4.2	8.1 ± 0.8	18.1 ± 0.8	40 ± 2.6	7.9 ± 1.5	9.0 ± 1.4	25.0 ± 1.6	9.0 ± 1.8	7.1 ± 1.2	0.4 ± 0.06
2003gd	···	···	···	···	···	···	···	···	···	···	···	···
2003hd	78.1 ± 11.2	119.1 ± 30.9	56.8 ± 9.4	4.9 ± 1.1	16.1 ± 3.1	33.910	4.6 ± 2.8	7.9 ± 4.5	15.4 ± 3.3	0.0 ± 0.0	0.0 ± 0.0	0.65 ± 0.26
2003hg	···	···	···	···	···	···	···	···	···	···	···	···
2003hk	32.6 ± 18.4	123.2 ± 12.4	39.2 ± 3.7	9.3 ± 3.9	17.6 ± 2.3	34.6 ± 3.6	0.0 ± 0.0	0.0 ± 0.0	44.3 ± 6.1	0.0 ± 0.0	0.0 ± 0.0	0.26 ± 0.18
2003hl	50.4 ± 6.1	118.3 ± 22.1	32.6 ± 9.9	6.8 ± 2.4	22.1 ± 3.9	39.5 ± 4.1	15.4 ± 2.9	19.2 ± 2.6	35.9 ± 5.5	5.6 ± 2.6	1.1 ± 2.2	0.43 ± 0.13
2003hn	61.4 ± 5.0	178.7 ± 22.4	60.0 ± 5.4	7.2 ± 1.1	17.5 ± 1.5	39.1 ± 5.7	10.2 ± 1.8	13.3 ± 1.5	31.5 ± 5.6	4.3 ± 0.9	5.3 ± 0.8	0.34 ± 0.07
2003ho	68.4 ± 9.8	269.8 ± 54.9	69.1 ± 4.6	5.4 ± 1.3	16.9 ± 1.9	42.7 ± 3.2	7.9 ± 1.8	8.3 ± 0.7	36.1 ± 2.9	0.0 ± 0.0	0.0 ± 0.0	0.25 ± 0.08
2003ib	···	···	···	···	···	···	···	···	···	···	···	···
2003ip	60.9 ± 5.2	191.4 ± 18.1	71.2 ± 10.8	0.0 ± 0.0	9.3 ± 5.2	43 ± 9.7	6.5 ± 1.4	12.0 ± 1.0	33.2 ± 3.6	4.9 ± 0.6	5.9 ± 2.1	0.32 ± 0.05
2003iq	84.2 ± 13.6	157.9 ± 14.4	46.2 ± 7.2	7.8 ± 3.1	21.3 ± 1.8	37.7 ± 4.1	10.4 ± 3.6	10.7 ± 3.5	32.3 ± 6.9	3.4 ± 1.2	6.0 ± 2.0	0.53 ± 0.13

2003T	58.5 ± 21	153.6 ± 29.6	27.6 ± 10.1	11.5 ± 4.7	22.9 ± 2.9	38.2 ± 7.6	14.0 ± 2.9	14.9 ± 3.3	35.1 ± 5.5	18.7 ± 6.7	10.2 ± 2.2	0.38 ± 0.21
2004dy	· · ·	· · ·	· · ·	· · ·	· · ·	· · ·	· · ·	· · ·	· · ·	· · ·	· · ·	· · ·
2004ej	57.1 ± 9.8	114.6 ± 20.3	48.6 ± 9.7	9.1 ± 6.1	20.7 ± 1.7	44.0 ± 8.3	14.7 ± 4.3	21.8 ± 4.9	37.2 ± 6.1	6.4 ± 4.6	5.9 ± 3.7	0.50 ± 0.17
2004er	74.4 ± 10.7	154.3 ± 23.7	59.2 ± 14.7	3.2 ± 1.5	10.7 ± 2.3	34.3 ± 5.2	3.6 ± 0.7	6.4 ± 2.4	16.2 ± 3.3	0.4 ± 4.6	2.6 ± 0.7	0.48 ± 0.14
2004fb	70.1 ± 37.2	165.5 ± 26.1	59.1 ± 17.4	6.9 ± 0.5	18.7 ± 2.1	46.9 ± 20.4	$11.6 \pm 2 - 1$	16.8 ± 5.1	41.6 ± 26.8	10.8 ± 2.0	10.4 ± 1.2	0.42 ± 0.29
2004fc	34.8 ± 16.2	85.6 ± 37.9	16.2 ± 9.8	7.9 ± 2.1	18.7 ± 3.8	28.2 ± 6.1	10.2 ± 2.9	14.4 ± 5.7	23.1 ± 9.3	5.0 ± 2.1	6.6 ± 1.8	0.41 ± 0.36
2004fx	70.6 ± 11.7	168.9 ± 35.7	55.7 ± 8.3	8.6 ± 3.3	18.6 ± 4.1	30.7 ± 5.0	7.2 ± 4.1	4.4 ± 5.6	11.3 ± 4.2	2.7 ± 1.2	4.8 ± 5.4	0.42 ± 0.15
2005af	· · ·	· · ·	· · ·	· · ·	· · ·	· · ·	· · ·	· · ·	· · ·	· · ·	· · · · · ·	
2005an	51.9 ± 7.8	210.8 ± 27.1	74.4 ± 12.7	4.1 ± 0.4	15.4 ± 2.6	42.8 ± 5.9	12.1 ± 2.1	22.2 ± 3.5	18.4 ± 2.8	0.0 ± 0.0	10.5 ± 0.9	0.25 ± 0.06
2005dk	49.0 ± 8.3	166.6 ± 19.0	57.6 ± 4.5	5.4 ± 0.7	13.4 ± 1.2	32.7 ± 3.2	8.9 ± 2.7	11.1 ± 1.3	32.1 ± 14.6	4.2 ± 1.9	4.6 ± 1.9	0.29 ± 0.08
2005dn	66.6 ± 7.1	238.9 ± 54.3	77.9 ± 9.5	1.1 ± 2.2	3.9 ± 1.1	$48.0 \pm 10.$	0.0 ± 0.0	10.5 ± 1.2	30.7 ± 10.4	0.0 ± 0.0	0.0 ± 0.0	0.28 ± 0.09
2005dt	· · ·	· · ·	· · ·	· · ·	· · ·	· · ·	· · ·	· · ·	· · ·	· · ·	· · ·	· · ·
2005dw	· · ·	· · ·	· · ·	· · ·	· · ·	· · ·	· · ·	· · ·	· · ·	· · ·	· · ·	· · ·
2005dx	· · ·	· · ·	· · ·	· · ·	· · ·	· · ·	· · ·	· · ·	· · ·	· · ·	· · ·	· · ·
2005dz	77.2 ± 13.4	205 ± 41.1	50.4 ± 14.1	0.0 ± 0.0	20.3 ± 2.3	34.4 ± 4.8	0.0 ± 0.0	0.0 ± 0.0	0.0 ± 0.0	0.0 ± 0.0	0.0 ± 0.0	0.38 ± 0.141
2005es	· · ·	· · ·	· · ·	· · ·	· · ·	· · ·	· · ·	· · ·	· · ·	· · ·	· · ·	· · ·
2005J	77.2 ± 9.5	133.7 ± 30.3	64.0 ± 6.5	5.5 ± 1.8	15.9 ± 3.1	36.6 ± 4.4	8.6 ± 2.3	12.2 ± 3.1	23.2 ± 6.4	4.8 ± 2.7	3.9 ± 1.3	0.58 ± 0.201
2005K	· · ·	· · ·	· · ·	· · ·	· · ·	· · ·	· · ·	· · ·	· · ·	· · ·	· · ·	· · ·
2005lw	45.1 ± 7.2	210.0 ± 15.2	50.1 ± 5.4	0.0 ± 0.0	9.2 ± 1.5	60.0 ± 6.1	6.1 ± 1.9	7.0 ± 1.7	26.0 ± 4.1	3.5 ± 1.2	4.9 ± 1.6	0.21 ± 0.17
2005me	· · ·	· · ·	· · ·	· · ·	· · ·	· · ·	· · ·	· · ·	· · ·	· · ·	· · ·	· · ·
2005Z	65.9 ± 10.4	192.1 ± 35.7	56.8 ± 17.3	6.9 ± 1.5	12.7 ± 2.6	36.1 ± 13.7	10.4 ± 2.2	13.9 ± 4.6	49.2 ± 10.6	0.0 ± 0.0	0.0 ± 0.0	0.34 ± 0.118
2006ai	15.4 ± 4.6	173.2 ± 22.5	38.5 ± 4.4	3.2 ± 1.2	15.0 ± 2.5	36.8 ± 4.6	6.5 ± 2.9	7.8 ± 1.7	35.4 ± 3.1	0.0 ± 0.0	0.0 ± 0.0	0.09 ± 0.038
2006bc	· · ·	· · ·	· · ·	· · ·	· · ·	· · ·	· · ·	· · ·	· · ·	· · ·	· · ·	· · ·
2006be	62.2 ± 4.3	180.5 ± 7	68.1 ± 4.0	5.6 ± 1.3	15.1 ± 0.7	26.0 ± 2.1	8.0 ± 1.2	12.0 ± 1.2	20.0 ± 1.2	5.3 ± 1.0	0.0 ± 0.0	0.34 ± 0.037
2006bl	· · ·	· · ·	· · ·	· · ·	· · ·	· · ·	· · ·	· · ·	· · ·	· · ·	· · ·	· · ·
2006ee	62.6 ± 16.2	122.1 ± 22.5	24.5 ± 10.5	15.2 ± 3.2	26.6 ± 3.9	42.4 ± 9.8	14.6 ± 2.8	18.1 ± 5.2	39.1 ± 7.8	13.1 ± 5.4	14.1 ± 3.2	0.51 ± 0.227
2006it	· · ·	· · ·	· · ·	· · ·	· · ·	· · ·	· · ·	· · ·	· · ·	· · ·	· · ·	· · ·
2006iw	40.6 ± 4.2	94.7 ± 12.2	38.1 ± 4.3	3.5 ± 1.6	10.0 ± 1.2	16.0 ± 1.6	5.0 ± 0.8	6.7 ± 1.2	12.1 ± 2	0.0 ± 0.0	0.0 ± 0.0	0.43 ± 0.097
2006ms	· · ·	· · ·	· · ·	· · ·	· · ·	· · ·	· · ·	· · ·	· · ·	· · ·	· · ·	· · ·
2006qr	69.7 ± 20.6	133.1 ± 15.1	61.9 ± 11.3	11.5 ± 0.6	22.1 ± 4.9	44.0 ± 5.2	16.3 ± 4.1	20.2 ± 4.6	33.6 ± 9.4	8.8 ± 4.9	12.6 ± 3.2	0.52 ± 0.214
2006Y	10.4 ± 2.9	123.7 ± 27.3	25.5 ± 2.8	1.6 ± 0.5	6.7 ± 1.8	16.3 ± 6.1	0.0 ± 0.0	0.0 ± 0.0	15.8 ± 6	0.0 ± 0.0	0.0 ± 0.0	0.08 ± 0.042
2007aa	74.5 ± 10.5	119.7 ± 11.0	52.5 ± 5.8	9.6 ± 1.1	20.7 ± 1.8	35.1 ± 3.1	10.7 ± 2.1	13.1 ± 2.1	31.8 ± 5.9	1.1 ± 2.2	5.7 ± 1.6	0.62 ± 0.145
2007ab	72.4 ± 11.1	232.1 ± 26.4	84.6 ± 9.4	0.0 ± 0.0	17.5 ± 3.6	77.2 ± 13.4	6.6 ± 3.6	23.0 ± 4.4	32.9 ± 2	8.0 ± 2.1	12.0 ± 3.3	0.31 ± 0.083
2007av	97 ± 6.6	164.9 ± 22.2	46.4 ± 3.3	8.6 ± 1.5	21.8 ± 1.4	43.9 ± 3.5	10.9 ± 3.8	12.3 ± 1.8	29.4 ± 5.2	7.6 ± 2.9	8.3 ± 2.5	0.59 ± 0.119
2007bf	· · ·	· · ·	· · ·	· · ·	· · ·	· · ·	· · ·	· · ·	· · ·	· · ·	· · ·	· · ·
2007hm	44.1 ± 10.3	180.7 ± 36.8	56.2 ± 9.9	8.3 ± 0.7	16.6 ± 4.3	29.1 ± 16.3	9.8 ± 2.6	14.3 ± 3.4	22.3 ± 4.2	0.0 ± 0.0	0.0 ± 0.0	0.24 ± 0.105
2007il	63.9 ± 9.4	190.2 ± 36.5	66.4 ± 7.2	2.8 ± 2.1	13.4 ± 3.5	28.2 ± 6.3	0.0 ± 0.0	0.0 ± 0.0	15.6 ± 6.1	0.0 ± 0.0	0.0 ± 0.0	0.34 ± 0.114
2007it	· · ·	· · ·	· · ·	· · ·	· · ·	· · ·	· · ·	· · ·	· · ·	· · ·	· · ·	· · ·
2007ld	· · ·	· · ·	· · ·	· · ·	· · ·	· · ·	· · ·	· · ·	· · ·	· · ·	· · ·	· · ·
2007oc	35.5 ± 2.8	267.1 ± 22.4	70.1 ± 6.9	4.5 ± 1.5	8.0 ± 1.9	46.5 ± 8.6	4.3 ± 2.6	14.4 ± 3.9	43.6 ± 4.8	3.5 ± 1.5	2.9 ± 1.0	0.13 ± 0.022
2007od	32.9 ± 3.1	184.0 ± 22.5	65.2 ± 5.1	0.0 ± 0.0	14.7 ± 2.7	36.0 ± 6.8	0.0 ± 0.0	15.2 ± 2.7	16.4 ± 1.9	3.5 ± 0.6	5.3 ± 1.4	0.18 ± 0.039
2007P	· · ·	· · ·	· · ·	· · ·	· · ·	· · ·	· · ·	· · ·	· · ·	· · ·	· · ·	· · ·
2007sq	37.5 ± 10.2	125.9 ± 36.4	48.3 ± 14	4.52	6.8 ± 2.9	31.8 ± 7.5	5.1 ± 2.3	7.7 ± 3.3	22.4 ± 8.9	0.0 ± 0.0	0.0 ± 0.0	0.30 ± 0.167
2007U	31.1 ± 4.2	142.8 ± 32.4	54.3 ± 9.2	0.0 ± 0.0	12.0 ± 2.1	40.9 ± 4.3	10.0 ± 2.5	15.6 ± 2.5	17.1 ± 5.7	0.0 ± 0.0	0.0 ± 0.0	0.22 ± 0.079
2007W	67.2 ± 5.6	131.2 ± 21.7	38.1 ± 11.9	11.52	21.7 ± 2.6	36.5 ± 4.8	10.2 ± 3.6	16.0 ± 4.8	13.5 ± 3.2	4.6 ± 2.3	4.1 ± 2.3	0.51 ± 0.127
2007X	45.2 ± 6.8	223.8 ± 32.8	77.1 ± 10.7	0.0 ± 0.0	13.9 ± 2.9	49.4 ± 6.1	10.3 ± 3.2	16.4 ± 3.6	22.9 ± 9.2	5.6 ± 1.9	9.1 ± 2.4	0.20 ± 0.06
2007Z	· · ·	· · ·	· · ·	· · ·	· · ·	· · ·	· · ·	· · ·	· · ·	· · ·	· · ·	· · ·
2008ag	60.6 ± 8.2	185.2 ± 15.8	39.3 ± 12.2	10.7 ± 4.1	22.3 ± 1.7	38.9 ± 5.6	10.1 ± 1.9	14.6 ± 2.3	38.4 ± 5.1	3.3 ± 2.8	5.5 ± 2.2	0.33 ± 0.072
2008aw	17.8 ± 7.3	175.8 ± 18.8	47.1 ± 6.6	3.1 ± 1.3	12.4 ± 1.4	37.8 ± 4.4	6.4 ± 1.2	8.2 ± 1.6	38.8 ± 9.9	3.6 ± 1.6	3.6 ± 1.3	0.10 ± 0.051
2008bh	55.8 ± 11.2	216.8 ± 41.7	54.4 ± 5.6	4.7 ± 1.3	16.2 ± 2.0	36.2 ± 11.1	8.3 ± 2.2	9.8 ± 2.0	16.7 ± 7.9	5.2 ± 0.9	5.2 ± 0.8	0.26 ± 0.101
2008bk	57.5 ± 7.8	94.3 ± 12.0	31.9 ± 10.9	16.3 ± 1.2	24.6 ± 2.1	43.7 ± 3.5	14.8 ± 1.7	21.8 ± 3.1	20.1 ± 3.7	11.8 ± 1.2	10.5 ± 1.1	0.61 ± 0.16
2008bm	4.6 ± 0.2	16.1 ± 0.8	19.2 ± 1.3	9.1 ± 0.5	11.6 ± 0.6	19.8 ± 2.1	0.0 ± 0.0	0.0 ± 0.0	3.4 ± 0.2	0.0 ± 0.0	0.0 ± 0.0	0.29 ± 0.027

2008bp	...	...	...	...	...	...	...	...	...	...	...	...
2008br	15.8 ± 5.0	23.3 ± 17.9	22.3 ± 8.2	7.1 ± 1.8	7.2 ± 4.1	9.7 ± 7.8	8.8 ± 1.9	12.9 ± 1.1	12.4 ± 3.7	9.4 ± 2.1	6.7 ± 2.5	0.69 ± 0.752
2008bu	...	...	...	...	...	...	...	...	...	...	...	...
2008F	...	...	...	...	...	...	...	...	...	...	...	...
2008ga	85 ± 5.7	234.1 ± 13.2	60.0 ± 3.3	6.8 ± 1.5	17.0 ± 2.3	35.1 ± 2.1	7.1 ± 1.8	15.0 ± 1.7	55.0 ± 2.1	0.0 ± 0.0	0.0 ± 0.0	0.36 ± 0.045
2008gi	...	...	...	...	...	...	...	...	...	...	...	...
2008gr	35.5 ± 10.5	186.4 ± 41.5	56.6 ± 8.6	0.0 ± 0.0	7.3 ± 0.9	34.1 ± 2.6	4.7 ± 1.8	7.8 ± 3.0	30.9 ± 2.5	0.0 ± 0.0	0.0 ± 0.0	0.19 ± 0.099
2008H	63.3 ± 11.1	150.2 ± 21.0	33.0 ± 3.1	10.0 ± 2.1	22.2 ± 2.4	51.0 ± 5.2	14 ± 1.9	20.0 ± 2.1	54.1 ± 3.4	15.0 ± 2.2	14.0 ± 1.8	0.42 ± 0.132
2008hg	...	...	...	...	...	...	...	...	...	...	...	...
2008ho	...	...	...	...	...	...	...	...	...	...	...	...
2008if	26.1 ± 8.3	239.2 ± 58.9	61.8 ± 9.7	2.4 ± 1.1	9.3 ± 1.8	30.2 ± 5.3	4.7 ± 1.2	6.9 ± 1.3	48.3 ± 10.6	1.2 ± 0.5	3.7 ± 0.9	0.11 ± 0.06
2008il	...	...	...	...	...	...	...	...	...	...	...	...
2008in	54.8 ± 17.3	157.6 ± 49.6	36.6 ± 20.1	14.5 ± 3.4	26.9 ± 3.3	42.9 ± 5.7	14.7 ± 2.6	18.3 ± 4.2	38.8 ± 11.9	6.4 ± 3.4	8.3 ± 2.3	0.35 ± 0.22
2008K	40.5 ± 11.5	250.8 ± 44.5	80.4 ± 15.2	0.0 ± 0.0	17.4 ± 5.6	62.8 ± 19.1	0.0 ± 0.0	19.1 ± 6.8	41.5 ± 9.1	0.0 ± 0.0	0.0 ± 0.0	0.16 ± 0.07
2008M	54.0 ± 6.5	208.7 ± 27.7	72.9 ± 15.8	5.3 ± 2.1	20.2 ± 5.4	34.0 ± 8.1	4.9 ± 2.1	7.5 ± 2.4	30.3 ± 13.8	2.5 ± 0.9	1.6 ± 1.1	0.26 ± 0.06
2008W	46.7 ± 10.2	200.2 ± 21.9	60.4 ± 9.4	5.1 ± 1.9	16.4 ± 3.9	36.9 ± 5.8	7.7 ± 1.9	12.7 ± 4.1	45.9 ± 7.7	3.5 ± 1.4	4.6 ± 1.7	0.23 ± 0.08
2009aj	8.1 ± 1.6	46.7 ± 6.1	13 ± 2.2	6.2 ± 1.6	8.5 ± 1.9	13.9 ± 3.1	0.0 ± 0.0	0.0 ± 0.0	1.7 ± 0.6	0.0 ± 0.0	0.0 ± 0.0	0.17 ± 0.06
2009ao	40.2 ± 3.1	148.6 ± 11	54.5 ± 10.4	5.8 ± 6.2	18.5 ± 1.4	41.8 ± 5.7	9.3 ± 3.2	19.4 ± 2.6	24.2 ± 4.6	0.0 ± 0.0	9.1 ± 2.8	0.27 ± 0.04
2009au	5.9 ± 1.4	34.3 ± 11.1	12.8 ± 5.7	8.8 ± 2.8	11.9 ± 4.7	17.2 ± 7.5	6.1 ± 2.8	7.3 ± 3.3	7.9 ± 3.5	3.3 ± 0.6	5.6 ± 1.3	0.17 ± 0.09
2009bu	84.6 ± 7.3	146.5 ± 23.3	55.9 ± 5.1	3.6 ± 1.1	14.2 ± 2.6	26.4 ± 9.8	5.7 ± 2.2	6.1 ± 2.5	15.1 ± 1.5	0.0 ± 0.0	0.0 ± 0.0	0.58 ± 0.14
2009bz	...	...	...	...	...	...	...	...	...	...	...	...
2009N	75.7 ± 13.1	118.5 ± 20.7	39.1 ± 7.9	15.2 ± 1.9	25.4 ± 2.3	34.4 ± 6.8	13.7 ± 1.1	20.8 ± 4.1	24.5 ± 3.2	10.3 ± 2.1	9.6 ± 1.1	0.64 ± 0.22
2009W	...	...	...	...	...	...	...	...	...	...	...	...

Columns: (1) SN name; (2) pEW of H_α absorption component; (3) pEW of H_α emission component; (4) pEW of H_β; (5) pEW of Fe II 4924; (6) pEW of Fe II 5018; (7) pEW of Fe II 5169; (8) pEW of Fe II/Sc II; (9) pEW of Sc II Multiplet; (10) pEW of Na I D; (11) pEW of Ba II; (12) pEW of ScII; (13) Ratio of absoprtion to emission (a/e) of H_α P-Cygni profile.

Chapter 5

Summary

In this thesis, I have presented a spectroscopic and photometric analysis of type II Supernovae (SNe II) obtained by the Carnegie Supernova Project (CSP) plus previous campaigns between 1986 and 2009. A total of 123 SNe II with $\sim$ 900 spectra were analysed and correlated with photometric parameters. The expansion velocity of the ejecta in the photospheric phase, the pseudo-equivalent width, the ratio of absorption to emission of H_α and the velocity decline rate of H_β were measured at different epochs. To that aim, I estimated the explosion epochs. Pre-explosion images and the spectral matching technique were used with very good agreements.

In the first part of this work, I used 52 SNe II with available spectra around t_{tran} to study the diversity of the H_α P-Cygni profile. I found that supernovae with greater ejecta velocities have smaller H_α a/e (absorption over emission ratios), more rapidly declining light curves from maximum, during the plateau and radioactive tail phase, are brighter at all phases, have shorter optically thick phase durations. I discussed possible explanations of these results in terms of physical properties of SNe II, speculating that the most likely parameters which influence in H_α diversity are the mass and density profile of the hydrogen envelope, together with additional emission components due to circumstellar interaction.

In the second part, I expanded the analysis to the full coverage of the spectra. Here, I used the entire sample. I worked on a statistical analysis of the appearance of lines in SNe II with time. I found that the He I line disappears around one week post explosion, when the iron-group lines appear. Fe II, Sc II and Ba II lines appear faster in SNe with lower velocities. I also found that SNe with higher velocities are brighter, have smaller pseudo-equivalent widths, faster declining light curves, shorter optically thick duration phases and plateau durations, and higher Ni mass. Discussion is presented on the physical meaning of all of our defined observational spectral and photometric parameters. Thus, I speculate that the plateau duration is related with the hydrogen envelope mass at the moment of the explosion, the initial light-curve decline rate is related with the radius of the progenitor, and the expansion ejecta velocities with the explosion energy. Also, a statistical processing reveals a continuum in spectral and photometric parameters. I speculate that this suggests a continuum in the underlying progenitor population.

I also studied the nature of the extra absorption component on the blue side of H_α P-Cygni profile. I concluded that this component in early spectra (before 35 days) is associated with Si II $\lambda6355$, while in the plateau phase is related with high velocity features (HVFs) of hydrogen lines. I speculate that the detection of Si II $\lambda6355$ is related to the radius of the progenitor star, and the HV features with an interaction between the SN ejecta and circumstellar material.

Bibliography

Allington-Smith, J., Breare, M., Ellis, R., Gellatly, D., Glazebrook, K., Jorden, P., Maclean, J., Oates, P., Shaw, G., Tanvir, N., Taylor, K., Taylor, P., Webster, J., Worswick, S., Sep. 1994. A low-dispersion survey spectrograph (LDSS-2) for the William Herschel Telescope. PASP106, 983–991.

Anderson, J. P., Dessart, L., Gutierrez, C. P., Hamuy, M., Morrell, N. I., Phillips, M., Folatelli, G., Stritzinger, M. D., Freedman, W. L., González-Gaitán, S., McCarthy, P., Suntzeff, N., Thomas-Osip, J., Jun. 2014a. Analysis of blueshifted emission peaks in Type II supernovae. MNRAS441, 671–680.

Anderson, J. P., Gutiérrez, C. P., Dessart, L., Hamuy, M., Galbany, L., Morrell, N. I., Stritzinger, M. D., Phillips, M. M., Folatelli, G., Boffin, H. M. J., de Jaeger, T., Kuncarayakti, H., Prieto, J. L., May 2016. Type II supernovae as probes of environment metallicity: observations of host H II regions. A&A589, A110.

Anderson, J. P., et al., May 2014b. Characterizing the V-band Light-curves of Hydrogen-rich Type II Supernovae. ApJ786, 67.

Andrews, J. E., Gallagher, J. S., Clayton, G. C., Sugerman, B. E. K., Chatelain, J. P., Clem, J., Welch, D. L., Barlow, M. J., Ercolano, B., Fabbri, J., Wesson, R., Meixner, M., May 2010. SN 2007od: A Type IIP Supernova with Circumstellar Interaction. ApJ715, 541–549.

Arcavi, I., Gal-Yam, A., Cenko, S. B., Fox, D. B., Leonard, D. C., Moon, D.-S., Sand, D. J., Soderberg, A. M., Kiewe, M., Yaron, O., Becker, A. B., Scheps, R., Birenbaum, G., Chamudot, D., Zhou, J., Sep. 2012. Caltech Core-Collapse Project (CCCP) Observations of Type II Supernovae: Evidence for Three Distinct Photometric Subtypes. ApJ756, L30.

Arnett, W. D., May 1979. On the theory of Type I supernovae. ApJ230, L37–L40.

Barbon, R., Buondí, V., Cappellaro, E., Turatto, M., Nov. 1999. The Asiago Supernova Catalogue - 10 years after. A&AS139, 531–536.

Barbon, R., Cappellaro, E., Turatto, M., Jun. 1984. Radioactive decays and supernova light curves. A&A135, 27–31.

Barbon, R., Ciatti, F., Rosino, L., Feb. 1979. Photometric properties of type II supernovae. A&A72, 287–292.

Baron, E., Branch, D., Hauschildt, P. H., Filippenko, A. V., Kirshner, R. P., Challis, P. M., Jha, S., Chevalier, R., Fransson, C., Lundqvist, P., Garnavich, P., Leibundgut, B., McCray, R., Michael, E., Panagia, N., Phillips, M. M., Pun, C. S. J., Schmidt, B., Sonneborn, G., Suntzeff, N. B., Wang, L., Wheeler, J. C., Dec. 2000. Preliminary Spectral Analysis of the Type II Supernova 1999EM. ApJ545, 444–448.

Bersten, M. C., Mar. 2013. Comparing Hydrodynamic Models with Observations of Type II Plateau Supernovae. ArXiv e-prints.

Blinnikov, S. I., Bartunov, O. S., Jun. 1993. Non-Equilibrium Radiative Transfer in Supernova Theory - Models of Linear Type-II Supernovae. A&A273, 106.

Blondin, S., Tonry, J. L., Sep. 2007. Determining the Type, Redshift, and Age of a Supernova Spectrum. ApJ666, 1024–1047.

Branch, D., Falk, S. W., Uomoto, A. K., Wills, B. J., McCall, M. L., Rybski, P., Mar. 1981. The type II supernova 1979c in M100 and the distance to the Virgo cluster. ApJ244, 780–804.

Buta, R. J., Jun. 1982. Photometric observations of the bright Type II supernova 1980K in NGC 6946. PASP94, 578–585.

Buzzoni, B., Delabre, B., Dekker, H., Dodorico, S., Enard, D., Focardi, P., Gustafsson, B., Nees, W., Paureau, J., Reiss, R., Dec. 1984. The ESO Faint Object Spectrograph and Camera (EFOSC). The Messenger 38, 9–13.

Cappellaro, E., Danziger, I. J., della Valle, M., Gouiffes, C., Turatto, M., Jan. 1995a. The bright linear type II SN 1990K. A&A293, 723–732.

Cappellaro, E., Danziger, I. J., Turatto, M., Nov. 1995b. SN 1986E eight years after outburst: a link to SN 1957D? MNRAS277, 106–112.

Catchpole, R. M., Menzies, J. W., Monk, A. S., Wargau, W. F., Pollaco, D., Carter, B. S., Whitelock, P. A., Marang, F., Laney, C. D., Balona, L. A., Feast, M. W., Lloyd Evans, T. H. H., Sekiguchi, K., Laing, J. D., Kilkenny, D. M., Spencer Jones, J., Roberts, G., Cousins, A. W. J., van Vuuren, G., Winkler, H., Nov. 1987. Spectroscopic and photometric observations of SN 1987a. II - Days 51 to 134. MNRAS229, 15P–25P.

Catchpole, R. M., Whitelock, P. A., Feast, M. W., Menzies, J. M., Glass, I. S., Marang, F., Laing, J. D., Spencer Jones, J. H., Roberts, G., Balona, L. A., Carter, B. S., Laney, C. D., Evans, L. T., Sekiguchi, K., Hutchinson, G. G., Maddison, R., Albinson, J., Evans, A., Allen, F. A., Winkler, H., Fairall, A., Corbally, C., Davies, J. K., Parker, Q. A., Apr. 1988. Spectroscopic and photometric observations of SN 1987A. III - Days 135 to 260. MNRAS231, 75p–89p.

Chevalier, R. A., Aug. 1976. The hydrodynamics of Type II supernovae. ApJ207, 872–887.

Chugai, N. N., Chevalier, R. A., Utrobin, V. P., Jun. 2007. Optical Signatures of Circumstellar Interaction in Type IIP Supernovae. ApJ662, 1136–1147.

Clocchiatti, A., Benetti, S., Wheeler, J. C., Wren, W., Boisseau, J., Cappellaro, E., Turatto, M., Patat, F., Swartz, D. A., Harkness, R. P., Brotherton, M. S., Wills, B., Hemenway, P., Cornell, M., Frueh, M., Kaiser, M. B., Mar. 1996. A Study of SN 1992H in NGC 5377. AJ111, 1286.

Contreras, C., Hamuy, M., Phillips, M. M., Folatelli, G., Suntzeff, N. B., Persson, S. E., Stritzinger, M., Boldt, L., González, S., Krzeminski, W., Morrell, N., Roth, M., Salgado, F., José Maureira, M., Burns, C. R., Freedman, W. L., Madore, B. F., Murphy, D., Wyatt, P., Li, W., Filippenko, A. V., Feb. 2010. The Carnegie Supernova Project: First Photometry Data Release of Low-Redshift Type Ia Supernovae. AJ139, 519–539.

Dekker, H., Delabre, B., Dodorico, S., Jan. 1986. ESO's Multimode Instrument for the Nasmyth focus of the 3.5 M New Technology Telescope. In: Crawford, D. L. (Ed.), Instrumentation in astronomy VI. Vol. 627 of Proc. SPIE. pp. 339–348.

Dessart, L., Blondin, S., Brown, P. J., Hicken, M., Hillier, D. J., Holland, S. T., Immler, S., Kirshner, R. P., Milne, P., Modjaz, M., Roming, P. W. A., Mar. 2008. Using Quantitative Spectroscopic Analysis to Determine the Properties and Distances of Type II Plateau Supernovae: SN 2005cs and SN 2006bp. ApJ675, 644–669.

Dessart, L., Gutierrez, C. P., Hamuy, M., Hillier, D. J., Lanz, T., Anderson, J. P., Folatelli, G., Freedman, W. L., Ley, F., Morrell, N., Persson, S. E., Phillips, M. M., Stritzinger, M., Suntzeff, N. B., May 2014. Type II Plateau supernovae as metallicity probes of the Universe. MNRAS440, 1856–1864.

Dessart, L., Hillier, D. J., Jul. 2005. Quantitative spectroscopy of photospheric-phase type II supernovae. A&A437, 667–685.

Dessart, L., Hillier, D. J., Feb. 2006. Quantitative spectroscopic analysis of and distance to SN1999em. A&A447, 691–707.

Dessart, L., Hillier, D. J., Jan. 2008. Time-dependent effects in photospheric-phase Type II supernova spectra. MNRAS383, 57–74.

Dessart, L., Hillier, D. J., Jan. 2011. Non-LTE time-dependent spectroscopic modelling of Type II-plateau supernovae from the photospheric to the nebular phase: case study for 15 and 25 $M_{\odot}$ progenitor stars. MNRAS410, 1739–1760.

Dessart, L., Hillier, D. J., Waldman, R., Livne, E., Aug. 2013a. Type II-Plateau supernova radiation: dependences on progenitor and explosion properties. MNRAS433, 1745–1763.

Dessart, L., Livne, E., Waldman, R., Jul. 2010. Shock-heating of stellar envelopes: a possible common mechanism at the origin of explosions and eruptions in massive stars. MNRAS405, 2113–2131.

Dessart, L., Waldman, R., Livne, E., Hillier, D. J., Blondin, S., Feb. 2013b. Radiative properties of pair-instability supernova explosions. MNRAS428, 3227–3251.

Dressler, A., Bigelow, B., Hare, T., Sutin, B., Thompson, I., Burley, G., Epps, H., Oemler, A., Bagish, A., Birk, C., Clardy, K., Gunnels, S., Kelson, D., Shectman, S., Osip, D., Mar. 2011. IMACS: The Inamori-Magellan Areal Camera and Spectrograph on Magellan-Baade. PASP123, 288–332.

Dwek, E., Nov. 1983. The infrared echo of a type II supernova with a circumstellar dust shell - Applications to SN 1979c and SN 1980k. ApJ274, 175–183.

Elias-Rosa, N., Van Dyk, S. D., Li, W., Miller, A. A., Silverman, J. M., Ganeshalingam, M., Boden, A. F., Kasliwal, M. M., Vinkó, J., Cuillandre, J.-C., Filippenko, A. V., Steele, T. N., Bloom, J. S., Griffith, C. V., Kleiser, I. K. W., Foley, R. J., May 2010. The Massive Progenitor of the Type II-linear Supernova 2009kr. ApJ714, L254–L259.

Elias-Rosa, N., Van Dyk, S. D., Li, W., Silverman, J. M., Foley, R. J., Ganeshalingam, M., Mauerhan, J. C., Kankare, E., Jha, S., Filippenko, A. V., Beckman, J. E., Berger, E., Cuillandre, J.-C., Smith, N., Nov. 2011. The Massive Progenitor of the Possible Type II-Linear Supernova 2009hd in Messier 66. ApJ742, 6.

Fabbri, J., Otsuka, M., Barlow, M. J., Gallagher, J. S., Wesson, R., Sugerman, B. E. K., Clayton, G. C., Meixner, M., Andrews, J. E., Welch, D. L., Ercolano, B., Dec. 2011. The effects of dust on the optical and infrared evolution of SN 2004et. MNRAS418, 1285–1307.

Faran, T., Poznanski, D., Filippenko, A. V., Chornock, R., Foley, R. J., Ganeshalingam, M., Leonard, D. C., Li, W., Modjaz, M., Nakar, E., Serduke, F. J. D., Silverman, J. M., Jul. 2014a. Photometric and spectroscopic properties of Type II-P supernovae. MNRAS442, 844–861.

Faran, T., Poznanski, D., Filippenko, A. V., Chornock, R., Foley, R. J., Ganeshalingam, M., Leonard, D. C., Li, W., Modjaz, M., Serduke, F. J. D., Silverman, J. M., Nov. 2014b. A sample of Type II-L supernovae. MNRAS445, 554–569.

Fesen, R. A., Gerardy, C. L., Filippenko, A. V., Matheson, T., Chevalier, R. A., Kirshner, R. P., Schmidt, B. P., Challis, P., Fransson, C., Leibundgut, B., van Dyk, S. D., Feb. 1999. Late-Time Optical and Ultraviolet Spectra of SN 1979C and SN 1980K. AJ117, 725–735.

Filippenko, A. V., 1997. Optical Spectra of Supernovae. ARA&A35, 309–355.

Filippenko, A. V., Matheson, T., Ho, L. C., Oct. 1993. The "Type IIb" Supernova 1993J in M81: A Close Relative of Type Ib Supernovae. ApJ415, L103.

Folatelli, G., Morrell, N., Phillips, M. M., Hsiao, E., Campillay, A., Contreras, C., Castellón, S., Hamuy, M., Krzeminski, W., Roth, M., Stritzinger, M., Burns, C. R., Freedman, W. L., Madore, B. F., Murphy, D., Persson, S. E., Prieto, J. L., Suntzeff, N. B., Krisciunas, K., Anderson, J. P., Förster, F., Maza, J., Pignata, G., Rojas, P. A., Boldt, L., Salgado, F., Wyatt, P., Olivares E., F., Gal-Yam, A., Sako, M., Aug. 2013. Spectroscopy of Type Ia Supernovae by the Carnegie Supernova Project. ApJ773, 53.

Folatelli, G., Phillips, M. M., Burns, C. R., Contreras, C., Hamuy, M., Freedman, W. L., Persson, S. E., Stritzinger, M., Suntzeff, N. B., Krisciunas, K., Boldt, L., González, S., Krzeminski, W., Morrell, N., Roth, M., Salgado, F., Madore, B. F., Murphy, D., Wyatt, P., Li, W., Filippenko, A. V., Miller, N., Jan. 2010. The Carnegie Supernova Project: Analysis of the First Sample of Low-Redshift Type-Ia Supernovae. AJ139, 120–144.

Galbany, L., Hamuy, M., Phillips, M. M., Suntzeff, N. B., Maza, J., de Jaeger, T., Moraga, T., González-Gaitán, S., Krisciunas, K., Morrell, N. I., Thomas-Osip, J., Krzeminski, W., González, L., Antezana, R., Wishnjewski, M., McCarthy, P., Anderson, J. P., Gutiérrez, C. P., Stritzinger, M., Folatelli, G., Anguita, C., Galaz, G., Green, E. M., Impey, C., Kim, Y.-C., Kirhakos, S., Malkan, M. A., Mulchaey, J. S., Phillips, A. C., Pizzella, A., Prosser, C. F., Schmidt, B. P., Schommer, R. A., Sherry, W., Strolger, L.-G., Wells, L. A., Williger, G. M., Feb. 2016. UBVRIz Light Curves of 51 Type II Supernovae. AJ151, 33.

Gutiérrez, C. P., et al., May 2014. H_α Spectral Diversity of Type II Supernovae: Correlations with Photometric Properties. ApJ786, L15.

Gutiérrez, C. P., et al., 2016. "spectral diversity of type ii supernovae paper i: Obervations, sample characterization and spectral lines evolution". in preparation.

Hamuy, M., Jan. 2003. Observed and Physical Properties of Core-Collapse Supernovae. ApJ582, 905–914.

Hamuy, M., Folatelli, G., Morrell, N. I., Phillips, M. M., Suntzeff, N. B., Persson, S. E., Roth, M., Gonzalez, S., Krzeminski, W., Contreras, C., Freedman, W. L., Murphy, D. C., Madore, B. F., Wyatt, P., Maza, J., Filippenko, A. V., Li, W., Pinto, P. A., Jan. 2006. The Carnegie Supernova Project: The Low-Redshift Survey. PASP118, 2–20.

Hamuy, M., Maza, J., Phillips, M. M., Suntzeff, N. B., Wischnjewsky, M., Smith, R. C., Antezana, R., Wells, L. A., Gonzalez, L. E., Gigoux, P., Navarrete, M., Barrientos, F., Lamontagne, R., della Valle, M., Elias, J. E., Phillips, A. C., Odewahn, S. C., Baldwin, J. A., Walker, A. R., Williams, T., Sturch, C. R., Baganoff, F. K., Chaboyer, B. C., Schommer, R. A., Tirado, H., Hernandez, M., Ugarte, P., Guhathakurta, P., Howell, S. B., Szkody, P., Schmidtke, P. C., Roth, J., Dec. 1993. The 1990 Calan/Tololo Supernova Search. AJ106, 2392–2407.

Hamuy, M., Maza, J., Pinto, P. A., Phillips, M. M., Suntzeff, N. B., Blum, R. D., Olsen, K. A. G., Pinfield, D. J., Ivanov, V. D., Augusteijn, T., Brillant, S., Chadid, M., Cuby, J.-G., Doublier, V., Hainaut, O. R., Le Floc'h, E., Lidman, C., Petr-Gotzens, M. G., Pompei, E., Vanzi, L., Jul. 2002. Optical and Infrared Spectroscopy of SN 1999ee and SN 1999ex. AJ124, 417–429.

Hamuy, M., Phillips, M. M., Suntzeff, N. B., Schommer, R. A., Maza, J., Smith, R. C., Lira, P., Aviles, R., Dec. 1996. The Morphology of Type IA Supernovae Light Curves. AJ112, 2438.

Hamuy, M., Pinto, P. A., Feb. 2002. Type II Supernovae as Standardized Candles. ApJ566, L63–L65.

Hamuy, M., Pinto, P. A., Maza, J., Suntzeff, N. B., Phillips, M. M., Eastman, R. G., Smith, R. C., Corbally, C. J., Burstein, D., Li, Y., Ivanov, V., Moro-Martin, A., Strolger, L. G., de Souza, R. E., dos Anjos, S., Green, E. M., Pickering, T. E., González, L., Antezana, R., Wischnjewsky, M., Galaz, G., Roth, M., Persson, S. E., Schommer, R. A., Sep. 2001. The Distance to SN 1999em from the Expanding Photosphere Method. ApJ558, 615–642.

Hamuy, M. A., 2001. Type II supernovae as distance indicators. Ph.D. thesis, The University of Arizona.

Harutyunyan, A. H., et al., Sep. 2008. ESC supernova spectroscopy of non-ESC targets. A&A488, 383–399.

Howell, D. A., et al., Dec. 2005. Gemini Spectroscopy of Supernovae from the Supernova Legacy Survey: Improving High-Redshift Supernova Selection and Classification. ApJ634, 1190–1201.

Hoyle, F., Fowler, W. A., Nov. 1960. Nucleosynthesis in Supernovae. ApJ132, 565.

Iben, Jr., I., Tutukov, A. V., Feb. 1984. Supernovae of type I as end products of the evolution of binaries with components of moderate initial mass (M not greater than about 9 solar masses). ApJS54, 335–372.

Immler, S., Fesen, R. A., Van Dyk, S. D., Weiler, K. W., Petre, R., Lewin, W. H. G., Pooley, D., Pietsch, W., Aschenbach, B., Hammell, M. C., Rudie, G. C., Oct. 2005. Late-Time X-Ray, UV, and Optical Monitoring of Supernova 1979C. ApJ632, 283–293.

Inserra, C., Pastorello, A., Turatto, M., Pumo, M. L., Benetti, S., Cappellaro, E., Botticella, M. T., Bufano, F., Elias-Rosa, N., Harutyunyan, A., Taubenberger, S., Valenti, S., Zampieri, L., Jul. 2013. Moderately luminous Type II supernovae. A&A555, A142.

Inserra, C., Turatto, M., Pastorello, A., Benetti, S., Cappellaro, E., Pumo, M. L., Zampieri, L., Agnoletto, I., Bufano, F., Botticella, M. T., Della Valle, M., Elias Rosa, N., Iijima, T., Spiro, S., Valenti, S., Oct. 2011. The Type IIP SN 2007od in UGC 12846: from a bright maximum to dust formation in the nebular phase. MNRAS417, 261–279.

Inserra, C., Turatto, M., Pastorello, A., Pumo, M. L., Baron, E., Benetti, S., Cappellaro, E., Taubenberger, S., Bufano, F., Elias-Rosa, N., Zampieri, L., Harutyunyan, A., Moskvitin, A. S., Nissinen, M., Stanishev, V., Tsvetkov, D. Y., Hentunen, V. P., Komarova, V. N., Pavlyuk, N. N., Sokolov, V. V., Sokolova, T. N., May 2012. The bright Type IIP SN 2009bw, showing signs of interaction. MNRAS422, 1122–1139.

Jerkstrand, A., Smartt, S. J., Fraser, M., Fransson, C., Sollerman, J., Taddia, F., Kotak, R., Apr. 2014. The nebular spectra of SN 2012aw and constraints on stellar nucleosynthesis from oxygen emission lines. MNRAS439, 3694–3703.

Jones, M. I., Hamuy, M., Lira, P., Maza, J., Clocchiatti, A., Phillips, M., Morrell, N., Roth, M., Suntzeff, N. B., Matheson, T., Filippenko, A. V., Foley, R. J., Leonard, D. C., May 2009. Distance Determination to 12 Type II Supernovae Using the Expanding Photosphere Method. ApJ696, 1176–1194.

Kasen, D., Woosley, S. E., Oct. 2009. Type II Supernovae: Model Light Curves and Standard Candle Relationships. ApJ703, 2205–2216.

Kotak, R., Meikle, W. P. S., Farrah, D., Gerardy, C. L., Foley, R. J., Van Dyk, S. D., Fransson, C., Lundqvist, P., Sollerman, J., Fesen, R., Filippenko, A. V., Mattila, S., Silverman, J. M., Andersen, A. C., Höflich, P. A., Pozzo, M., Wheeler, J. C., Oct. 2009. Dust and The Type II-Plateau Supernova 2004et. ApJ704, 306–323.

Kromer, M., Sim, S. A., Fink, M., Röpke, F. K., Seitenzahl, I. R., Hillebrandt, W., Aug. 2010. Double-detonation Sub-Chandrasekhar Supernovae: Synthetic Observables for Minimum Helium Shell Mass Models. ApJ719, 1067–1082.

Leonard, D. C., Filippenko, A. V., Ardila, D. R., Brotherton, M. S., Jun. 2001. Is It Round? Spectropolarimetry of the Type II-p Supernova 1999EM. ApJ553, 861–885.

Leonard, D. C., Filippenko, A. V., Gates, E. L., Li, W., Eastman, R. G., Barth, A. J., Bus, S. J., Chornock, R., Coil, A. L., Frink, S., Grady, C. A., Harris, A. W., Malkan, M. A., Matheson, T., Quirrenbach, A., Treffers, R. R., Jan. 2002a. The Distance to SN 1999em in NGC 1637 from the Expanding Photosphere Method. PASP114, 35–64.

Leonard, D. C., Filippenko, A. V., Li, W., Matheson, T., Kirshner, R. P., Chornock, R., Van Dyk, S. D., Berlind, P., Calkins, M. L., Challis, P. M., Garnavich, P. M., Jha, S., Mahdavi, A., Nov. 2002b. A Study of the Type II-Plateau Supernova 1999gi and the Distance to its Host Galaxy, NGC 3184. AJ124, 2490–2505.

Li, W., Van Dyk, S. D., Filippenko, A. V., Cuillandre, J.-C., Feb. 2005. On the Progenitor of the Type II Supernova 2004et in NGC 6946. PASP117, 121–131.

Li, W., et al., Dec. 2011. Exclusion of a luminous red giant as a companion star to the progenitor of supernova SN 2011fe. Nature480, 348–350.

Litvinova, I. I., Nadezhin, D. K., Jan. 1983. Hydrodynamical models of type II supernovae. Ap&SS89, 89–113.

Litvinova, I. Y., Nadezhin, D. K., May 1985. Determination of Integrated Parameters for Type-II Supernovae. Soviet Astronomy Letters 11, 145–147.

Maguire, K., Di Carlo, E., Smartt, S. J., Pastorello, A., Tsvetkov, D. Y., Benetti, S., Spiro, S., Arkharov, A. A., Beccari, G., Botticella, M. T., Cappellaro, E., Cristallo, S., Dolci, M., Elias-Rosa, N., Fiaschi, M., Gorshanov, D., Harutyunyan, A., Larionov, V. M., Navasardyan, H., Pietrinferni, A., Raimondo, G., di Rico, G., Valenti, S., Valentini, G., Zampieri, L., May 2010. Optical and near-infrared coverage of SN 2004et: physical parameters and comparison with other Type IIP supernovae. MNRAS404, 981–1004.

Marino, R. A., Rosales-Ortega, F. F., Sánchez, S. F., Gil de Paz, A., Vílchez, J., Miralles-Caballero, D., Kehrig, C., Pérez-Montero, E., Stanishev, V., Iglesias-Páramo, J., Díaz, A. I., Castillo-Morales, A., Kennicutt, R., López-Sánchez, A. R., Galbany, L., García-Benito, R., Mast, D., Mendez-Abreu, J., Monreal-Ibero, A., Husemann, B., Walcher, C. J., García-Lorenzo, B., Masegosa, J., Del Olmo Orozco, A., Mourão, A. M., Ziegler, B., Mollá, M., Papaderos, P., Sánchez-Blázquez, P., González Delgado, R. M., Falcón-Barroso, J., Roth, M. M., van de Ven, G., Califa Team, Nov. 2013. The O3N2 and N2 abundance indicators revisited: improved calibrations based on CALIFA and T_e-based literature data. A&A559, A114.

Maund, J. R., Fraser, M., Reilly, E., Ergon, M., Mattila, S., Mar. 2015. Whatever happened to the progenitors of supernovae 2008cn, 2009kr and 2009md? MNRAS447, 3207–3217.

Maund, J. R., Smartt, S. J., Jun. 2005. Hubble Space Telescope imaging of the progenitor sites of six nearby core-collapse supernovae. MNRAS360, 288–304.

Menzies, J. W., Catchpole, R. M., van Vuuren, G., Winkler, H., Laney, C. D., Whitelock, P. A., Cousins, A. W. J., Carter, B. S., Marang, F., Lloyd Evans, T. H. H., Roberts, G., Kilkenny, D., Spencer Jones, J., Sekiguchi, K., Fairall, A. P., Wolstencroft, R. D., Aug. 1987. Spectroscopic and photometric observations of SN 1987a - The first 50 days. MNRAS227, 39P–49P.

Milisavljevic, D., Fesen, R. A., Kirshner, R. P., Challis, P., Feb. 2009. The Evolution of Late-Time Optical Emission from SN 1979C. ApJ692, 839–843.

Minkowski, R., Aug. 1941. Spectra of Supernovae. PASP53, 224.

Misra, K., et al., Oct. 2007. Type IIP supernova SN 2004et: a multiwavelength study in X-ray, optical and radio. MNRAS381, 280–292.

Moriya, T. J., Pruzhinskaya, M. V., Ergon, M., Blinnikov, S. I., Jan. 2016. On the nature of rapidly fading Type II supernovae. MNRAS455, 423–430.

Nakar, E., Poznanski, D., Katz, B., Jun. 2016. The Importance of ^{56}Ni in Shaping the Light Curves of Type II Supernovae. ApJ823, 127.

Nomoto, K., Feb. 1982. Accreting white dwarf models for type I supernovae. I - Presupernova evolution and triggering mechanisms. ApJ253, 798–810.

Nomoto, K., Iwamoto, K., Suzuki, T., Pols, O. R., Yamaoka, H., Hashimoto, M., Hoflich, P., van den Heuvel, E. P. J., 1996. The Origin of Type Ib-Ic-IIb-IIL Supernovae and Binary Star Evolution. In: van Paradijs, J., van den Heuvel, E. P. J., Kuulkers, E. (Eds.), Compact Stars in Binaries. Vol. 165 of IAU Symposium. p. 119.

Olivares, F., Oct. 2008. The Standard Candle Method for Type II-Plateau Supernovae. ArXiv e-prints.

Pakmor, R., Kromer, M., Taubenberger, S., Sim, S. A., Röpke, F. K., Hillebrandt, W., Mar. 2012. Normal Type Ia Supernovae from Violent Mergers of White Dwarf Binaries. ApJ747, L10.

Pastorello, A., Baron, E., Branch, D., Zampieri, L., Turatto, M., Ramina, M., Benetti, S., Cappellaro, E., Salvo, M., Patat, F., Piemonte, A., Sollerman, J., Leibundgut, B., Altavilla, G., Jul. 2005. SN 1998A: explosion of a blue supergiant. MNRAS360, 950–962.

Pastorello, A., Ramina, M., Zampieri, L., Navasardyan, H., Salvo, M., Fiaschi, M., Oct. 2003. Observational Properties of Type II Plateau Supernovae. ArXiv Astrophysics e-prints.

Pastorello, A., Sauer, D., Taubenberger, S., Mazzali, P. A., Nomoto, K., Kawabata, K. S., Benetti, S., Elias-Rosa, N., Harutyunyan, A., Navasardyan, H., Zampieri, L., Iijima, T., Botticella, M. T., di Rico, G., Del Principe, M., Dolci, M., Gagliardi, S., Ragni, M., Valentini, G., Aug. 2006. SN 2005cs in M51 - I. The first month of evolution of a subluminous SN II plateau. MNRAS370, 1752–1762.

Pastorello, A., Valenti, S., Zampieri, L., Navasardyan, H., Taubenberger, S., Smartt, S. J., Arkharov, A. A., Bärnbantner, O., Barwig, H., Benetti, S., Birtwhistle, P., Botticella, M. T., Cappellaro, E., Del Principe, M., di Mille, F., di Rico, G., Dolci, M., Elias-Rosa, N., Efimova, N. V., Fiedler, M., Harutyunyan, A., Höflich, P. A., Kloehr, W., Larionov, V. M., Lorenzi, V., Maund, J. R., Napoleone, N., Ragni, M., Richmond, M., Ries, C., Spiro, S., Temporin, S., Turatto, M., Wheeler, J. C., Apr. 2009. SN 2005cs in M51 - II. Complete evolution in the optical and the near-infrared. MNRAS394, 2266–2282.

Pastorello, A., Zampieri, L., Turatto, M., Cappellaro, E., Meikle, W. P. S., Benetti, S., Branch, D., Baron, E., Patat, F., Armstrong, M., Altavilla, G., Salvo, M., Riello, M., Jan. 2004. Low-luminosity Type II supernovae: spectroscopic and photometric evolution. MNRAS347, 74–94.

Patat, F., Barbon, R., Cappellaro, E., Turatto, M., Feb. 1994. Light curves of type II supernovae. 2: The analysis. A&A282, 731–741.

Podsiadlowski, P., Joss, P. C., Hsu, J. J. L., May 1992. Presupernova evolution in massive interacting binaries. ApJ391, 246–264.

Pooley, D., Lewin, W. H. G., Fox, D. W., Miller, J. M., Lacey, C. K., Van Dyk, S. D., Weiler, K. W., Sramek, R. A., Filippenko, A. V., Leonard, D. C., Immler, S., Chevalier, R. A., Fabian, A. C., Fransson, C., Nomoto, K., Jun. 2002. X-Ray, Optical, and Radio Observations of the Type II Supernovae 1999em and 1998S. ApJ572, 932–943.

Popov, D. V., Sep. 1993. An analytical model for the plateau stage of Type II supernovae. ApJ414, 712–716.

Raskin, C., Timmes, F. X., Scannapieco, E., Diehl, S., Fryer, C., Oct. 2009. On Type Ia supernovae from the collisions of two white dwarfs. MNRAS399, L156–L159.

Roy, R., Kumar, B., Benetti, S., Pastorello, A., Yuan, F., Brown, P. J., Immler, S., Fatkhullin, T. A., Moskvitin, A. S., Maund, J., Akerlof, C. W., Wheeler, J. C., Sokolov, V. V., Quimby, R. M., Bufano, F., Kumar, B., Misra, K., Pandey, S. B., Elias-Rosa, N., Roming, P. W. A., Sagar, R., Aug. 2011. SN 2008inBridging the Gap between Normal and Faint Supernovae of Type IIP. ApJ736, 76.

Sahu, D. K., Anupama, G. C., Srividya, S., Muneer, S., Nov. 2006. Photometric and spectroscopic evolution of the Type IIP supernova SN 2004et. MNRAS372, 1315–1324.

Sanders, N. E., Soderberg, A. M., Gezari, S., Betancourt, M., Chornock, R., Berger, E., Foley, R. J., Challis, P., Drout, M., Kirshner, R. P., Lunnan, R., Marion, G. H., Margutti, R., McKinnon, R., Milisavljevic, D., Narayan, G., Rest, A., Kankare, E., Mattila, S., Smartt, S. J., Huber, M. E., Burgett, W. S., Draper, P. W., Hodapp, K. W., Kaiser, N., Kudritzki, R. P., Magnier, E. A., Metcalfe, N., Morgan, J. S., Price, P. A., Tonry, J. L., Wainscoat, R. J., Waters, C., Apr. 2014. Towards Characterization of the Type IIP Supernova Progenitor Population: a Statistical Sample of Light Curves from Pan-STARRS1. ArXiv e-prints.

Schlafly, E. F., Finkbeiner, D. P., Aug. 2011. Measuring Reddening with Sloan Digital Sky Survey Stellar Spectra and Recalibrating SFD. ApJ737, 103.

Schlegel, E. M., May 1990. A new subclass of Type II supernovae? MNRAS244, 269–271.

Schlegel, E. M., Apr. 1996. On the Early Spectroscopic Distinction of Type II Supernovae. AJ111, 1660.

Schmidt, B. P., Kirshner, R. P., Schild, R., Leibundgut, B., Jeffery, D., Willner, S. P., Peletier, R., Zabludoff, A. I., Phillips, M. M., Suntzeff, N. B., Hamuy, M., Wells, L. A., Smith, R. C., Baldwin, J. A., Weller, W. G., Navarette, M., Gonzalez, L., Filippenko, A. V., Shields, J. C., Steidel, C. C., Perlmutter, S., Pennypacker, C., Smith, C. K., Porter, A. C., Boroson, T. A., Stathakis, R., Cannon, R., Peters, J., Horine, E., Freeman, K. C., Womble, D. S., Stone, R. P. S., Marschall, L. A., Phillips, A. C., Saha, A., Bond, H. E., Jun. 1993. Photometric and spectroscopic observations of SN 1990E in NGC 1035 - Observational constraints for models of type II supernovae. AJ105, 2236–2250.

Sim, S. A., Fink, M., Kromer, M., Röpke, F. K., Ruiter, A. J., Hillebrandt, W., Mar. 2012. 2D simulations of the double-detonation model for thermonuclear transients from low-mass carbon-oxygen white dwarfs. MNRAS420, 3003–3016.

Smartt, S. J., Sep. 2009. Progenitors of Core-Collapse Supernovae. ARA&A47, 63–106.

Smartt, S. J., Apr. 2015. Observational Constraints on the Progenitors of Core-Collapse Supernovae: The Case for Missing High-Mass Stars. 32, e016.

Smartt, S. J., Eldridge, J. J., Crockett, R. M., Maund, J. R., May 2009. The death of massive stars - I. Observational constraints on the progenitors of Type II-P supernovae. MNRAS395, 1409–1437.

Smartt, S. J., Maund, J. R., Hendry, M. A., Tout, C. A., Gilmore, G. F., Mattila, S., Benn, C. R., Jan. 2004. Detection of a Red Supergiant Progenitor Star of a Type II-Plateau Supernova. Science 303, 499–503.

Spiro, S., Pastorello, A., Pumo, M. L., Zampieri, L., Turatto, M., Smartt, S. J., Benetti, S., Cappellaro, E., Valenti, S., Agnoletto, I., Altavilla, G., Aoki, T., Brocato, E., Corsini, E. M., Di Cianno, A., Elias-Rosa, N., Hamuy, M., Enya, K., Fiaschi, M., Folatelli, G., Desidera, S., Harutyunyan, A., Howell, D. A., Kawka, A., Kobayashi, Y., Leibundgut, B., Minezaki, T., Navasardyan, H., Nomoto, K., Mattila, S., Pietrinferni, A., Pignata, G., Raimondo, G., Salvo, M., Schmidt, B. P., Sollerman, J., Spyromilio, J., Taubenberger, S., Valentini, G., Vennes, S., Yoshii, Y., Jan. 2014. Underluminous Type II Plateau Supernovae: II. Pointing towards moderate mass precursors. ArXiv e-prints.

Stritzinger, M. D., et al., Nov. 2011. The Carnegie Supernova Project: Second Photometry Data Release of Low-redshift Type Ia Supernovae. AJ142, 156.

Taddia, F., Stritzinger, M. D., Sollerman, J., Phillips, M. M., Anderson, J. P., Ergon, M., Folatelli, G., Fransson, C., Freedman, W., Hamuy, M., Morrell, N., Pastorello, A., Persson, S. E., Gonzalez, S., Jan. 2012. The Type II supernovae 2006V and 2006au: two SN 1987A-like events. A&A537, A140.

Taddia, F., et al., Jul. 2013. Carnegie Supernova Project: Observations of Type IIn supernovae. A&A555, A10.

Takáts, K., Pumo, M. L., Elias-Rosa, N., Pastorello, A., Pignata, G., Paillas, E., Zampieri, L., Anderson, J. P., Vinkó, J., Benetti, S., Botticella, M.-T., Bufano, F., Campillay, A., Cartier, R., Ergon, M., Folatelli, G., Foley, R. J., Förster, F., Hamuy, M., Hentunen, V.-P., Kankare, E., Leloudas, G., Morrell, N., Nissinen, M., Phillips, M. M., Smartt, S. J., Stritzinger, M., Taubenberger, S., Valenti, S., Van Dyk, S. D., Haislip, J. B., LaCluyze, A. P., Moore, J. P., Reichart, D., Feb. 2014. SN 2009N: linking normal and subluminous Type II-P SNe. MNRAS438, 368–387.

Turatto, M., 2003. Classification of Supernovae. In: Weiler, K. (Ed.), Supernovae and Gamma-Ray Bursters. Vol. 598 of Lecture Notes in Physics, Berlin Springer Verlag. pp. 21–36.

Turatto, M., Cappellaro, E., Benetti, S., Danziger, I. J., Nov. 1993. Observations of Type-II Plateau Supernovae - Supernova 1988A Supernova 1988H and Supernova 1989C. MNRAS265, 471.

Turatto, M., Mazzali, P. A., Young, T. R., Nomoto, K., Iwamoto, K., Benetti, S., Cappellaro, E., Danziger, I. J., de Mello, D. F., Phillips, M. M., Suntzeff, N. B., Clocchiatti, A., Piemonte, A., Leibundgut, B., Covarrubias, R., Maza, J., Sollerman, J., May 1998. The Peculiar Type II Supernova 1997D: A Case for a Very Low 56Ni Mass. ApJ498, L129.

Valenti, S., Howell, D. A., Stritzinger, M. D., Graham, M. L., Hosseinzadeh, G., Arcavi, I., Bildsten, L., Jerkstrand, A., McCully, C., Pastorello, A., Piro, A. L., Sand, D., Smartt, S. J., Terreran, G., Baltay, C., Benetti, S., Brown, P., Filippenko, A. V., Fraser, M., Rabinowitz, D., Sullivan, M., Yuan, F., Mar. 2016. The Diversity of Type II Supernova vs. The Similarity in Their Progenitors. ArXiv e-prints.

Van Dyk, S. D., Li, W., Filippenko, A. V., Nov. 2003. On the Progenitor of the Type II-Plateau Supernova 2003gd in M74. PASP115, 1289–1295.

Webbink, R. F., Feb. 1984. Double white dwarfs as progenitors of R Coronae Borealis stars and Type I supernovae. ApJ277, 355–360.

Woosley, S. E., Hartmann, D., Pinto, P. A., Nov. 1989. Hard emission at late times from SN 1987A. ApJ346, 395–404.

Yoon, S.-C., Woosley, S. E., Langer, N., Dec. 2010. Type Ib/c Supernovae in Binary Systems. I. Evolution and Properties of the Progenitor Stars. ApJ725, 940–954.

Young, T. R., Dec. 2004. A Parameter Study of Type II Supernova Light Curves Using 6 M_{solar} He Cores. ApJ617, 1233–1250.

Zhang, J., Wang, X., Mazzali, P. A., Bai, J., Zhang, T., Bersier, D., Huang, F., Fan, Y., Mo, J., Wang, J., Yi, W., Wang, C., Xin, Y., Liangchang, Zhang, X., Lun, B., Wang, X., He, S., Walker, E. S., Dec. 2014. Optical and Ultraviolet Observations of a Low-velocity Type II Plateau Supernova 2013am in M65. ApJ797, 5.

Appendix A

SNe II spectral series

Here I present the SN II spectral series for a sample of 123 SNe.

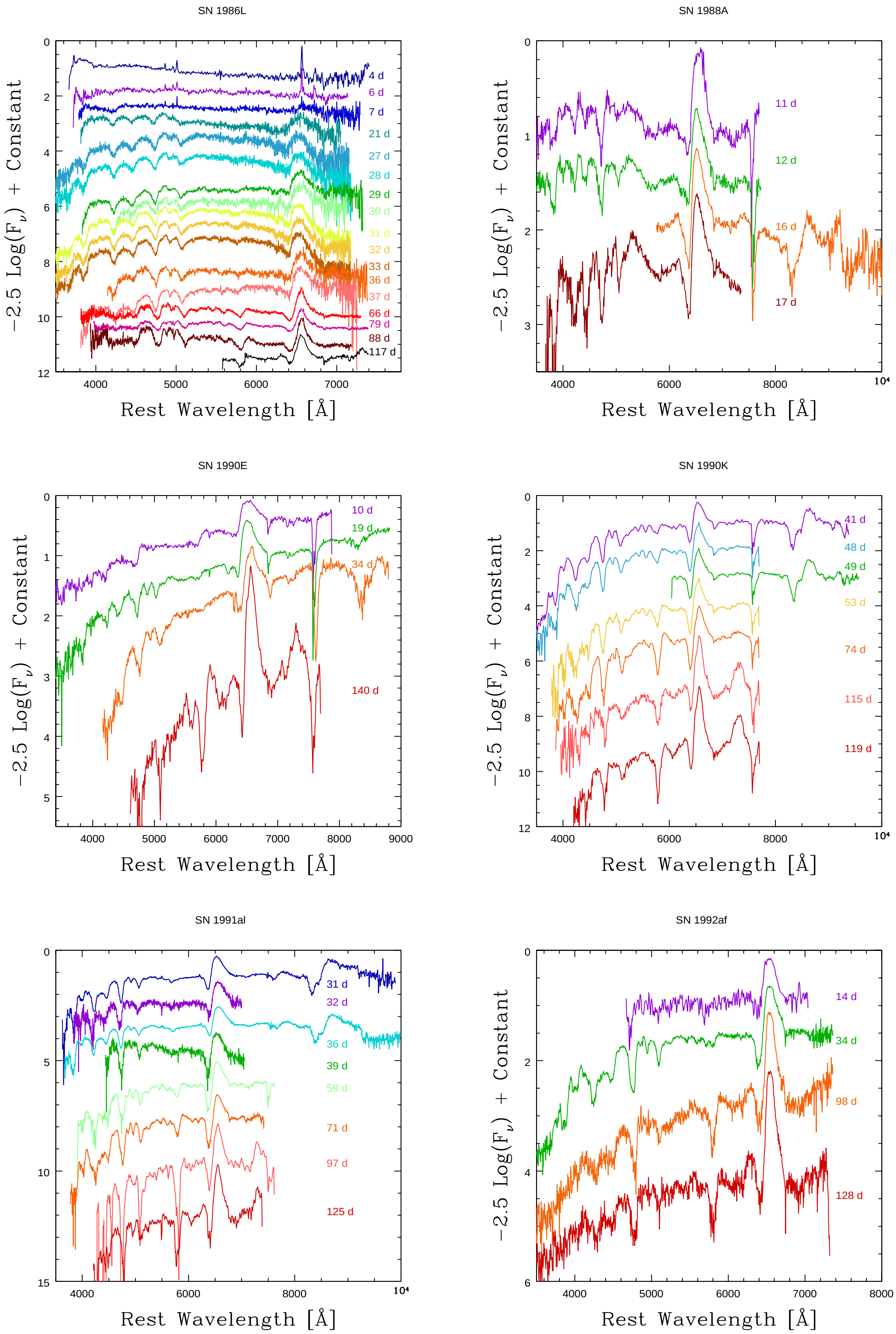

Figure A.1 SN II spectral series. The wavelength axis is corrected for the recession velocity of the host galaxy.

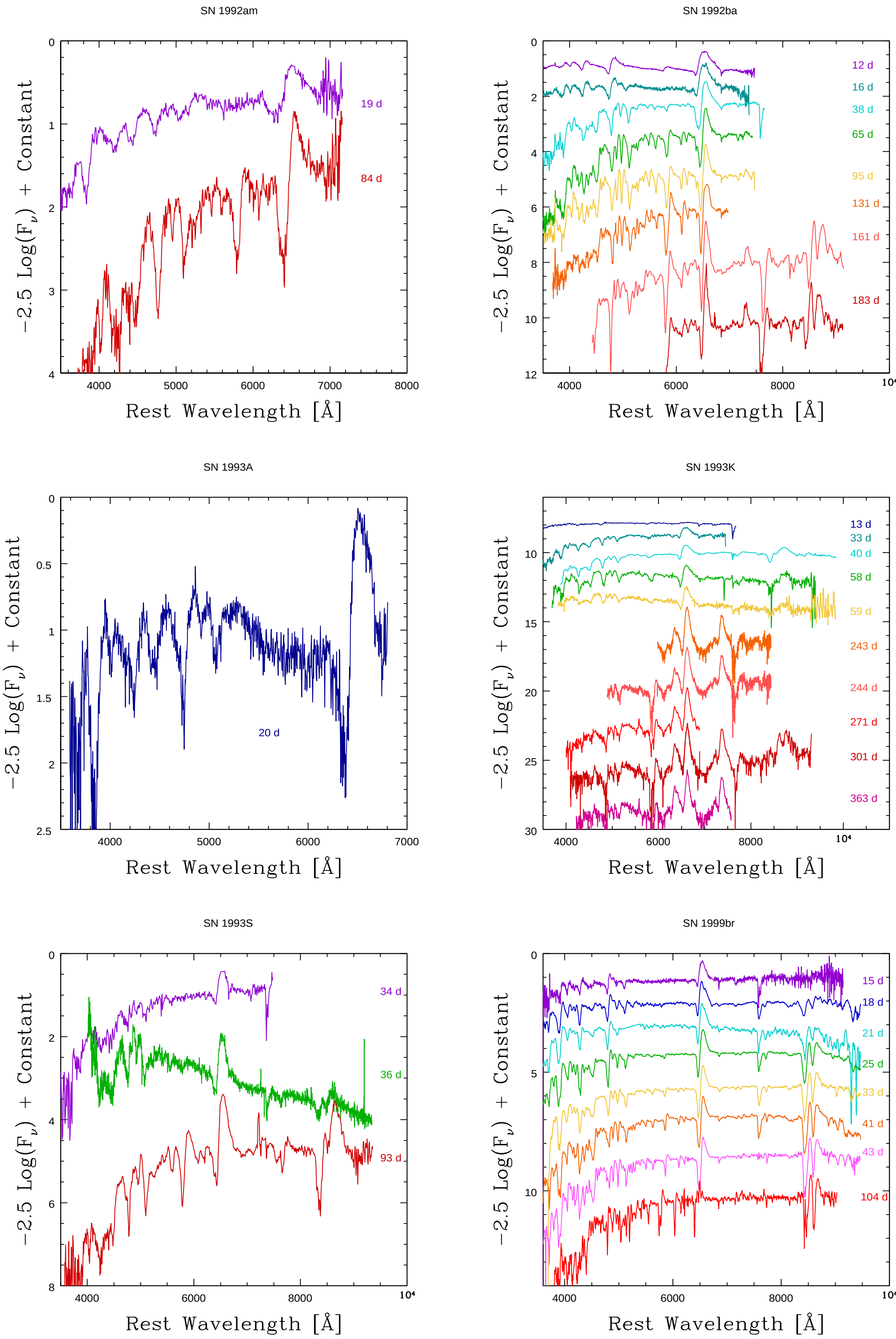

Figure A.2 SN II spectral series. The wavelength axis is corrected for the recession velocity of the host galaxy.

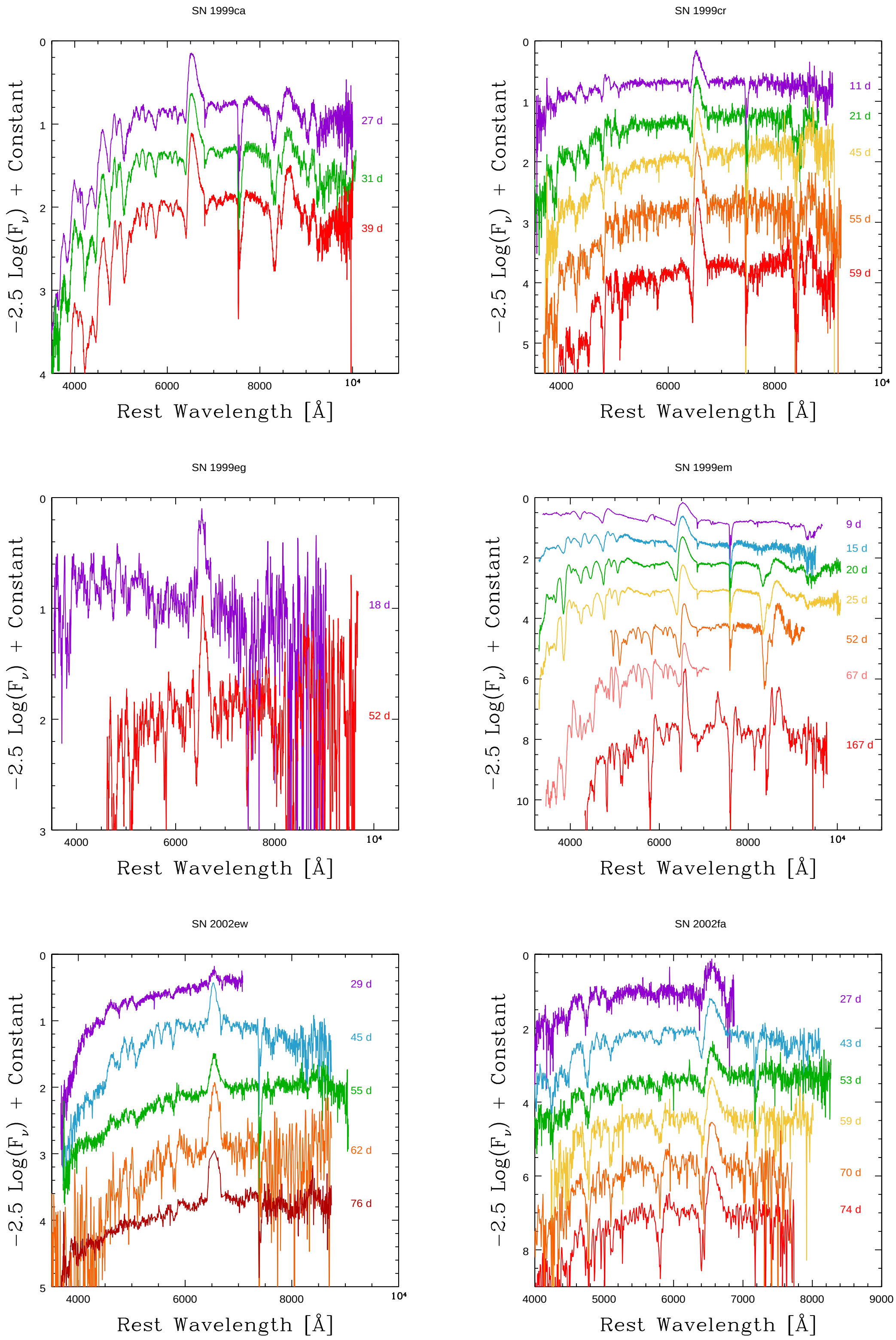

Figure A.3 SN II spectral series. The wavelength axis is corrected for the recession velocity of the host galaxy.

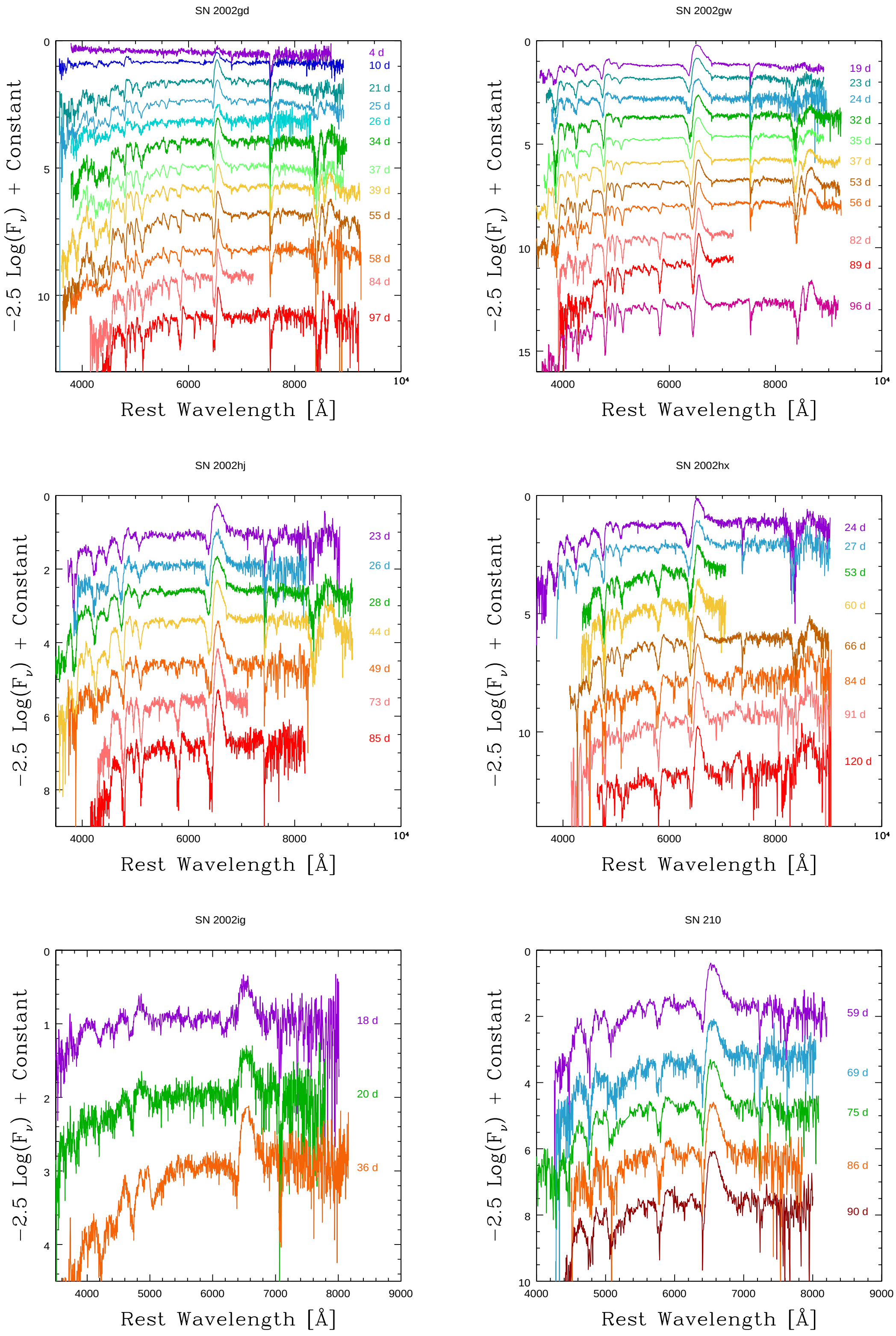

Figure A.4 SN II spectral series. The wavelength axis is corrected for the recession velocity of the host galaxy.

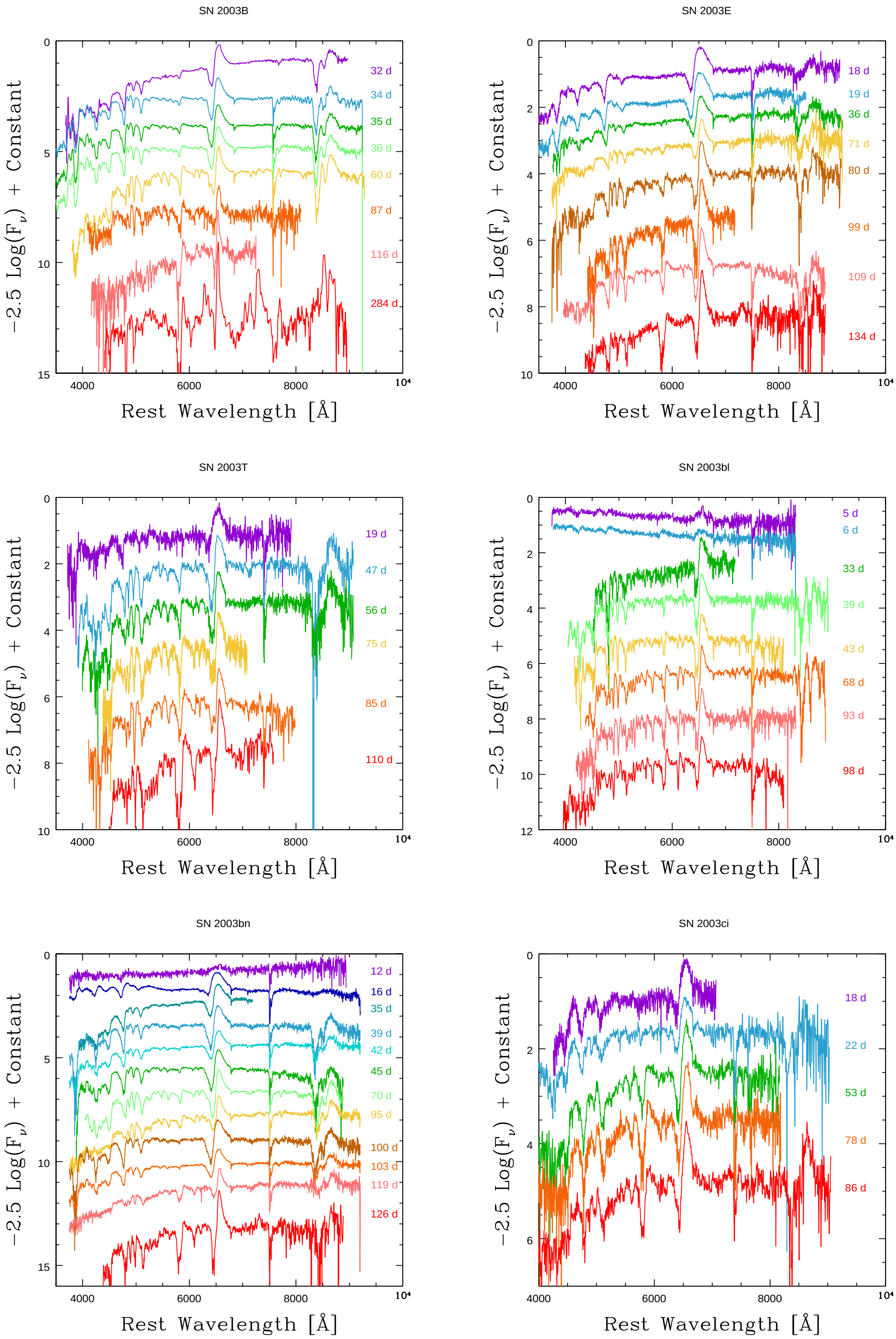

Figure A.5 SN II spectral series. The wavelength axis is corrected for the recession velocity of the host galaxy.

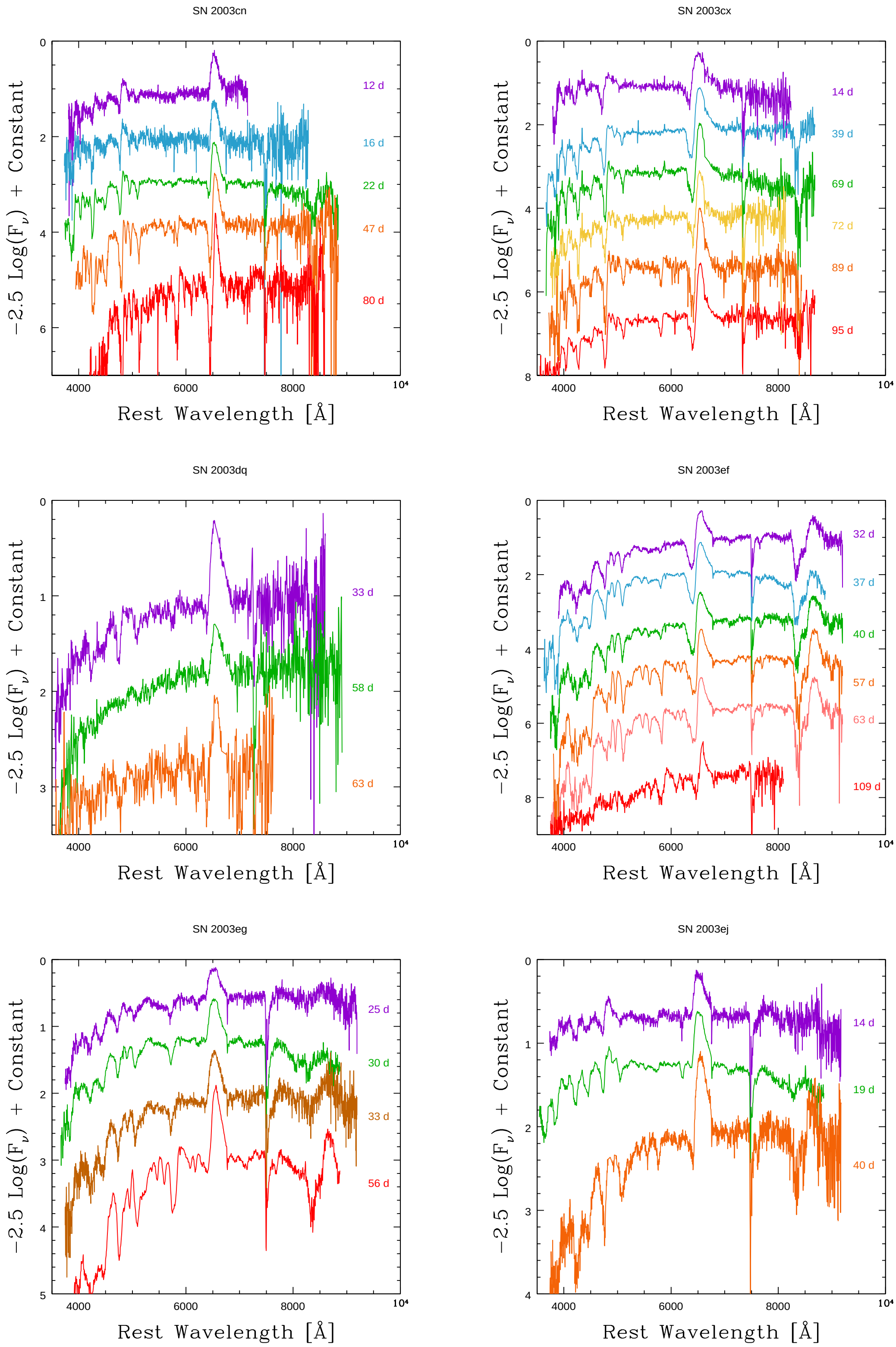

Figure A.6 SN II spectral series. The wavelength axis is corrected for the recession velocity of the host galaxy.

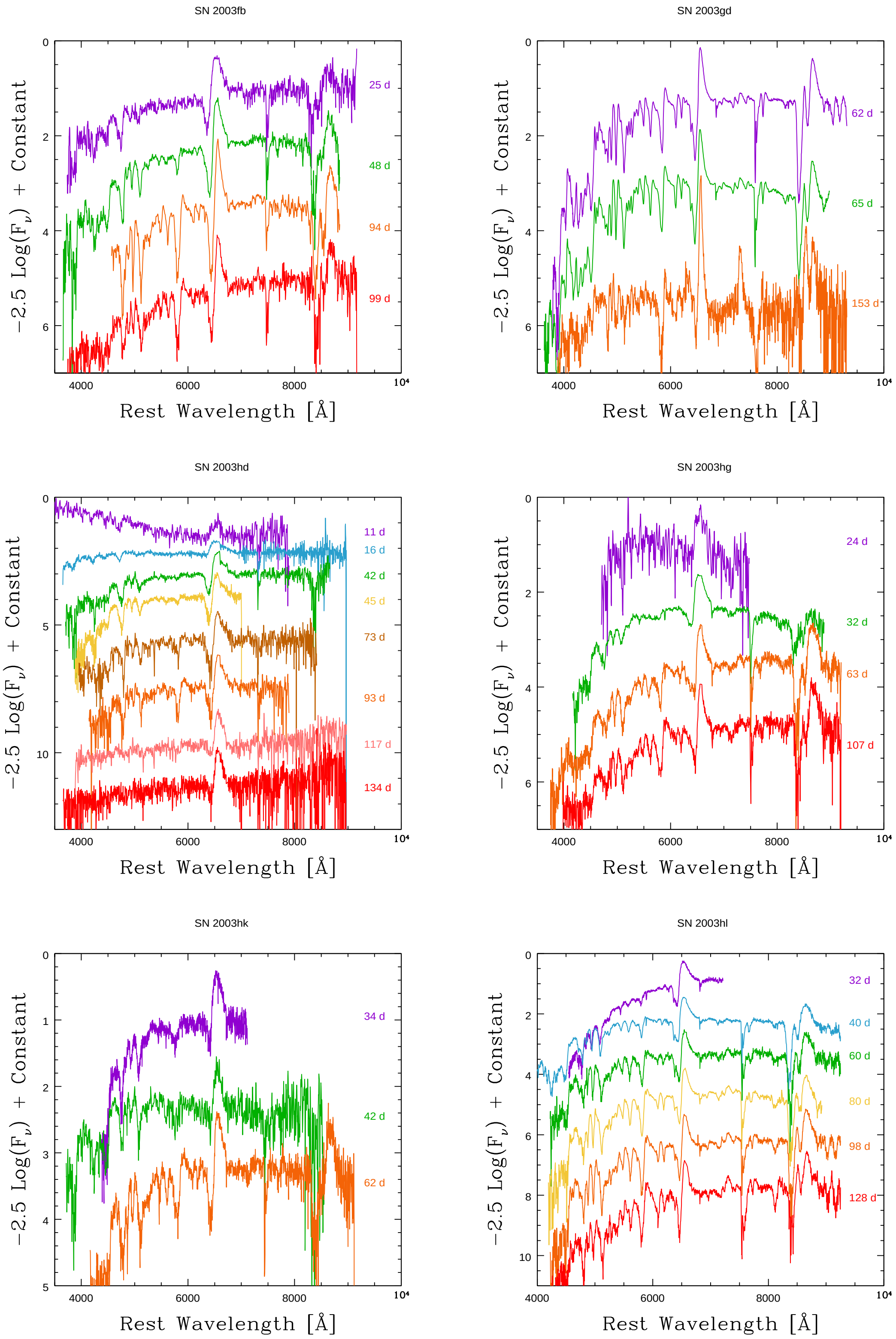

Figure A.7 SN II spectral series. The wavelength axis is corrected for the recession velocity of the host galaxy.

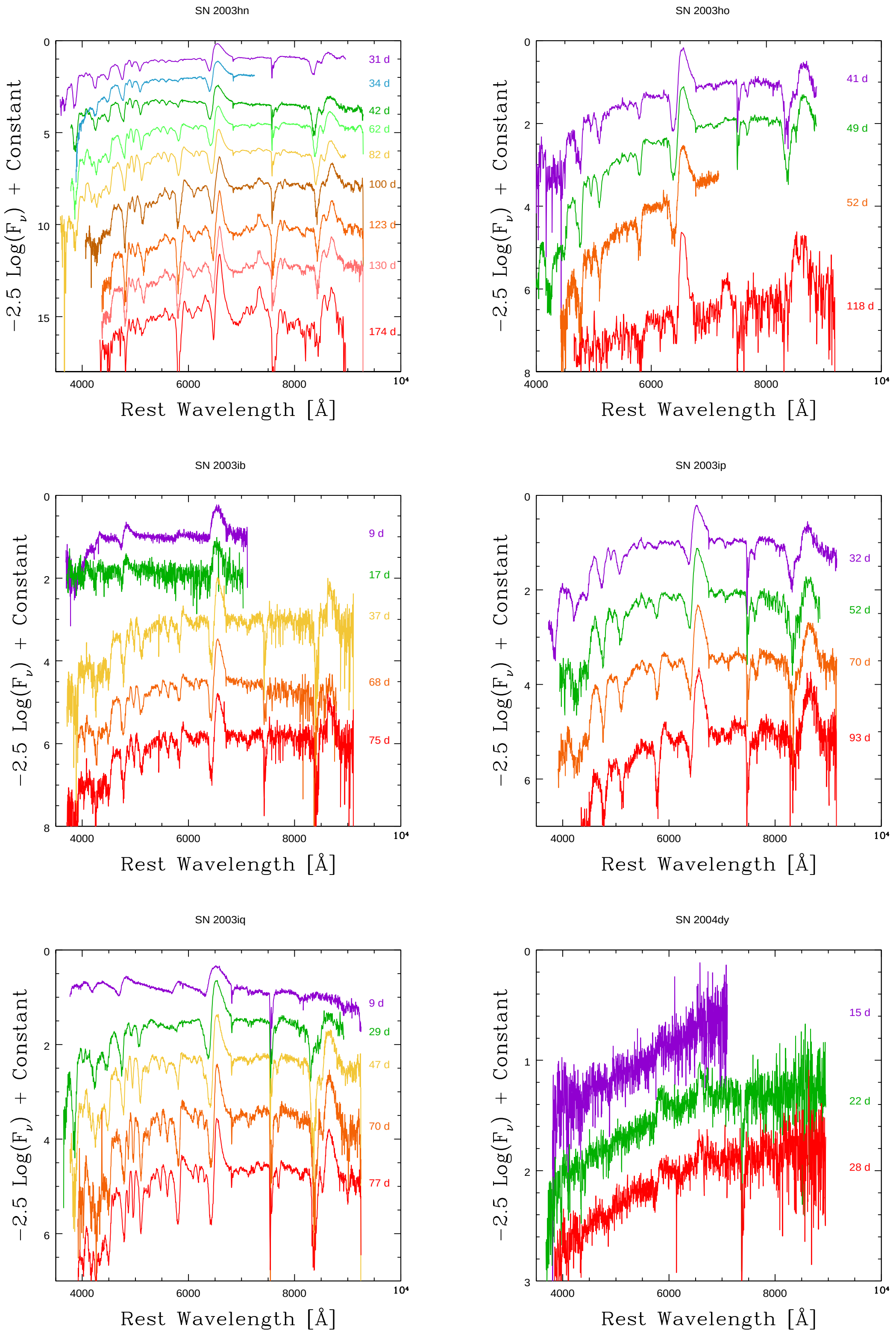

Figure A.8 SN II spectral series. The wavelength axis is corrected for the recession velocity of the host galaxy.

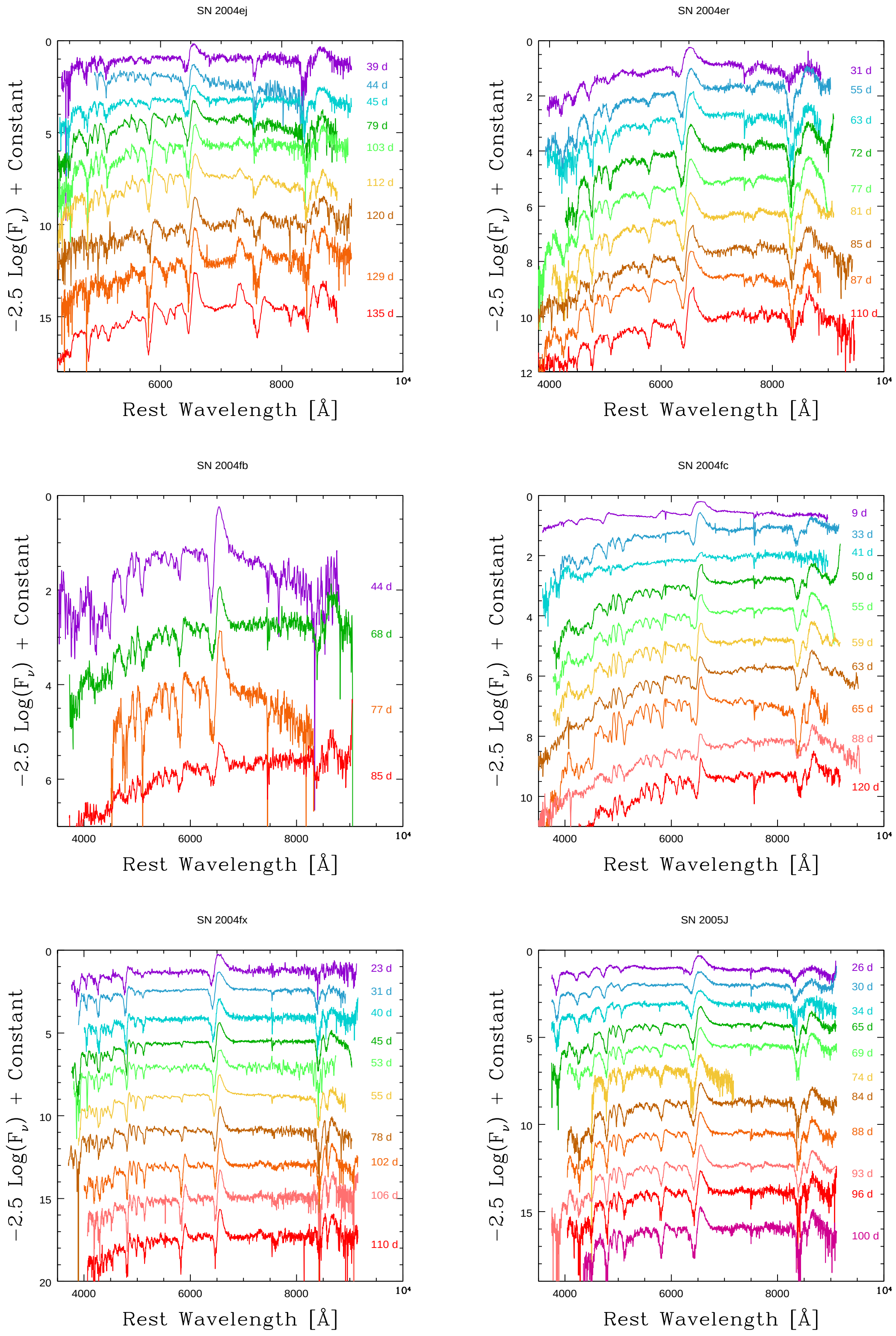

Figure A.9 SN II spectral series. The wavelength axis is corrected for the recession velocity of the host galaxy.

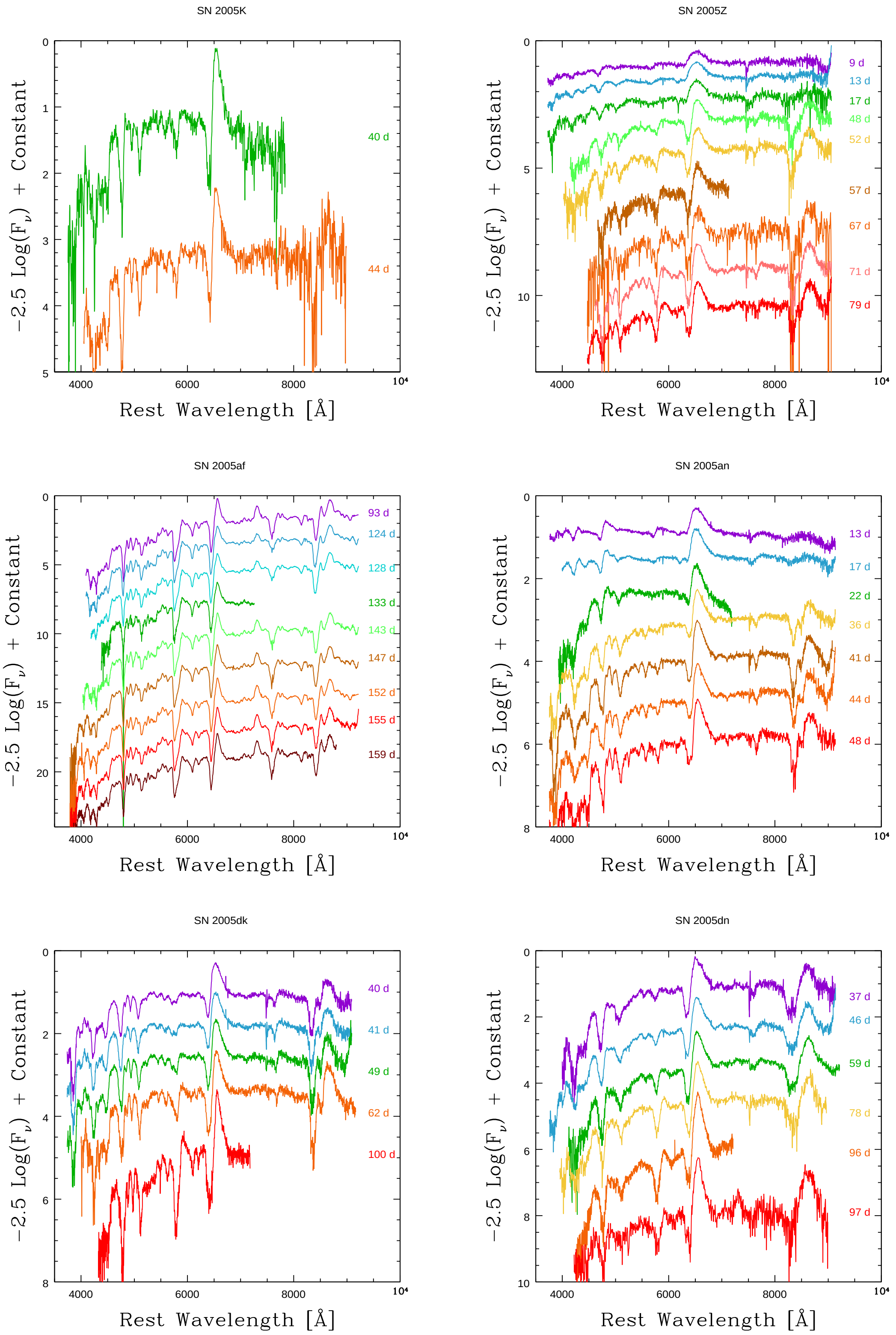

Figure A.10 SN II spectral series. The wavelength axis is corrected for the recession velocity of the host galaxy.

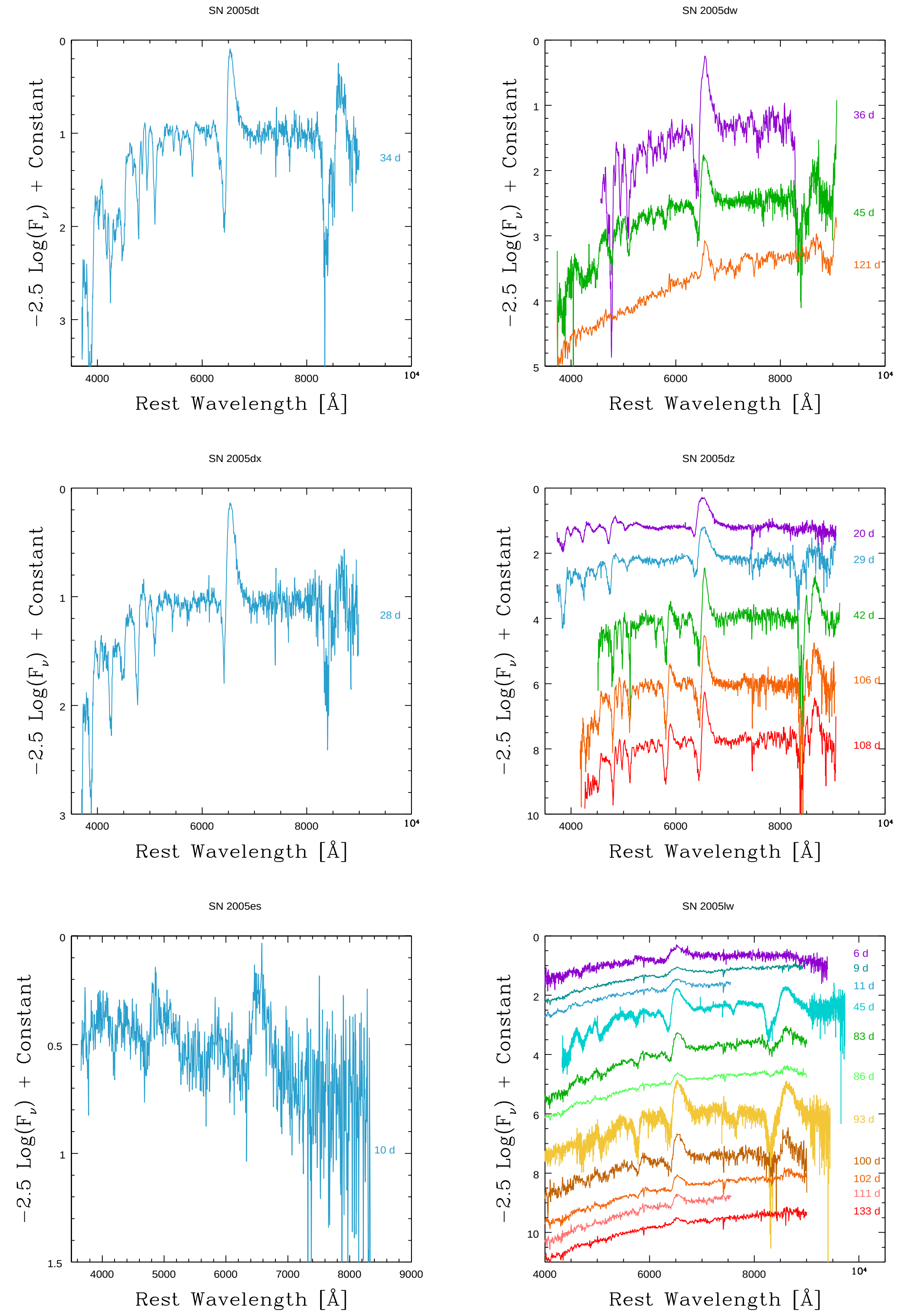

Figure A.11 SN II spectral series. The wavelength axis is corrected for the recession velocity of the host galaxy.

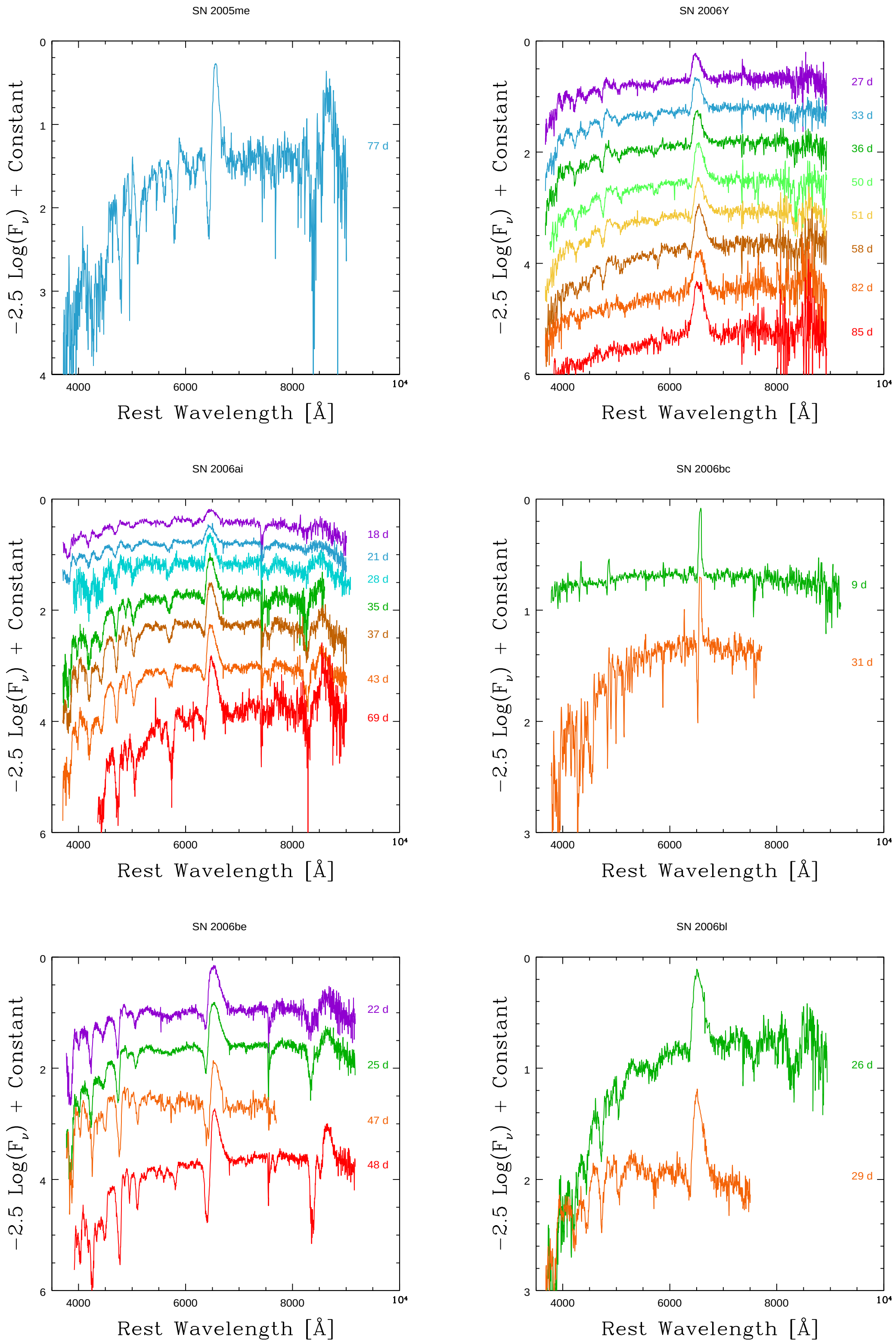

Figure A.12 SN II spectral series. The wavelength axis is corrected for the recession velocity of the host galaxy.

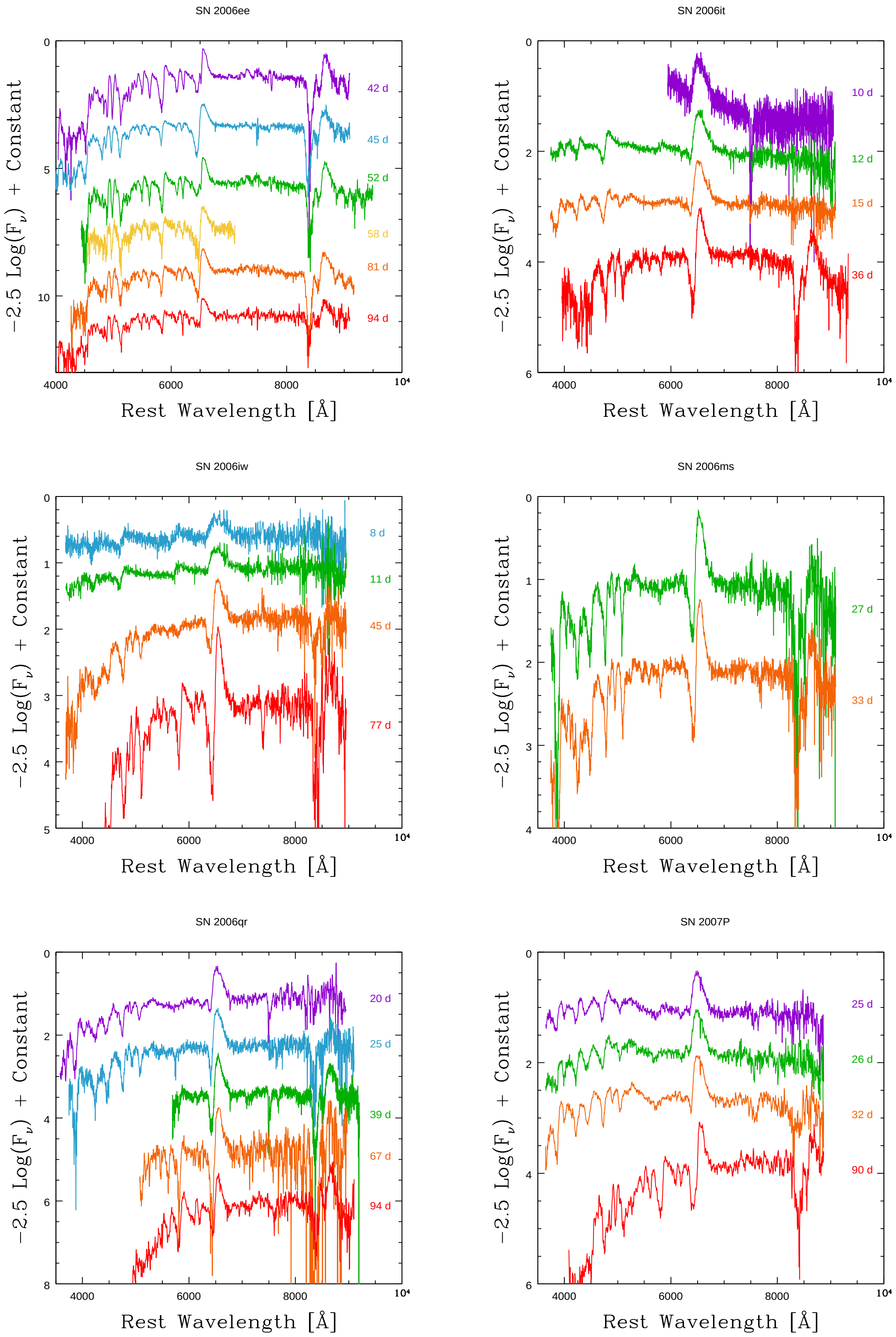

Figure A.13 SN II spectral series. The wavelength axis is corrected for the recession velocity of the host galaxy.

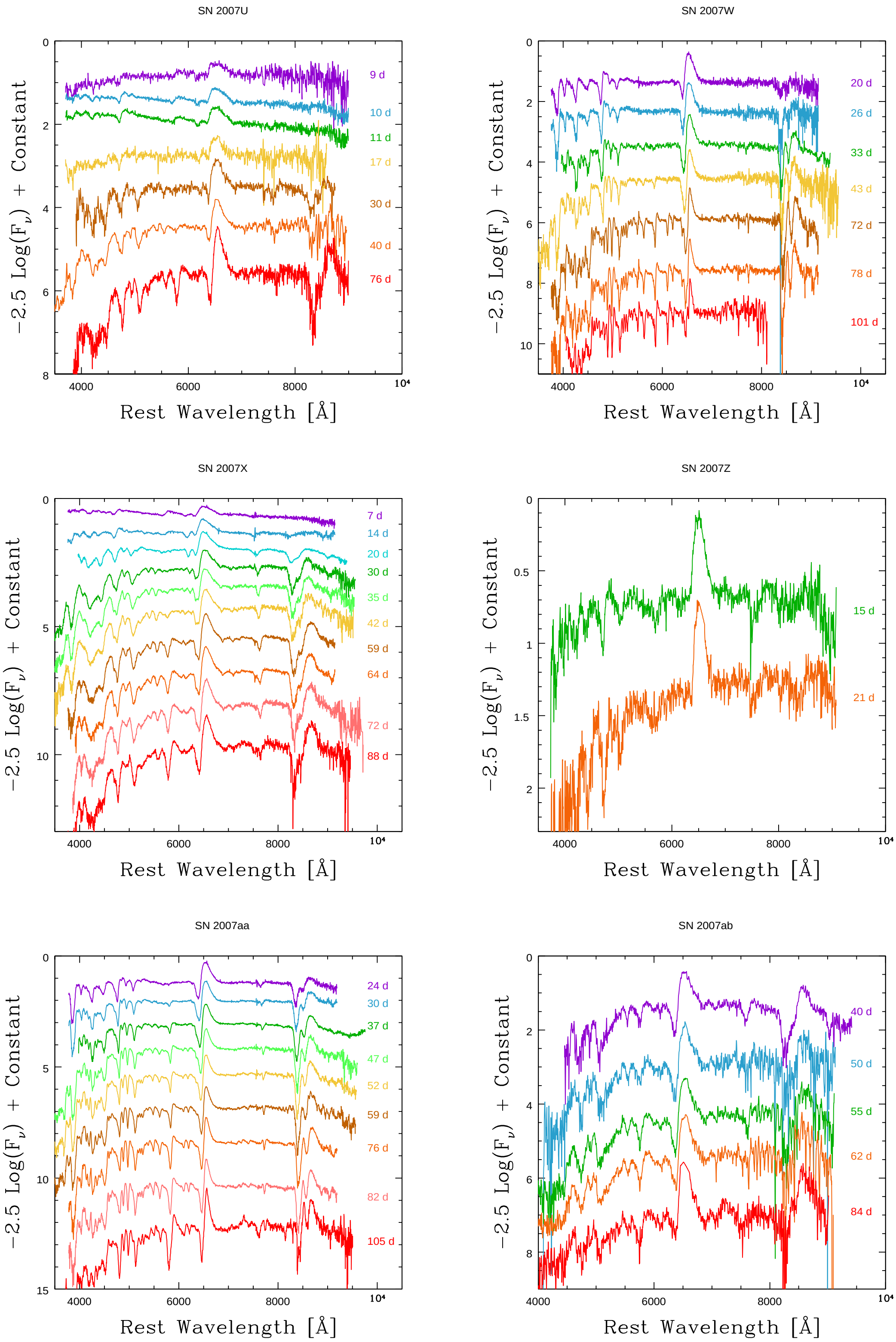

Figure A.14 SN II spectral series. The wavelength axis is corrected for the recession velocity of the host galaxy.

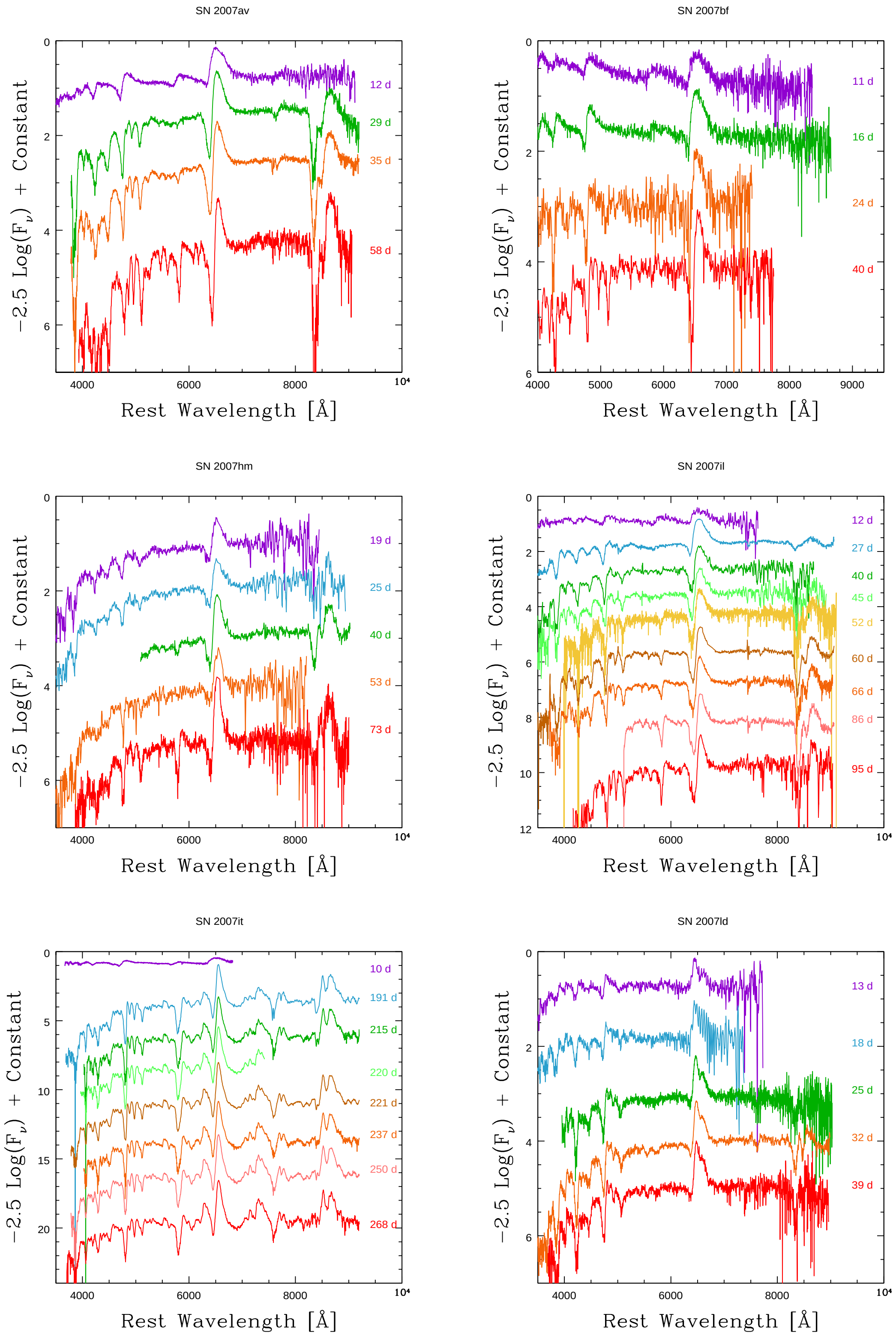

Figure A.15 SN II spectral series. The wavelength axis is corrected for the recession velocity of the host galaxy.

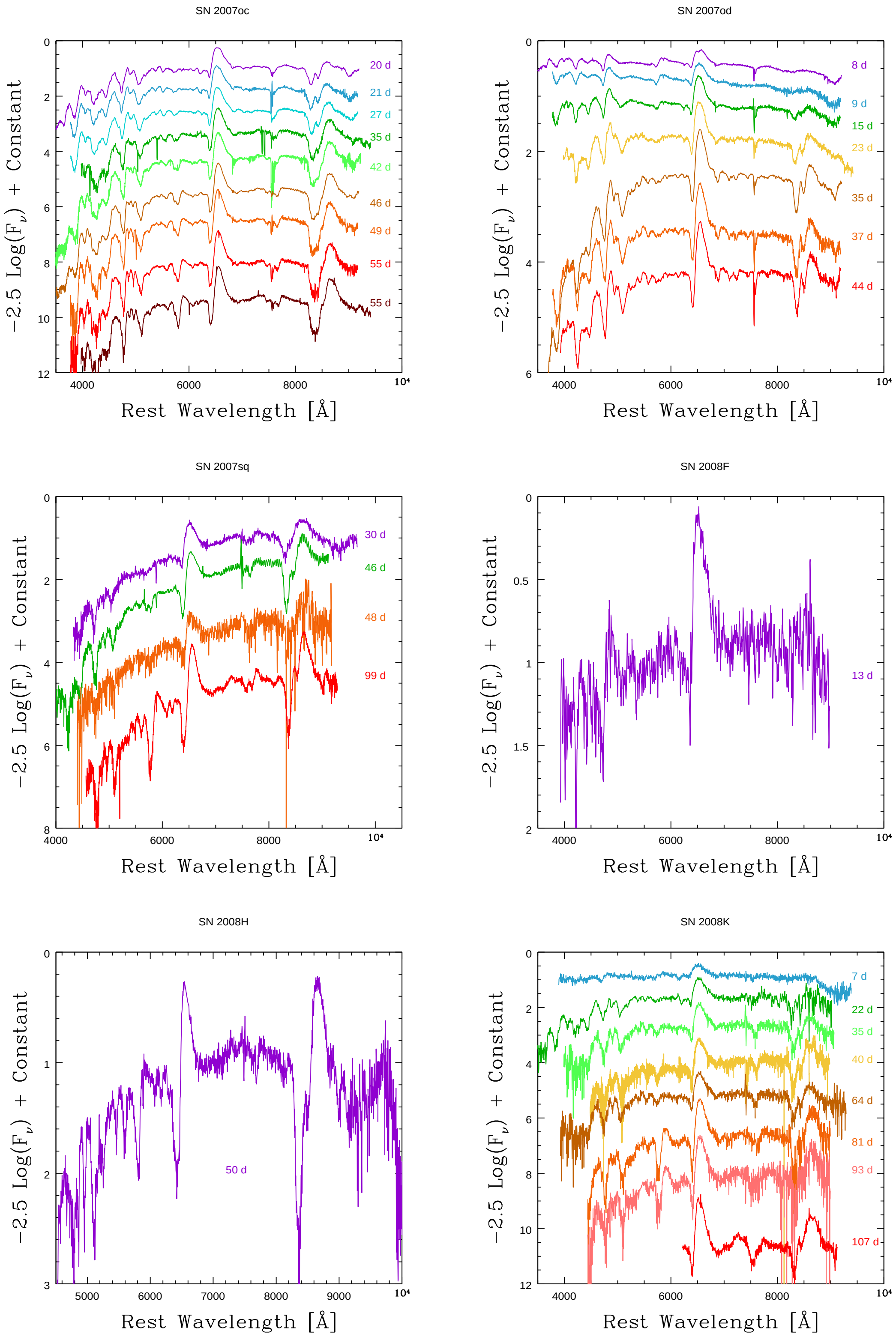

Figure A.16 SN II spectral series. The wavelength axis is corrected for the recession velocity of the host galaxy.

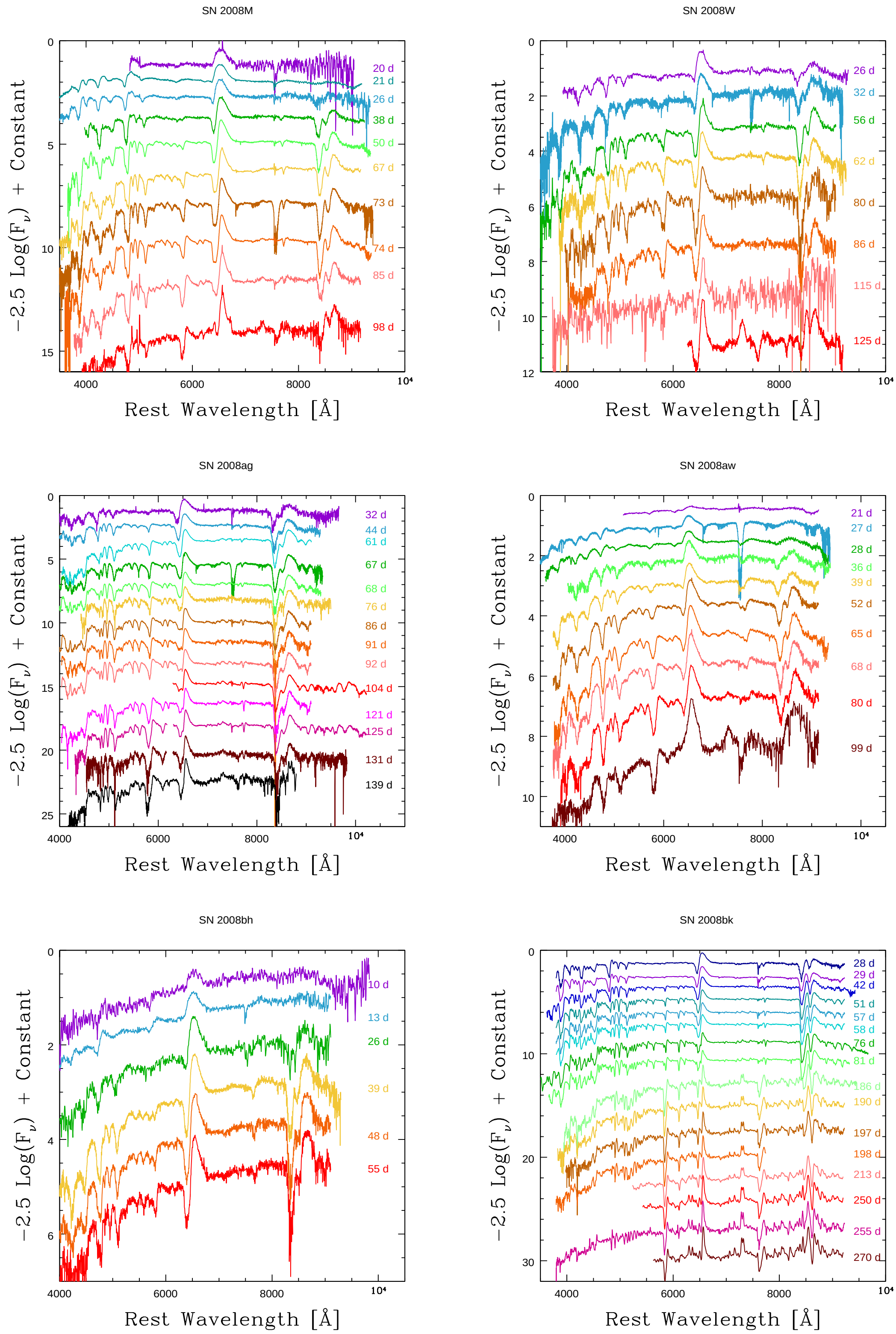

Figure A.17 SN II spectral series. The wavelength axis is corrected for the recession velocity of the host galaxy.

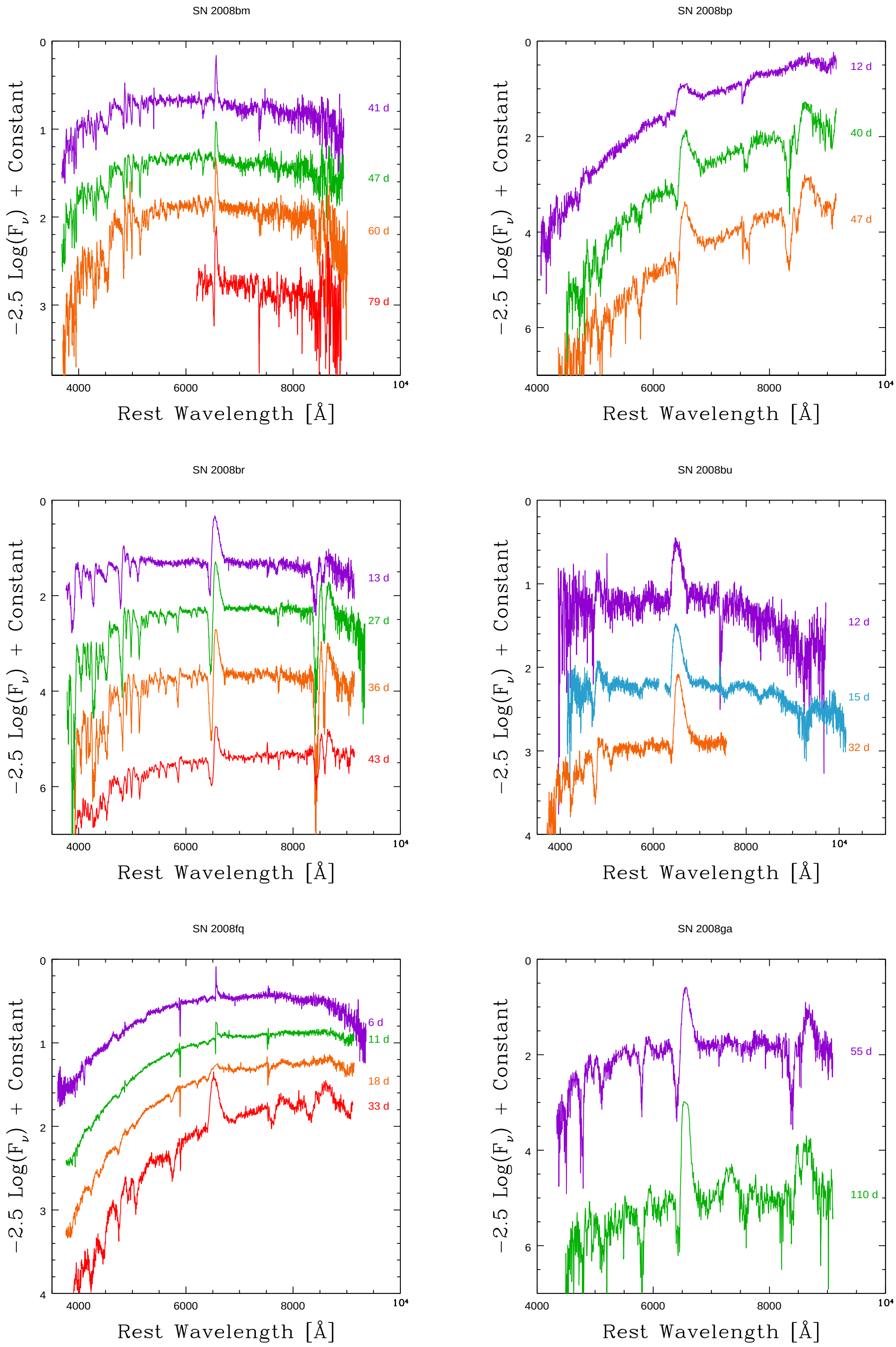

Figure A.18 SN II spectral series. The wavelength axis is corrected for the recession velocity of the host galaxy.

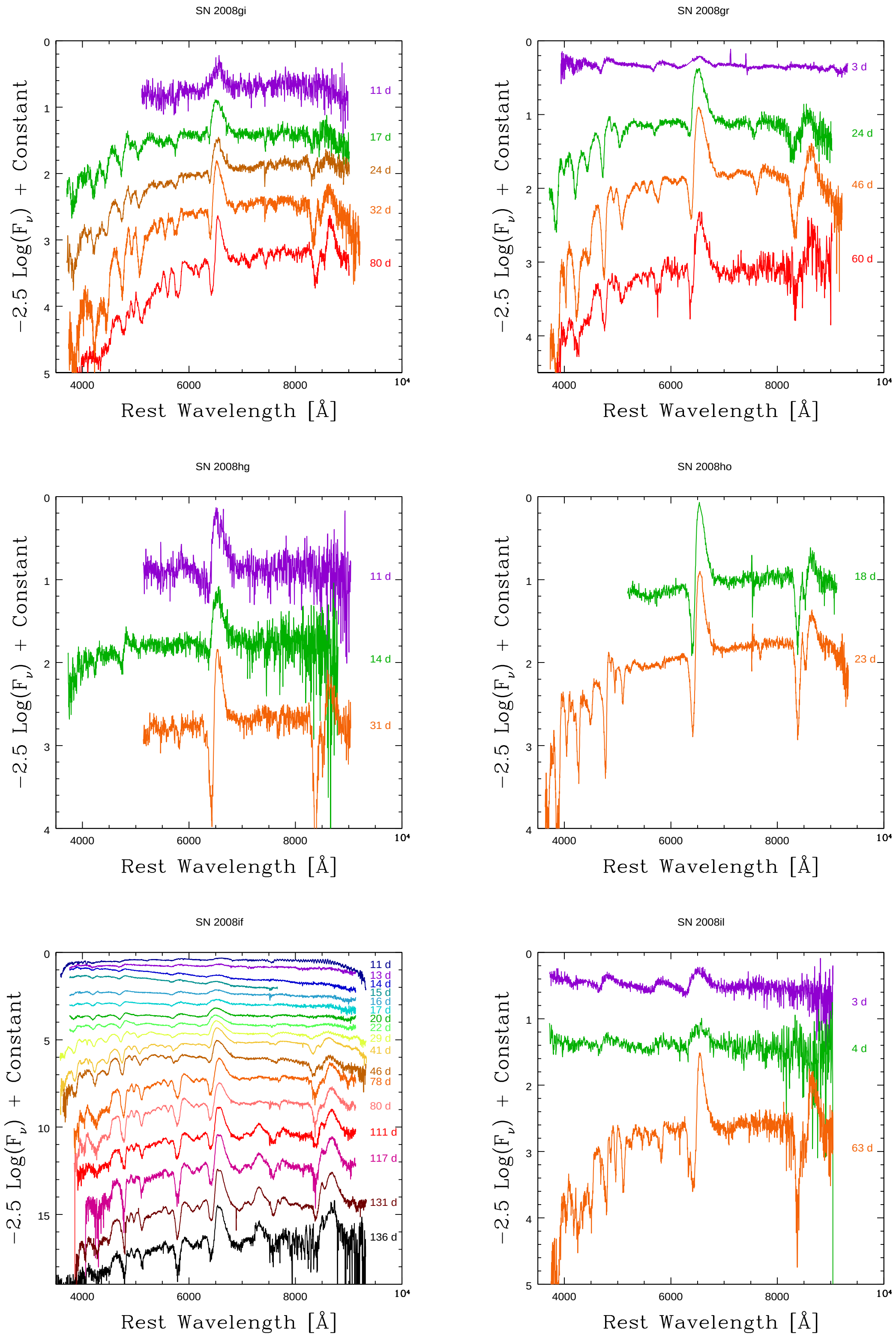

Figure A.19 SN II spectral series. The wavelength axis is corrected for the recession velocity of the host galaxy.

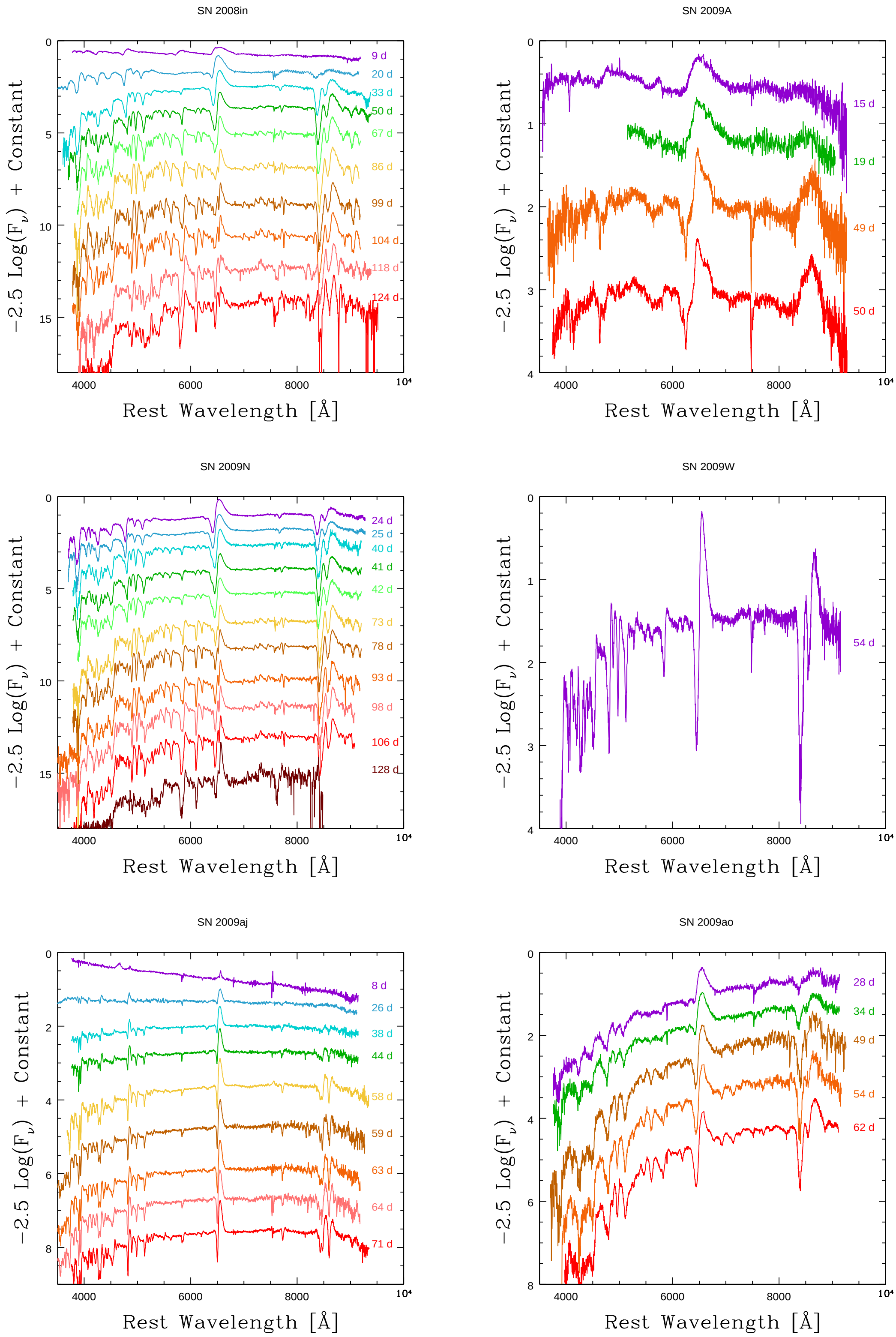

Figure A.20 SN II spectral series. The wavelength axis is corrected for the recession velocity of the host galaxy.

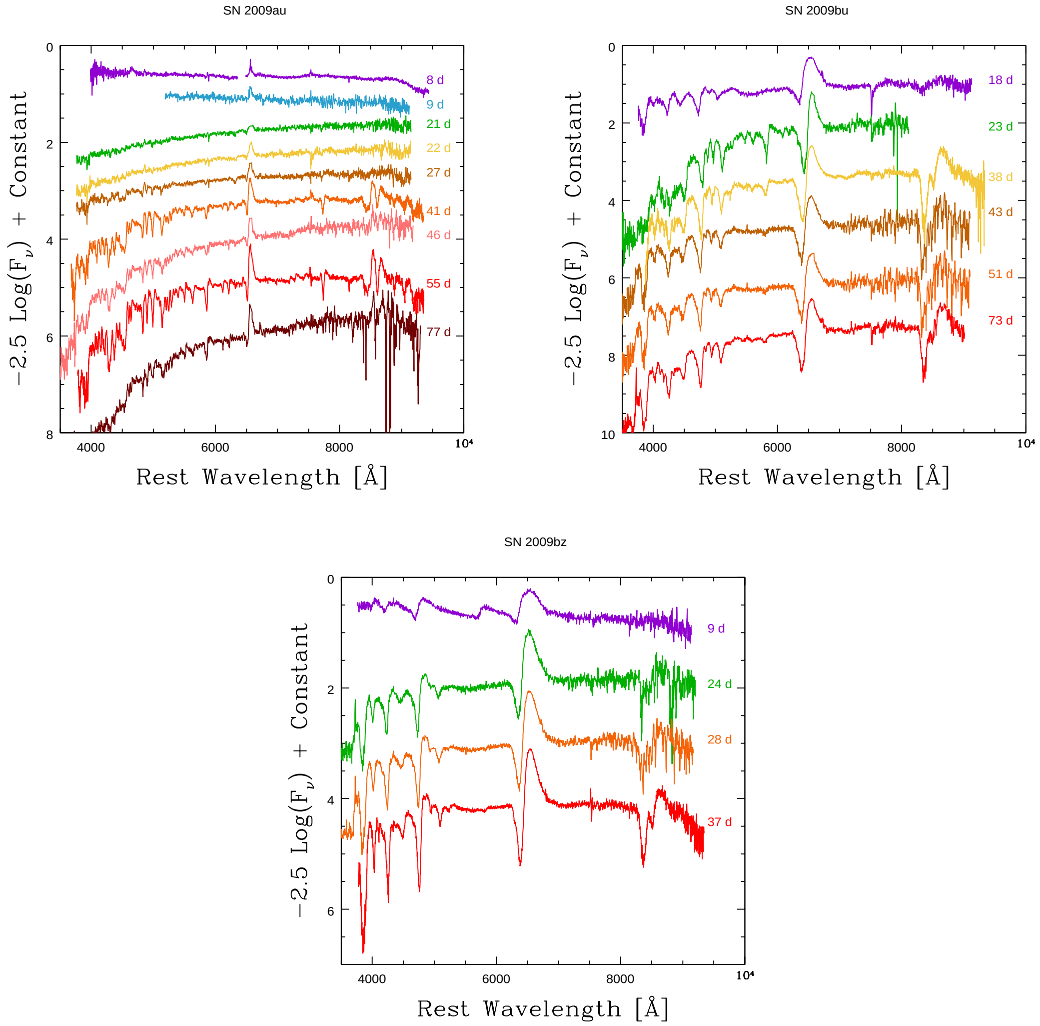

Figure A.21 SN II spectral series. The wavelength axis is corrected for the recession velocity of the host galaxy.

Appendix B

SNe II spectral matching technique

Here I present the SN II spectral matching technique.

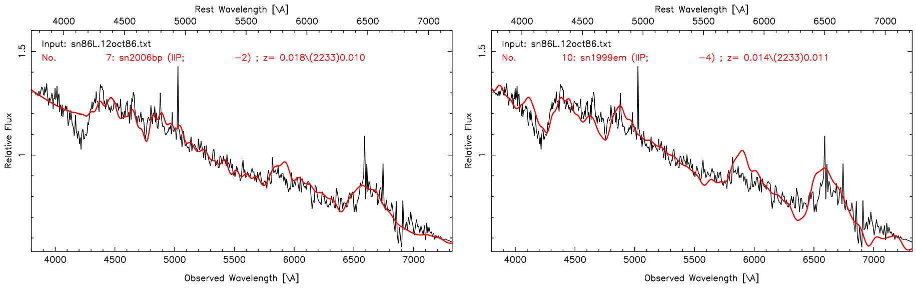

Figure B.1 Best spectral matching of SN 1986L using SNID.

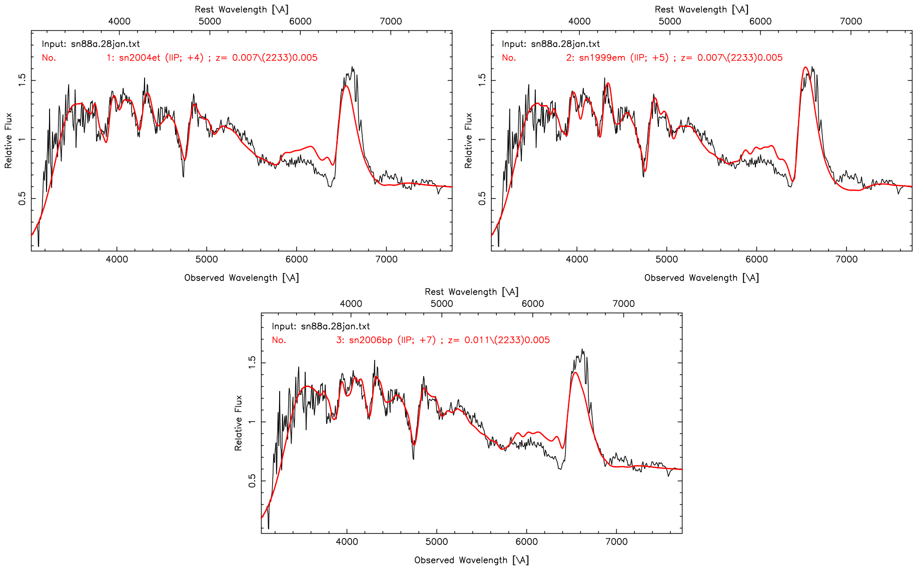

Figure B.2 Best spectral matching of SN 1988A using SNID.

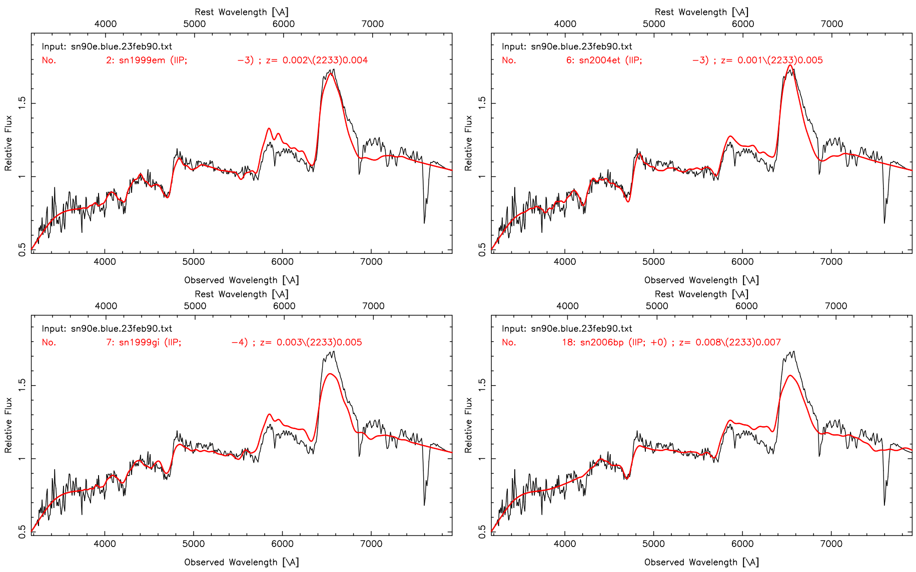

Figure B.3 Best spectral matching of SN 1990E using SNID.

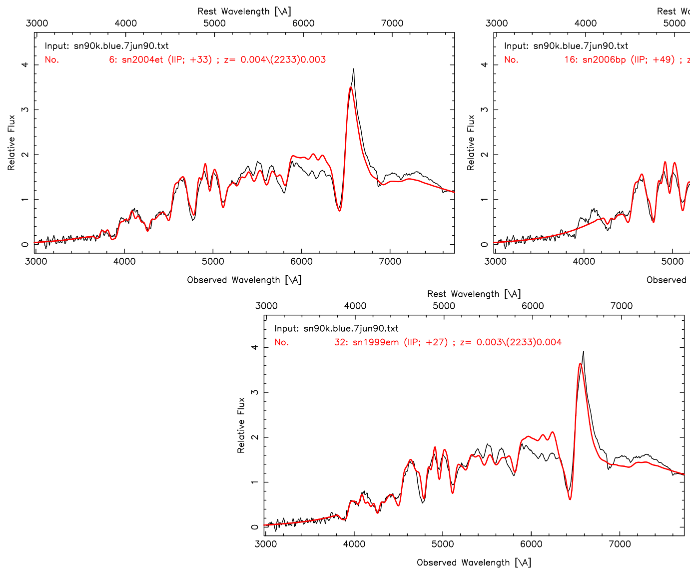

Figure B.4 Best spectral matching of SN 1990K using SNID.

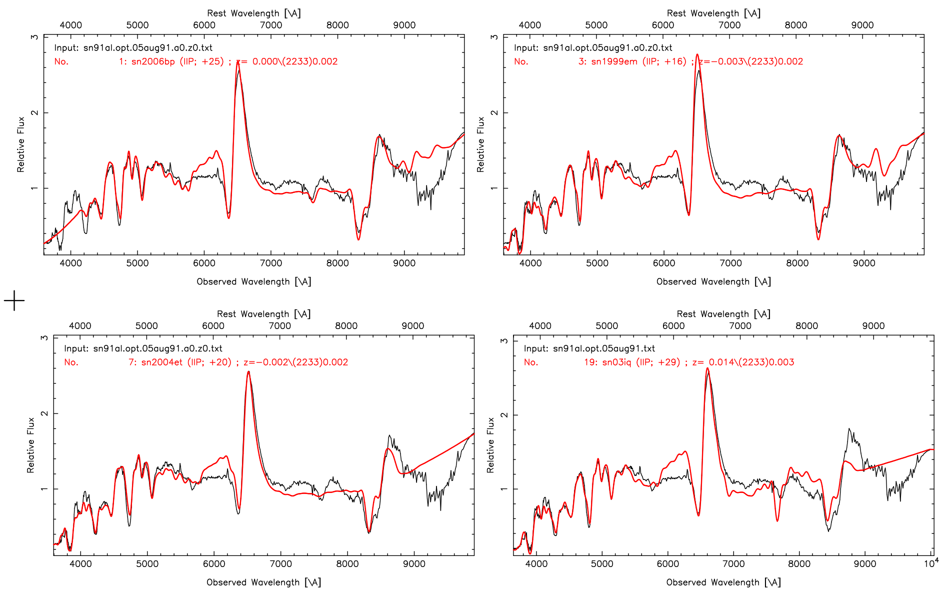

Figure B.5 Best spectral matching of SN 1991al using SNID.

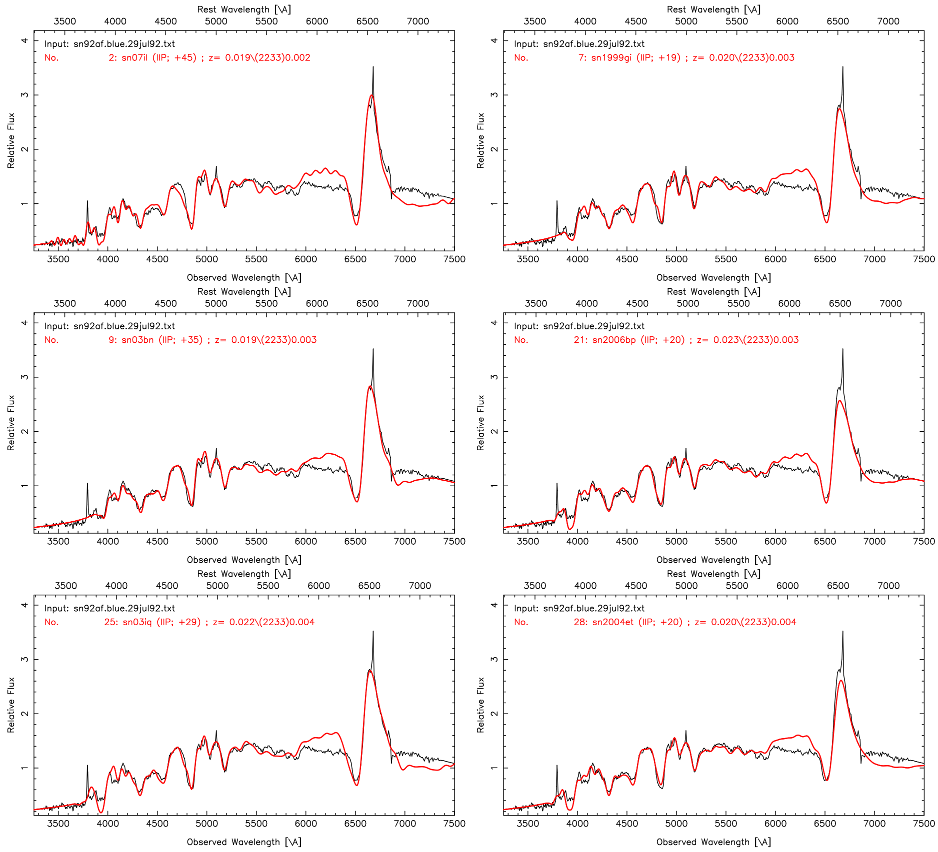

Figure B.6 Best spectral matching of SN 1992af using SNID.

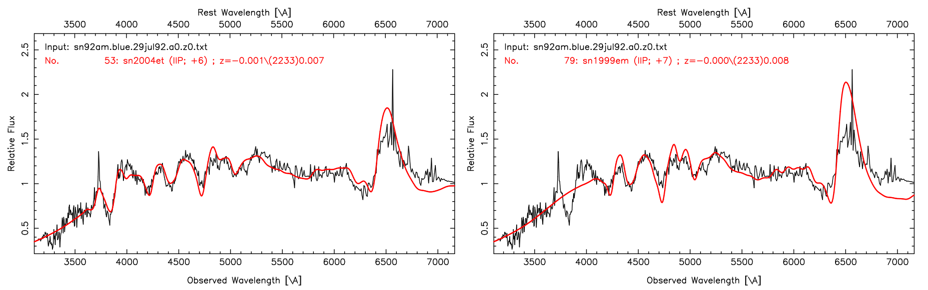

Figure B.7 Best spectral matching of SN 1992am using SNID.

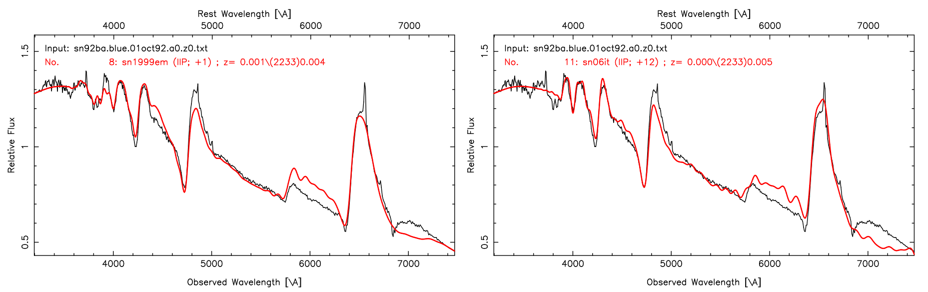

Figure B.8 Best spectral matching of SN 1992ba using SNID.

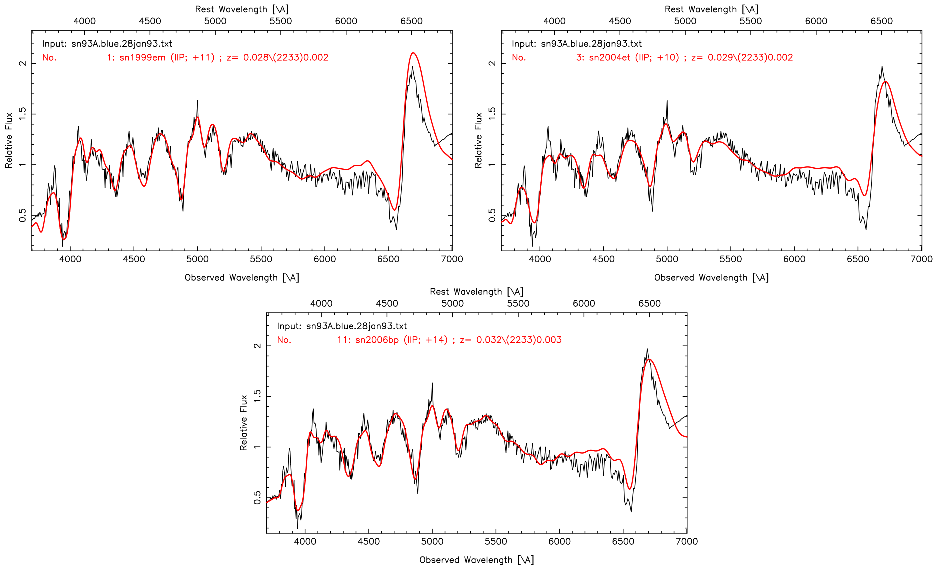

Figure B.9 Best spectral matching of SN 1993A using SNID.

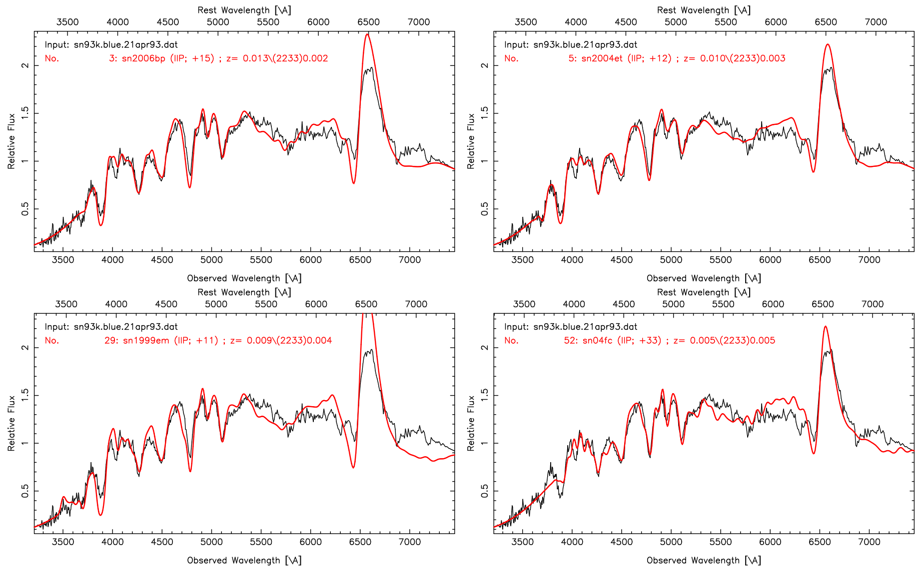

Figure B.10 Best spectral matching of SN 1993K using SNID.

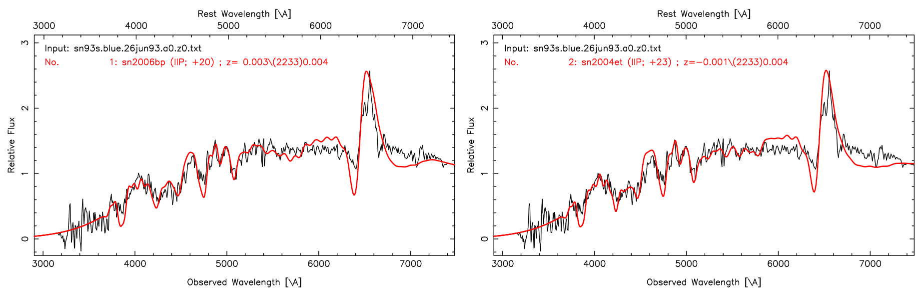

Figure B.11 Best spectral matching of SN 1993S using SNID.

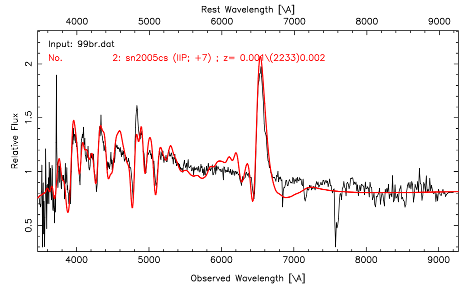

Figure B.12 Best spectral matching of SN 1999br using SNID.

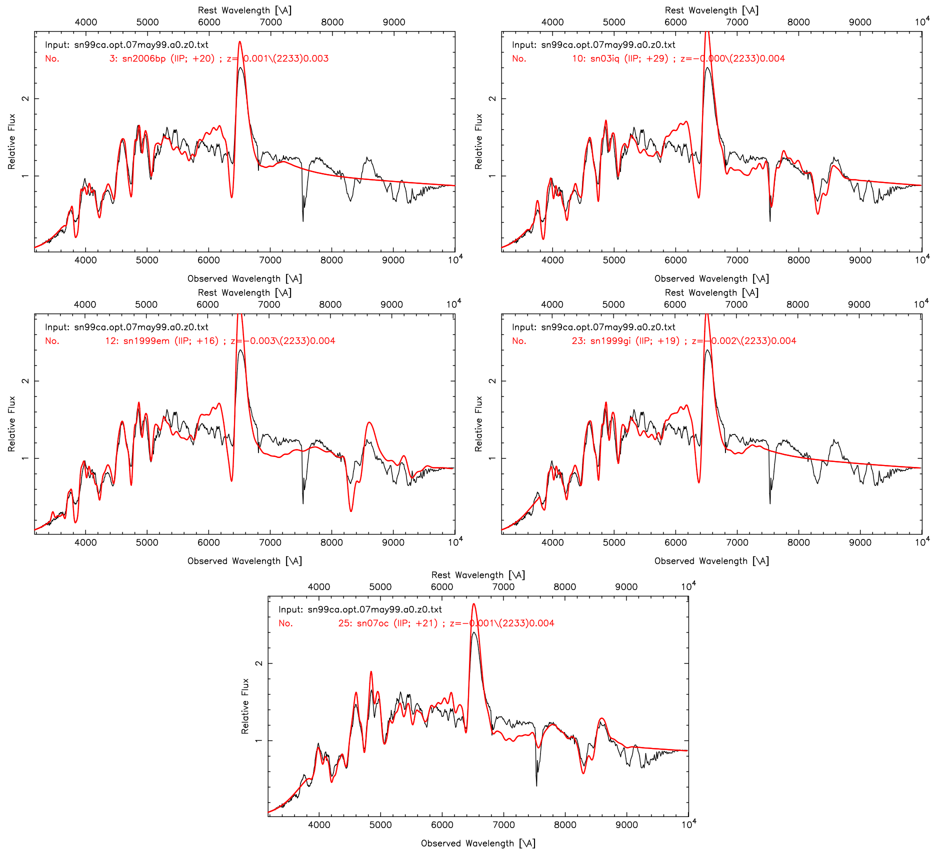

Figure B.13 Best spectral matching of SN 1999ca using SNID.

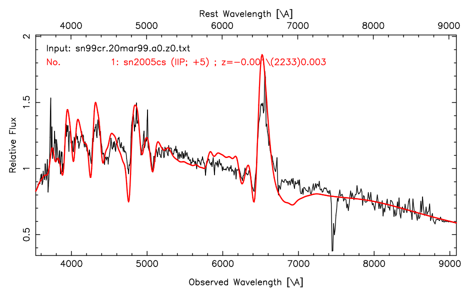

Figure B.14 Best spectral matching of SN 1999cr using SNID.

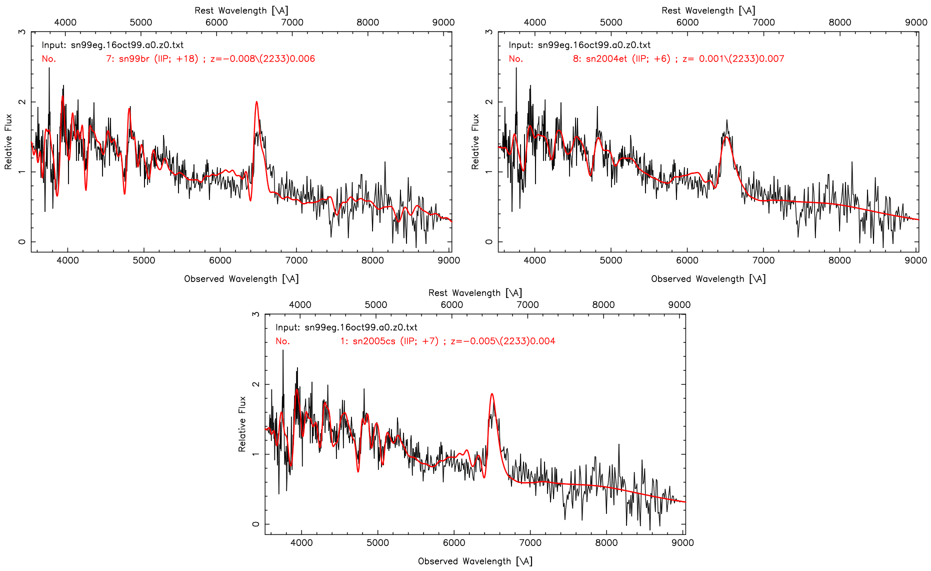

Figure B.15 Best spectral matching of SN 1999eg using SNID.

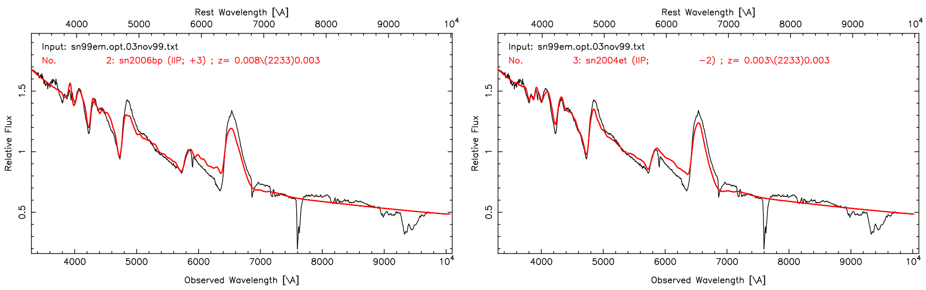

Figure B.16 Best spectral matching of SN 1999em using SNID.

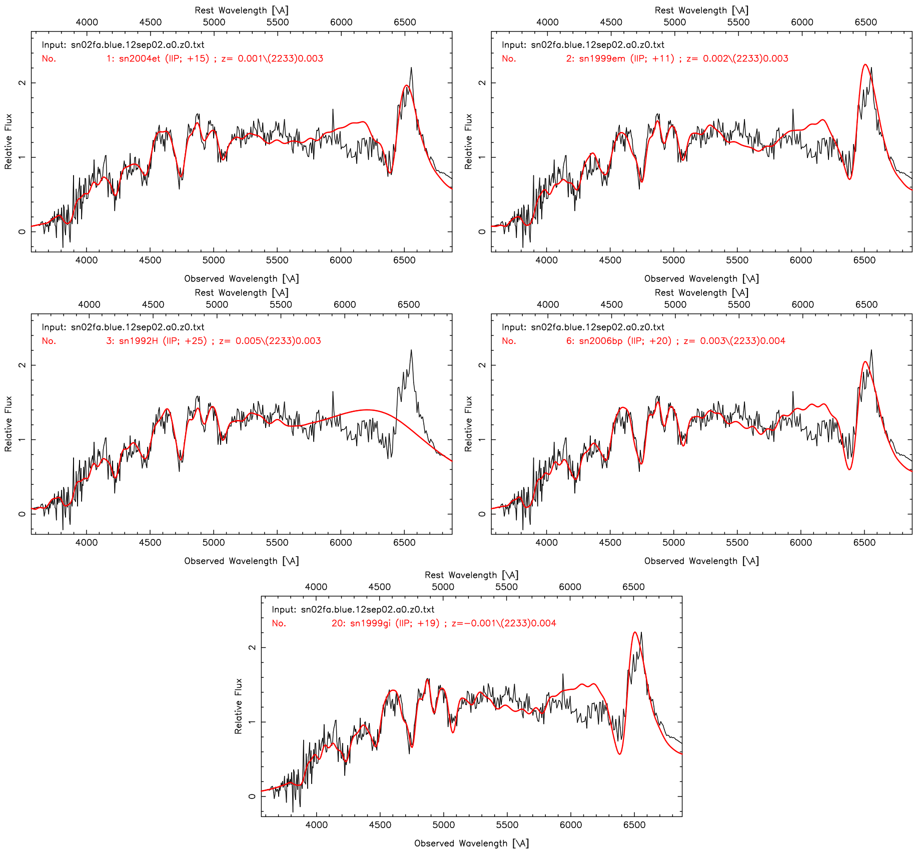

Figure B.17 Best spectral matching of SN 2002fa using SNID.

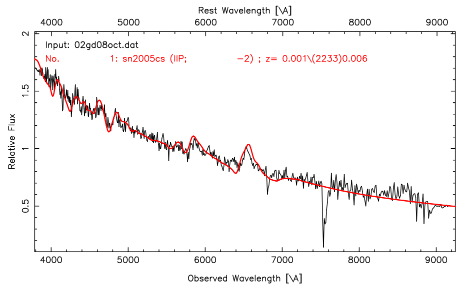

Figure B.18 Best spectral matching of SN 2002gd using SNID.

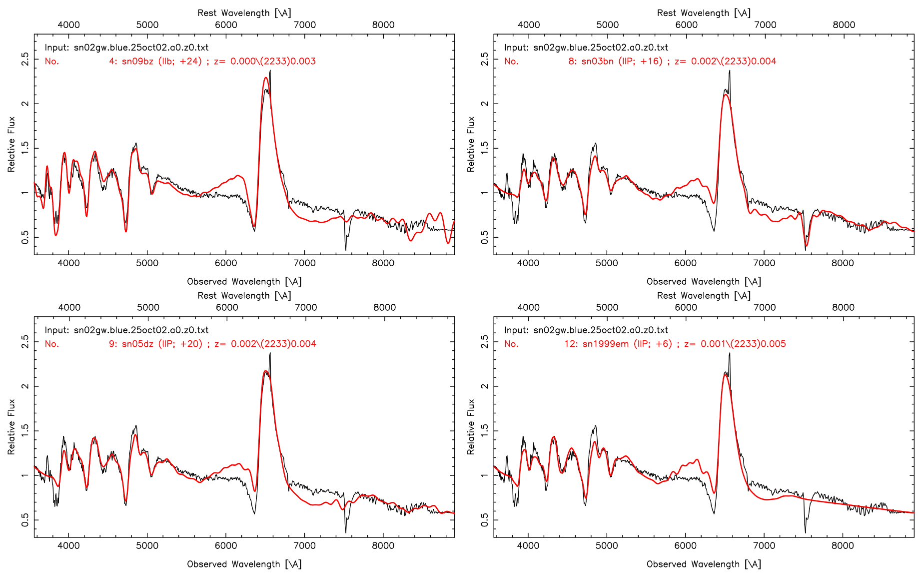

Figure B.19 Best spectral matching of SN 2002gw using SNID.

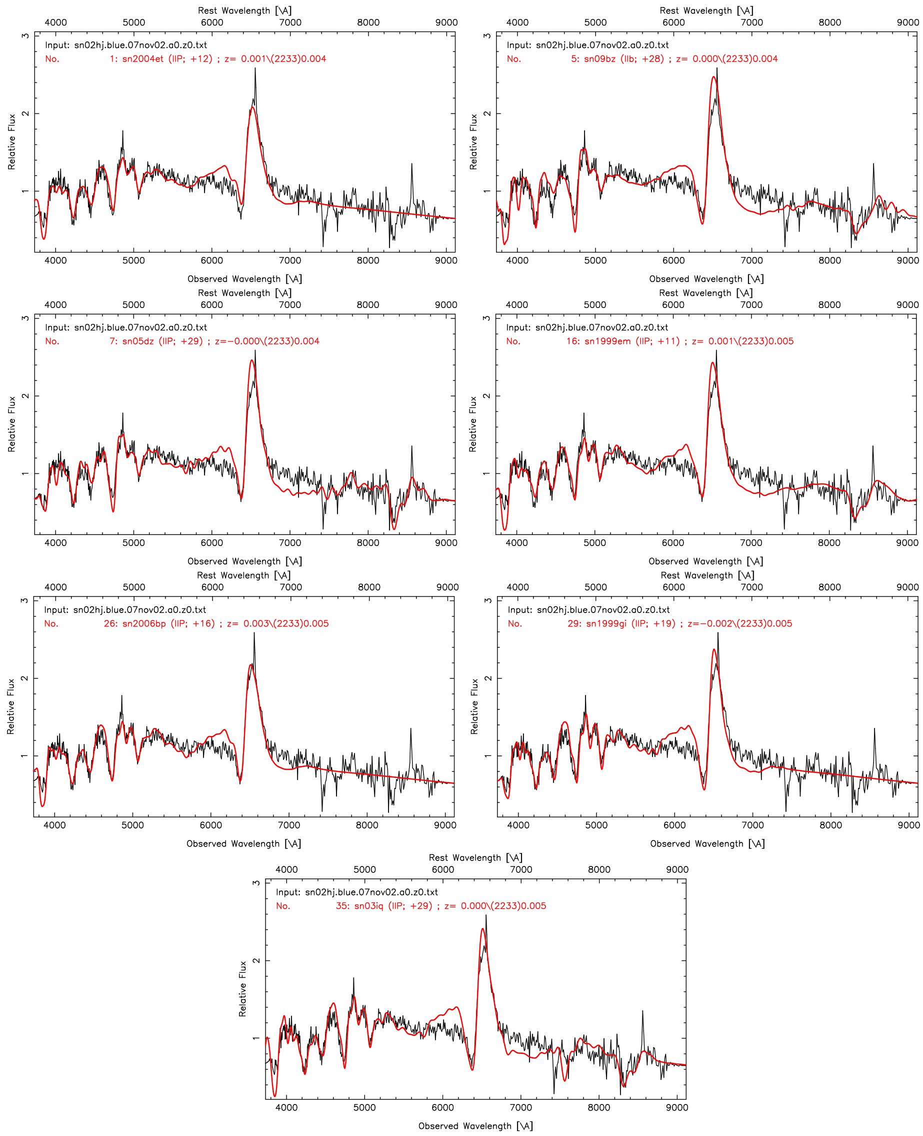

Figure B.20 Best spectral matching of SN 2002hj using SNID.

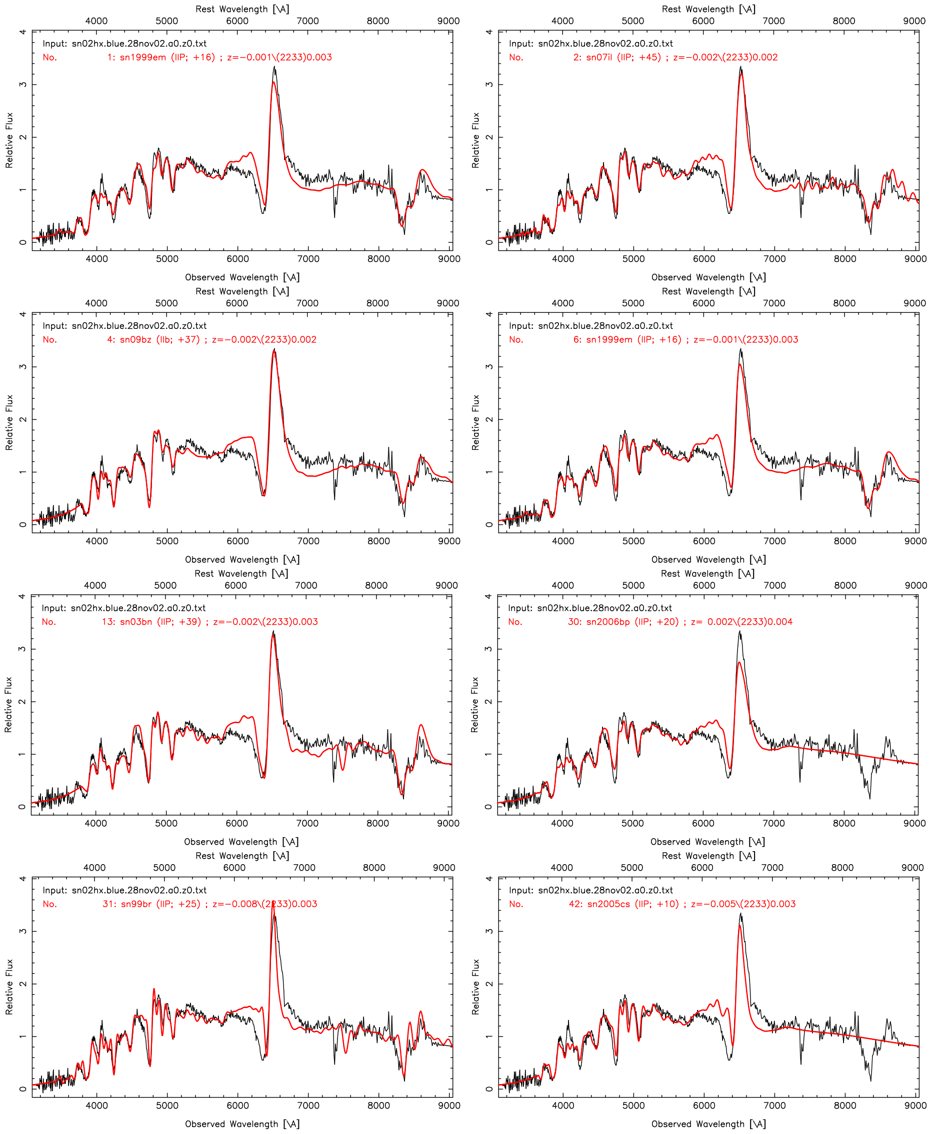

Figure B.21 Best spectral matching of SN 2002hx using SNID.

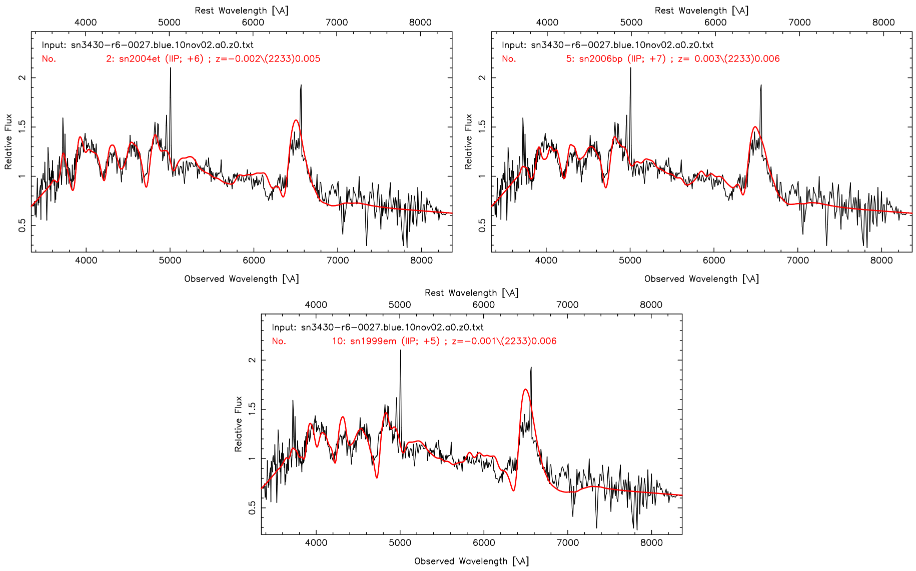

Figure B.22 Best spectral matching of SN 2002ig using SNID.

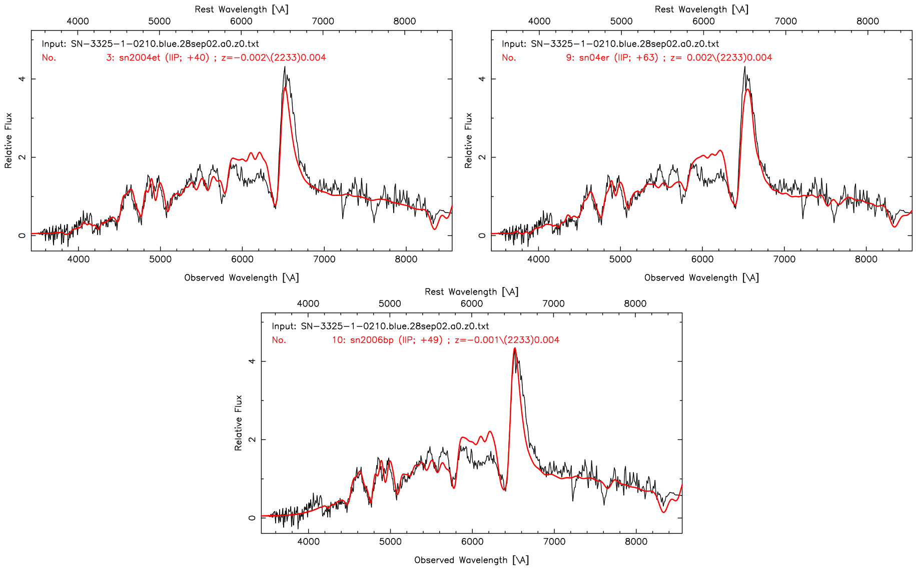

Figure B.23 Best spectral matching of SN 210 using SNID.

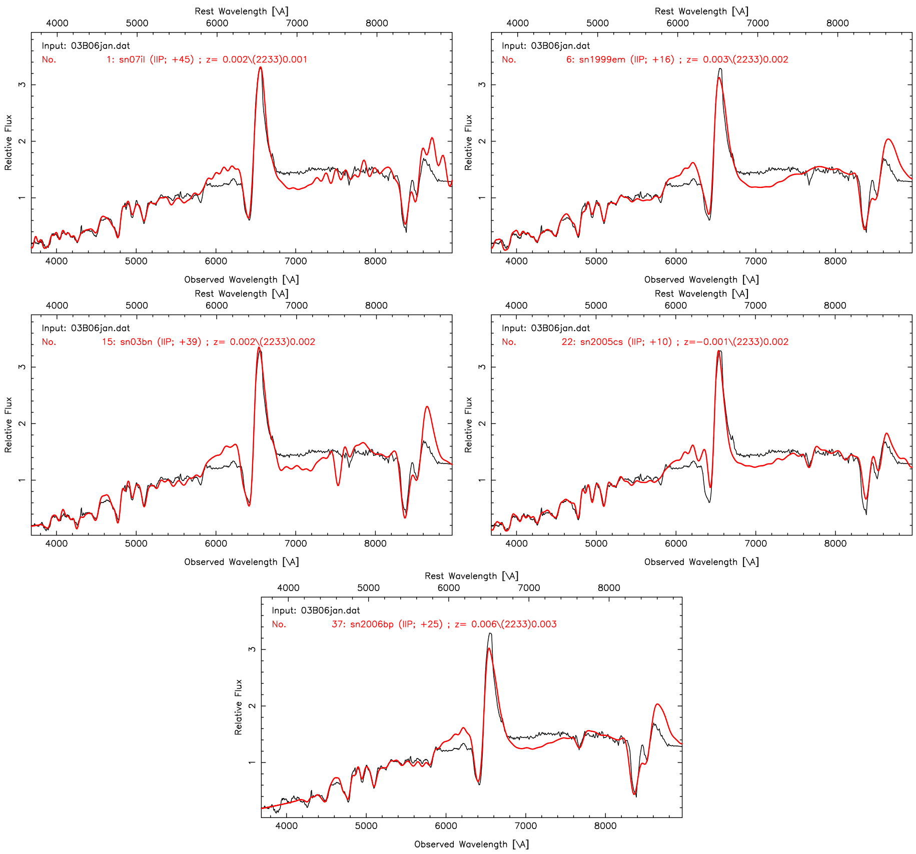

Figure B.24 Best spectral matching of SN 2003B using SNID.

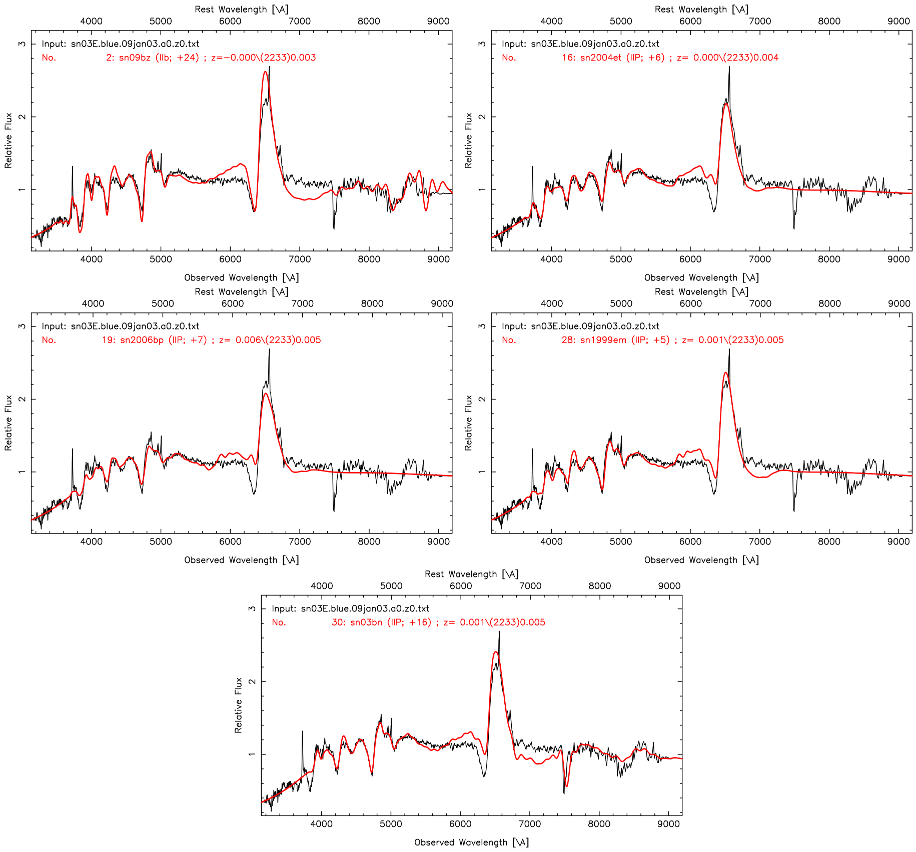

Figure B.25 Best spectral matching of SN 2003E using SNID.

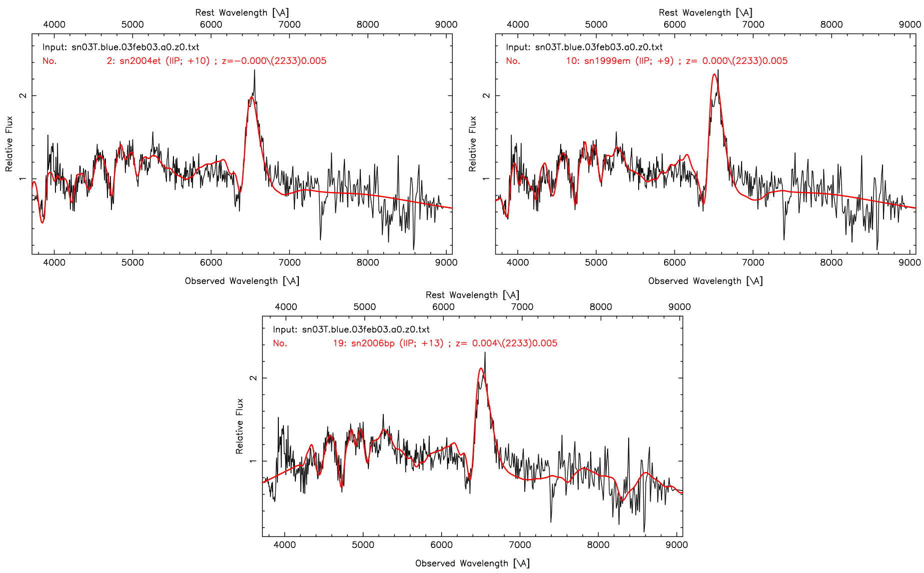

Figure B.26 Best spectral matching of SN 2003T using SNID.

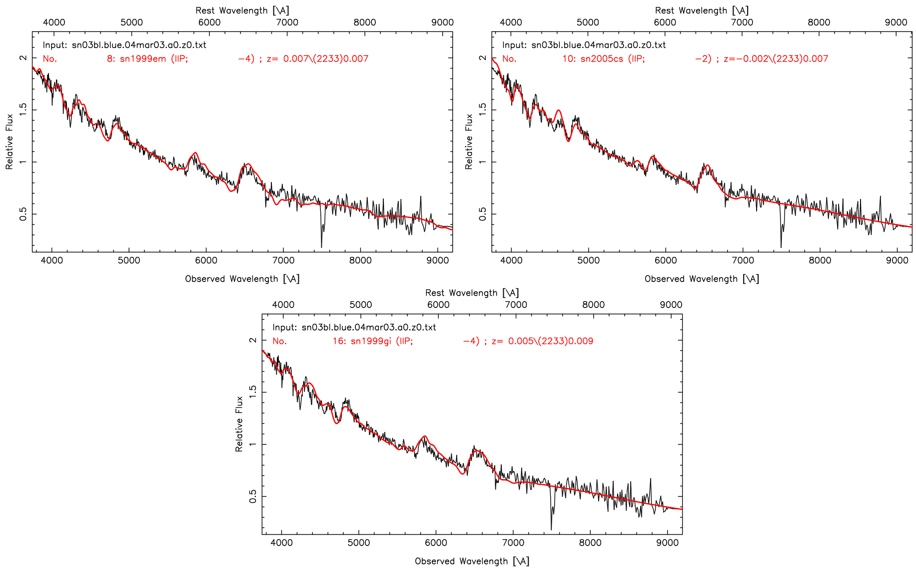

Figure B.27 Best spectral matching of SN 2003bl using SNID.

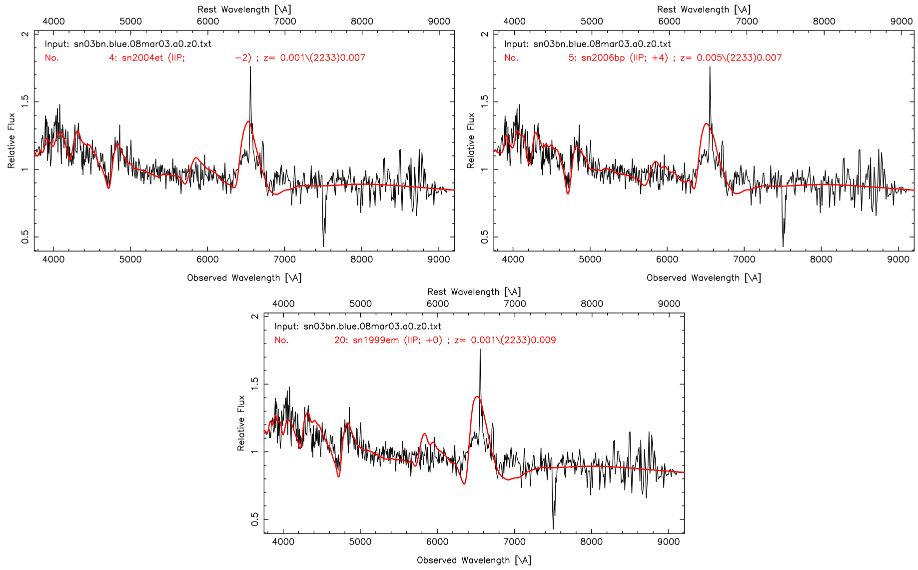

Figure B.28 Best spectral matching of SN 2003bn using SNID.

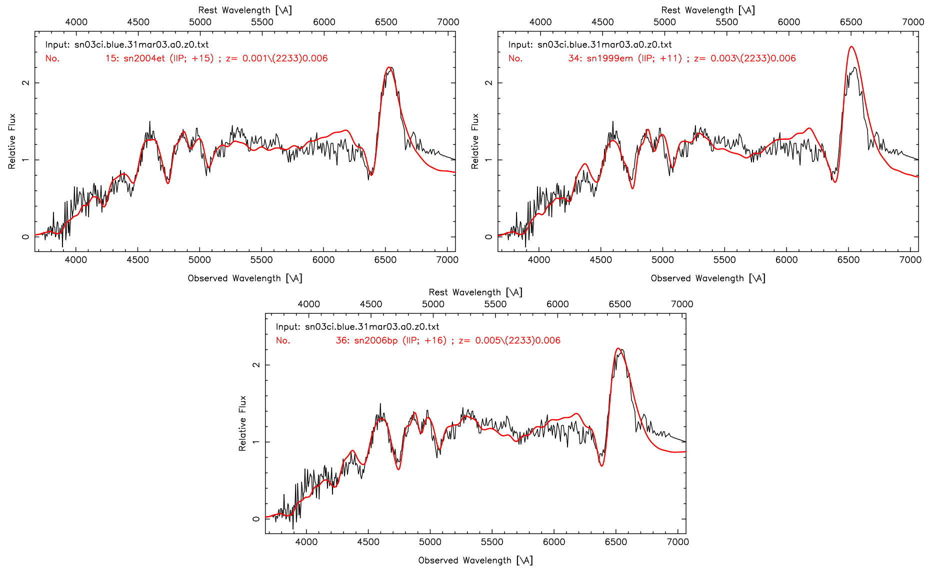

Figure B.29 Best spectral matching of SN 2003ci using SNID.

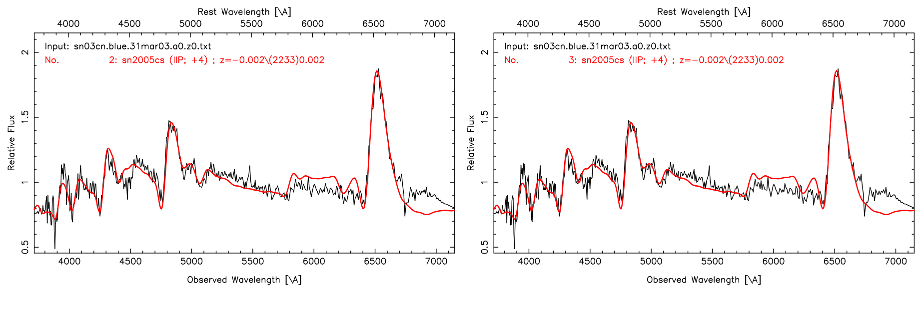

Figure B.30 Best spectral matching of SN 2003cn using SNID.

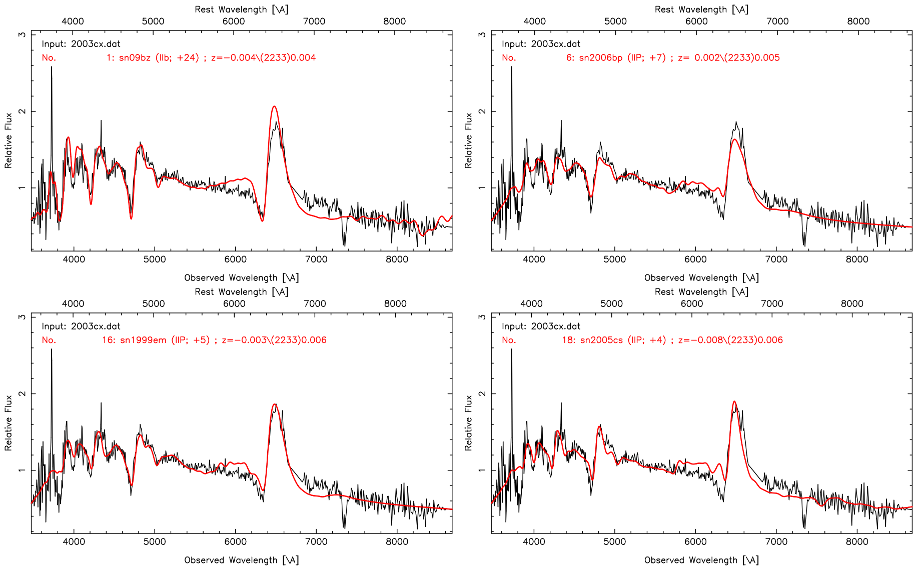

Figure B.31 Best spectral matching of SN 2003cx using SNID.

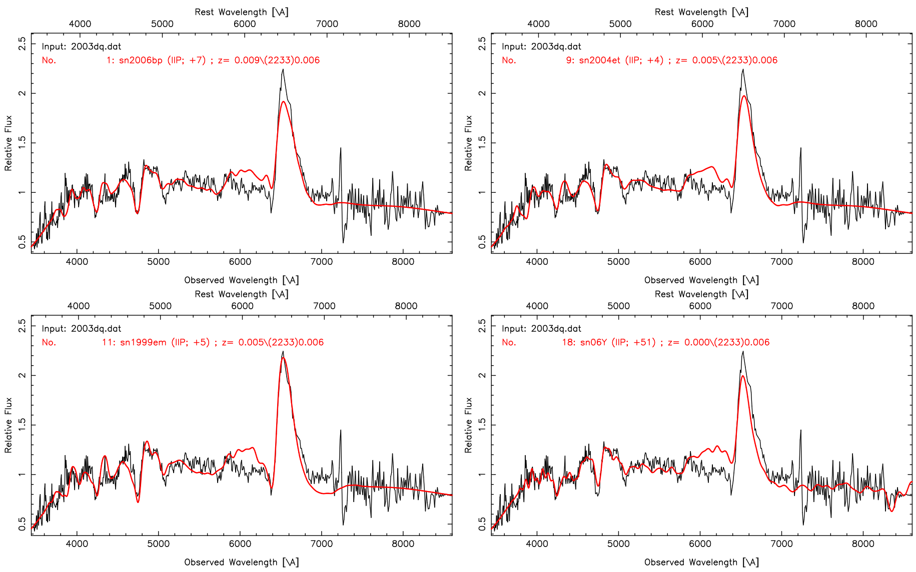

Figure B.32 Best spectral matching of SN 2003dq using SNID.

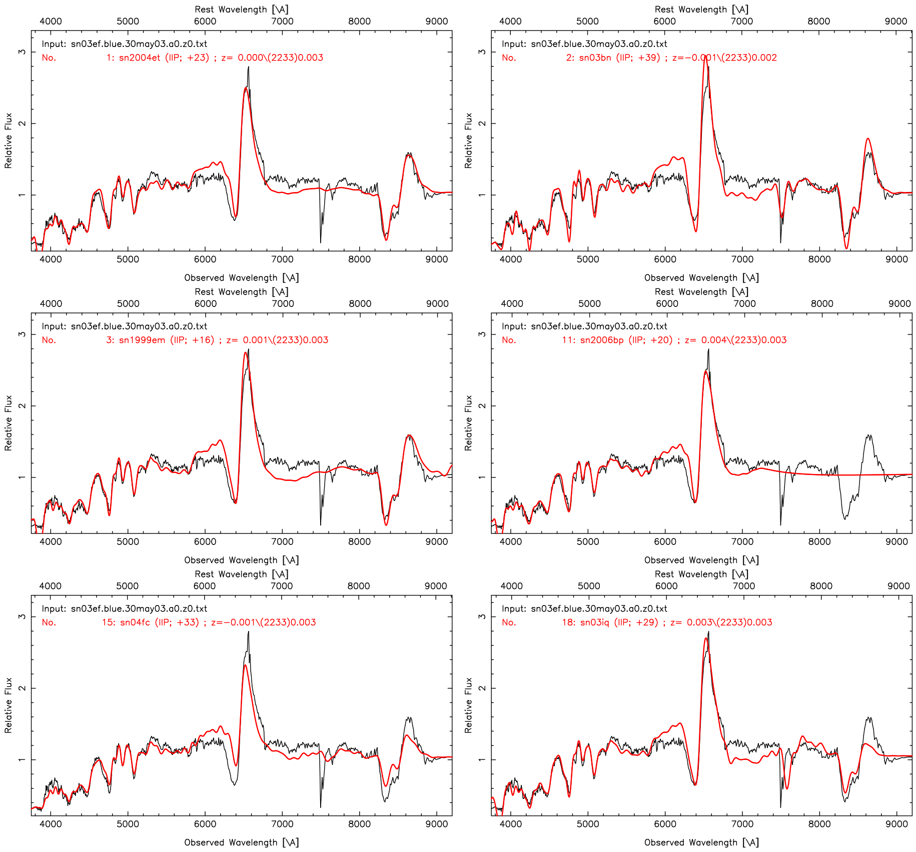

Figure B.33 Best spectral matching of SN 2003ef using SNID.

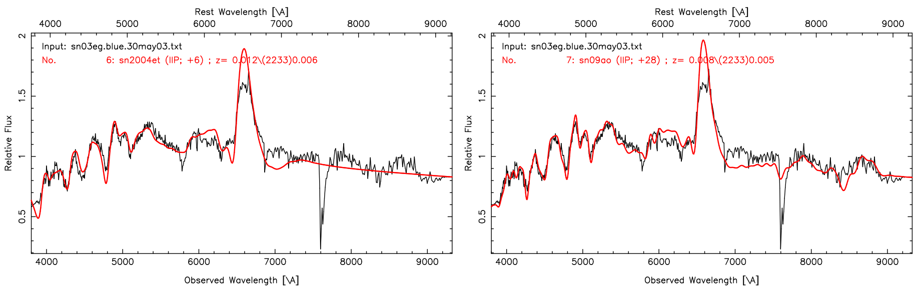

Figure B.34 Best spectral matching of SN 2003eg using SNID.

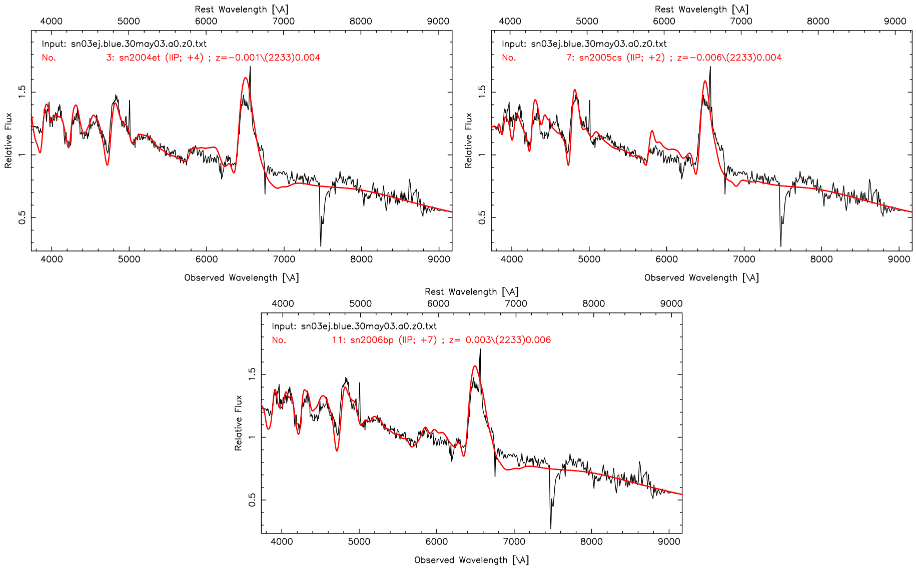

Figure B.35 Best spectral matching of SN 2003ej using SNID.

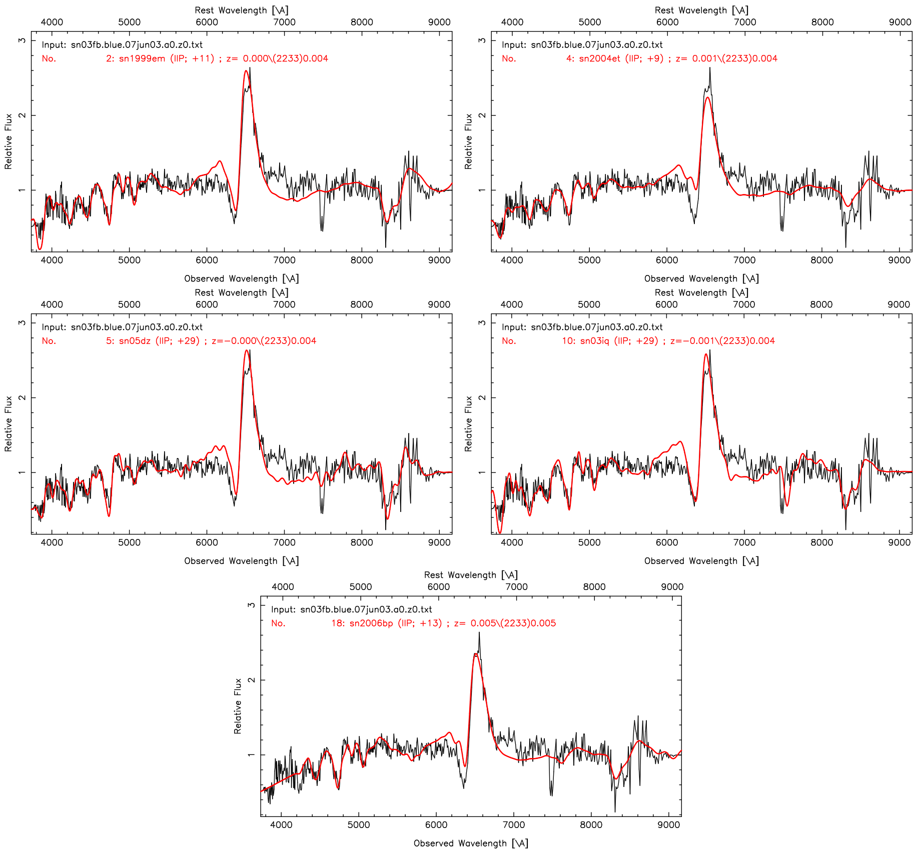

Figure B.36 Best spectral matching of SN 2003fb using SNID.

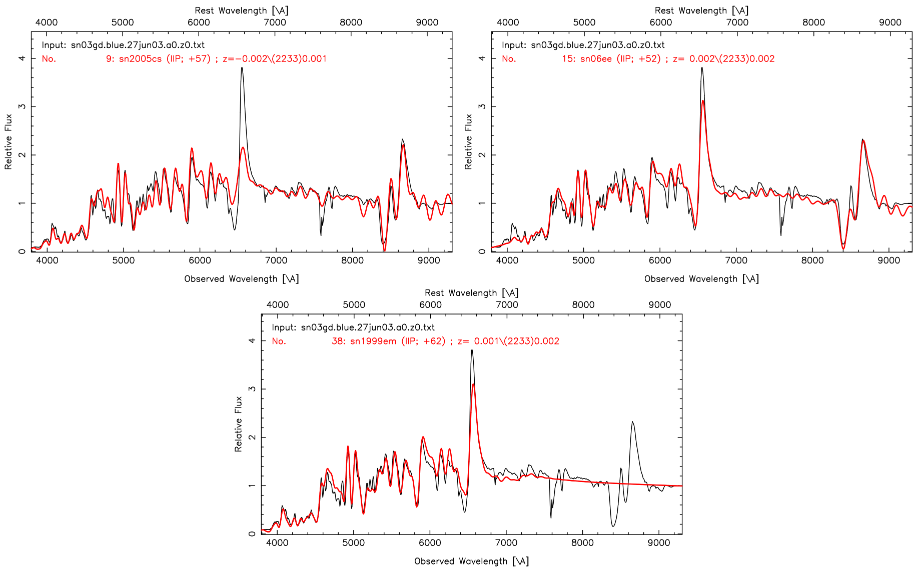

Figure B.37 Best spectral matching of SN 2003gd using SNID.

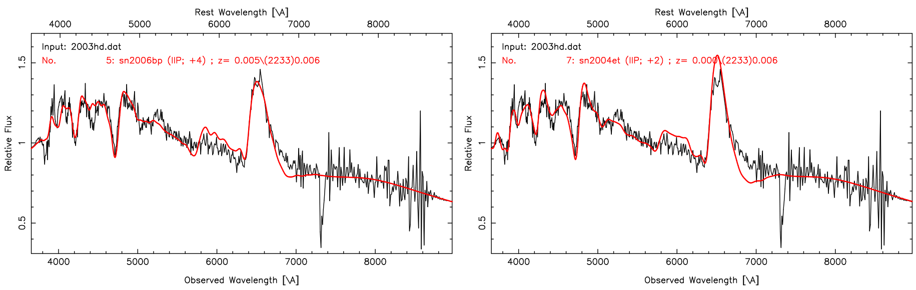

Figure B.38 Best spectral matching of SN 2003hd using SNID.

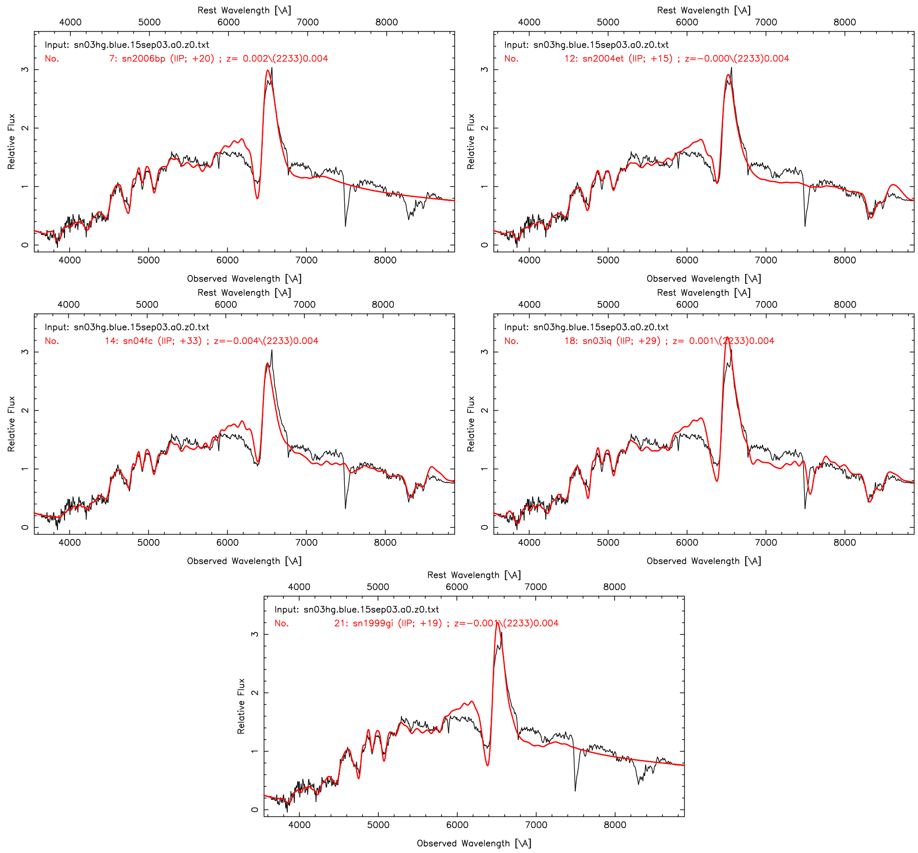

Figure B.39 Best spectral matching of SN 2003hg using SNID.

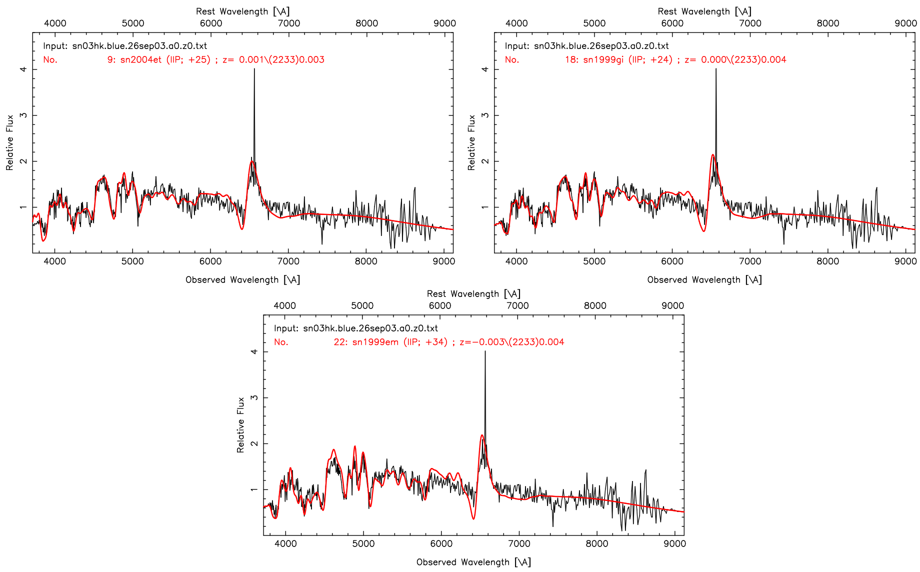

Figure B.40 Best spectral matching of SN 2003hk using SNID.

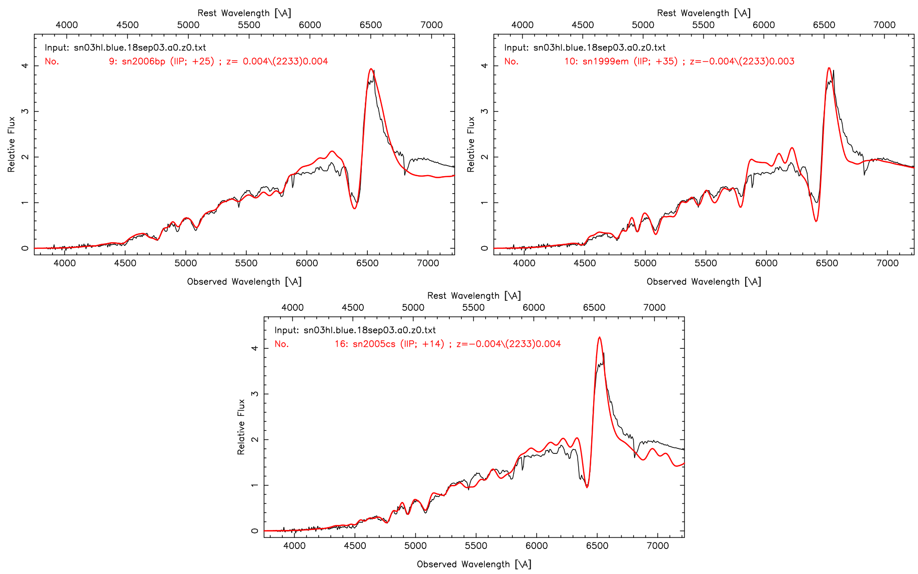

Figure B.41 Best spectral matching of SN 2003hl using SNID.

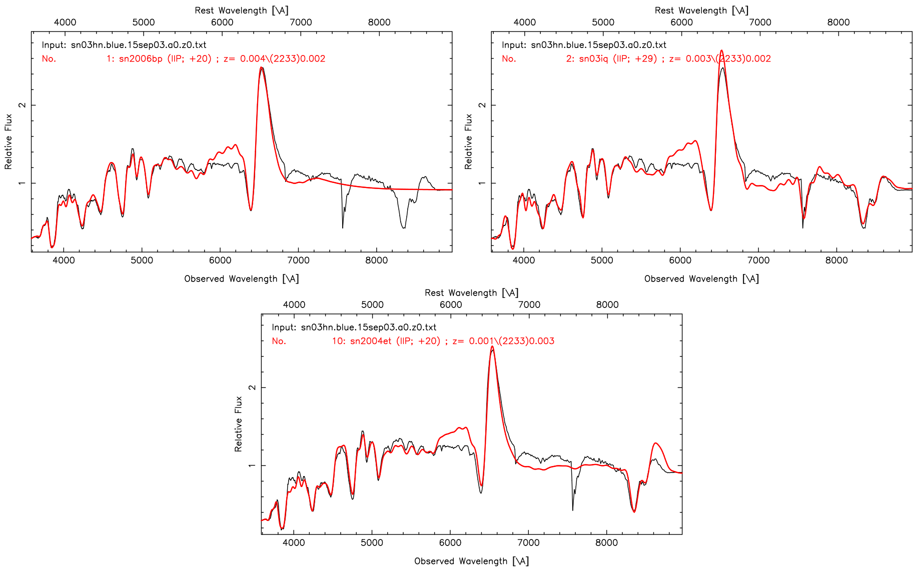

Figure B.42 Best spectral matching of SN 2003hn using SNID.

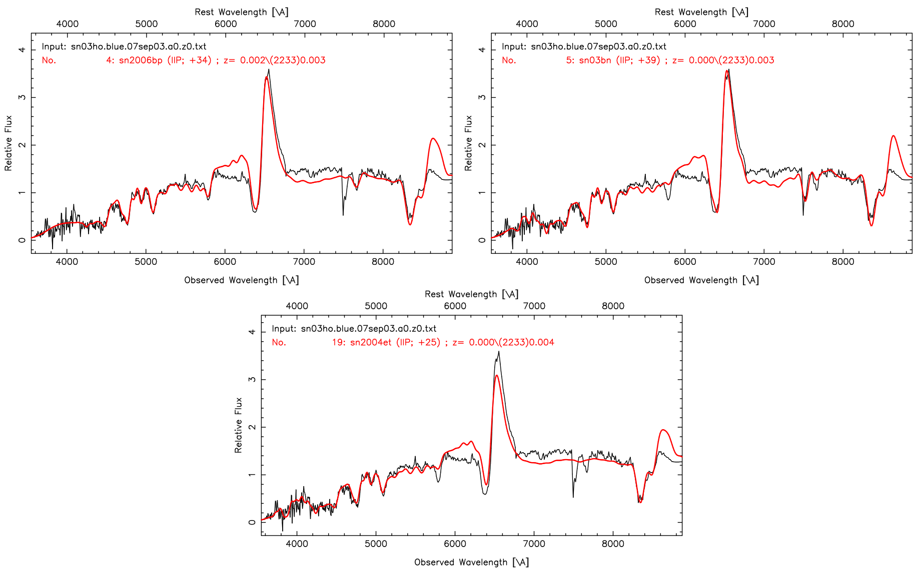

Figure B.43 Best spectral matching of SN 2003ho using SNID.

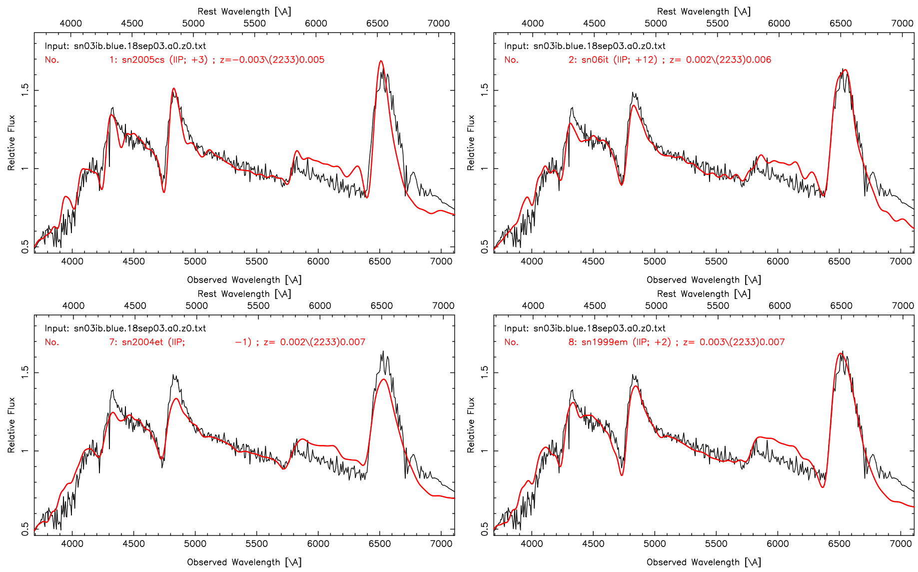

Figure B.44 Best spectral matching of SN 2003ib using SNID.

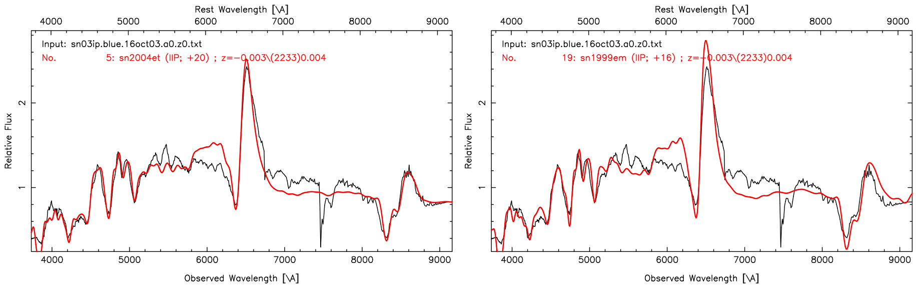

Figure B.45 Best spectral matching of SN 2003ip using SNID.

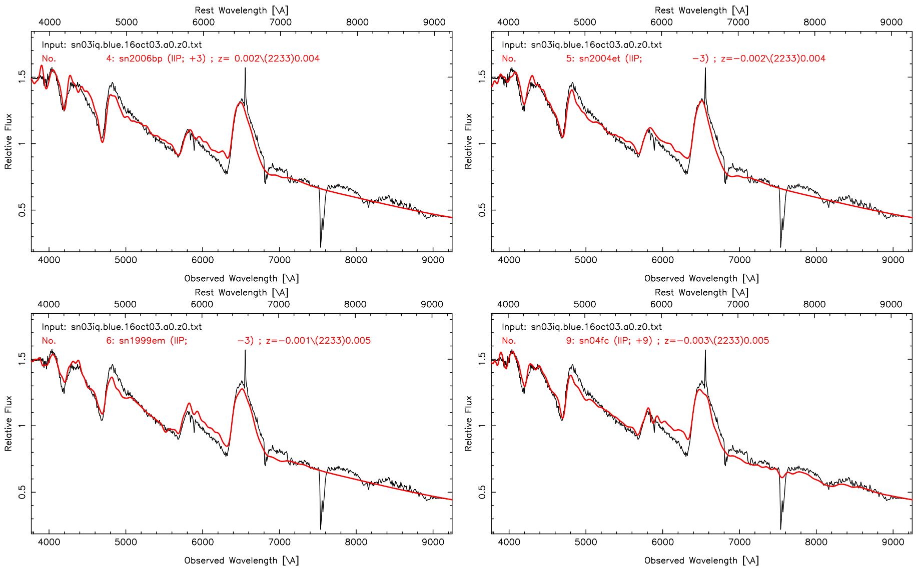

Figure B.46 Best spectral matching of SN 2003iq using SNID.

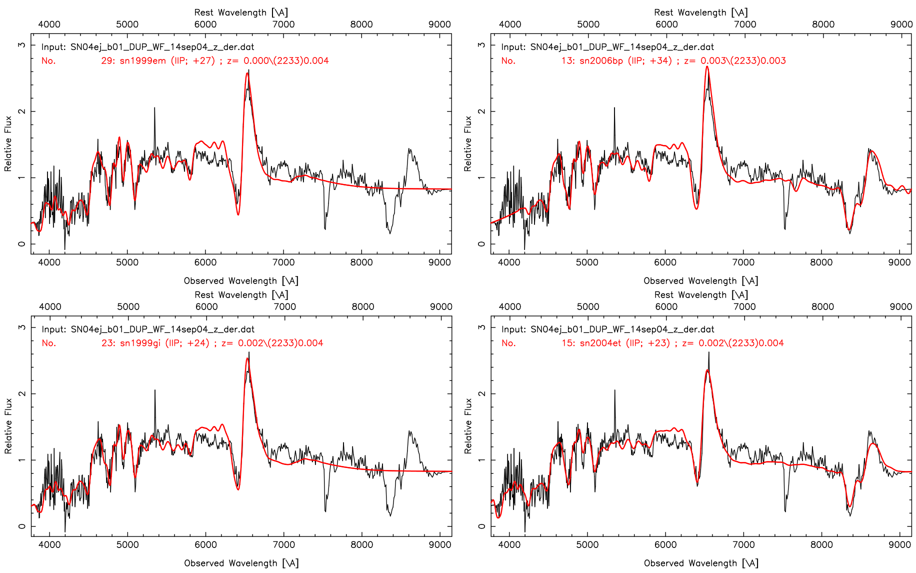

Figure B.47 Best spectral matching of SN 2004ej using SNID.

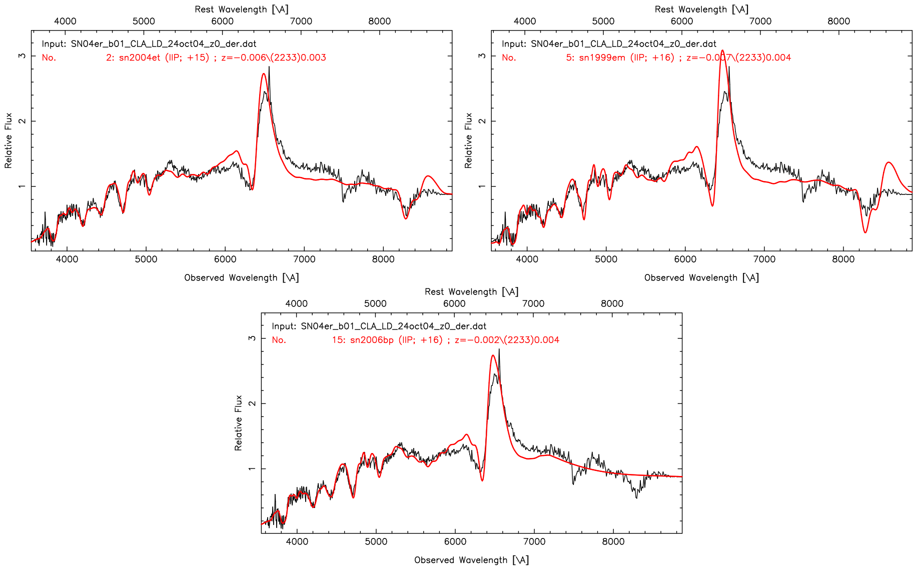

Figure B.48 Best spectral matching of SN 2004er using SNID.

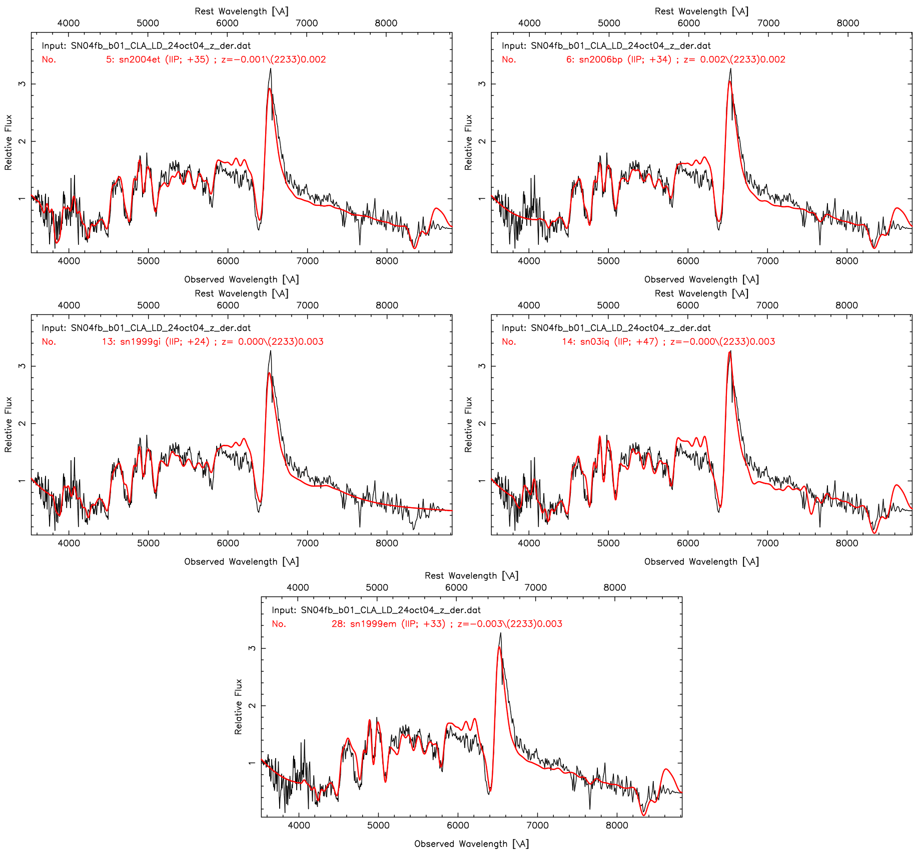

Figure B.49 Best spectral matching of SN 2004fb using SNID.

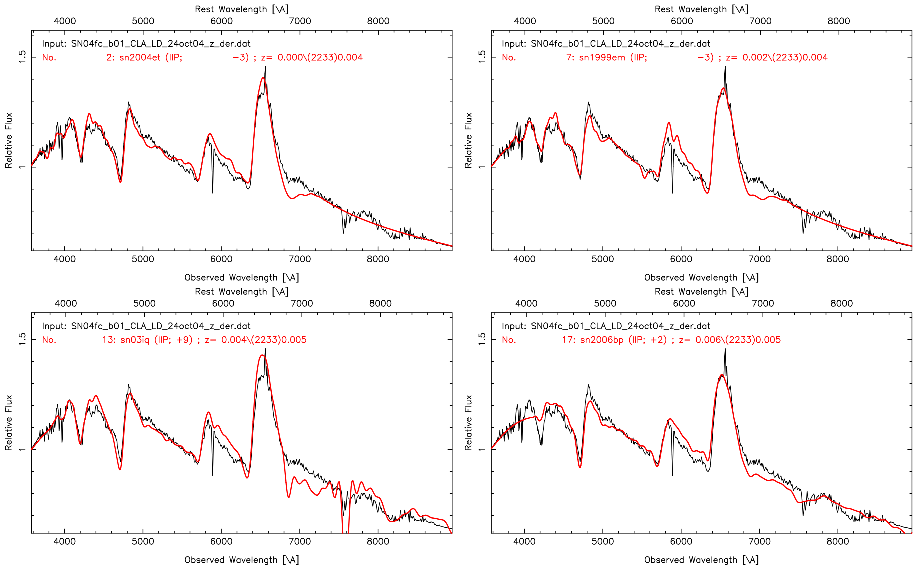

Figure B.50 Best spectral matching of SN 2004fc using SNID.

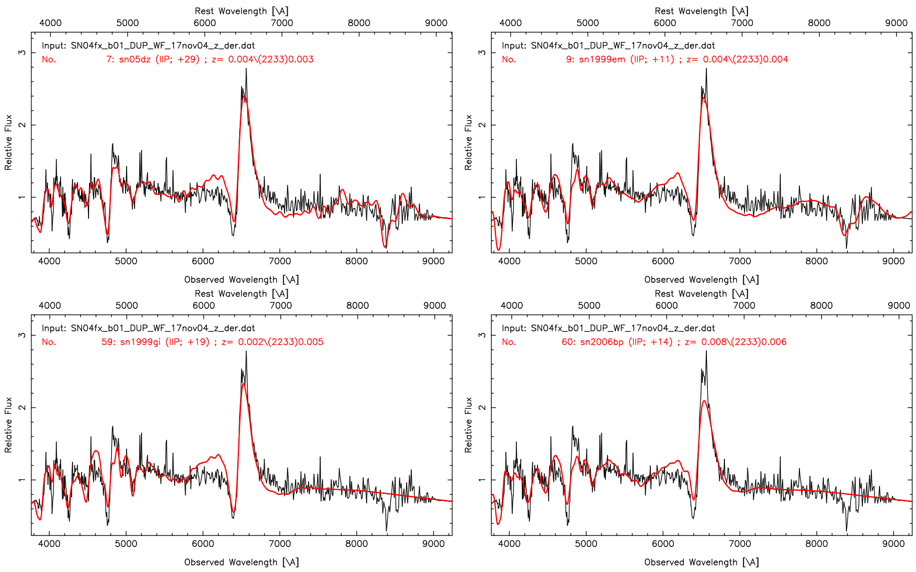

Figure B.51 Best spectral matching of SN 2004fx using SNID.

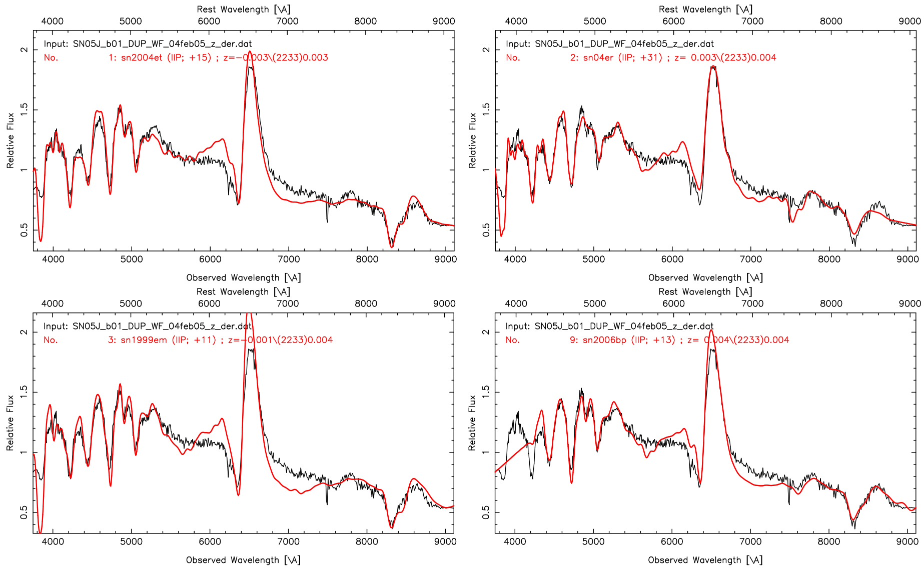

Figure B.52 Best spectral matching of SN 2005J using SNID.

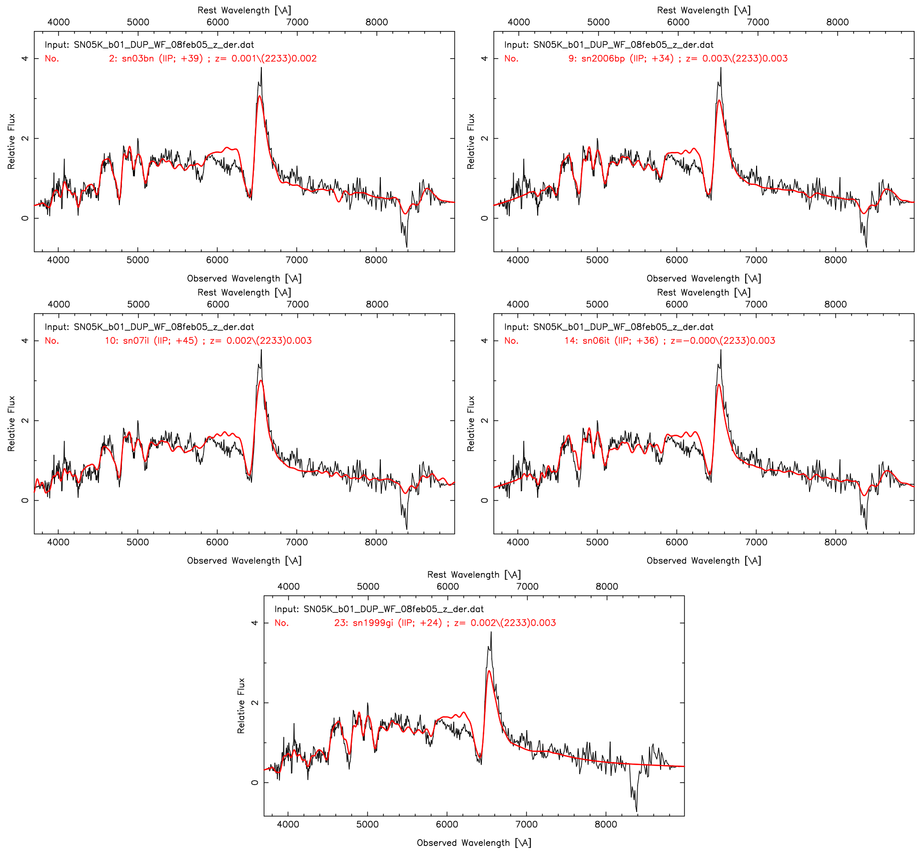

Figure B.53 Best spectral matching of SN 2005K using SNID.

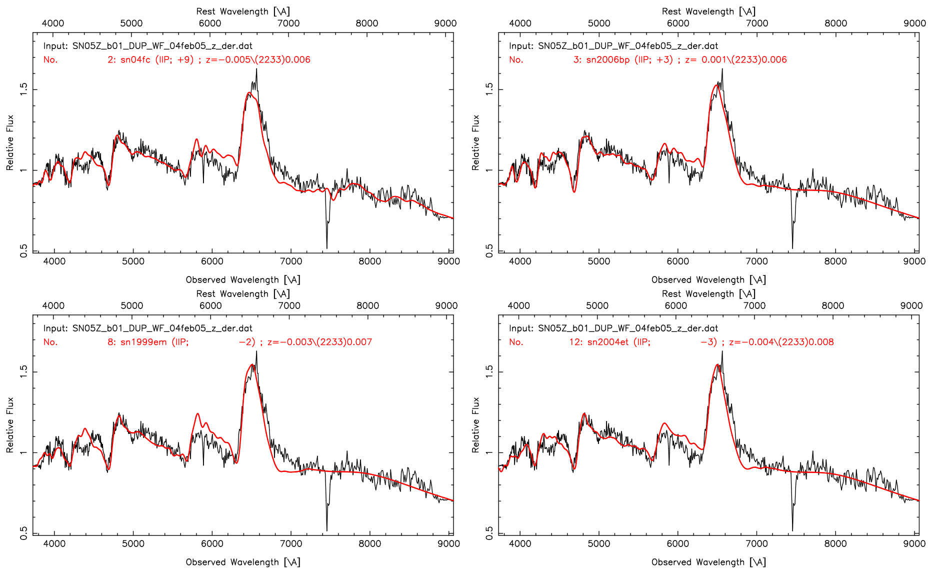

Figure B.54 Best spectral matching of SN 2005Z using SNID.

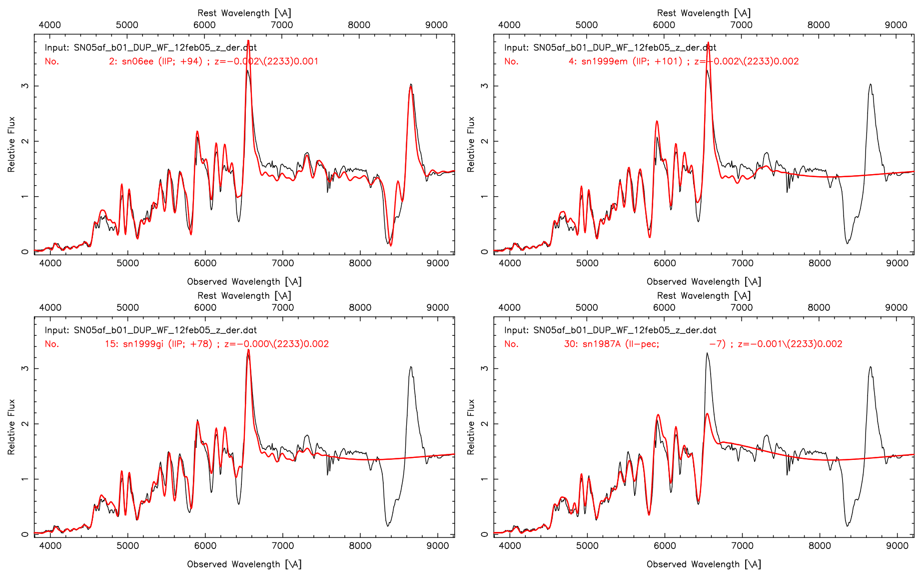

Figure B.55 Best spectral matching of SN 2005af using SNID.

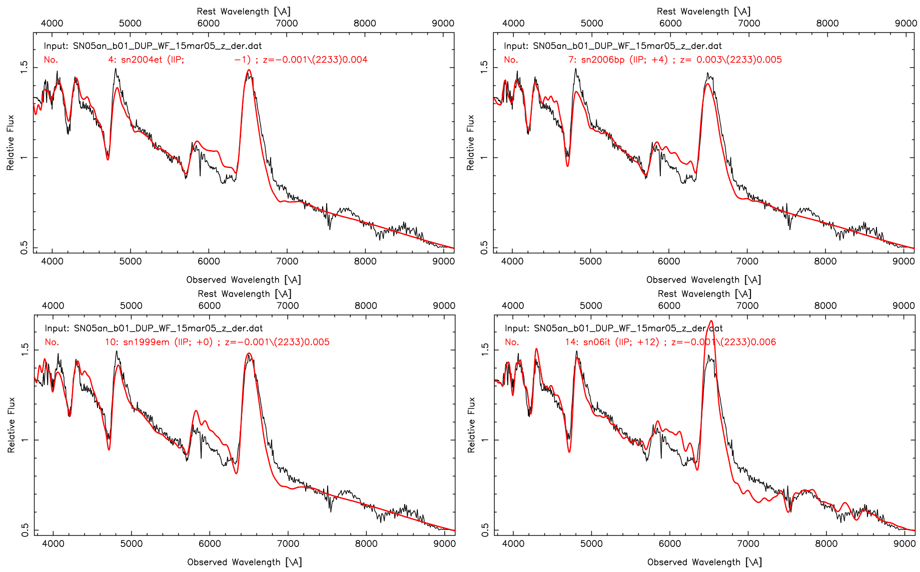

Figure B.56 Best spectral matching of SN 2005an using SNID.

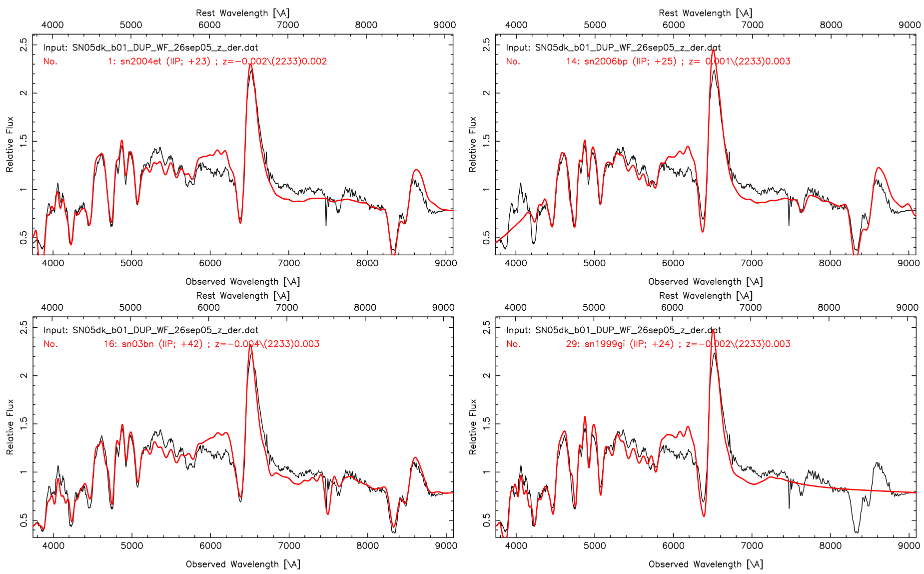

Figure B.57 Best spectral matching of SN 2005dk using SNID.

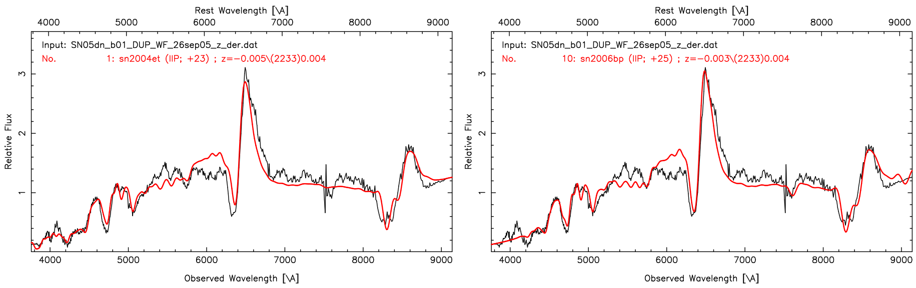

Figure B.58 Best spectral matching of SN 2005dn using SNID.

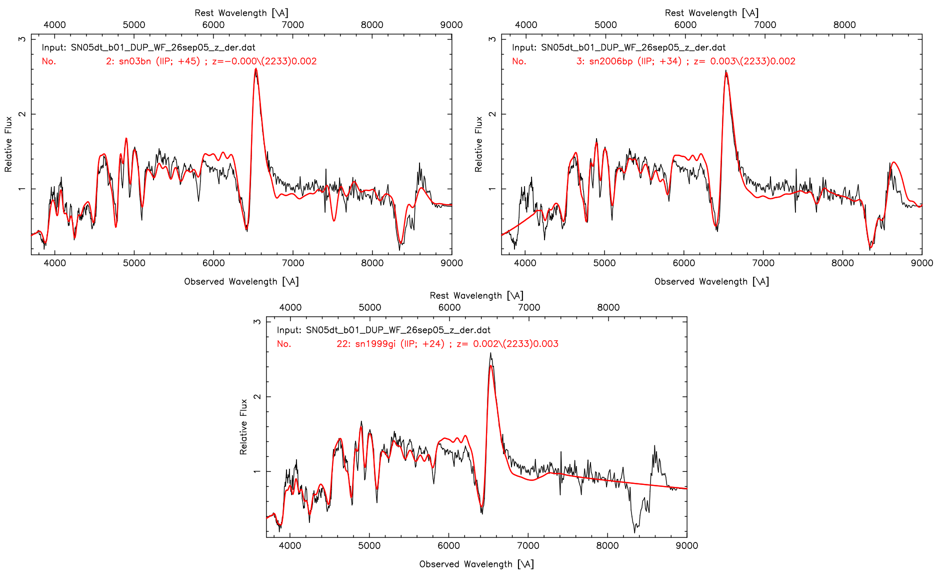

Figure B.59 Best spectral matching of SN 2005dt using SNID.

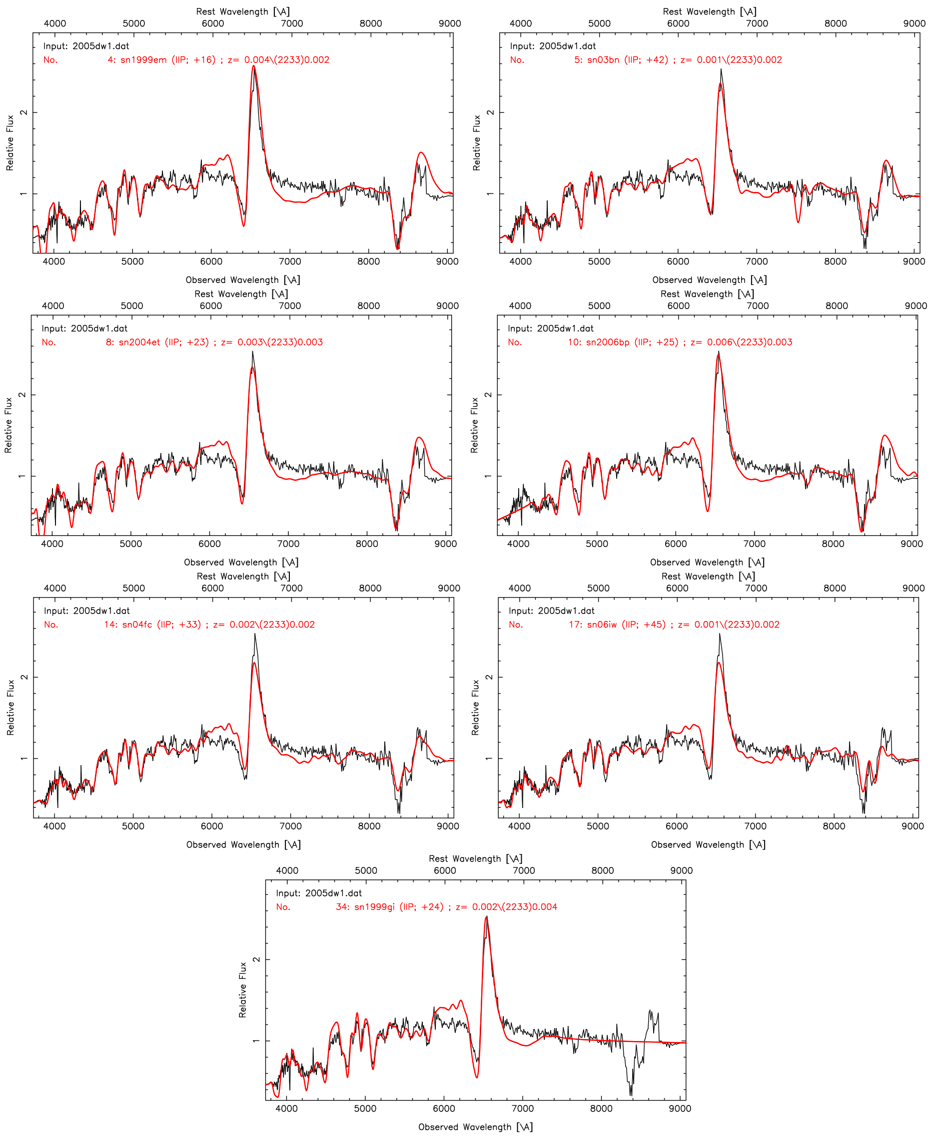

Figure B.60 Best spectral matching of SN 2005dw using SNID.

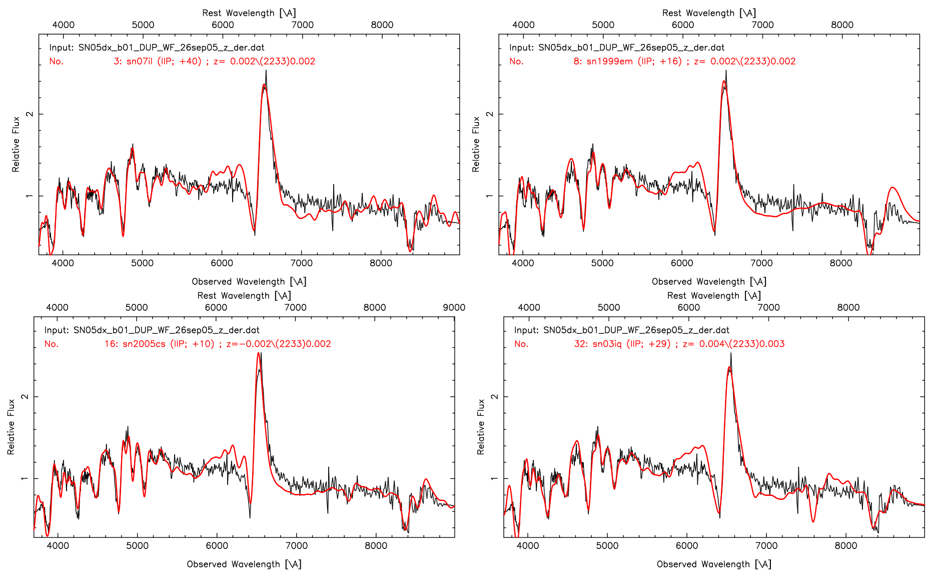

Figure B.61 Best spectral matching of SN 2005dx using SNID.

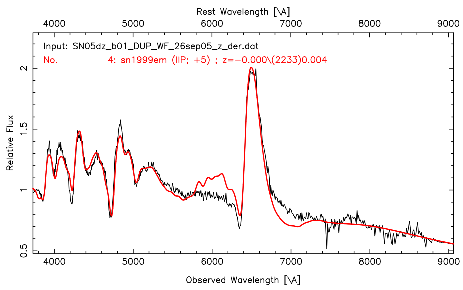

Figure B.62 Best spectral matching of SN 2005dz using SNID.

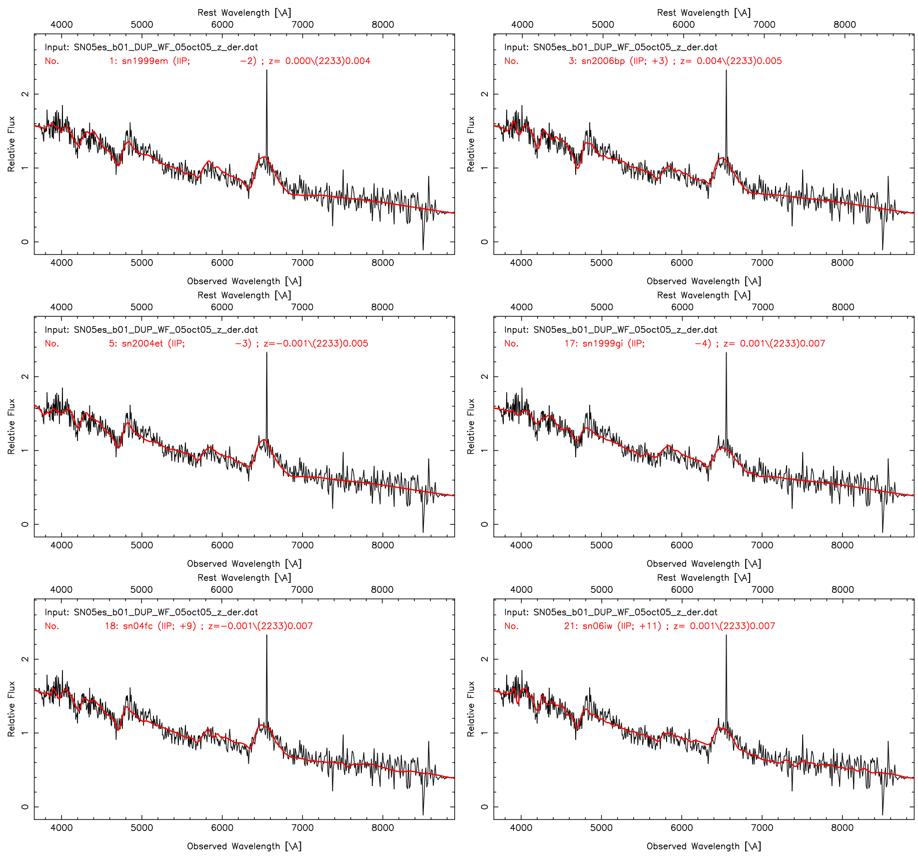

Figure B.63 Best spectral matching of SN 2005es using SNID.

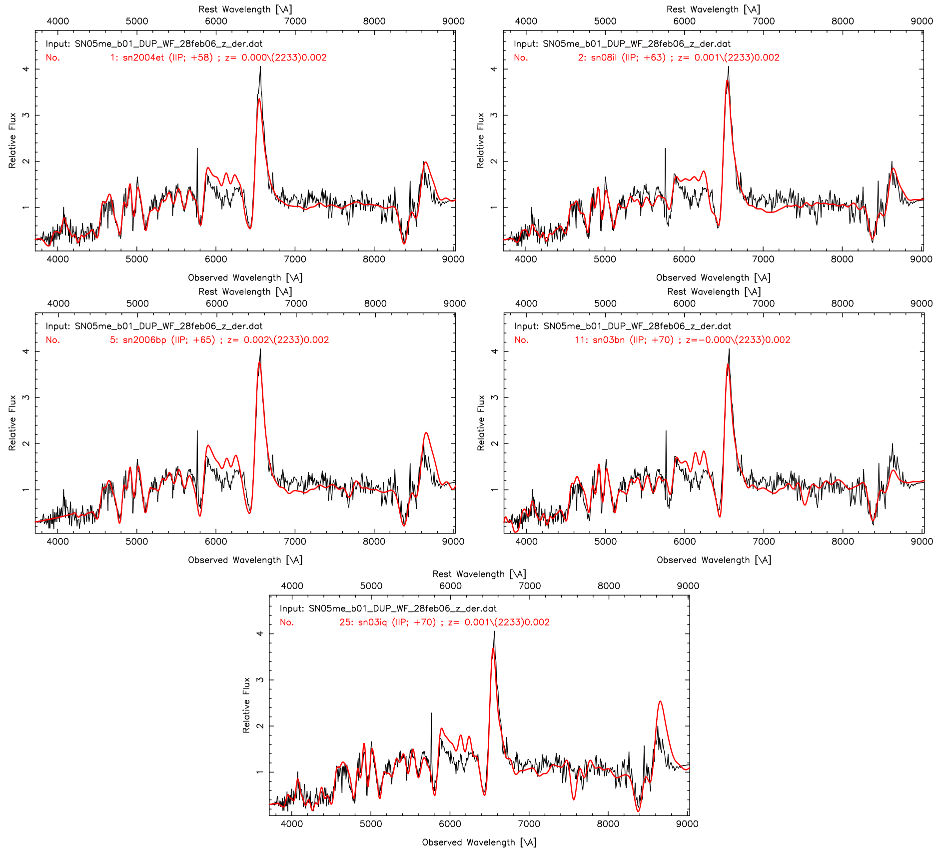

Figure B.64 Best spectral matching of SN 2005me using SNID.

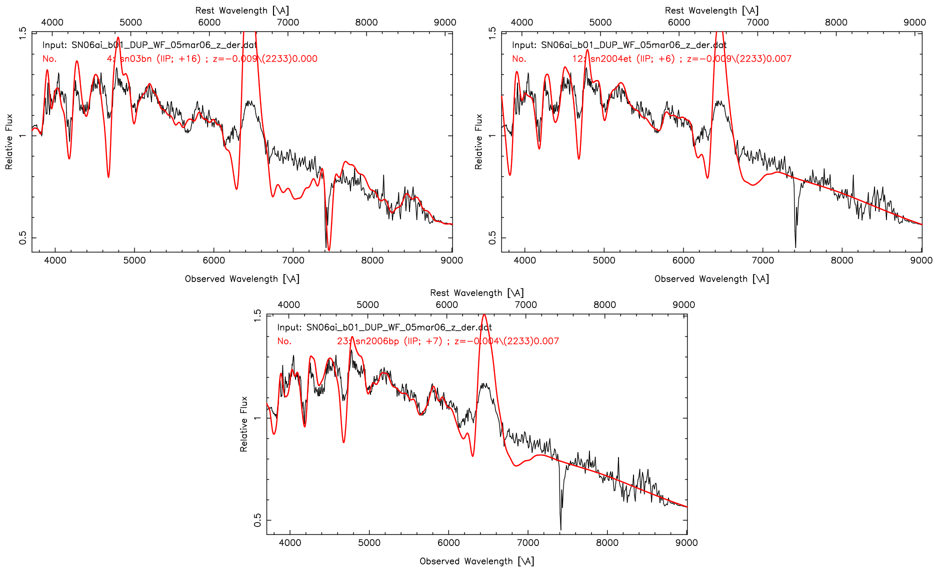

Figure B.65 Best spectral matching of SN 2006ai using SNID.

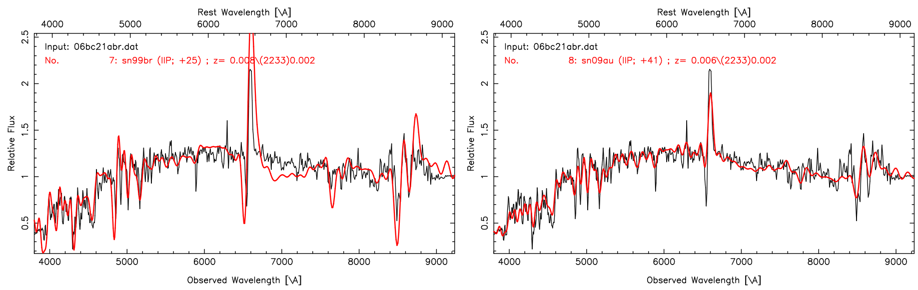

Figure B.66 Best spectral matching of SN 2006bc using SNID.

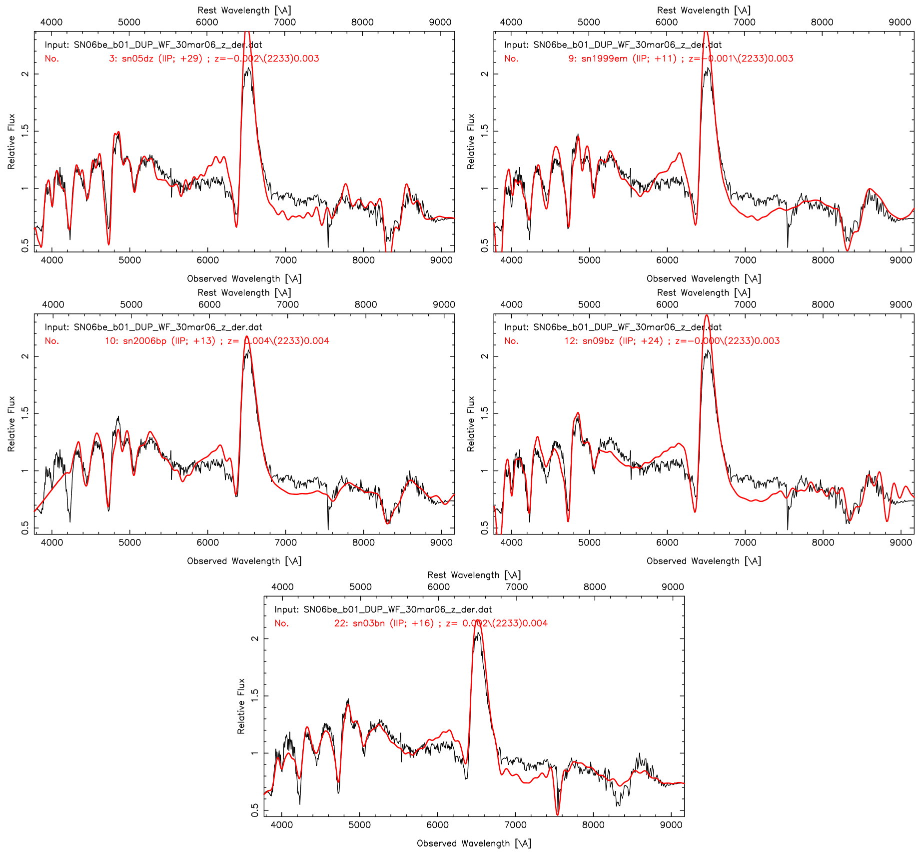

Figure B.67 Best spectral matching of SN 2006be using SNID.

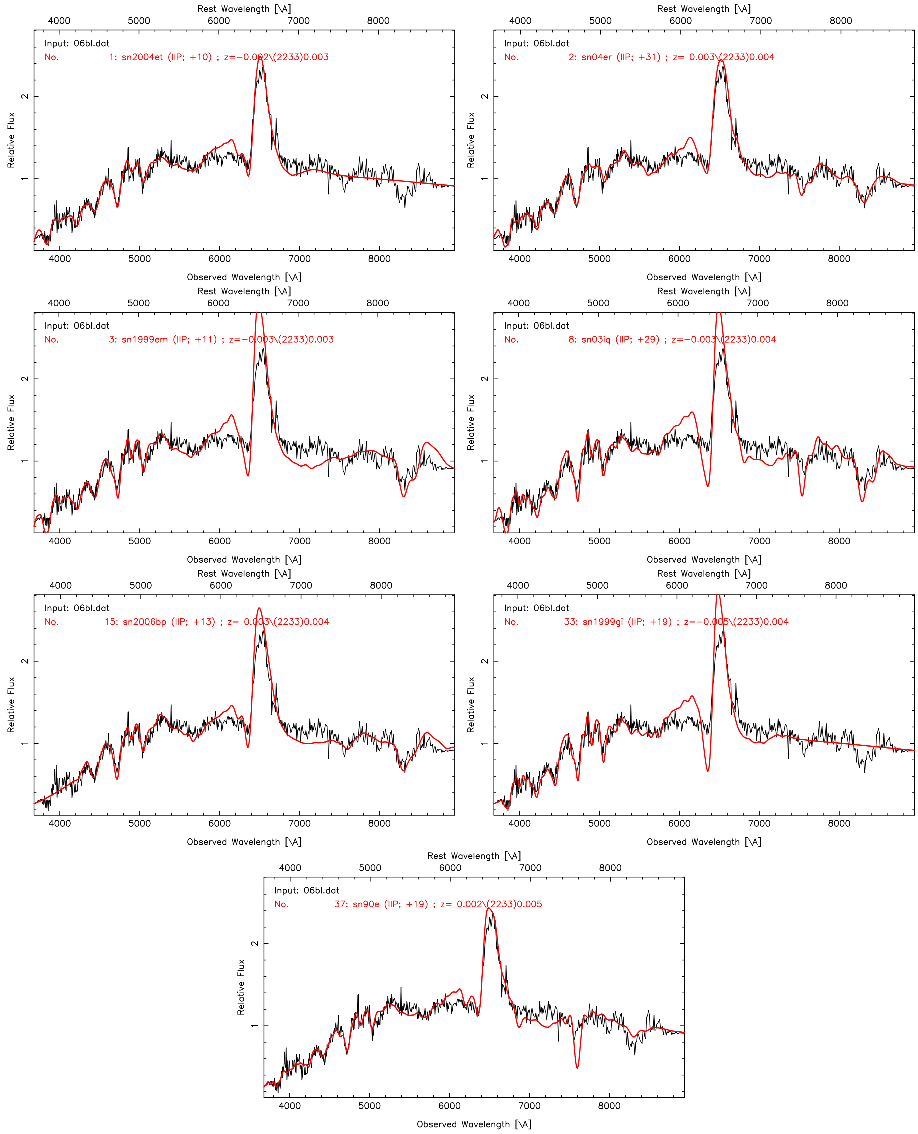

Figure B.68 Best spectral matching of SN 2006bl using SNID.

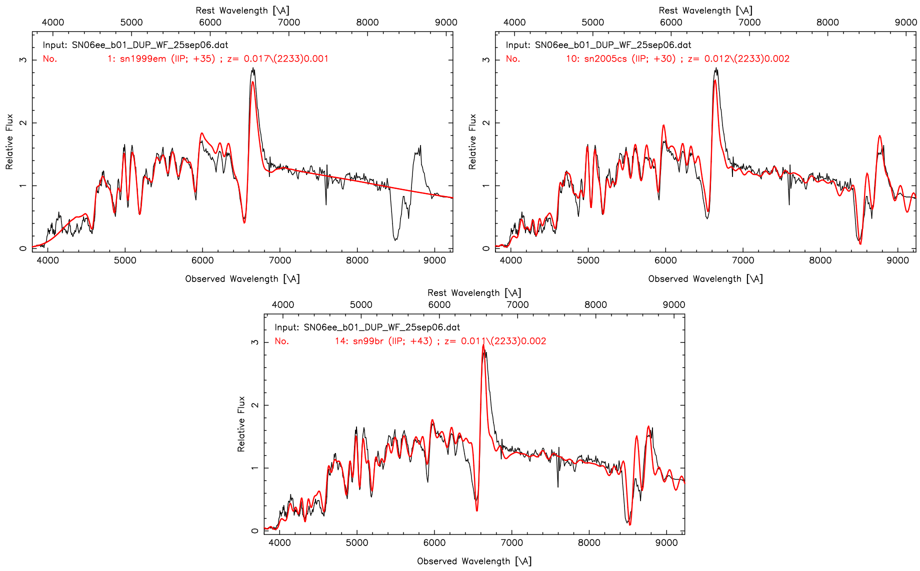

Figure B.69 Best spectral matching of SN 2006ee using SNID.

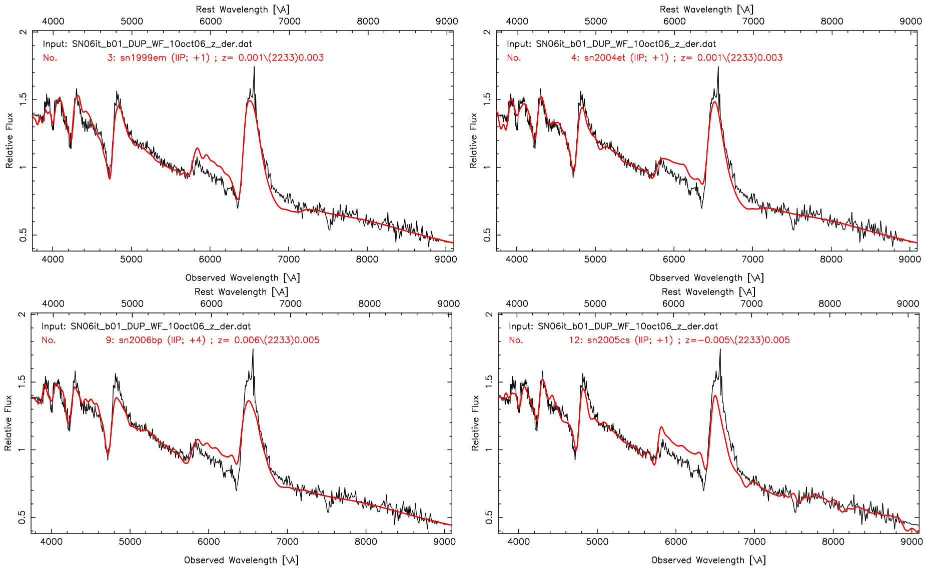

Figure B.70 Best spectral matching of SN 2006it using SNID.

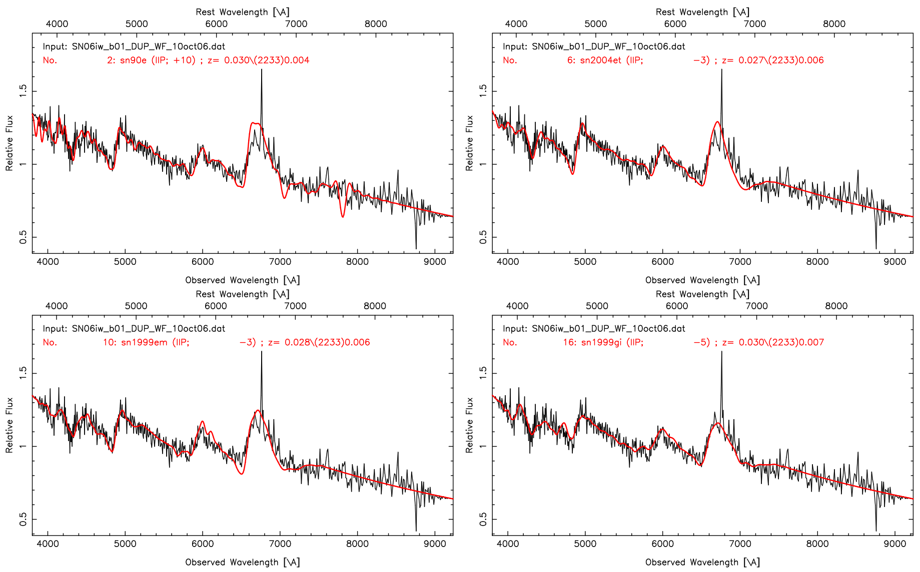

Figure B.71 Best spectral matching of SN 2006iw using SNID.

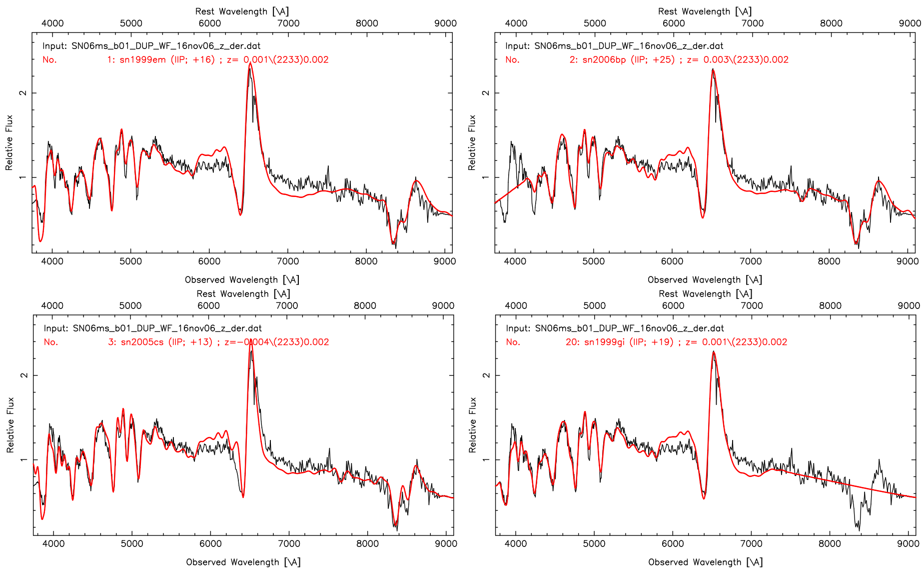

Figure B.72 Best spectral matching of SN 2006ms using SNID.

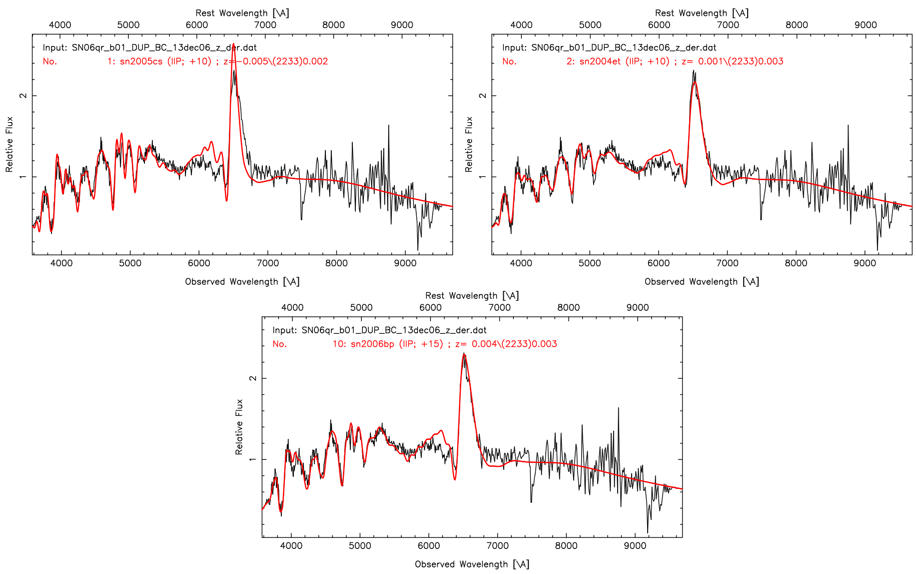

Figure B.73 Best spectral matching of SN 2006qr using SNID.

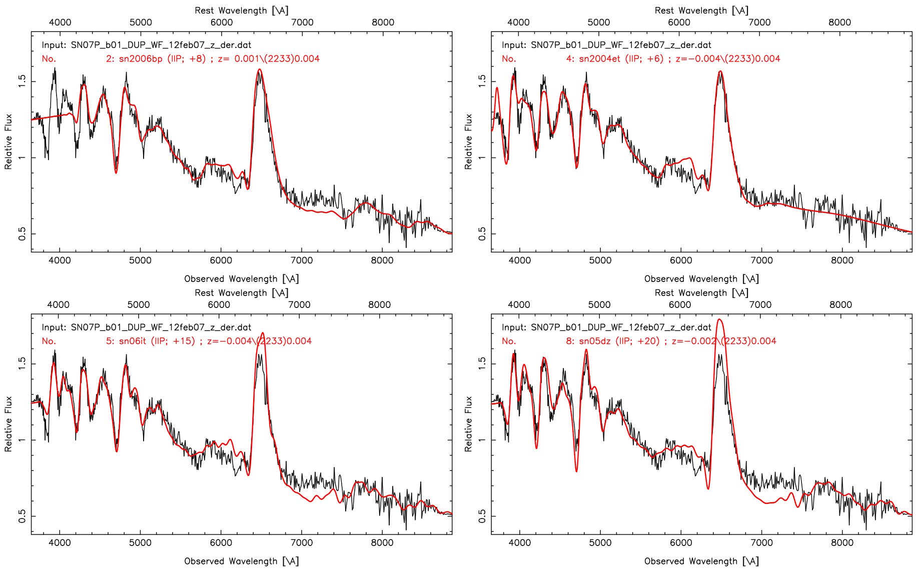

Figure B.74 Best spectral matching of SN 2007P using SNID.

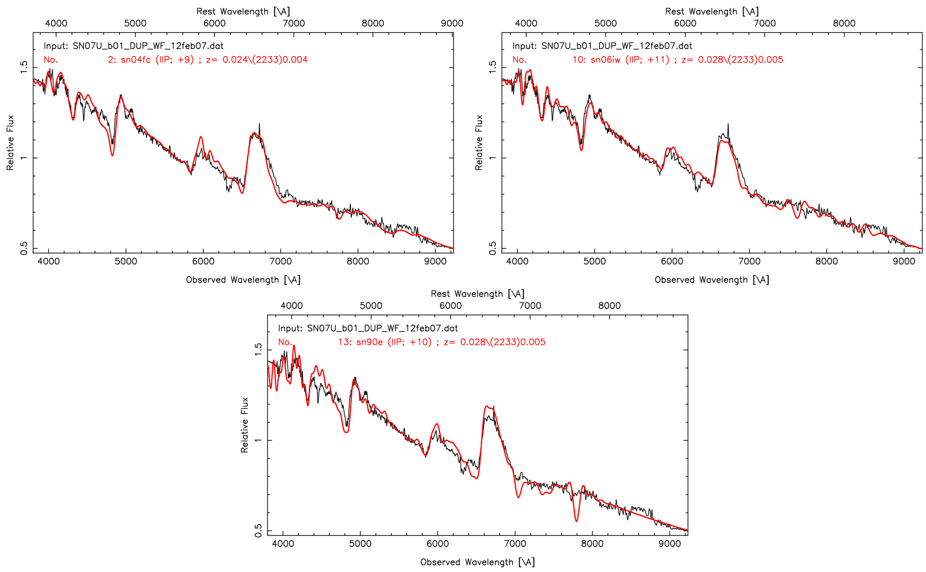

Figure B.75 Best spectral matching of SN 2007U using SNID.

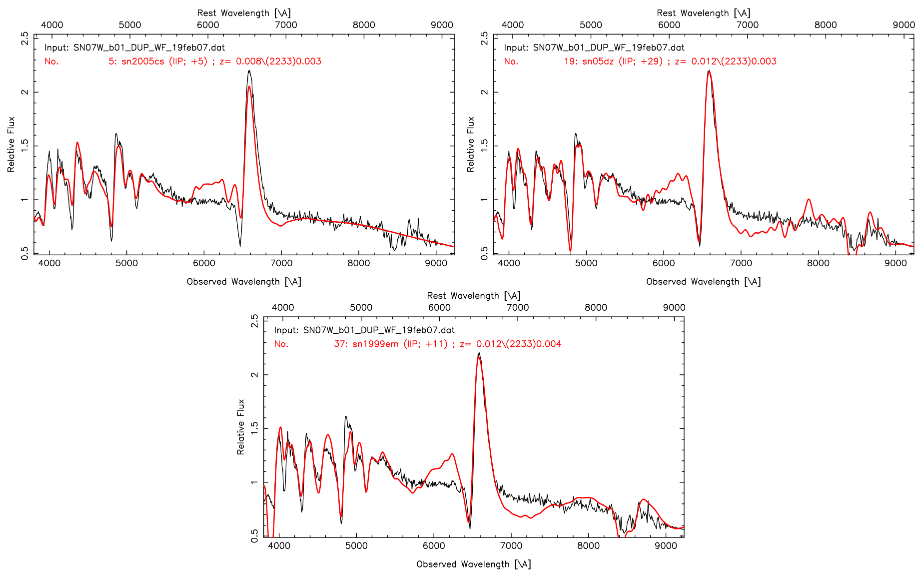

Figure B.76 Best spectral matching of SN 2007W using SNID.

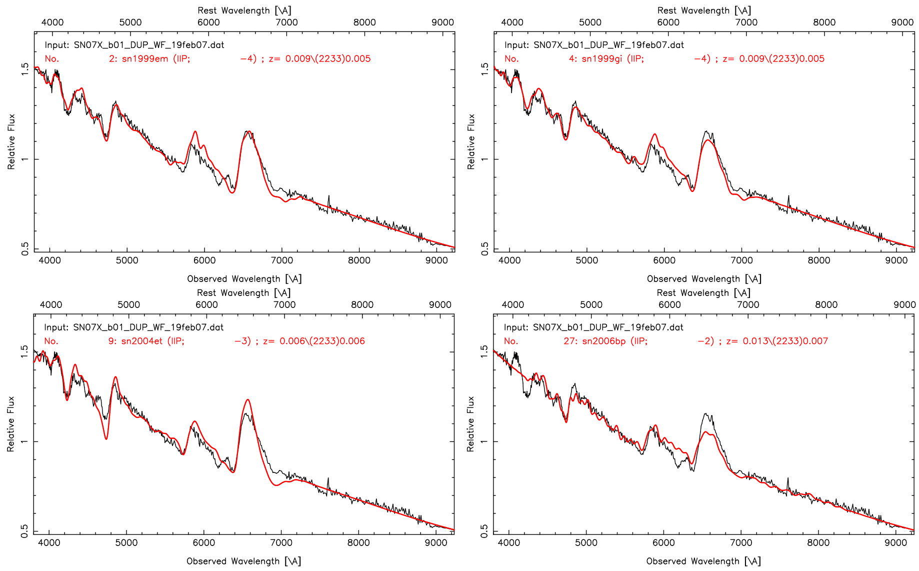

Figure B.77 Best spectral matching of SN 2007X using SNID.

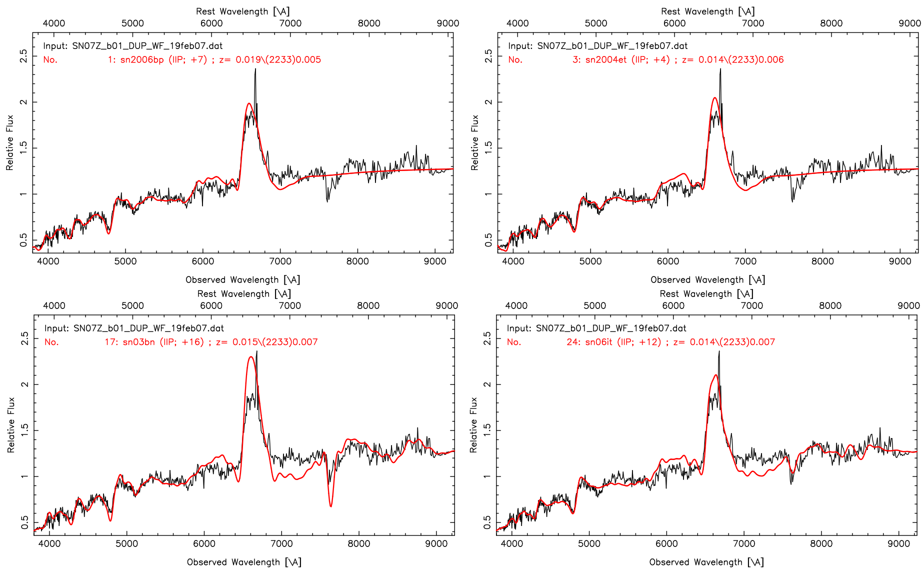

Figure B.78 Best spectral matching of SN 2007Z using SNID.

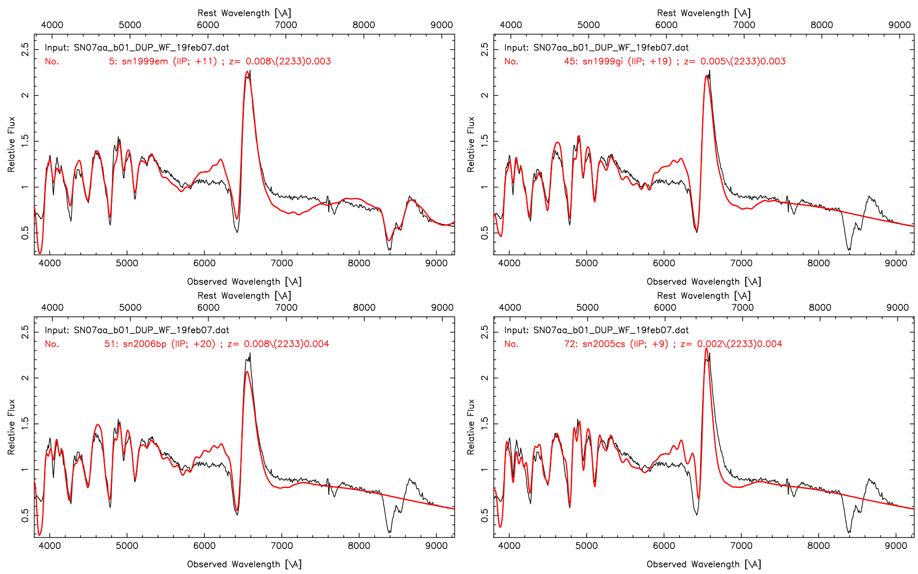

Figure B.79 Best spectral matching of SN 2007aa using SNID.

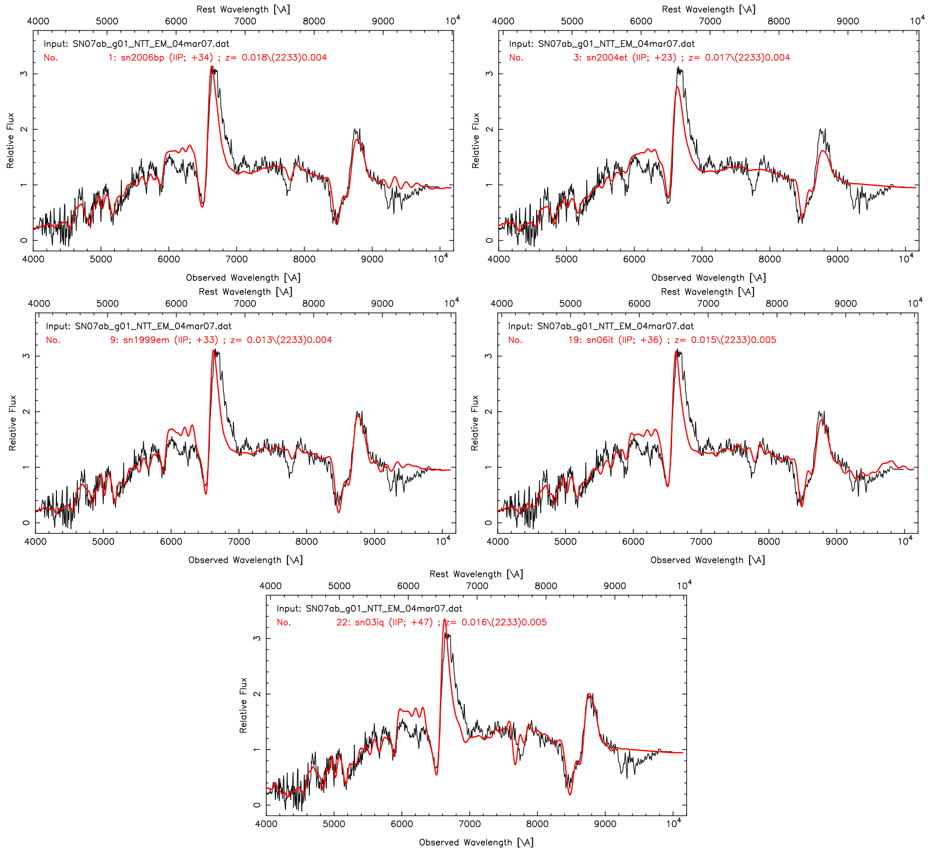

Figure B.80 Best spectral matching of SN 2007ab using SNID.

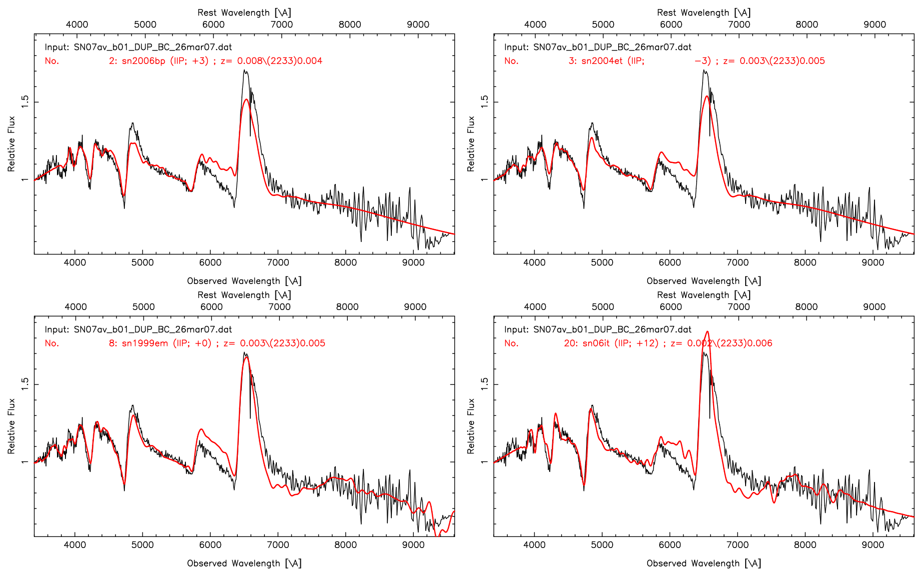

Figure B.81 Best spectral matching of SN 2007av using SNID.

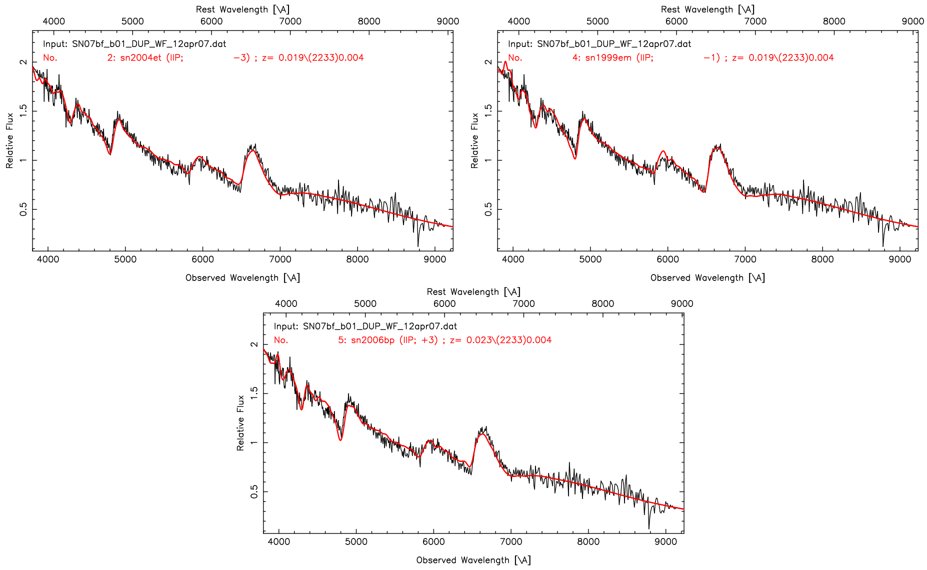

Figure B.82 Best spectral matching of SN 2007bf using SNID.

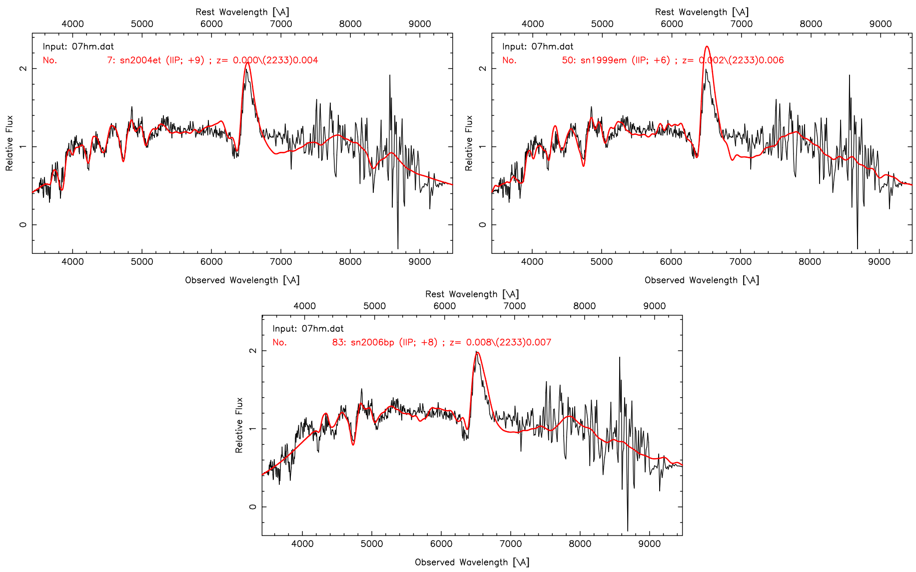

Figure B.83 Best spectral matching of SN 2007hm using SNID.

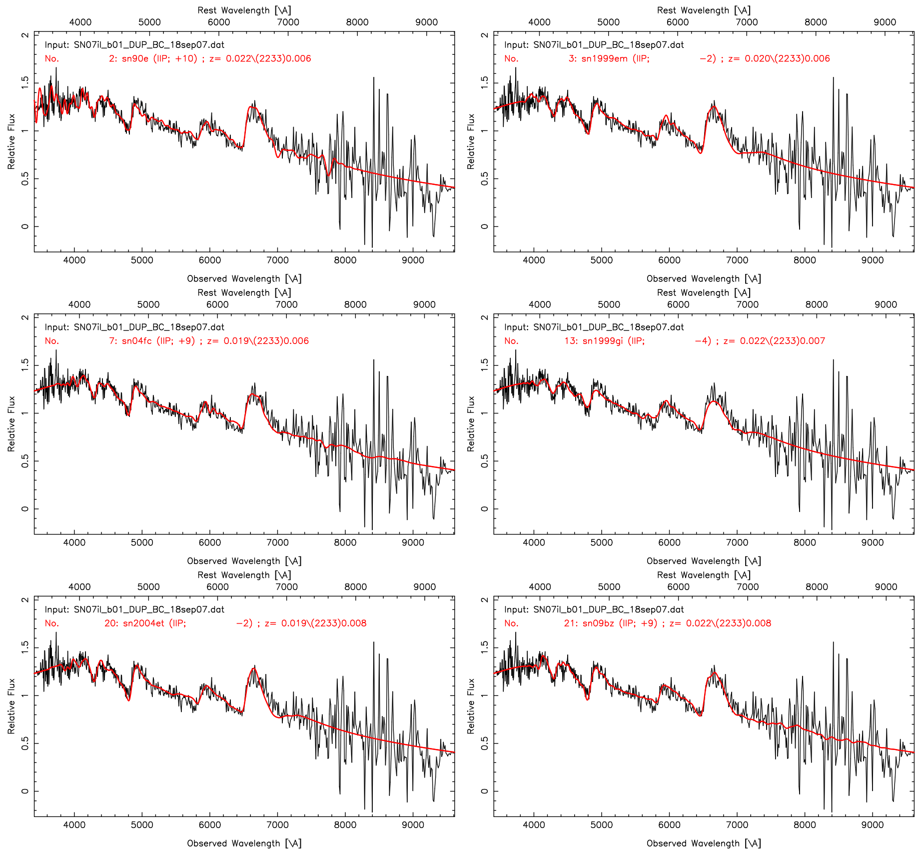

Figure B.84 Best spectral matching of SN 2007il using SNID.

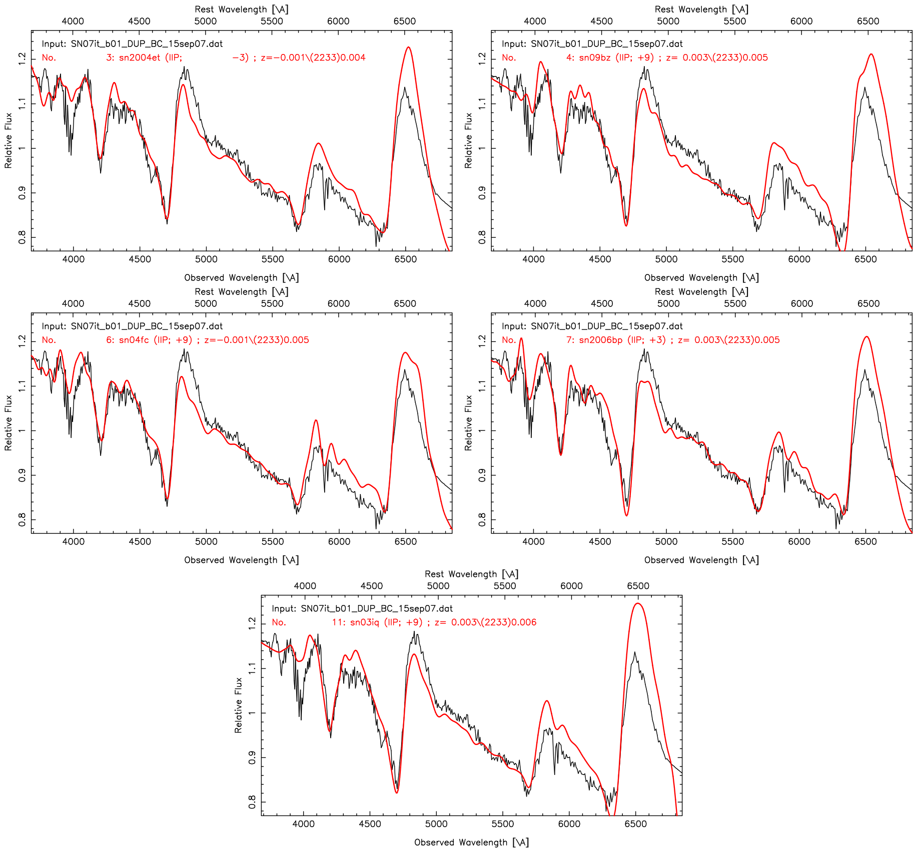

Figure B.85 Best spectral matching of SN 2007it using SNID.

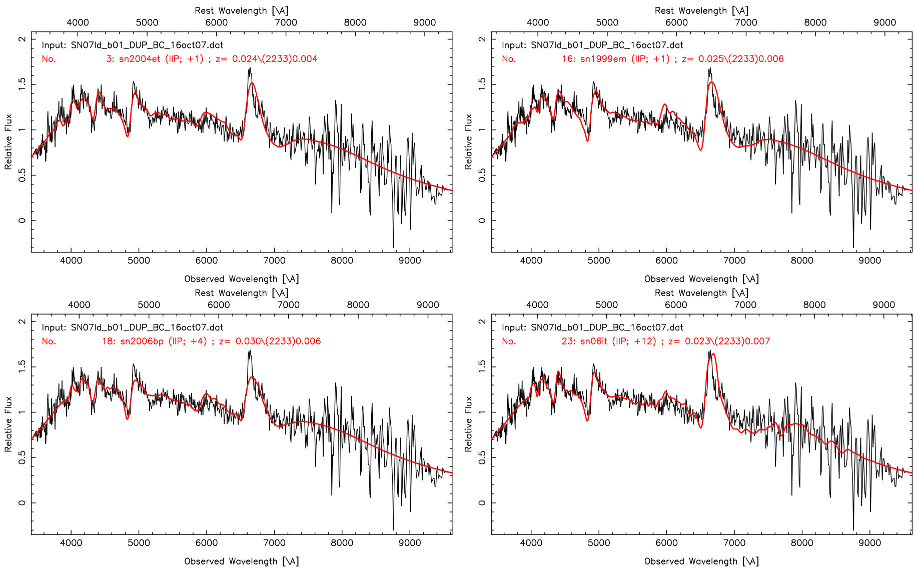

Figure B.86 Best spectral matching of SN 2007ld using SNID.

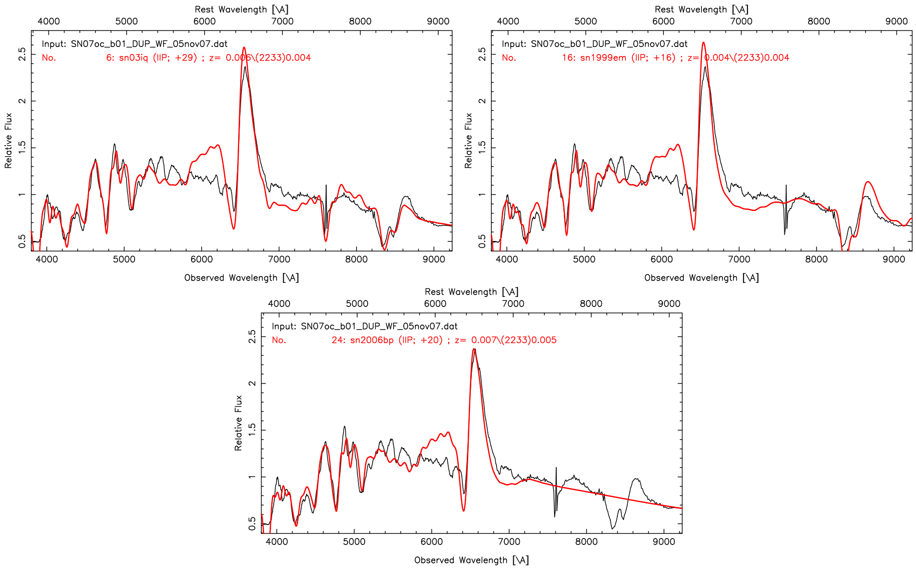

Figure B.87 Best spectral matching of SN 2007oc using SNID.

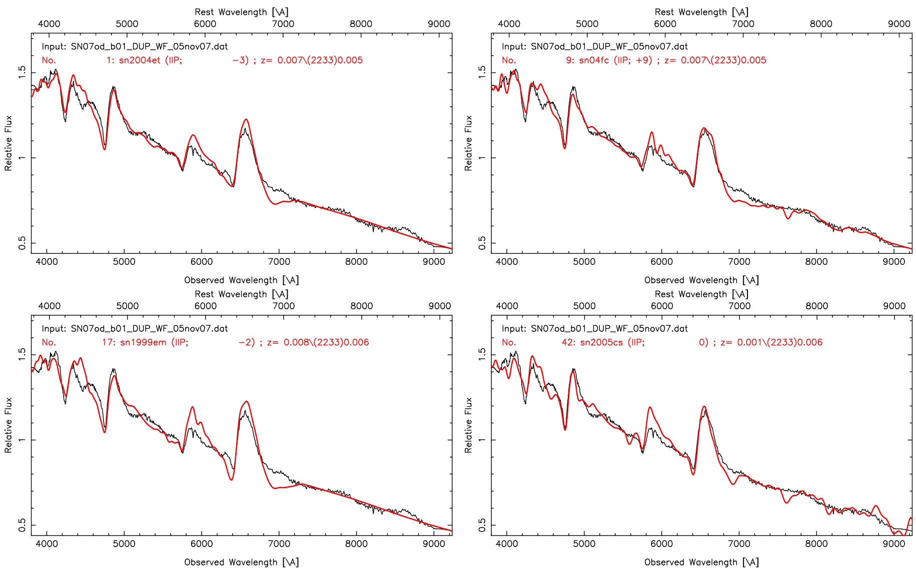

Figure B.88 Best spectral matching of SN 2007od using SNID.

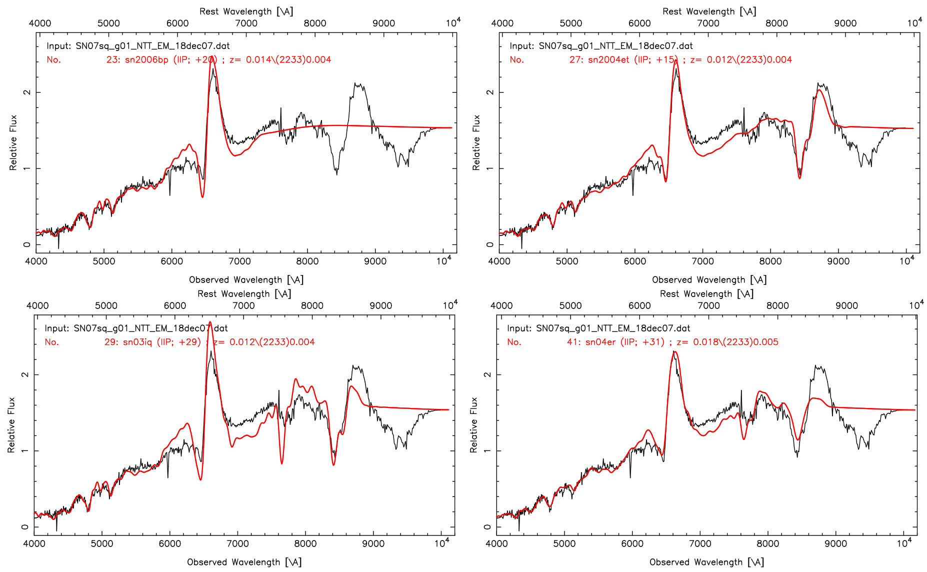

Figure B.89 Best spectral matching of SN 2007sq using SNID.

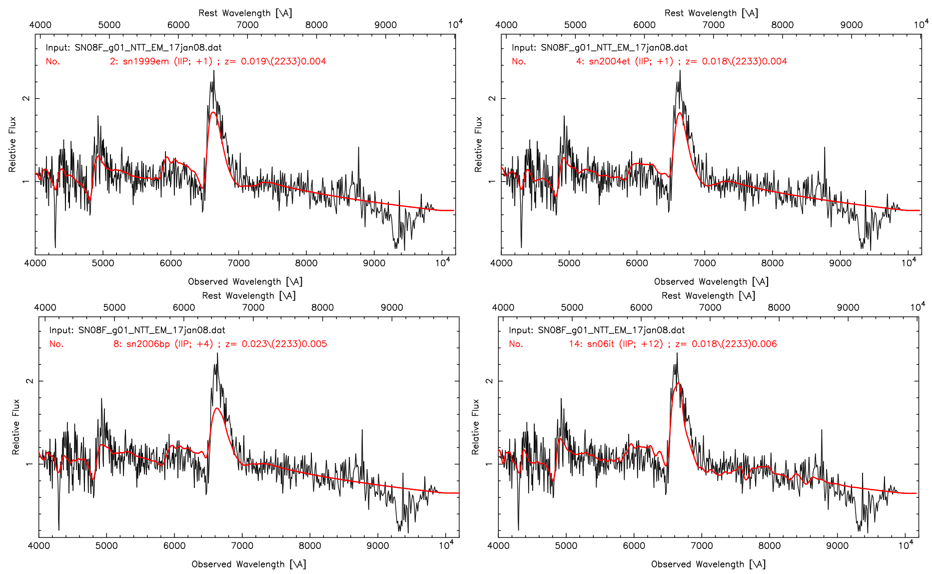

Figure B.90 Best spectral matching of SN 2008F using SNID.

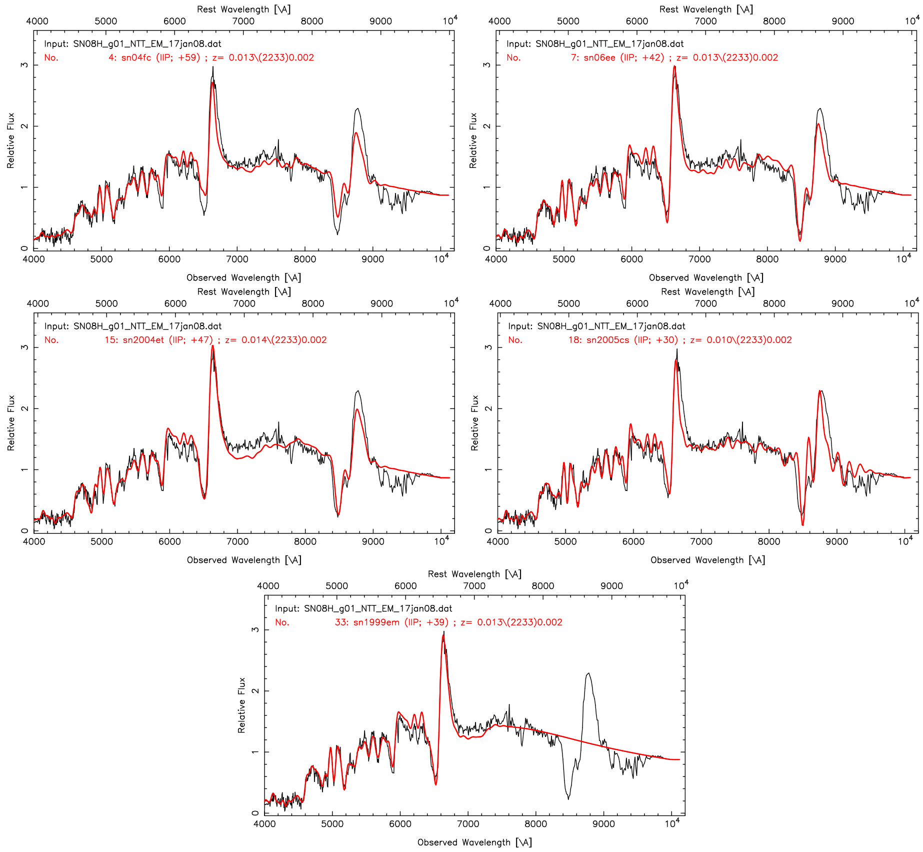

Figure B.91 Best spectral matching of SN 2008H using SNID.

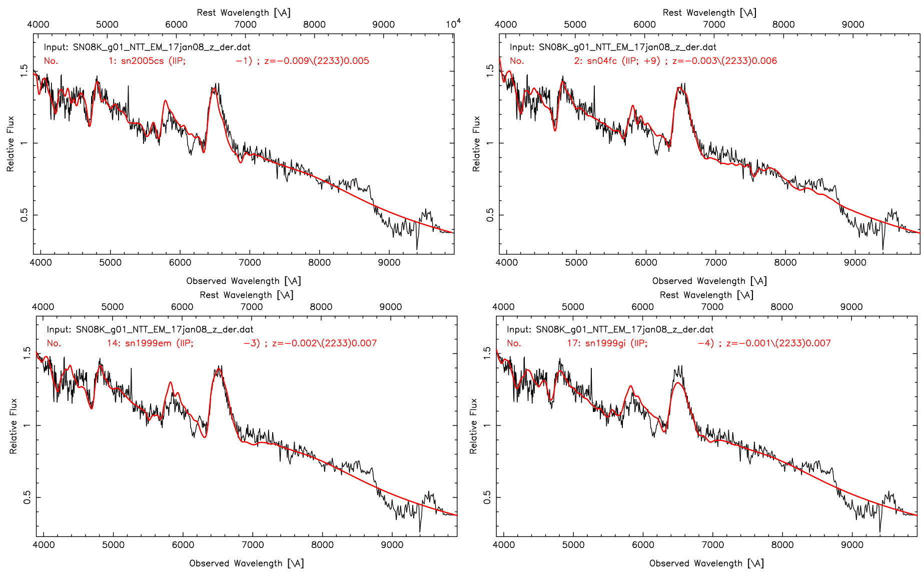

Figure B.92 Best spectral matching of SN 2008K using SNID.

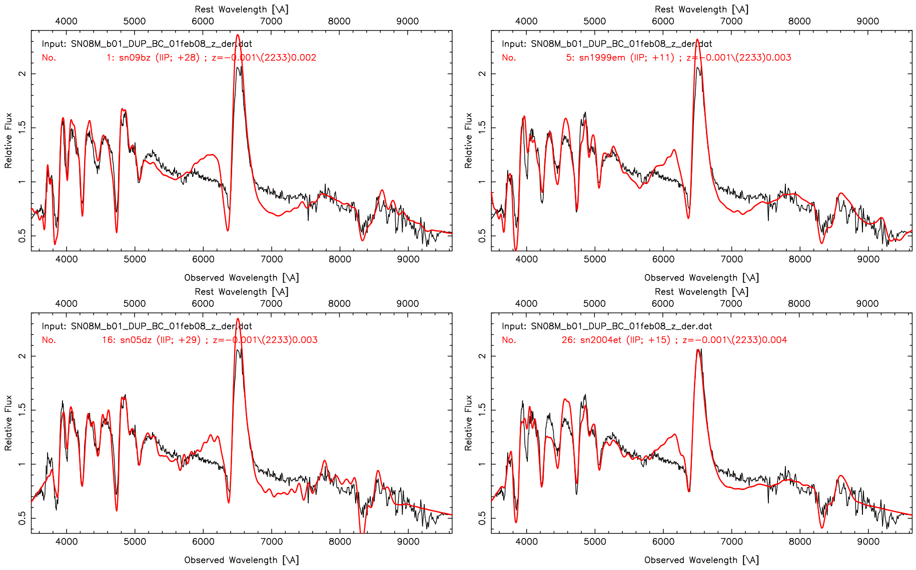

Figure B.93 Best spectral matching of SN 2008M using SNID.

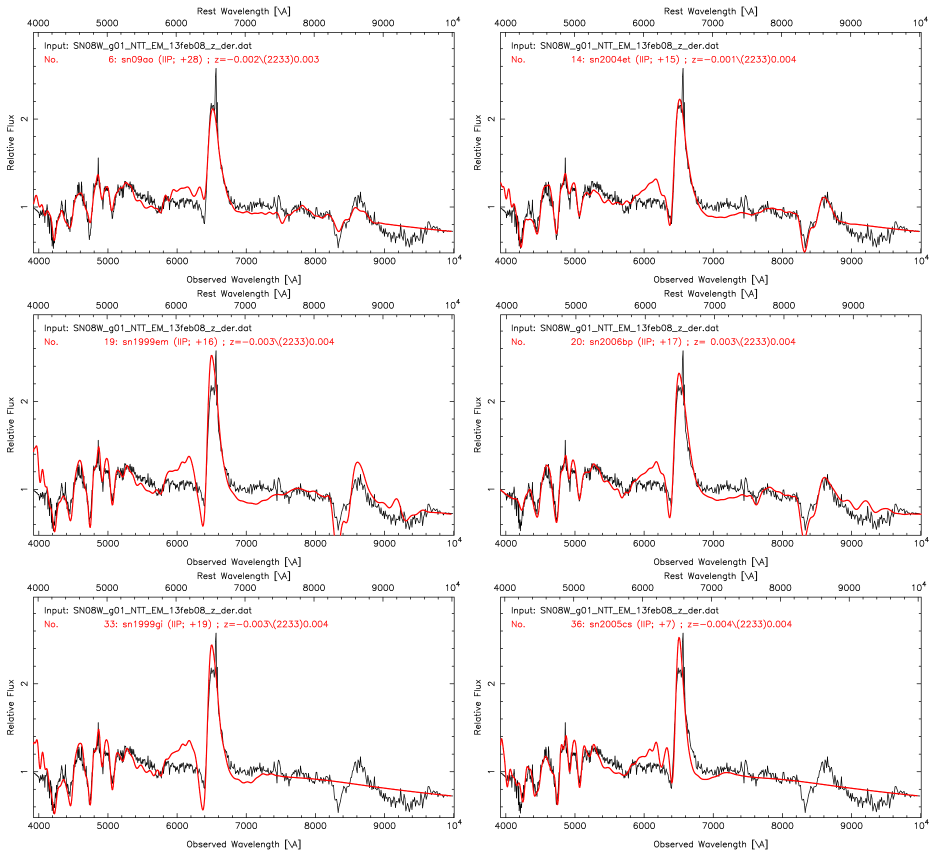

Figure B.94 Best spectral matching of SN 2008W using SNID.

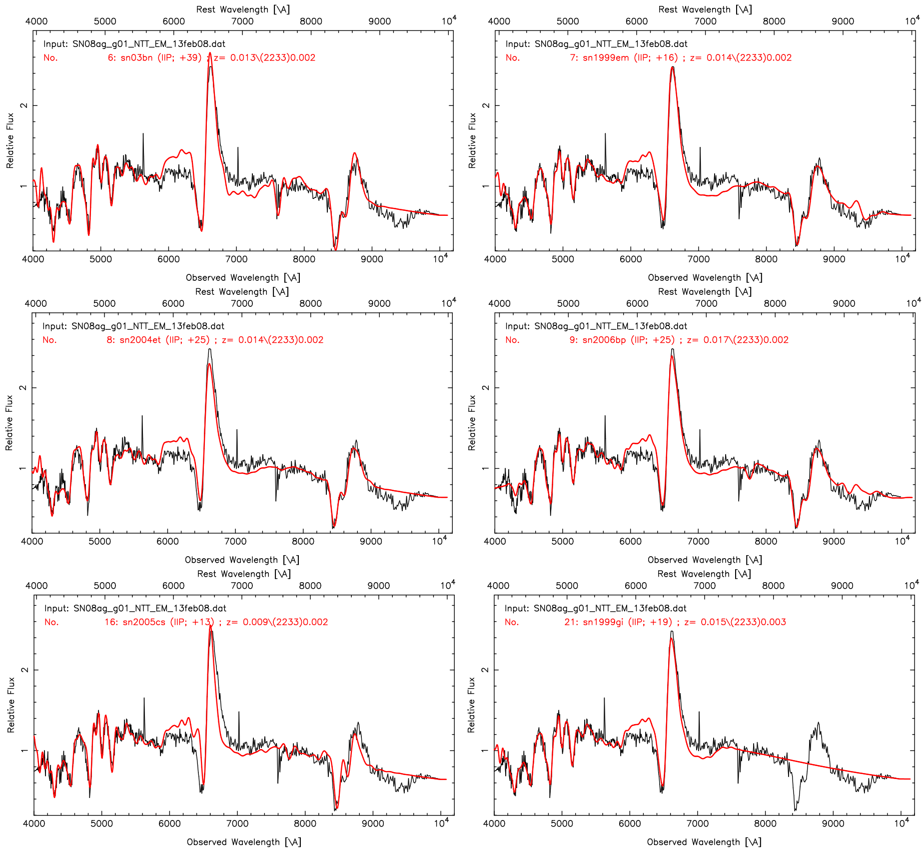

Figure B.95 Best spectral matching of SN 2008ag using SNID.

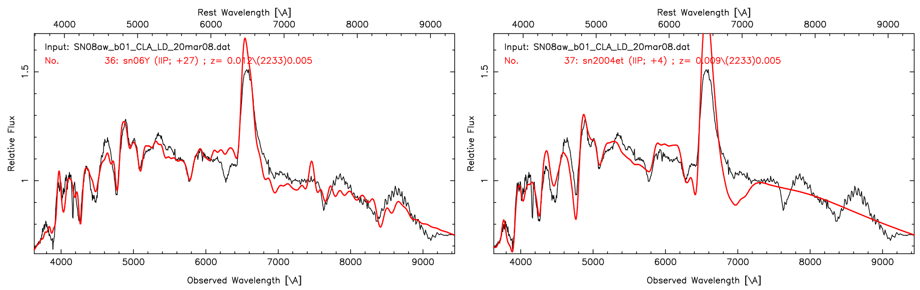

Figure B.96 Best spectral matching of SN 2008aw using SNID.

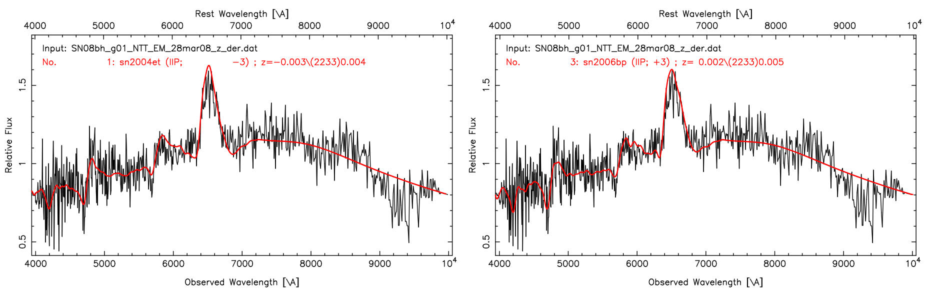

Figure B.97 Best spectral matching of SN 2008bh using SNID.

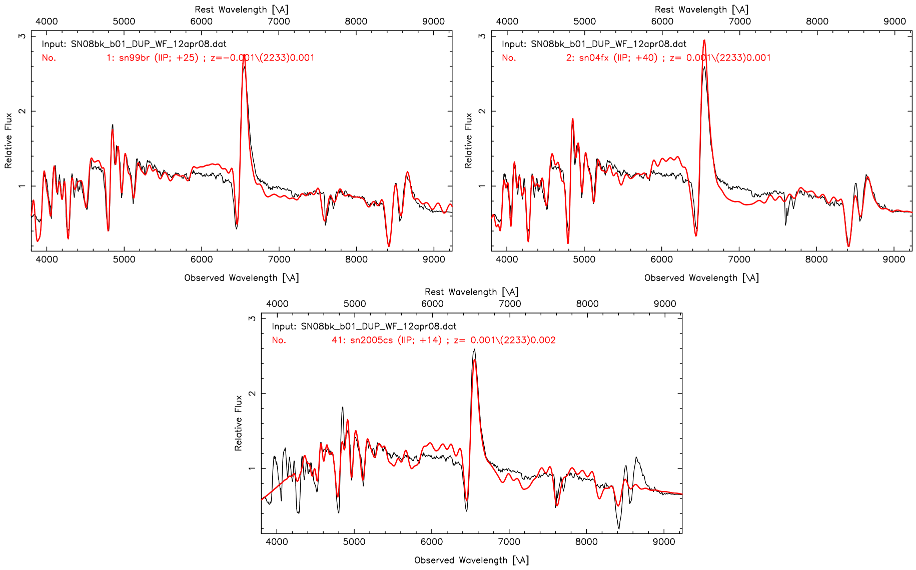

Figure B.98 Best spectral matching of SN 2008bk using SNID.

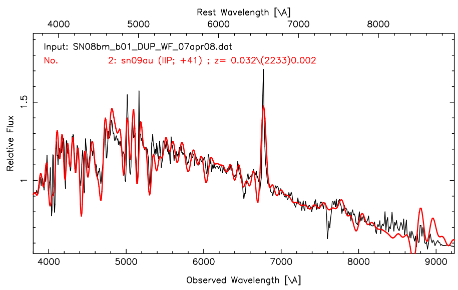

Figure B.99 Best spectral matching of SN 2008bm using SNID.

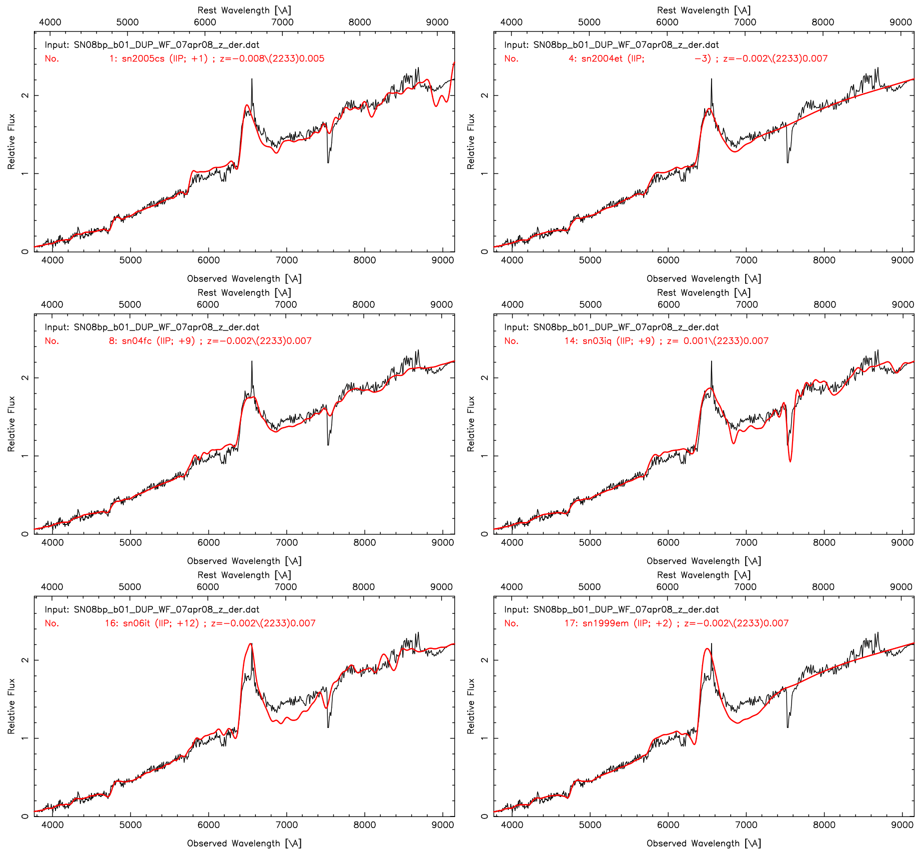

Figure B.100 Best spectral matching of SN 2008bp using SNID.

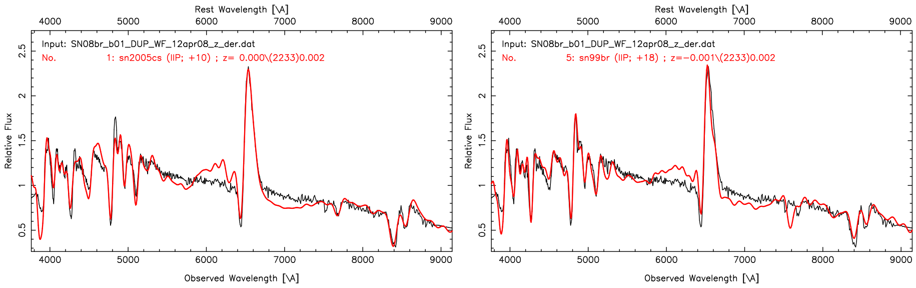

Figure B.101 Best spectral matching of SN 2008br using SNID.

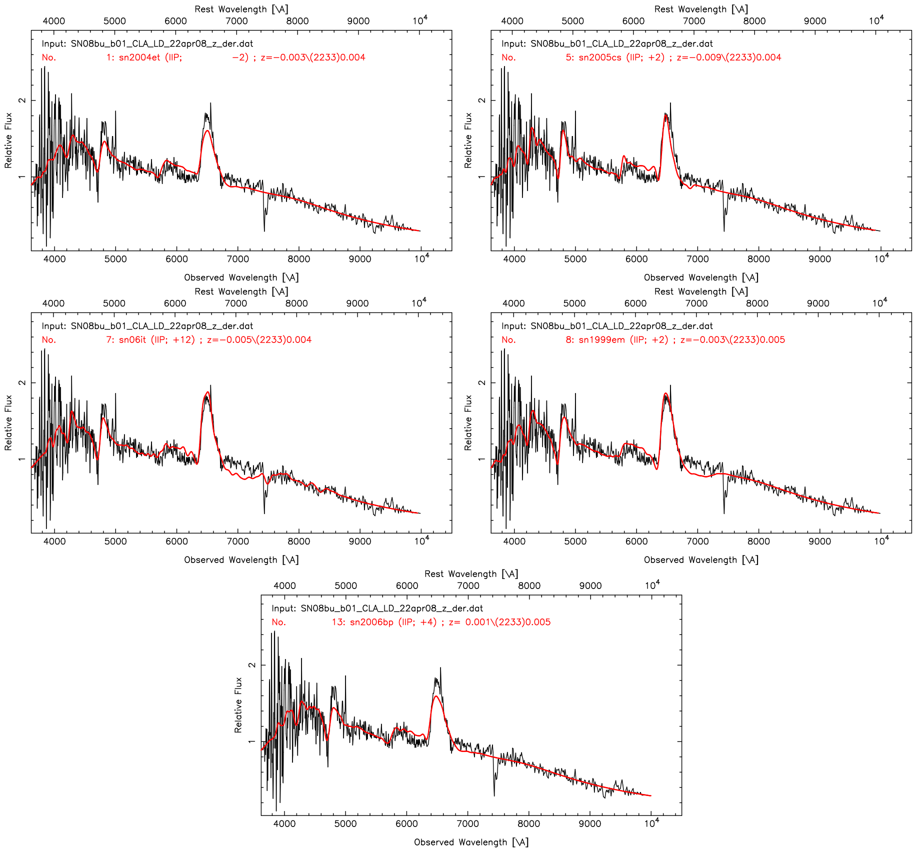

Figure B.102 Best spectral matching of SN 2008bu using SNID.

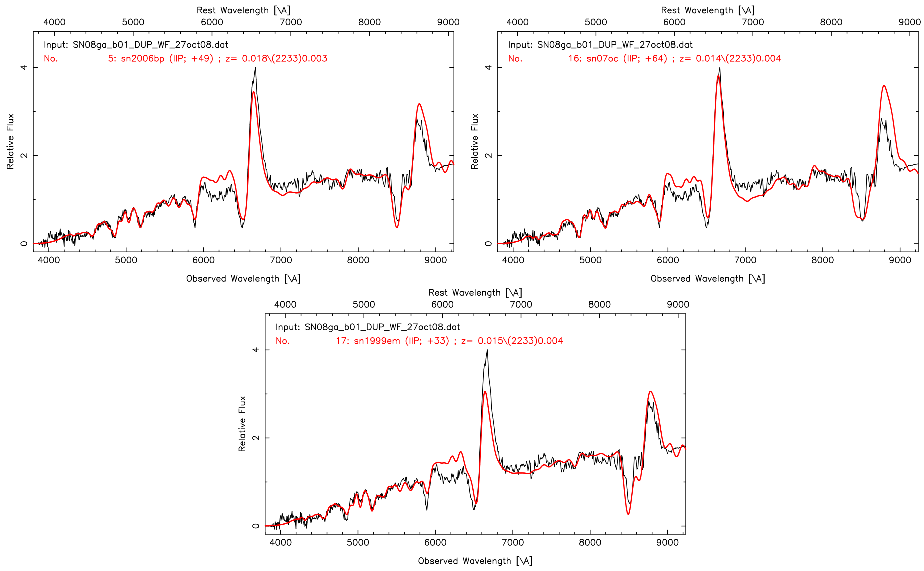

Figure B.103 Best spectral matching of SN 2008ga using SNID.

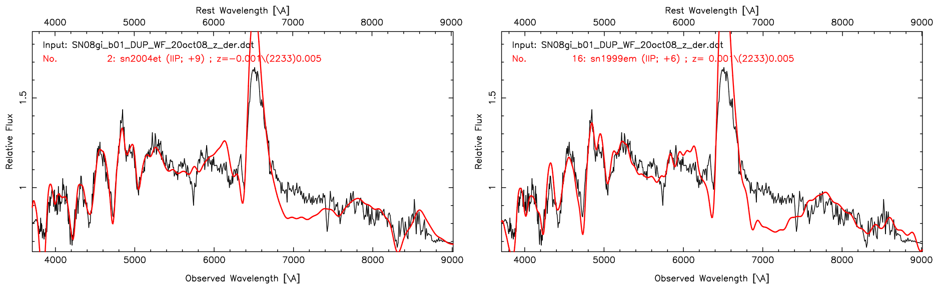

Figure B.104 Best spectral matching of SN 2008gi using SNID.

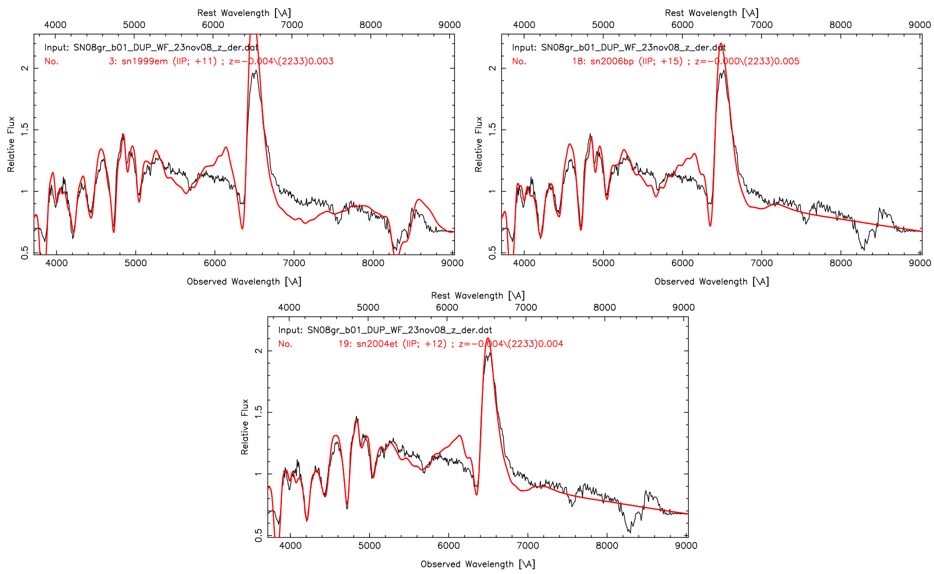

Figure B.105 Best spectral matching of SN 2008gr using SNID.

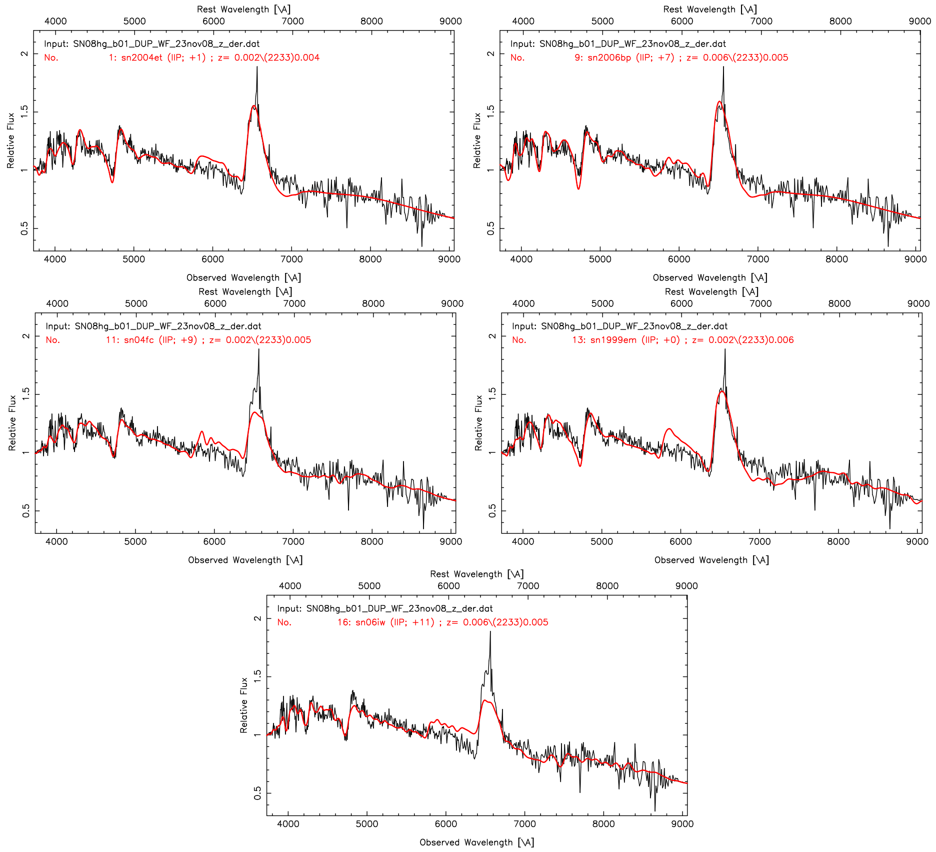

Figure B.106 Best spectral matching of SN 2008hg using SNID.

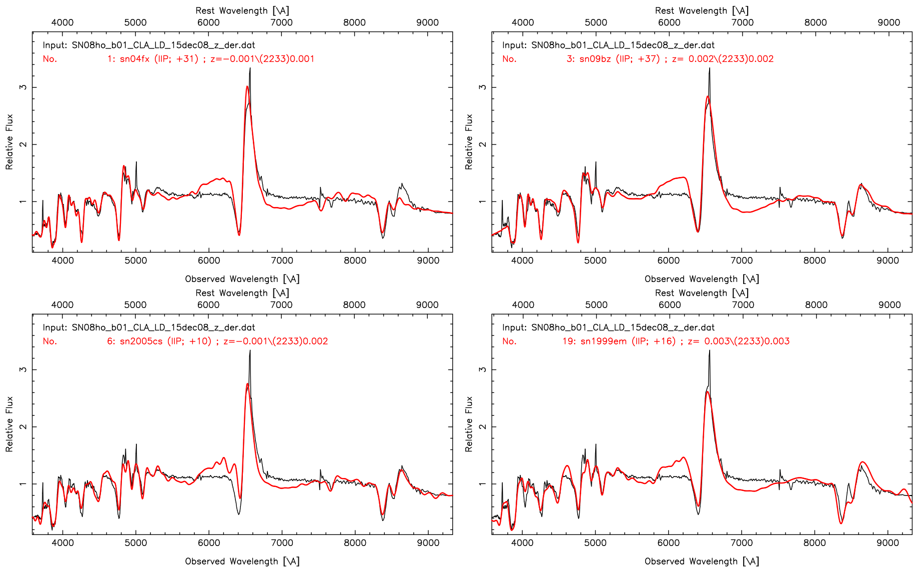

Figure B.107 Best spectral matching of SN 2008ho using SNID.

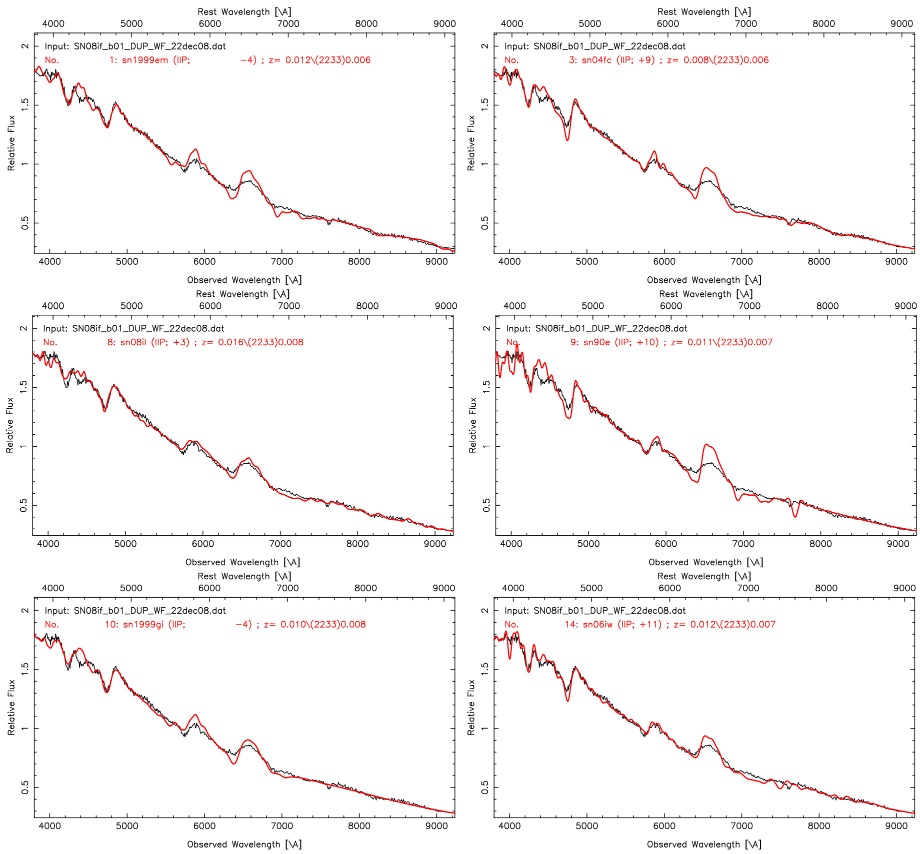

Figure B.108 Best spectral matching of SN 2008if using SNID.

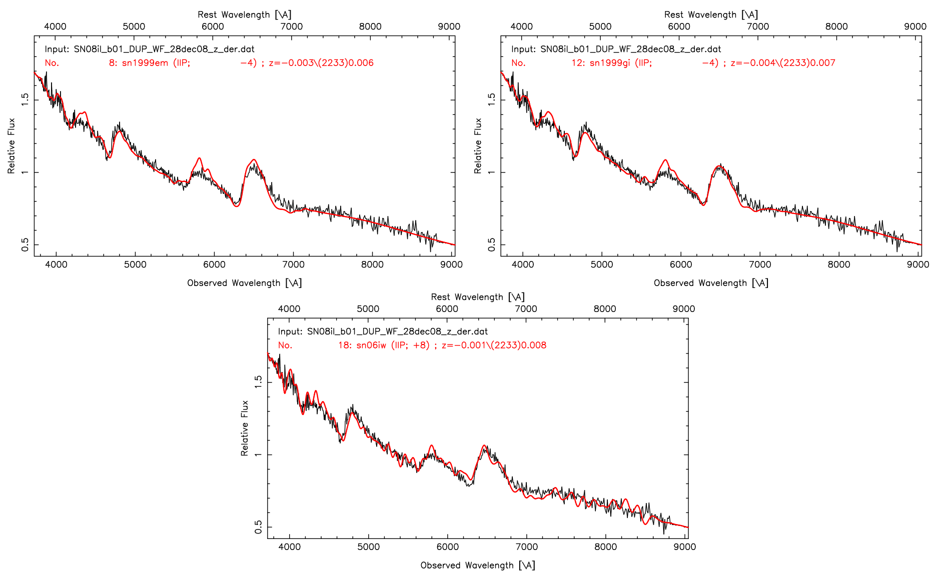

Figure B.109 Best spectral matching of SN 2008il using SNID.

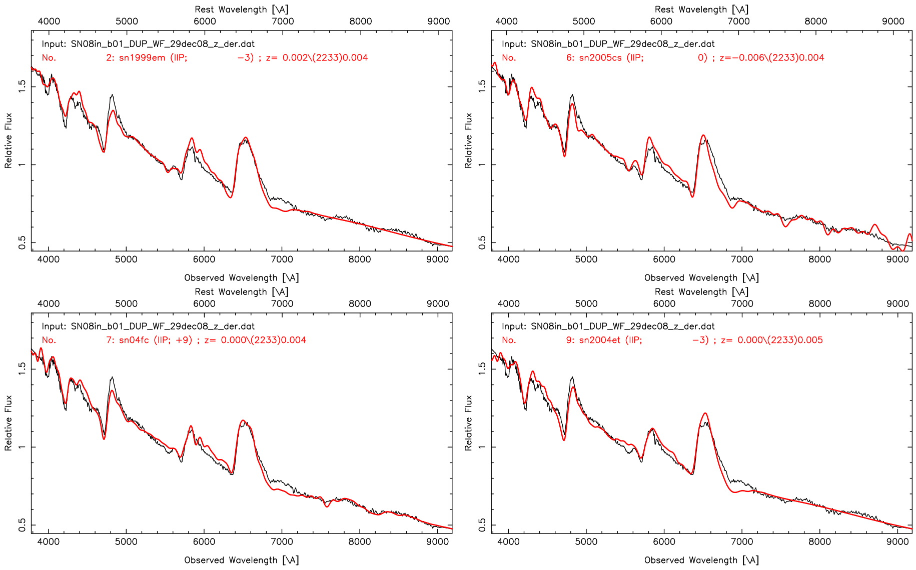

Figure B.110 Best spectral matching of SN 2008in using SNID.

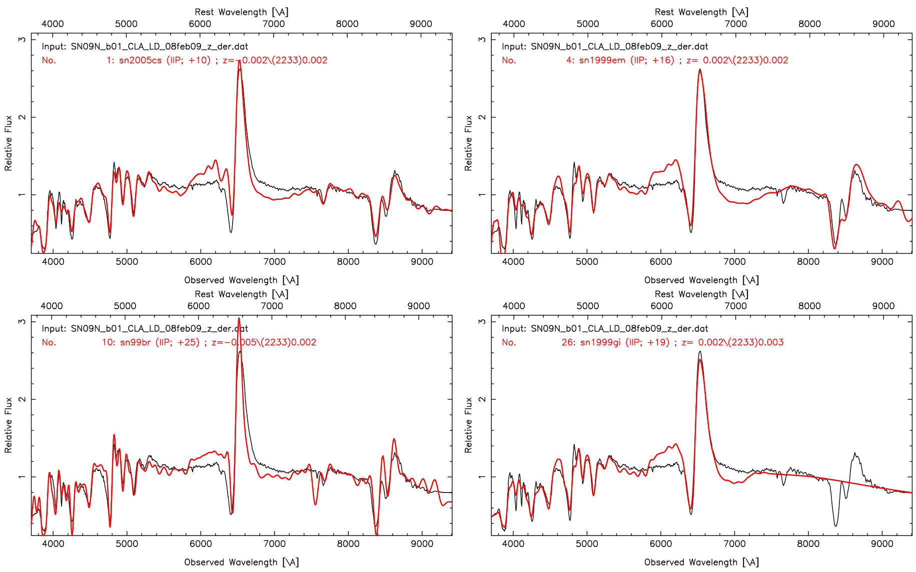

Figure B.111 Best spectral matching of SN 2009N using SNID.

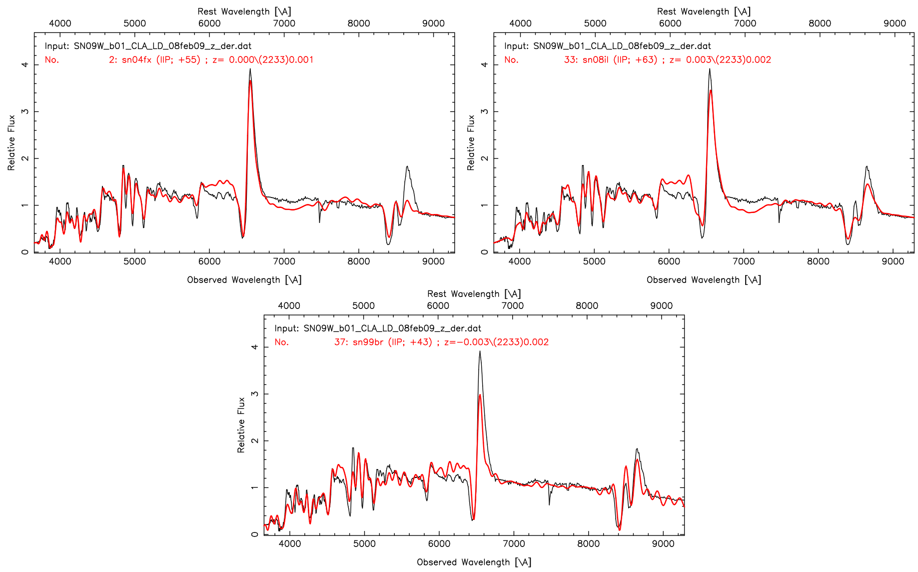

Figure B.112 Best spectral matching of SN 2009W using SNID.

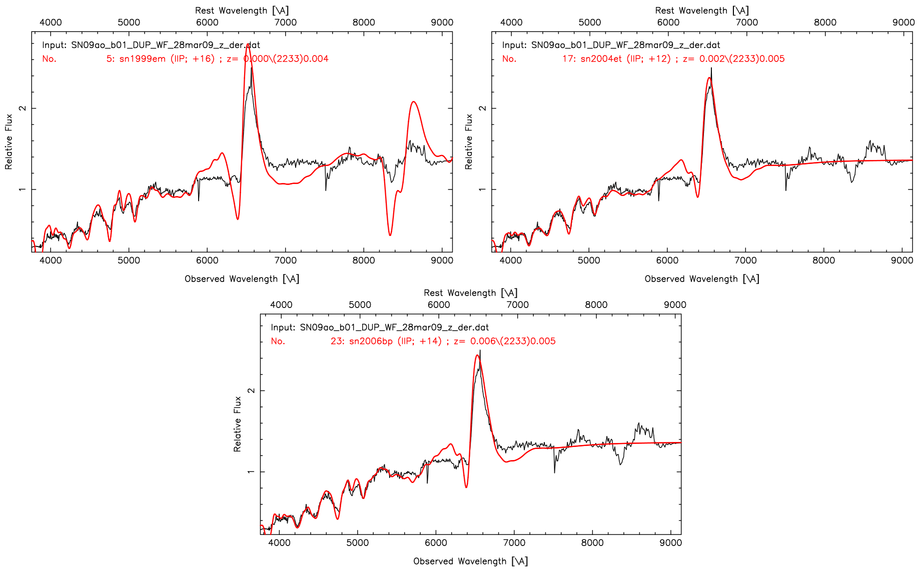

Figure B.113 Best spectral matching of SN 2009ao using SNID.

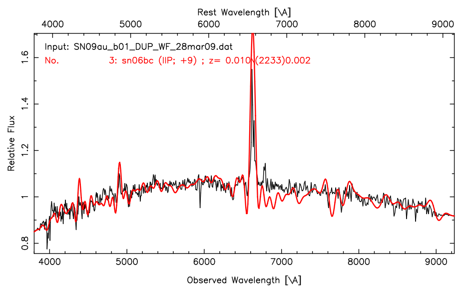

Figure B.114 Best spectral matching of SN 2009au using SNID.

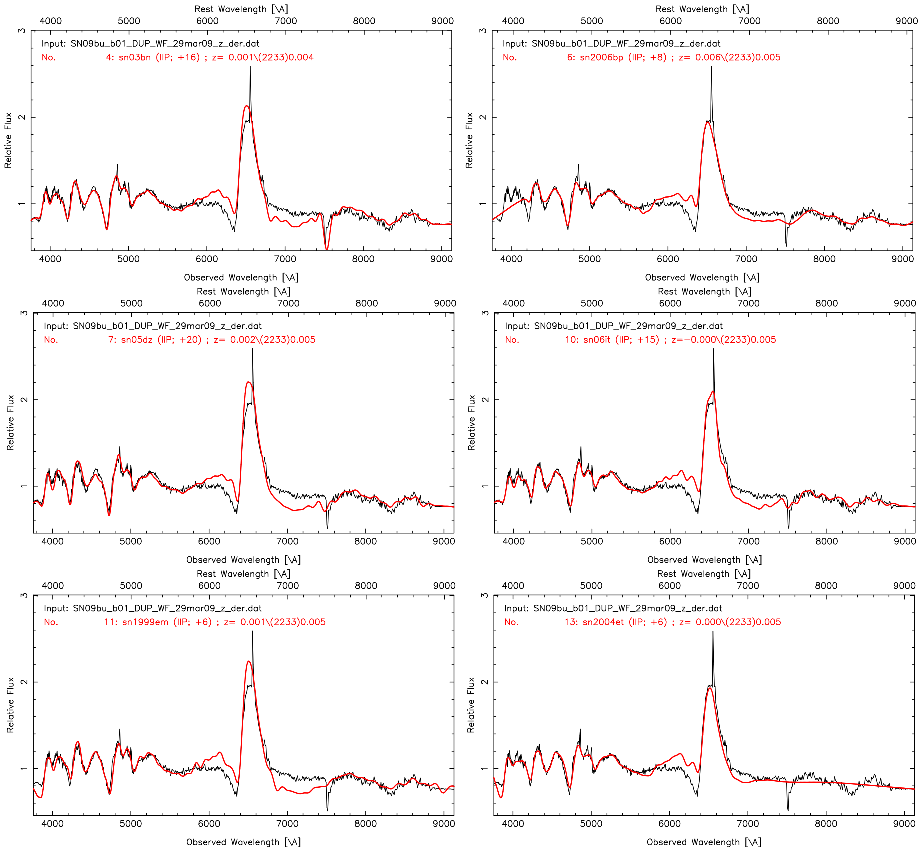

Figure B.115 Best spectral matching of SN 2009bu using SNID.

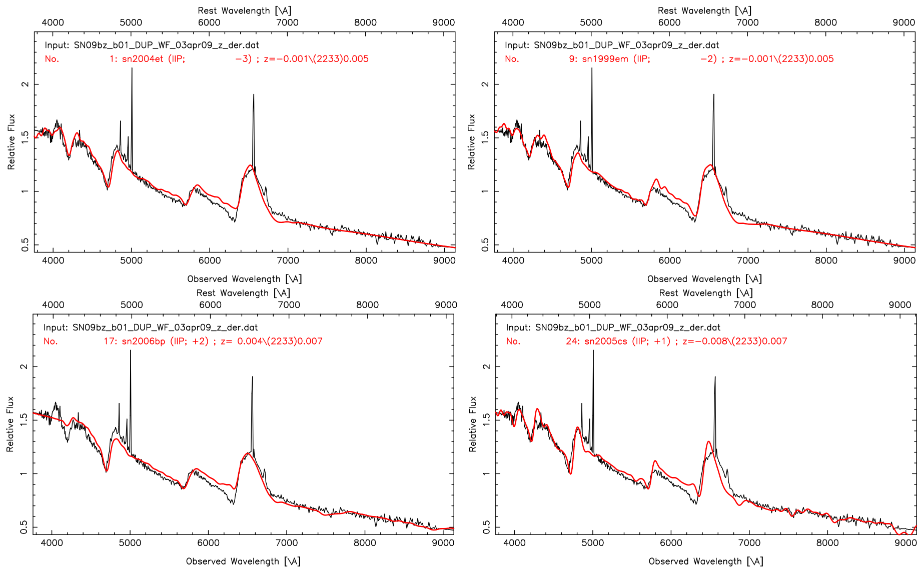

Figure B.116 Best spectral matching of SN 2009bz using SNID.